Department of Civil Engineering

Characterization of Amplitudes of Strong Ground Motion and Response Time Histories

J.M. Pauschke
J. Chatterjee

A Report on a Research Project Sponsored by the
National Science Foundation
Grant No. CEE83 - 07187

University of Pennsylvania
Philadelphia, PA
May 1986

ABSTRACT

This study investigate two methods to characterize the largest amplitudes of ground motion and response time histories. First, rms acceleration is investigated as ground motion and response parameters to characterize the strong motion amplitudes sustained over a given duration. While rms acceleration is shown to be linearly related to the peak acceleration of the ground motion or response time history, it does not consistently summarize the same of number of cycles of ground motion or response whose amplitudes will exceed the magnitude of the rms acceleration. Rms acceleration does not retain specific information on the near maximum peaks of a time history.

Second, a methodology is presented which does enable prediction of the expected amplitudes of specific peaks of ground motion and response time histories. The upper half-tail exponential and Rayleigh distributions proposed by Deherrera and Zsutty (1982) are shown to predict the largest peaks of ground motion acceleration, velocity, and displacement and acceleration response time histories better than the traditional exponential and Rayleigh distributions. Characterization of the probability distributions of the largest peaks of an earthquake time history enables information to be retained on all the near maximum peaks of the time history. This presents a more comprehensive description of the expected loading demands and response than the traditionally characterized maximum value and rms acceleration parameters of an earthquake time history.

TABLE OF CONTENTS

LIST OF TABLES

LIST OF FIGURES

XX

CHAPTER 1

INTRODUCTION

1.1 BACKGROUND

For simplicity in seismic hazard analysis and seismic design, an entire expected ground motion or response time history must be summarized by only a few parameters which reflect the duration, the amplitude levels, and the frequency content of the time history. While the frequency content of an earthquake time history is typically represented by the Fourier amplitude spectrum or the response spectrum of a single-degree-of-freedom (SDOF) oscillator, the duration and the amplitude levels of ground motion and structural response have been characterized by a number of different parameters.

The duration of the strong motion portion of an earthquake time history should represent the total time or the equivalent number of cycles over which the largest and most damaging amplitudes of motion occur. The duration of strong ground motion is required for the selection of representative input records for response studies of soils and structures and for generation of artificial accelerograms. For response, duration becomes important to characterize cyclic behavior, such as low-cycle fatigue.

A number of time domain definitions have been proposed to characterize strong ground motion. For a given earthquake record, however, the strong motion duration and the times of the start and the end of the strong motion defining the duration depend on the duration definition assumed. The use of a given duration measure is dependent on whether the ground motion duration is to be related to specific amplitude levels of the time history, to satisfy certain energy relationships, or to be a function of wave arrival and faulting characteristics. Typically, the time domain measures of duration are defined independent of their influence on structural response.

The amplitudes of strong ground motion and response time histories directly characterize the levels of loading and response. Traditionally, the amplitudes of an earthquake time history are represented by only one specific amplitude level of the time history: by the maximum value of the time history, e.g., the peak acceleration, or by a lesser amplitude level, e.g., root-mean-square (rms) acceleration or effective peak acceleration (EPA). Consequently, specific information is not retained on the amplitude levels and the duration of all the lesser, but near maximum amplitudes of the time history.

Therefore, this study investigates two methods to characterize the largest amplitudes and strong motion duration of ground motion and response time histories. First, the dependence of the two-parameter characterization of an earthquake time history, namely, rms acceleration, which characterizes the amplitudes sustained over a given duration, on the duration measure is addressed for ground motion and response time histories. Because a number of studies have addressed the use of rms acceleration as a ground motion parameter, this study primarily focuses on rms acceleration as a response parameter.

Second, the adequacy of selected exponential and exponential-like (Rayleigh and Weibull) probability distributions to predict the largest peaks of ground motion and response time histories is investigated. Characterization of the probability distribution of the largest peaks enables specific information on each of the expected largest peaks of an earthquake time history to be retained. Hence information is also implicitly retained on the duration of these peaks in terms of cyclic behavior.

Because this study focuses on the characterization of the duration and the amplitude levels of earthquake time histories, Sections 1.2 and 1.3 briefly review

parameters which have been developed to characterize the duration and the amplitude levels, respectively, of strong ground motion and structural response. Section 1.4 presents an overview of the methodology of this study to characterize the amplitudes and the duration of the maximum and near maximum peaks of earthquake time histories.

1.2 DURATION OF STRONG GROUND MOTION AND STRUCTURAL RESPONSE

In the time domain, the duration, T, of the strong motion portion of an accelerogram is defined as the elapsed time between the time of initial build-up of the strong motion, T_1, and the time corresponding to the end of the strong motion, T_2, as illustrated in Figure 1.1 where:

$$T = T_2 - T_1 \tag{1.1}$$

Because it is not clear what definitions of T_1 and T_2 are most appropriate for a transient signal, T_1 and T_2 have been determined for acceleration time histories based on different time domain measures of duration.

Strong ground motion duration has been defined in the time domain by Bolt (1973), Trifunac and Brady (1975), McCann and Shah (1979), McCann (1980), McGuire

and Hanks (1980), Bond, et al., (1980), and Vanmarcke and Lai (1977, 1980). Duration has also been defined in terms of an equivalent number of cycles for use in liquefaction studies (e.g., Seed and Idriss, 1971; Seed, et al., 1975). Procedures to determine the times T_1 and T_2 corresponding to the beginning and the end of the strong motion duration T in equation (1.1), respectively, are briefly discussed below for each time domain measure of duration. The first two definitions discussed below, which have been proposed by Bolt (1973) and Trifunac and Brady (1975), will be investigated in Chapter 2 as duration measures for calculation of rms acceleration.

Bolt (1973) defines "bracketed duration" as the elapsed time between the first (T_1) and the last (T_2) excursions of the acceleration time history greater than a prescribed cutoff level, such as 0.05g (where g represents the acceleration due to gravity), as shown in Figure 1.2. The bracketed duration is directly dependent on the amplitude levels of the accelerogram. Therefore, accelerograms with a peak ground acceleration (PGA) less than the specified cutoff level will have zero duration.

Trifunac and Brady (1975) define duration as the time during which a predetermined percentage of total energy would be input to a structure. For use in

earthquake engineering, Arias (1970) has demonstrated that the area under a squared acceleration time history is equivalent to the total energy per unit mass dissipated by all single degree of freedom oscillators. If a(t) is the acceleration time history and T is the total duration of the ground acceleration, then the Arias Intensity, I, is defined as:

$$I = \int_0^T [a(t)]^2 \, dt \qquad (1.2)$$

Duration should be based on that intensity which is closely related to the strong motion contributing significantly to the seismic energy. Accordingly, Trifunac and Brady (1975) define duration to be the time interval to accumulate between five and ninety-five percent of the total Arias Intensity. Hence, T_1 and T_2 are the times at which five and ninety-five percent, respectively, of the total energy is accumulated, as shown in Figure 1.3.

McCann and Shah (1979) and McCann (1980) define duration in a manner consistent with the use of rms acceleration as a ground motion parameter to summarize the amplitudes sustained over the strong ground motion duration. In the time domain, the rms acceleration, a_{rms}, of an acceleration time history, a(t), is defined

over a given strong motion duration T in equation (1.1) as:

$$a_{rms} = \{\frac{1}{T} \int_{T_1}^{T_2} [a(t)]^2 dt\}^{1/2} \quad (1.3)$$

The cumulative rms acceleration of the time history is calculated at each time step of the digitized time history from equation (1.3) by initially letting T_1 be equal to zero and time T_2 be equal to the total time at each time step. Then the time T_1 in equation (1.1) for this definition is the time at which the cumulative rms acceleration of the time-reversed accelerogram starts a steady decrease. The upper limit T_2 is found by applying the same procedure to the original acceleration time history, but the origin of the time history is now the value of T_1 computed from the time-reversed accelerogram.

In a study of the 1971 San Fernando, CA, accelerograms, McGuire and Hanks (1980) define T_1 as the time of the S-wave arrival and time T_2 equal to T_1 + 10 seconds. The duration T of all records is assumed to be equal to the faulting duration of 10 seconds. Bond, et al., (1980) define the times T_1 and T_2 to be the first and the last times, respectively, of the direct S-wave arrival.

Vanmarcke and Lai (1980) propose a definition of duration derived from the theory of stationary Gaussian

random processes. They assume that the strong motion portion of the record can be defined, in a total sense, by an equivalent stationary time history with a constant frequency spectrum intensity equal to that of the entire strong motion record. The duration T and the corresponding rms acceleration, a_{rms}, are derived in this method to guarantee that the total energy, I, in equation (1.2) is preserved and a constant relationship between PGA and a_{rms} is satisfied. This duration definition does not determine explicit values of T_1 and T_2. However, if the time of occurrence of the PGA is T_p, then the times T_1 and T_2 in equation (1.1) can be defined as:

$$T_1 = T_p - T/2 \qquad (1.4)$$

$$T_2 = T_p + T/2 \qquad (1.5)$$

Bolt`s duration is directly dependent on the specific amplitude levels of the acceleration time history. Hence a value of zero duration will be given by this definition if the cutoff level is less than the PGA of the accelerogram. However, all other duration measures discussed above are defined in terms of satisfying either various energy or wave arrival relationships and hence are not explicitly dependent on the amplitude

levels. For these definitions, the duration of the accelerogram will always be greater than zero.

In addition, several of the time domain definitions of duration do not show consistent trends when regressed as functions of earthquake intensity measures and distance from source to site. For example, Bolt's (1973) bracketed duration, based on a specific acceleration amplitude cutoff level, increases with increasing Richter magnitude and decreases with increasing distance from source to site. The Trifunac and Brady duration measure, attenuated by Trifunac and Brady (1975), Trifunac and Westermo (1977), and Dobry, et al., (1978), increases both with increasing magnitude and increasing distance from source to site but decreases with increasing Modified Mercalli Intensity (MMI). For the 1971 San Fernando, CA earthquake records, McCann (1980) and Bond, et al., (1980) did not observe any noticeable trends for duration as a function of distance from source to site. Vanmarcke and Lai (1977, 1980) found that duration increases both as a function of increasing magnitude and increasing epicentral distance.

However, the above studies indicate considerable scatter in the duration measures as a function of magnitude and distance from source to site. McGuire and Barnhard (1979) have found that when the duration

measures proposed by Bolt (1973) and Trifunac and Brady (1975) are regressed as a function of magnitude, distance, soil type, and component direction, the residual uncertainty is even larger than that typically calculated in regression studies for PGA. Consequently, the characterization of the duration of ground motion accelerograms is highly dependent on the definition of duration chosen. Different duration measures will lead to different relationships of duration as functions of a seismic severity parameter and source to site distance.

Moreover, these ground motion durations are defined independently of their effects on structural response. For example, O'Rourke, et al., (1982) investigate the correlation between the Trifunac and Brady (1975) definition to measure the duration of building response recorded from the 1971 San Fernando, CA earthquake and four measures of the causative ground motion duration. Comparisons between the ground motion durations and the response duration indicate that the match between strong ground motion duration and structural response duration is a function of the natural period of the structure. For structures with fundamental natural periods less than two seconds, strong structural response begins approximately two seconds after the starting time T_1 of strong ground motion determined by any of the four duration

measures. For many longer period structures, strong structural response begins after the end of the strong ground motion duration and none of the ground motion duration measures matches well with the time during which strong structural response occurs.

As discussed above, the proposed time domain definitions of duration result in different characterization of strong ground motion. The attenuation behavior of ground motion duration is dependent on the assumed duration definition. Characterization of ground motion duration in terms of cyclic behavior, however, avoids the need to explicitly define duration. The implicit cyclic behavior of ground motion and response time histories will be addressed in this study by retaining information on the largest peaks of earthquake time histories.

1.3 AMPLITUDES OF STRONG GROUND MOTION AND STRUCTURAL RESPONSE

This section briefly reviews parameters which characterize the amplitude levels of strong ground motion and structural response.

1.3.1 AMPLITUDES OF STRONG GROUND MOTION

Parameters which characterize the amplitude levels of strong ground motion include the following:

- Peak ground acceleration (PGA), peak ground velocity (PGV), peak ground displacement (PGD) (e.g., as reviewed in Idriss, 1978; Campbell, 1985)
- Effective peak acceleration (EPA), effective peak velocity (EPV) (Seed and Idriss, 1971; Schnabel and Seed, 1973; Ploessel and Slosson, 1974; Newmark, 1976; Whitman, 1978; Donovan, et al., 1978; Blume, 1979; Bolt and Abrahamson, 1982).
- Root-mean-square (rms) acceleration (Vanmarcke, 1976; Vanmarcke and Lai, 1977, 1980; Mortgat and Shah, 1978; Hanks, 1979, 1982; McCann and Shah, 1979; Mortgat, 1979; McCann, 1980; Bond, et al., 1980; McGuire and Hanks, 1980; Hanks and McGuire, 1981; McCann and Boore, 1983)

For many of these amplitude parameters, attenuation relationships have been derived to predict the expected parameter at a site as a function of magnitude, distance from source to site, and local site geology. Idriss (1978) and Campbell (1985) review available attenuation formulas. In addition, a number of these parameters have been investigated as normalization parameters to reduce the coefficient of variation of statistically derived seismic design response spectra (e.g., Nau and Hall, 1982, 1984).

The most widely-used characterization of strong ground motion is PGA, the maximum absolute amplitude of the ground motion acceleration time history. PGA has

been a convenient parameter to characterize seismic hazard since it can be directly scaled from the accelerogram. PGA has also been extensively used as a normalization parameter to derive statistical seismic design response spectra.

It is well-recognized, however, that PGA is not necessarily the most important feature of a ground motion time history which affects the structural response (Schnabel and Seed, 1973; Dizon, 1977; Donovan, et al., 1978). Observations from a number of earthquakes have confirmed that the duration of the strong ground motion influences significantly the degree of damage to both structures and soils. Examination of records obtained from the June 27, 1966, Parkfield, CA earthquake indicates that little damage may be associated with large accelerations if the duration is short (Cloud, 1967; Housner, 1975). PGA has also been shown to be a poor indicator of the energy demands on a structure and of the damage potential of the earthquake excitation (Kennedy, 1981).

As an improvement over the use of PGA to characterize strong ground motion, a number of definitions of EPA have been proposed. EPA typically defines a lesser, near maximum amplitude level of the acceleration time history or an amplitude level sustained over a prescribed

number of cycles. Schnabel and Seed (1973) illustrate that a 25 to 35 percent reduction of the PGA will affect the spectral accelerations by less than ten percent. Hence, in many cases, the EPA of ground motion on rock may be about 25 to 30 percent of the PGA. Newmark (1976), Housner and Jennings (1977), and Blume (1979) define EPA as the zero-period spectral acceleration value of the design response spectrum.

Seed and Idriss (1971) define "average equivalent uniform acceleration" as the average acceleration of an equivalent uniform number of cycles. Ploessel and Slosson (1974) define "respectable high ground acceleration" as the average acceleration of the several largest peaks which are repeated a significant number of times, generally about five to ten times, in the time history. Whitman (1978) defines EPA to be the intensity of ground motion which produces the same response as the actual motion when applied over a standard duration. Finally, Bolt and Abrahamson (1982) define EPA to be the 90^{th} percentile acceleration of the time history.

Definitions of duration proposed for strong ground motion gave impetus to the development of a two-parameter description of strong ground motion, namely, rms acceleration, which by its definition in the time domain is coupled with duration, as a summary of the amplitude

levels of an accelerogram sustained over a given strong motion duration. In the time domain, the rms acceleration, a_{rms}, of an acceleration time history a(t) is defined over a given duration T by equation (1.3).

An advantage of using rms acceleration to characterize ground motion is that this parameter can be directly predicted from the properties of the seismic source, e.g., the seismic moment and the stress drop. Also, because rms acceleration is an average statistic of the accelerogram, it should be insensitive to isolated peaks that might contribute to the large uncertainty in prediction of PGA. For a stationary Gaussian process, the rms acceleration will have considerably lower variation than the peak value. However, based on an analysis of the 1971 San Fernando, CA earthquake records, McCann and Boore (1983) found that rms acceleration, when regressed as a function of distance, has only a slightly lower logarithmic standard deviation than the PGA and concluded that the rms acceleration does not provide a more stable measure of ground motion than does PGA.

The rms acceleration description of strong ground motion requires the selection of the most appropriate definition of duration needed to compute the rms acceleration in equation (1.3). None of the time domain definitions proposed for duration have been widely

accepted to be the most suitable measure of strong ground motion duration. Consequently, the rms acceleration computed from equation (1.3) is dependent on the duration measure selected.

Another point of concern with the use of rms acceleration as a ground motion parameter is the apparent loss of information on particular acceleration levels. Mortgat and Shah (1978) and Mortgat (1979), however, have shown that rms acceleration is related by a constant K_p to an acceleration level, A_p, which has a given probability p of being exceeded. The constant K_p depends only on the probability level p. However, their characterization does not give information on the actual number of cycles in the time history which will exceed A_p.

To avoid the need to explicitly define duration and yet retain information on both the amplitude levels of and the duration of an acceleration time history, Mortgat and Shah (1978), Mortgat (1979), Zsutty and Deherrera (1979), and Deherrera and Zsutty (1982) have demonstrated that the largest peaks of ground motion and response time histories can be predicted from exponential, Rayleigh, Weibull, or Gamma functions. The Rayleigh distribution is also extensively used in random vibration analysis to model the peaks of the time history of a narrowband, stationary Gaussian process (Crandall and Mark, 1963;

Newland, 1975). However, in random vibration analysis, the Rayleigh distribution is typically used to determine the average number of exceedances above or below a given amplitude level. Information on the expected amplitudes sustained over a given number of cycles, however, cannot be obtained from random vibration analysis.

Zsutty and Deherrera (1979) and Deherrera and Zsutty (1982), however, have retained specific information on the largest peaks of an accelerogram by modeling the probability distributions of the largest peaks with the upper half-tail of exponential, Rayleigh, and Weibull probability distributions. In their study, a peak is defined as the maximum absolute amplitude between two consecutive zero crossings of the ground motion acceleration time history. As shown in Figure 1.4, the k^{th} largest peak, X(k), is the k^{th} peak in the time history when the peaks are ranked in descending order from the largest, X(1), to the smallest peak. The peak X(k) then summarizes the amplitude for which there will be k/2 cycles of ground motion acceleration exceeding this amplitude.

From the parameters of the proposed exponential half-tail (EHT) distributions and extremal statistics, the mean value of a specific peak X(k) of interest can be predicted. Consequently, their approach retains infor-

mation explicitly on specific amplitude levels and implicitly on the duration of an accelerogram. This methodology will be utilized extensively in this study as an improvement over the use of the ground motion parameters discussed above to characterize the amplitudes of strong ground motion acceleration, velocity, and displacement time histories.

1.3.2 AMPLITUDES OF STRUCTURAL RESPONSE

To characterize the amplitude levels of the response of a single-degree-of-freedom (SDOF) oscillator subjected to strong ground motion, statistically derived, seismic design response spectra plot the maximum value only of the response time history (e.g., Blume, et al., 1972; Mohraz, et al., 1972; Newmark, et al., 1973; Hall, et al., 1975a,b; Mohraz, 1976, Seed, et al., 1976b; Kiremidjian and Shah, 1978; Nau and Hall, 1982). It is well-recognized, however, that structural response to seismic excitation is not governed by the occurrence of a single maximum amplitude value but rather by an overall duration of response amplitudes sustained above a given level. By retaining information on only one single maximum response amplitude, present response spectrum techniques ignore information on the amplitude levels and the duration of

the lesser, but near maximum peak values of the response time history.

As a measure of "effective acceleration" of structural response, Mortgat and Shah (1978) present rms acceleration spectra to represent a summary of response peaks using a definition of response duration in which the response is arbitrarily terminated when the response acceleration peaks reach 10% of the largest response peak and thereafter did not exceed that value. The resulting rms acceleration spectra for a number of input ground motions are similar in shape but "smoother" than traditional maximum acceleration response spectra. No study is made, however, by Mortgat and Shah (1978), to investigate the sensitivity of the rms acceleration of response to other possible definitions of response duration. Consequently, this study will address the sensitivity of rms acceleration as a response parameter to various time domain definitions of response duration.

To characterize both the duration and the amplitude levels of the response of a SDOF oscillator subjected to strong ground motion, several researchers have eliminated the need to explicitly define response duration by retaining information on the cyclic behavior of the response. Perez (1973, 1980) plots tripartite response spectra for the response amplitudes sustained for a

given number of cycles of a linear SDOF oscillator subjected to ground motion records from the 1971 San Fernando, CA earthquake. Perez and Brady (1984) plot the average ratio of the relative displacement amplitudes sustained over a given number of cycles to the maximum displacement of the response time history as a function of the oscillator period. This approach, however, requires a statistical study of the maximum response sustained over each specific number of cycles in question. Similarly, Prince (1984) plots, as a function of the oscillator period, the ratio of the number of response peaks which exceed a given fraction of the maximum response to the total number of peaks in the response time history.

Deherrera and Zsutty (1982) have suggested that the largest peaks of SDOF oscillator response can also be modelled by the EHT probability distributions considered for ground motion studies. This methodology would retain information on specific levels of the largest response amplitudes and would eliminate the need to derive explicit relationships for each specific maximum and near maximum amplitude of the response time history as in Perez and Brady (1984) and Prince (1984). Consequently this study will also investigate the adequacy of

the EHT distributions to model the largest amplitudes of response time histories.

1.4 SCOPE AND OBJECTIVES

This study investigates parameters which characterize both the amplitudes and the duration of the largest peaks of ground motion and response time histories. While the emphasis of this study focuses on parameters which summarize the response time history of a linear, elastic SDOF oscillator, for insight and for completeness, the parameters are also investigated for strong ground motion.

First, rms acceleration, defined by equation (1.3), is investigated as a parameter which summarizes the largest amplitudes of ground motion and response time histories. Because a number of studies have addressed the use of rms acceleration as a ground motion parameter, emphasis is given in this study to the investigation of rms acceleration as a response parameter. The objectives are to determine the sensitivity of rms acceleration to the duration measure over which the rms aceleration is computed from equation (1.3) and to characterize the levels of loading and response which are described by rms acceleration.

Rms acceleration is investigated for ground motion and response as a function of the duration measures proposed by Bolt (1973) and Trifunac and Brady (1975). For response, average rms acceleration spectra are presented for the response of a SDOF oscillator with 2, 5, and 10% of critical damping for soil and rock sites.

Second, this study investigates the adequacy of the exponential, Rayleigh, and Weibull distributions to model and predict the largest peaks of strong ground motion, SDOF oscillator response, and recorded building response time histories. The objective is to retain information on both the amplitudes and the duration of the strong motion portion of a ground motion or response time history without having to explicitly define duration as required by the rms acceleration parameter.

The traditional exponential and Rayleigh distributions, as well as the EHT probability distributions (exponential, Rayleigh, and Weibull) proposed by Deherrera and Zsutty (1982) to characterize ground motion acceleration, are used to model the largest peaks of earthquake time histories. Hence, this study extends the EHT model to characterize the largest peaks of ground motion velocity and displacement time histories and of linear, elastic SDOF oscillator and recorded building acceleration response time histories.

The adequacy of the probability distributions investigated to predict selected values of the k^{th} largest peaks of ground motion and response time histories is investigated. For response, the average actual acceleration spectra for the first, second, fifth, tenth, and twentieth largest peaks of response time histories of a SDOF oscillator with 5% critical damping are compared to the average acceleration spectra computed for these largest peaks predicted from the investigated probability distributions. For recorded building response from the 1971 San Fernando, CA earthquake, the EHT distribution (exponential, Rayleigh, or Weibull) which best models the largest peaks of a given building response time history is determined and compared to trends observed for SDOF oscillator response.

Chapter 2 addresses the appropriateness of rms acceleration as a ground motion and response parameter. In Chapters 3 and 4, the exponential, Rayleigh, and Weibull distributions are used to characterize the probability distributions of the largest amplitudes of strong ground motion and response time histories, respectively. Finally, Chapter 5 summarizes the results of this study and suggests extensions of this study for future research.

CHAPTER 2

ROOT-MEAN-SQUARE ACCELERATION AS STRONG GROUND MOTION AND RESPONSE PARAMETERS

2.1 INTRODUCTION

This chapter investigates the use of root-mean-square (rms) acceleration defined in equation (1.3) as a parameter to summarize the amplitude levels sustained over the strong motion duration of ground motion and linear, elastic single-degree-of-freedom (SDOF) oscillator response time histories. Because a number of studies have addressed the use of rms acceleration as a ground motion parameter, this chapter focuses primarily on the characterization of rms acceleration as a parameter to summarize the amplitude levels and duration of SDOF oscillator response.

The objectives of this chapter are the following:

- to illustrate the sensitivity of strong motion duration and the corresponding rms acceleration to different time domain definitions of duration,
- to determine the levels of loading and response which are characterized by rms acceleration by illustrating the following:
  - the relationship between the maximum acceleration and the rms acceleration of the time history;
  - the number of cycles of the time history whose amplitudes will exceed the magnitude of the rms acceleration.

To accomplish these objectives, the following four duration-dependent quantities are investigated in this

chapter for strong ground motion and linear, elastic SDOF oscillator response:

1) the strong ground duration,
2) the corresponding rms acceleration,
3) the relationship between the maximum acceleration and the rms acceleration of the time history,
4) the peak number k of the kth largest acceleration peak of the time history whose absolute amplitude is nearest to the magnitude of the computed rms acceleration.

As discussed in Chapter 1, a number of different time domain definitions have been proposed to characterize strong ground motion duration. Because the durations proposed by Bolt (1973) and Trifunac and Brady (1975) are the most widely-used definitions in the literature, these two definitions are selected in this study as duration measures of ground motion and response. A brief review of these duration measures has been presented in Chapter 1. These two duration measures are also selected to illustrate the sensitivity of the four duration-dependent parameters defined above to an amplitude-dependent duration (Bolt's) and an amplitude-independent duration (Trifunac and Brady's). A cutoff value of 0.05g is used in Bolt's definition for both ground motion and response calculations.

As illustrated in Figure 1.4, a peak is also defined in this chapter as the maximum absolute amplitude between

two consecutive zero crossings of the ground motion or response acceleration time history. Again, the k^{th} largest peak, X(k), is the k^{th} peak in the time history when the peaks are ranked in descending order from the largest, X(1), to smallest peak. The peak X(k) then summarizes the amplitude for which there will be k/2 cycles of motion exceeding this amplitude. Hence, item (4) describes the number of cycles (k/2) of the ground motion or response time history whose amplitudes will exceed the computed rms acceleration value. Consequently, items (3) and (4) both illustrate the levels of loading and response characterized by rms acceleration. The relationship between maximum acceleration and rms acceleration will also be compared to the relationship between maximum acceleration and the parameter $1/\lambda$ of the exponential-like probability distributions investigated in Chapters 3 and 4 to characterize the largest peaks of ground motion and response acceleration time histories, respectively.

Section 2.2 discusses the data base of ground motion records analyzed and site geology classifications considered in this investigation. The four duration-dependent parameters in Section 2.1 are investigated in Sections 2.3 and 2.4 for strong ground motion and SDOF oscillator response, respectively. Finally, Section 2.5 summarizes rms acceleration as ground motion and response parameters.

2.2 DATA BASE OF GROUND MOTION RECORDS

The data base of 112 strong ground motion records used to investigate rms acceleration are listed in Table 2.1. These ground motion records represent the two orthogonal, horizontal ground motion components recorded at 56 recording stations. Of the 112 horizontal ground motion records considered, 68 records have been selected from the Volume II records published by the California Institute of Technology (1973). In this group of records, 34 are from earthquakes prior to 1971 and 34 are from the 9 February 1971 San Fernando, CA earthquake. The remaining 44 records are from the 15 October 1979 Imperial Valley, CA earthquake and have been processed by Brady, Perez, and Mork (1982).

To investigate the influence of site geology, the the recording stations are divided into two site geology categories: "soil" and "rock". Site category "rock" corresponds to the rock category per Seed, et al., (1976 a,b). Site category "soil" includes both the "stiff soil conditions" and the "deep cohesionless soil conditions" per the same references. Of the 112 records considered, 86 and 26 records correspond to soil and rock sites, respectively. While other researchers have considered more refined "soil" classifications (e.g., Seed, et al., 1976a,b; Dobry, Idriss, and Ng, 1978; McGuire and Hanks, 1980), the two

categories used in this study will adequately illustrate the effects of site geology as in other studies which utilized only two site categories (e.g., in Vanmarcke and Lai, 1977, 1980; McGuire, 1978; and McCann, 1980).

2.3 RMS ACCELERATION AS A GROUND MOTION PARAMETER

This section presents a brief characterization of rms acceleration as a ground motion parameter. The objective of this study is only to illustrate general trends in the four duration-dependent ground motion parameters listed in Section 2.1 which have not been identified in previous investigations of rms acceleration. These duration-dependent parameters are computed for each strong ground motion record listed in Table 2.1 and are summarized in Table 2.2 as a function of Bolt's and Trifunac and Brady's duration measures.

The parameters in Table 2.2 are also graphed in Figures 2.1 to 2.7 for combined soil and rock sites. While considerable scatter is evident for many of the parameters graphed in these figures, the scatter may be reduced by incorporating the dependence of these parameters on earthquake magnitude, distance from source to site, and other geophysical parameters. In Figures 2.1 to 2.7 and in the figures of Section 2.4, Bolt's and Trifunac and Brady's duration measures are referred to as "Bolt" and

"T & B", respectively.

Figure 2.1 graphs PGA vs. ground motion duration for Bolt's and Trifunac and Brady's durations. While considerable scatter of the data is evident, the upper graph for Bolt's duration indicates that Bolt's ground motion duration slightly increases with increasing PGA. Such behavior is expected since Bolt's duration is directly related to specific amplitude levels of the time history. For the data base considered, the PGA of six ground motion records is less than 0.05g. Hence, Bolt's duration for these records will be zero.

On the other hand, because Trifunac and Brady's duration is based on energy considerations and is independent of a specific amplitude level, this definition will always give a nonzero value of duration. The lower graph in Figure 2.1, which plots PGA vs. Trifunac and Brady's duration, shows the ground motion duration increases with decreasing PGA. Consequently, Bolt's and Trifunac and Brady's durations show opposite trends as a function of PGA.

A comparison of Bolt's duration vs. Trifunac and Brady's duration is graphed in Figure 2.2. This graph indicates that for about two-thirds of the ground motion records considered, Trifunac and Brady's durations are larger than Bolt's durations. Also, Figure 2.2 shows that

for the six records with Bolt's duration equal to zero, Trifunac and Brady's duration ranged between about 12 and 32 seconds. Consequently, an explicit time domain representation of ground motion duration is sensitive to the definition of duration assumed. As also discussed in Chapter 1, different duration definitions give different characterizations of the ground motion duration of a given acceleration record.

Figure 2.3 graphs the rms accelerations computed by equation (1.3) as a function of duration for the ground motion durations listed in Table 2.2 and shown in Figures 2.1 and 2.2. While the graph of rms acceleration vs. duration from Bolt's definition shows considerable scatter, the graph of rms acceleration vs. duration from Trifunac and Brady's definition shows a definite trend of decreasing rms acceleration with increasing duration.

A comparison of the rms accelerations computed from Bolt's and Trifunac and Brady's durations is graphed in Figure 2.4. While Figure 2.2 shows considerable scatter in the durations computed from these two definitions, Figure 2.4 indicates that the corresponding rms accelerations computed from these two definitions show less sensitivity to the duration definition. An inspection of Table 2.2 also shows that for a given record, the smaller of the two duration values computed from Bolt's and Trifunac and

Brady's definitions results in the larger value of the rms acceleration.

To investigate the relationship between PGA and rms acceleration, Table 2.2 lists the ratio of PGA to rms acceleration (PGA/RMS) for the rms acceleration computed for each ground motion record from Bolt's and Trifunac and Brady's durations. Correspondingly, Figure 2.5 graphs PGA vs. rms acceleration computed from these two duration measures. As indicated in Table 2.2 and Figure 2.5, the rms acceleration values computed from both definitions of duration show a definite linear relationship between PGA and rms acceleration. This linear relationship is most distinct for the rms accelerations computed from Trifunac and Brady's duration measure. The outliers shown in the upper right hand corner in Figure 2.5 for PGA vs. rms acceleration computed from Bolt's duration correspond to the Pacoima Dam records from the 1971 San Fernando, CA earthquake (C041 S16E and C041 S74W).

Hence rms acceleration appears to be a scaling down of the PGA. Because rms acceleration represents a summary of the strong motion amplitudes, this linear trend implies that the PGA does contain information on the lesser, but near maximum ground motion peaks.

The ratio of PGA/RMS, however, may be less than 1 for Bolt's duration. If the accelerogram contains only a few

time steps whose amplitudes exceed the cutoff level for Bolt's definition (i.e., the PGA is just slightly larger than the cutoff level), then the resulting rms acceleration computed from equation (1.3) may slightly exceed the PGA. For example, for the record A003 S90W, the PGA is just slightly greater than 0.05g, the duration is 0.14 seconds, and the PGA/RMS ratio is equal to 0.95.

To determine if the ratio of PGA/RMS is a function of the definition of duration used to compute the rms acceleration, Figure 2.6 plots this ratio as a function of Bolt's duration vs. Trifunac and Brady's duration. For the majority of records considered, the ratio of PGA/RMS acceleration is generally bounded between 3 and 6 for both definitions of duration and hence is relatively independent of the duration measure..

Finally, the last two columns in Table 2.2 list the peak number, k, of the k^{th} largest peak of the ground motion time history whose absolute amplitude is closest to the computed rms acceleration value. Of interest is whether rms acceleration summarizes the same number of cycles of ground motion for for each record and for each duration measure. An inspection of the peak numbers k in Table 2.2 indicates that there is considerable variation of k from record to record and for a given record, between the two duration measures. For a given ground motion record,

the smaller of the rms accelerations computed from the two definitions of duration describes a lesser amplitude of the time history and therefore will correspond to a larger peak number. The maximum value observed for k in this data base is 124 for record IV01 230 for the rms acceleration computed from Trifunac and Brady's duration. Hence for this record, there will be 62 cycles of ground motion whose amplitudes exceed the rms acceleration value of 24.36 cm/sec^2 . For this same record, the peak number corresponding to the rms acceleration from Bolt's duration is 84 and there will be 42 cycles of ground motion whose amplitudes exceed the rms acceleration value of 34.79 cm/sec^2.

Figure 2.7 compares the peak number corresponding to the rms accelerations from Bolt's and Trifunac and Brady's durations. The considerable scatter evident in this graph indicates that the number of cycles of ground motion characterized by rms acceleration varies from record to record, is not constant for a given duration definition, and for a given record, is not the same for both duration measures. Therefore, rms acceleration does not represent an amplitude sustained over a consistent number of cycles for all ground motion records and duration measures. Consequently, because a linear relationship is noted between PGA and rms acceleration, rms acceleration does

give specific information on the magnitude of only one other peak in the time history, the PGA. Specific information is not retained on the relative magnitudes of the near maximum peaks.

In summary, this section briefly investigated the dependence of rms acceleration on the duration measures given by Bolt (1973) and Trifunac and Brady (1975). The following dependence on the duration measures have been noted for rms acceleration as a parameter of strong ground motion:

- The ground motion duration is sensitive to the duration definition.
- The rms acceleration is dependent on the duration measure but is not as sensitive to the duration measure as the calculated value of duration.
- The ratio of PGA/RMS ranges between values of 3 and 6 for both duration measures.
- The rms acceleration does not consistently summarize the same number of cycles and hence same level of loading for each ground motion time history and for each duration measure.

The next section addresses the dependence of rms acceleration as a response parameter on the duration measures given by Bolt (1973) and Trifunac and Brady (1975) investigated as duration measures of response.

2.4 RMS ACCELERATION AS A RESPONSE PARAMETER

The four duration-dependent parameters listed in section 2.1 are computed for the response of a linear, elastic SDOF oscillator subjected to the strong ground motion records listed in Table 2.1. Calculation of the response of a SDOF oscillator subjected to strong ground motion requires solving the equation of motion for a viscously damped, linear, elastic SDOF oscillator shown in Figure 2.8. The equation of motion of a SDOF oscillator at any time t is given as:

$$m * \ddot{x}(t) + c * \dot{x}(t) + k * x(t) = -m * a(t) \qquad (2.1)$$

where

- m = mass of the system
- c = viscous damping of the system
- k = stiffness of the system
- $\ddot{x}(t)$ = relative acceleration
- $\dot{x}(t)$ = relative velocity
- x(t) = relative displacement
- a(t) = ground motion acceleration input

If equation (2.1) is divided by the mass m, then the equation of motion becomes

$$\ddot{x}(t) + 2 * \beta * \omega * \dot{x}(t) + \omega^2 * x(t) = -a(t) \qquad (2.2)$$

where

$\omega = (k/m)^{1/2}$ = natural frequency of the oscillator

$\beta = c/2\omega m$ = percent of critical damping

The linear, elastic response given by equation (2.2) is computed using the numerical procedure outline in Nigam and Jennings (1968). The response is calculated for forty (40) oscillator periods between 0.03 second and 30 seconds at 13 equally-spaced oscillator periods for each cycle of the logarithmic scale. The response is computed for 2, 5, and 10% of critical damping.

2.4.1 PRELIMINARY INVESTIGATION

As a preliminary investigation, the four duration-dependent parameters are computed for the acceleration response of a SDOF oscillator with 2, 5, and 10% of critical damping subjected to eight well-studied ground motion records taken from Table 2.1: A001 S00E, A004 S69E, A015 S80E, B029 N86E, B034 N85E, C041 S16E, C048 N00W, and IV19 230 (Bond). These parameters are graphed in Figures 2.9 through 2.21 as a function of Bolt's and Trifunac and Brady's duration definitions.

First, of interest in response calculations is the number of cycles of response experienced rather than the explicit time domain duration. If the time domain duration of the response of a SDOF oscillator with a given period is known, then the corresponding number of cycles of response is equal to the duration multiplied by the oscillator period. Therefore, the response durations determined from Bolt's and Trifunac and Brady's durations are expressed in terms of number of cycles and are graphed in Figures 2.9, 2.10, and 2.11.

Figures 2.9 and 2.10 graph, as a function of 2, 5, and 10% damping and oscillator period, the number of cycles of response computed from Bolt's and Trifunac and Brady's durations, respectively. Because the response at higher periods will often have peak accelerations less than 0.05g, Bolt's duration and the corresponding number of cycles will be zero at these periods. Two trends are apparent in these graphs. First, the number of cycles of response is independent of damping. Second, because the actual number of cycles in the total response time history decreases at the longer periods, the number of cycles of response for these duration measures decreases as the oscillator period increases.

Figures 2.11 and 2.12 compare the number of cycles of oscillator response and the calculated time domain dura-

tions, respectively, computed from the two definitions of duration for 5% damping. In general, for periods less than about 1 or 2 seconds, the number of cycles (or duration) of response from Bolt's duration exceeds the number of cycles (or duration) from Trifunac and Brady's duration. Beyond periods of about 1 or 2 seconds, the number of cycles (or duration) calculated from Bolt's definition becomes less than the number of cycles calculated from Trifunac and Brady's definition. Consequently, the duration or the number of cycles of response is dependent on the duration measure as observed for ground motion.

Second, the corresponding rms accelerations computed by equation (1.3) for the response durations given by Bolt's and Trifunac and Brady's definitions are shown in Figures 2.13 and 2.14, respectively, for 2, 5, and 10% damping. These rms acceleration spectra have been normalized by the PGA. In general, the rms acceleration spectra show the same shape as the traditionally plotted maximum acceleration spectra and the magnitudes generally decrease with increasing damping.

Comparisons of the rms acceleration spectra for 5% damping computed from Bolt's and Trifunac and Brady's durations are shown in Figure 2.15. Typically for oscillator periods less than 0.1 second or greater than about 1 second, the rms accelerations computed from the two

definitions of duration are similar in magnitude. Between 0.1 second and 1 to 2 second, the rms accelerations computed from Trifunac and Brady's durations are considerably larger than from Bolt's duration for the response to several of the ground motion records, e.g., B034 N85E, C041 S16E, C048 N00W, and Bond 230. As for ground motion, this trend is also expected since in Figure 2.12, Trifunac and Brady's durations in this period range for these records are considerably smaller than Bolt's durations. Hence, the magnitude of rms acceleration is dependent on the duration measure.

Third, as for ground motion, also investigated is the relationship between the peak acceleration and the rms acceleration of a given response time history. The objective is to determine if the rms acceleration of a response time history is a constant fraction of the peak acceleration of the time history. Figures 2.16 and 2.17 graph the ratio of rms acceleration to peak acceleration as a function of damping and oscillator period for Bolt's and Trifunac and Brady's durations, respectively. Interestingly, both figures indicate that while the ratio of rms acceleration to peak acceleration is independent of damping, this ratio increases from 0.25 to about 0.50 with increasing oscillator period.

For Bolt's duration, this ratio may, in some cases,

exceed a value of 1. For oscillator periods where Bolt's duration tends toward zero as the peak acceleration of the response slightly exceeds the cutoff level of 0.05g, there will be only a few time steps in the response time history whose acceleration exceeds 0.05g. Consequently, the rms acceleration calculated by equation (1.3) will approach the peak acceleration or may even slightly exceed the peak value. Hence, the ratio of rms to peak acceleration, as shown in Figure 2.16 for the response to A004 S69E and Bond 230, may approach or exceed a value of 1.

A comparison of the ratio of rms to peak (maximum) acceleration for 5% damping as a function of the two duration definitions is shown in Figure 2.18. Except for those oscillator periods where Bolt's duration tends toward zero and hence this ratio takes on a value near 1, the two duration definitions give reasonably similar values of this ratio (between 0.25 and 0.50) as the oscillator period increases. Hence, the rms acceleration appears to be a scaling down of the peak acceleration for both duration measures as also observed for ground motion.

Fourth and finally, of interest is the peak number k of the k^{th} largest peak of time history which corresponds to the amplitude level of the rms acceleration. Hence, this peak number k is simply twice the number of cycles of response whose amplitudes will exceed the amplitude level

of the rms acceleration. Figures 2.19 and 2.20 graph, based on the rms accelerations computed from Bolt's and Trifunac and Brady's durations, respectively, for 2, 5, and 10% damping, the peak number k of the k^{th} largest peak of the response time history whose absolute amplitude is nearest to the rms acceleration amplitude.

In general, these two figures show that for both duration measures, as the percent of critical damping increases, the peak number k corresponding to the rms acceleration decreases. For both duration measures, the peak number k is also a function of oscillator period and reaches a maximum between periods of 0.05 second and 0.2 second. Consequently, for a given duration measure, rms acceleration does not summarize a consistent level of response for all oscillator periods and damping values.

Figure 2.21 compares the peak number for the rms accelerations for 5% damping computed from the two definitions of duration. As observed for ground motion, the larger rms acceleration value of response from the two duration measures (Figure 2.15), corresponding to the smaller duration value (Figure 2.12), typically corresponds to the lower peak number k (Figure 2.21). This figure shows that the rms accelerations computed from the two duration measures also do not consistently summarize the same number of cycles of response.

In summary, the duration dependence observed for rms acceleration as a ground motion parameter has also been observed for rms acceleration as a response parameter. Specifically, the following trends have been observed for response rms acceleration computed from Bolt's and Trifunac and Brady's durations:

- The response duration (number of cycles of response) is dependent on the duration measure.
- The magnitude of the rms acceleration is dependent on the duration measure.
- The rms acceleration is a scaling down (between 0.25 and 0.50) of the peak acceleration of the response time history.
- The rms acceleration does not consistently summarize the same level of response but is a function of damping, oscillator period, and the duration measure.

2.4.2 AVERAGE RMS ACCELERATION SPECTRA

To facilitate a more comprehensive characterization of rms acceleration as a response parameter, average peak acceleration spectra, average rms acceleration spectra, and average rms/peak acceleration spectra are computed for the response of a SDOF oscillator with 2, 5, and 10% critical damping subjected to the ground motion records listed in Table 2.1. These average spectra are computed separately

for soil and rock sites. The average peak acceleration and average rms acceleration spectra are normalized by the PGA of the input ground motion record.

Average peak acceleration spectra (denoted as SA), which are traditionally plotted for SDOF oscillator response, are shown in Figure 2.22 for soil and rock sites for 2, 5, and 10% of critical damping. These spectra will be compared to the average rms acceleration spectra computed below. The coefficient of variation of the average peak acceleration spectra is shown in Figure 2.23. For both soil and rock sites, the coefficient of variation decreases with increasing percent of critical damping and generally increases with increasing oscillator period.

Average rms acceleration spectra for the rms accelerations computed from Bolt's and Trifunac and Brady's durations are shown in Figures 2.24 and 2.25 for soil and rock sites, respectively. The average rms acceleration spectra have similar shapes as the traditional average peak acceleration spectra shown in Figure 2.22. Average rms acceleration spectra are not computed for Bolt's durations at periods greater than about 8 and 2 seconds for soil and rock sites, respectively. Beyond these periods, there were very few, if any, response records whose peak acceleration exceeded the cutoff level of 0.05g.

The coefficient of variation of the average rms acceleration spectra computed for soil and rock sites are shown in Figures 2.26 and 2.27, respectively. The coefficient of variation of the average rms acceleration spectra for soil sites computed from Bolt's duration fluctuates about a value of 0.4 as a function of oscillator period and damping. With the exception of a few sporadic deviations, a similar trend in the coefficient of variation is observed for rock sites for Bolt's duration.

The coefficient of variation of the average rms acceleration spectra computed from Trifunac and Brady's duration, however, shows similar behavior as the coefficient of variation in Figure 2.23 for the average peak acceleration spectra. In general, the coefficient of variation based on Trifunac and Brady's duration decreases with increasing damping, increases with increasing oscillator period, and is slightly higher than the coefficient of variation of the traditional average peak acceleration spectra.

Figure 2.28 compares, for soil and rock sites for 5% damping, the average peak acceleration spectrum and the average rms acceleration spectra computed from Bolt's and Trifunac and Brady's durations. For both soil and rock sites, the average rms acceleration spectra have similar shape as the average peak acceleration spectrum and hence

appear to be a scaling down of the average peak acceleration spectrum. This relationship is explored in more detail below.

A comparison of the coefficient of variation of the average peak acceleration in Figure 2.23 and of the average rms acceleration spectra in Figures 2.26 and 2.27 is shown in Figure 2.29. The following trends are noted for both rock and soil sites. For periods less than 1 second, the coefficient of variation of the average peak acceleration spectrum is less than the coefficient of variation of the average rms acceleration spectra computed from the two duration measures. However, for periods greater than about 1 second, the average rms acceleration spectrum computed from Bolt's duration gives the lowest coefficient of variation. The coefficient of variation of the average rms acceleration spectrum computed from Trifunac and Brady's duration is greater than the coefficient of variation of the average peak acceleration spectrum for all oscillator periods.

A comparison of the average rms acceleration spectra for 5% damping computed from Bolt's and Trifunac and Brady's durations is shown in Figures 2.30 and 2.31 for soil and rock sites, respectively. For periods between 0.1 second and about 0.5 to 1.0 second, the average rms acceleration spectra computed from Trifunac and Brady's

duration for both soil and rock sites are greater than the spectra computed from Bolt's duration. At all other periods, the rms acceleration spectra computed from Bolt's duration are slightly greater. Consequently, the average rms acceleration spectra are sensitive to the duration measure.

Figures 2.32 and 2.33 compare the average rms acceleration spectra computed from Bolt's and Trifunac and Brady's durations, respectively, as a function of the site geology conditions. For both definitions of duration, the following trends are observed. For periods less than about 0.1 second, the spectra for soil and rock sites are essentially identical. For periods between 0.1 second and about 0.5 second, the response for rock sites exceeds the response for soil sites. For periods greater than about 0.5 second, the response for soil sites is amplified greater than the response for rock sites. Hence, the average rms acceleration spectra show similar sensitivity to local site geology as observed for average peak acceleration spectra, e.g., Seed, et al., (1976b); Mohraz (1976); Kiremidjian and Shah, (1978).

To verify if rms acceleration of response is a scaling down of the peak acceleration of the response time history as observed for ground motion, average rms acceleration/ peak acceleration spectra are graphed in Figures 2.34 and

2.35 for soil and rock sites, respectively, as a function of 2, 5, and 10% of critical damping. These figures show that for both soil and rock sites, the spectrum computed from Bolt's duration is independent of damping and increases with increasing oscillator period from about 0.25 to approximately 0.7. The spectrum computed from Trifunac and Brady's duration, however, is dependent on damping, generally increases with oscillator period, and ranges between 0.25 and 0.50.

A comparison of the rms/peak acceleration spectra for Bolt's and Trifunac and Brady's durations for 5% damping is shown in Figure 2.36. For periods less than about 1 second, the rms/peak values are independent of the duration measure. For periods greater than 1 second, the rms/peak values are greater for Bolt's duration.

The coefficient of variation of the spectra shown in Figures 2.34 and 2.35 is shown in Figures 2.37 and 2.38, respectively. The coefficient of variation is seen to slightly increase with increasing damping. Typically the coefficient of variation fluctuates between 0.2 and 0.3 as a function of oscillator period.

Consequently, the average rms acceleration spectrum is a scaling down of the average peak acceleration spectrum. The scaling down, however, is a function of the oscillator period, the percent of critical damping, and the

duration measure. However, the average rms acceleration spectrum given by Trifunac and Brady's duration gives a more uniform scaling as a function of oscillator period than the average rms acceleration spectrum given by Bolt's duration. Again, this implies that the peak (maximum) acceleration of the time history does retain information on the lesser, near maximum amplitudes sustained over the strong motion duration.

2.5 CONCLUSIONS

In summary, as a ground motion and a response parameter, rms acceleration has been shown to be dependent on the duration measures defined by Bolt (1973) and Trifunac and Brady (1975) to calculate the rms acceleration from equation (1.3). For both ground motion and response, the following trends have been noted for the rms acceleration parameter:

- The rms acceleration is dependent on the duration measure.
- A linear relationship is observed between the rms acceleration and the peak acceleration of the ground motion or response time history. For response, the relationship is dependent on the oscillator period and the percent of critical damping.

- The rms acceleration does not consistently summarize the same levels of loading or response for each duration measure.

While rms acceleration is a summary of the amplitudes over a given strong motion duration and is observed to be related to the peak acceleration of the ground motion or response time history, no further information can be obtained from the rms acceleration representation on the amplitudes of the lesser, near maximum amplitudes of the ground motion or response time history. Consequently, the next two chapters present a methodology to characterize the largest amplitudes, or peaks, in ground motion and SDOF response time histories in terms of the probability distributions of the largest peaks of the time history. An interesting observation in these next two chapters is that for the investigated exponential-like probability distributions, the parameter $1/\lambda$ of the distributions has similar behavior as the rms acceleration parameter of ground motion and SDOF oscillator response.

CHAPTER 3

CHARACTERIZATION OF THE AMPLITUDES OF THE LARGEST PEAKS OF STRONG GROUND MOTION TIME HISTORIES

3.1 INTRODUCTION

Of interest to engineers for seismic hazard analysis and seismic design is the characterization of the strong motion portion of an expected ground motion record during which the largest amplitudes of excitation occur. Traditionally, the largest amplitudes of a ground motion acceleration, velocity, or displacement time history have been characterized by the maximum absolute amplitude of the time history, i.e., the peak ground acceleration (PGA), peak ground velocity (PGV), or peak ground displacement (PGD), respectively. Hence, specific information on the amplitudes and the duration of the lesser, but near maximum peaks of a ground motion time history is not retained.

While root-mean-square (rms) acceleration discussed in Chapter 2 does represent a summary of the amplitudes sustained over a given strong motion duration of the time history, such representation does not, however, retain specific information on the relative magnitudes and the number of cycles of potentially damaging, near maximum amplitudes of the strong ground motion record. Information on the largest peaks of ground motion acceleration and

velocity time histories is needed for load level and energy considerations. For most applications in seismic hazard analysis, typically the maximum value of the ground motion displacement time history, i.e., PGD, is of interest.

Consequently, this chapter investigates the adequacy of the exponential, Rayleigh, and Weibull probability distributions to model the maximum and near maximum amplitudes, or peaks, of ground motion records. The objective is to present a methodology to retain information explicitly on the amplitudes of the largest peaks and hence implicitly on the duration of the strong motion portion of a ground motion time history. Characterization of the largest peaks of ground motion acceleration, velocity, and displacement time histories is presented.

A peak is again defined in this chapter as shown in Figure 3.1 as the maximum absolute amplitude between two consecutive zero crossings of a ground motion acceleration, velocity, or displacement time history. The k^{th} largest peak, X(k), is then the k^{th} peak of the ground motion time history when the peaks are ranked in descending order from the largest to smallest peak. The first peak, X(1), corresponds to the PGA, PGV, or PGD of a ground motion acceleration, velocity, or displacement time history, respectively. The peak X(k) then represents the amplitude for which there will be k/2 cycles of ground motion

excitation exceeding this amplitude. Using extremal statistics, prediction of the largest peaks from exponential or exponential-like (Rayleigh and Weibull) probability distributions enables information to be retained on the specific peak amplitude level X(k) corresponding to an implicit duration of k/2 cycles.

Prediction of the largest peaks of ground motion time histories is investigated for the recorded strong ground motion discussed in Section 3.2. The data base of ground motion records in Table 2.1 used for the investigation of rms acceleration in Chapter 2 is expanded in this chapter for the ground motion study. The selection of the probability distributions investigated is discussed in Section 3.3. Model verification of the adequacy of the investigated probability distributions to predict the largest peaks of ground motion time histories is presented in Section 3.4. Section 3.5 illustrates the relationships between PGA, PGV, PGD, and the parameter $1/\lambda$ of the exponential and exponential-like probability distributions. The sensitivity of the predicted peaks to the number of peaks in the distribution is addressed in Section 3.6. Finally, Section 3.7 summarizes the findings of this ground motion investigation and recommends extensions of this study for future research.

3.2 GROUND MOTION RECORDS ANALYZED

Prediction of the largest peaks of ground motion time histories is investigated for 332 ground motion records selected from 35 earthquakes, primarily in the western United States, between 1933 and 1979. These ground motion records represent the two orthogonal, horizontal ground motion components at 166 recording stations. Table 3.1 lists the earthquakes considered by date, location, and Richter magnitude. Of the 332 records analyzed, 288 records representing 34 earthquakes have been selected from the Volume II records published by the California Institute of Technology (1973). Of the 288 Volume II records analyzed, 176 records correspond to horizontal components of ground motion from the 9 February 1971 San Fernando, CA earthquake. Forty-four (44) records have been selected from the 15 October 1979 Imperial Valley earthquake records processed by Brady, Perez, and Mork (1982).

As in Chapter 2, to investigate the influence of site geology conditions, the site conditions of the recording stations are divided into two site categories - "rock" and "soil" - using the site categories defined by Seed, et al., (1976a,b). Site category "rock" corresponds to rock sites "where rock was considered to be shale-like or sounder in characteristics as evidenced by a shear-wave velocity greater than about 2500 fps" per Seed,

et al., (1976a,b). In this investigation, the site category "soil" includes the following two soil site classifications per Seed, et al., (1976a,b):

1) "Stiff soil conditions - where rock as defined above was overlain by less than about 150 feet of stiff clay, sand, or gravel";

2) "Deep cohesionless soil conditions - where rock as defined above was overlain by at least 250 feet of generally cohesionless soils".

Table 3.2 presents a listing of the recording stations for the time histories analyzed and includes the earthquake I.D. number from Table 3.1, the Richter magnitude, the site geology condition, and the epicentral distance. Of the 332 records considered, 266 correspond to soil sites and 66 to rock sites.

3.3 SELECTION OF PROBABILITY DISTRIBUTION MODELS

The largest peaks of ground motion acceleration, velocity, and displacement time histories are modelled by the exponential and exponential-like (Rayleigh and Weibull) probability distributions listed in Table 3.3. This section discusses the selection and the theoretical basis of these probability distributions. The first two probability distributions listed in Table 3.3 are the traditional exponential and Rayleigh distributions. The remaining five probability distributions are the exponential half-tail (EHT) distributions developed by Deherrera

and Zsutty (1982). While Deherrera and Zsutty (1982) developed the EHT distributions to predict the largest peaks of ground motion acceleration records, this study extends these distributions to model the largest peaks of ground motion velocity and displacement time histories in this chapter and of response time histories in Chapter 4.

3.3.1 TRADITIONAL EXPONENTIAL, RAYLEIGH, AND WEIBULL PROBABILITY DISTRIBUTIONS

The first two probability distributions listed in Table 3.3 are the well-known exponential (Case 1) and Rayleigh (Case 2) distributions from probability theory (e.g., Ang and Tang, 1984). Both the exponential and Rayleigh distributions are used to model the probability distributions of the *entire* set of peaks of the ground motion records. Although the Weibull distribution will only be investigated as an EHT probability distribution, the theoretical basis of this distribution is also discussed below.

If the random variable X represents the set of peaks of a ground motion time history, then the exponential probability distribution function, $f_X(x)$, of the peaks is given as:

$$f_X(x) = \lambda e^{-\lambda x} \qquad (3.1)$$

where λ is the parameter of the exponential distribution. The mean, or expected value, E(X), and the variance, σ_X^2, of X are given as:

$$E(X) = 1/\lambda \tag{3.2}$$

$$\sigma_X^2 = 1/\lambda^2 \tag{3.3}$$

Note that the quantity $1/\lambda$ will have the same units as the random variable X. For example, if the random variable X represents acceleration peaks, then the quantity $1/\lambda$ in equation (3.2) will also have units of acceleration.

Deherrera and Zsutty (1982) have shown through a simple change of variable transformation that if the set of original peaks {X} of L ordered observations (from largest to smallest) given as:

$$\{X\} = \{X_1, X_2, \ldots, X_L\} \tag{3.4}$$

<u>is not</u> exponentially distributed, but the set of ordered, transformed peaks {Y} given as:

$$\{Y\} = \{Y_1, Y_2, \ldots, Y_L\} = \{X_1^n, X_2^n, \ldots, X_L^n\} \tag{3.5}$$

is exponentially distributed, then for n equal to 1, 1/2, or 2, the set {X} follows the exponential, Weibull, or Rayleigh distribution, respectively.

Hence, for the original, untransformed set of peaks {X}, the probability distribution functions $f_X^E(x)$, $f_X^W(x)$, and $f_X^R(x)$ corresponding to the exponential, Weibull, and Rayleigh distributions, respectively, are given as follows:

$$f_X^E(x) = \lambda_e \, e^{-\lambda_e x} \tag{3.6}$$

$$f_X^W(x) = \frac{\sqrt{\lambda_w} \; e^{-\sqrt{\lambda_w} \; x}}{2\sqrt{x}} \tag{3.7}$$

$$f_X^R(x) = 4 \, \lambda_r^2 \, x \, e^{-\lambda_r^2 \, x^2} \tag{3.8}$$

where λ_e, λ_w, and λ_r are the parameters of the exponential, Weibull, and Rayleigh distributions, respectively. For the transformed set of peaks {Y} given by equation (3.5), the probability distribution functions $f_Y^E(y)$, $f_Y^W(y)$, and $f_Y^R(y)$ corresponding to the exponential, Weibull, and Rayleigh distributions, respectively, have the following exponential-like forms:

$$f_Y^E(y) = \lambda_e \, e^{-\lambda_e \, y} \tag{3.9}$$

$$f_Y^W(y) = \sqrt{\lambda_w} \, e^{-\sqrt{\lambda_w} \, y} \tag{3.10}$$

$$f_y^R(y) = \lambda_r^2 \; e^{-\lambda_r^2 \; y} \qquad (3.11)$$

From the parameter λ equal to λ_e, λ_r, or λ_w for the exponential, Rayleigh, or Weibull distributions, respectively, and N, the number of peaks in the time history, the mean value of the expected k^{th} largest peak, $\bar{X}(k)$, can be predicted from extremal statistics per Gumbel (1958) as:

$$\bar{X}(k) = \frac{1}{\lambda} \left[\sum_{z=k}^{N} \frac{1}{z} \right]^m \qquad (3.12)$$

where m is equal to 1, 1/2, or 2 for an exponential, Rayleigh, or Weibull distribution, respectively. The mean value of the largest peak, $\bar{X}(1)$ can also be expressed in terms of the asymptotic formula:

$$\bar{X}(1) = 1/\lambda(\ln N + 0.577)^m \qquad (3.13)$$

where m is defined in equation (3.12).

3.3.2 EXPONENTIAL HALF-TAIL (EHT) DISTRIBUTIONS

The majority of the peaks of ground motion time histories, however, will consist of smaller amplitude peaks which do not contribute to the strong motion portion of the record. Consequently, inclusion of these smaller peaks will greatly reduce the accuracy of prediction of the larger peaks of the ground motion time history. In a

methodology to retain information on the lesser, but near maximum peaks without the influence of the smaller, less significant peaks, Deherrera and Zsutty (1982) developed the exponential half-tail (EHT) distribution to characterize only the upper median of a given population of peaks of the ground motion acceleration time history. The objectives of the EHT distribution are to emphasize the importance of the larger peaks over the smaller and less important peaks and to allow the EHT model to select the appropriate probability distribution function (exponential, Rayleigh, or Weibull) for the larger peaks without influence of the smaller peaks. The EHT model will be investigated in this chapter and in Chapter 4 and is briefly discussed below. A more extensive discussion is found in Deherrera and Zsutty (1982).

The EHT model describes the largest peaks above a median, m_y, by an exponential or exponential-like distribution (Rayleigh or Weibull) as shown in Figure 3.2. The use of the median as a cutoff point is chosen for convenience and because it is a well-established statistical quantity. If the exponential distribution describes the random variable Y, which represents the set of transformed peaks of a given time history, as:

$$f_Y(y) = \lambda\, e^{-\lambda y} \qquad (3.14)$$

then the median, m_y, of the exponential distribution is:

$$m_y = \ln(2)/\lambda \tag{3.15}$$

While the exponential distribution describing the larger peaks will also extend into the region of the smaller peaks, no probability statements will be in the lower half-tail region. Hence, the zone of validity of the EHT model is the upper half-tail of the exponential distribution as shown in Figure 3.2. The first and second moments, $E'[Y]$ and $E'[Y^2]$, respectively, of the EHT distribution are illustrated in Figure 3.2 and are as follows:

$$E'[Y] = \int_{m_y}^{\infty} y\, \lambda e^{-\lambda Y}\, dy = \frac{0.847}{\lambda} \tag{3.16}$$

$$E'[Y^2] = \int_{m_y}^{\infty} y^2\, \lambda e^{-\lambda Y}\, dy = \frac{1.933}{\lambda^2} \tag{3.17}$$

The half-tail moments can be used to find the exponential distribution that best describes the probabilistic behavior of the largest peaks above a median m_y. The median m_y can be related to the half-tail moments from equations (3.15), (3.16), and (3.17) as follows:

$$m_y = 0.819\ E'[Y] \tag{3.18}$$

or

$$m_y = 0.499 \{E'[Y^2]\}^{1/2} \qquad (3.19)$$

The median m_y is estimated for each time history by a trial and error procedure which assumes that each transformed peak Y_i, starting with the largest peak, is the median value. A check is made to determine if one or both of the guesses for the median in terms of the estimates in equations (3.18) or (3.19) is valid. The rank "i" of the peak which makes these equations valid is then equal to the sample half size N/2 and the largest i peaks, from Y_1 to Y_i, form the upper half-tail of a sample size N from an exponential distribution with the parameter λ. The parameter λ can be estimated from equations (3.16) and (3.17) as follows:

$$\lambda = 2.28 \frac{E'[Y]}{E'[Y^2]} \qquad (3.20)$$

The parameter λ and the sample size N are then used to predict the expected peaks $\bar{X}(k)$ from equations (3.12) and (3.13). The upper half-tail exponential, Rayleigh, and Weibull distributions are referred in the remainder of this study as the exponential (EHT), Rayleigh (EHT), and Weibull (EHT) distributions, respectively.

Two criteria have been proposed by Deherrera and Zsutty (1982) to determine whether the acceleration peaks of a given time history can be best predicted by the exponential (EHT), Rayleigh (EHT), or Weibull (EHT) distribution. The first criterion is a graphical procedure using an exponential probability distribution plot. Let the random variable Y represent the set of ordered peaks in equation (3.5) drawn from an exponential distribution. The probability that the random variable Y exceeds a given value Y_i, i.e., $P(Y > Y_i)$, is given by the exceedance distribution function (EDF) of the exponential distribution as:

$$P(Y > Y_i) = e^{-\lambda Y_i} \tag{3.21}$$

If N observations of Y_i are arranged in descending order, $Y_1 > Y_2 \ldots > Y_N$, then the EDF can be estimated by:

$$P(Y > Y_i) = i/(N + 1) \tag{3.22}$$

where i is the rank of the observation Y_i. If $i/(N + 1)$ is a valid estimate for the EDF of the exponential function, then equating equations (3.21) and (3.22) gives the relationship:

$$\lambda Y_i = -\ln[i/(N + 1)] \qquad (3.23)$$

If Y_i follows an exponential distribution, then the graph of $-\ln[i/(N + 1)]$ vs. Y_i would plot along a straight line with slope λ on exponential probability paper as shown in Figure 3.3 for the upper half-tail exponential distribution. Lack of exponentiality would plot as a marked nonlinear curve. Consequently, if the untransformed peaks {X} in equation (3.4) plot concave upward or concave downward on exponential probability paper, then the peaks may be assumed to be drawn from a Rayleigh or Weibull distribution, respectively, as illustrated in Figure 3.4. Figure 3.5 plots the untransformed acceleration, velocity, and displacement peaks recorded during the 1971 San Fernando earthquake at the base of the Holiday Inn Building at 1640 Marengo Street. The acceleration, velocity, and displacement peaks plot as Rayleigh, Rayleigh, and exponential distributions, respectively. Hence, to determine if the largest peaks of a given time history are best modelled by an exponential (EHT), Rayleigh (EHT), or Weibull (EHT) distribution, the peaks are plotted on exponential probability plot paper and the appropriate trend is noted.

However, to provide a more analytical criterion to determine the best EHT distribution which models the

largest peaks, the second criterion proposed by Deherrera and Zsutty (1982) is based on minimizing the weighted square difference between the observed and the predicted peaks in accordance with the rank of the peak. For a given EHT distribution, if Y_i is the observed i^{th} largest peak in the transformed space, Y_i^* is the predicted i^{th} peak from the given EHT distribution, D_i equals $Y_i - Y_i^*$, and W_i equals Y_i/Y_1, then the weighted error squared term, β^2, is equal to:

$$\beta^2 = \frac{\sum_{i=1}^{N/2} W_i D_i^2}{\sum_{i=1}^{N/2} W_i} \qquad (3.24)$$

The upper limit N/2 of the summations will be $N_e/2$, $N_r/2$, and $N_w/2$ for the exponential (EHT), Rayleigh (EHT), and Weibull (EHT) distributions, respectively. For a given accelerogram, the particular EHT probability distribution which minimizes the error term β^2 is then the distribution selected by the EHT model to characterize the distribution of the largest peaks of that record.

Consequently, this study initially assumes that the largest peaks of ground motion acceleration, velocity, and displacement time histories are modelled by the appropriate EHT distribution (exponential, Rayleigh, or Weibull) which minimizes β^2 in equation (3.24). Table 3.4 summarizes the

EHT distribution selected by equation (3.24) to minimize β^2 for each ground motion component (acceleration, velocity, and displacement) of the 332 ground motion records listed in Table 3.2. In Table 3.4, the exponential (EHT), Rayleigh (EHT), and Weibull (EHT) distributions are denoted by 0, 1, and 2, respectively. Also given in Table 3.4 are the corresponding EHT distribution parameters: $1/\lambda$ and N/2, the number of peaks of the upper half-tail of the distribution.

No trends are observed from Table 3.4 in the selections of the EHT distribution by equation (3.24) to model the velocity and displacement peaks given that the acceleration peaks are selected by equation (3.24) to follow a given EHT distribution. In addition, there is no apparent relationship between the distributions selected to model the largest acceleration, velocity, and displacement peaks of the two orthogonal components of ground motion at a particular recording station.

For comparison purposes, the percentage of ground motion records from Table 3.4 whose largest peaks are selected by the criterion in equation (3.24) to be modelled by the exponential (EHT), Rayleigh (EHT), or Weibull (EHT) distribution is shown in Table 3.5 for each ground motion component (acceleration, velocity, and displacement) and each local site category (soil and rock). Similarly,

Tables 3.6 and 3.7 summarize the percentage of records investigated from the 9 February 1971 San Fernando, CA and the 15 October 1979 Imperial Valley, CA earthquakes, respectively, whose largest peaks are selected by the criterion in equation (3.24) to follow one of the three EHT distributions. Typically, Tables 3.5, 3.6, and 3.7 show that for each ground motion component and site category, for the greatest percentage of records, the largest peaks are selected by equation (3.24) to follow the Rayleigh (EHT) distribution. The only exception to this trend is the favoring of the exponential (EHT) distribution for acceleration records for rock sites in Tables 3.5, 3.6 and 3.7 and velocity records for both rock and soil sites from the 1979 Imperial Valley earthquake in Table 3.7.

Consequently, because the exponential (EHT) and Rayleigh (EHT) distributions are generally favored over the Weibull (EHT) distribution, case 3 in Table 3.3 assumes that the largest peaks of the ground motion components of all 332 ground motion records follow the exponential (EHT) distribution. Similarly, case 4 in Table 3.3 assumes that the largest peaks of all 332 records follow the Rayleigh (EHT) distribution. Case 5 in Table 3.3, the General (EHT) distribution, allows the EHT model weighted criterion in equation (3.24) to select the best fit EHT distribution

for each of the 332 records, resulting in the EHT distributions listed in Table 3.4.

3.3.3 EHT DISTRIBUTIONS ASSUMING STANDARDIZED NUMBER OF PEAKS, N*

An important result in Deherrera and Zsutty (1982) is that for the purpose of predicting the expected k^{th} largest ground motion acceleration peak, X(k), the number of peaks N in equations (3.12) and (3.13), which varies from record to record, can be replaced by a standardized number of peaks, N*. The value of N* is derived from the slope of the plot of $1/\lambda$ vs. $1/\lambda(\ln N)^m$ where m is equal to 1, 1/2, or 2 for an exponential (EHT), Rayleigh (EHT), or Weibull (EHT) distribution, respectively. For example, the slope of the plot will be equal to ln N for the exponential (EHT) distribution and $(\ln N)^{1/2}$ for the Rayleigh (EHT) distribution.

Following the above procedure, N* is derived in this study for ground motion acceleration, velocity, and displacement records assuming that the largest peaks of all ground motion records follow Case 3, the exponential (EHT) distribution, and Case 4, the Rayleigh (EHT) distribution, in Table 3.3. Figures 3.6, 3.7, and 3.8 graph $1/\lambda$ vs. $1/\lambda\ (\ln N)^m$ for the exponential (EHT) and Rayleigh (EHT) distributions for combined soil and rock sites for ground

motion acceleration, velocity, and displacement, respectively. Table 3.8 lists the values derived for N* for the soil, rock, and combined soil and rock categories. The N* values computed for the three site geology categories are very similar in value. Hence N^* does not appear to be sensitive to the site conditions. For the exponential (EHT) distribution, N* is equal to 127, 37, and 20 for acceleration, velocity, and displacement records, respectively, considering soil and rock sites combined. Similarly, for the Rayleigh (EHT) distribution, N* is equal to 48, 25, and 14 for acceleration, velocity, and displacement records, respectively, considering soil and rock sites combined. Hence, acceleration records contain the largest number of peaks, and displacement records, the smallest. The sensitivity of the peaks predicted from equations (3.12) and (3.13) to the number of peaks, N, in the distribution is addressed in Section 3.7. The N* values derived for acceleration are in agreement with the values derived by Deherrera and Zsutty (1982).

Using the N* values given in Table 3.8, the N* exponential (EHT) and the N* Rayleigh (EHT) distributions in Table 3.3 (cases 6 and 7, respectively) assume that the largest peaks of ground motion time histories can be modelled by the exponential (EHT) and Rayleigh (EHT) distributions, respectively, but where the number of

peaks, N, is now replaced by the appropriate value of N*. The largest peaks then act as if they are derived from a standardized sample size N*.

3.3.4 SUMMARY

In summary, of the seven probability distributions considered in Table 3.3 to model the peaks of strong ground motion records, two of the probability distributions are the traditional exponential and Rayleigh distributions. The remaining five distributions are variations of the EHT distributions proposed by Deherrera and Zsutty (1982). The next section addresses the adequacy of these seven probability distributions to model and predict the largest peaks of ground motion time histories.

3.4 PREDICTION OF THE LARGEST PEAKS

The capability of the exponential and exponential-like probability distributions in Table 3.3 to predict the largest peaks of ground motion time histories is verified analytically and graphically in this section. The analytical verification is accomplished as follows:

1) by model verification through Kolmogorov-Smirnov goodness-of-fit tests for 1, 5, and 10% significance levels;

2) by minimization of the standard error between the observed peak X(k) and the predicted peak $\bar{X}(k)$ for selected values of the peak number k.

In conjunction with item (2) of the analytical verification, graphical verification is presented by plotting the observed peak X(k) vs. the predicted peak $\bar{X}(k)$ for selected peak numbers k.

3.4.1 KOLMOGOROV-SMIRNOV TESTS

First, Kolmogorov-Smirnov tests are performed for the first five probability distributions listed in Table 3.3. The percentage of ground motion records passing the 1, 5, and 10% significance levels for the Kolmogorov-Smirnov test are listed in Tables 3.9, 3.10, and 3.11 for ground motion acceleration, velocity, and displacement records, respectively, as a function of site geology conditions. The trends observed from the results of the Kolmogorov-Smirnov tests are the following:

1) Regardless of ground motion component (acceleration, velocity, or displacement) and site geology conditions (soil or rock), none of the records pass the Kolmogorov-Smirnov test at the 1, 5, and 10% significance levels when the peaks are modelled by the traditional exponential, traditional Rayleigh, and General (EHT)-Weibull (EHT) distributions.

2) Regardless of ground motion component and site geology conditions, at least 82% of the records pass the Kolmogorov-Smirnov test at the 1, 5, and 10% significance levels when the peaks are modelled by the exponential (EHT), Rayleigh (EHT), General (EHT)-Exponential (EHT), and General (EHT)-Rayleigh (EHT) distributions.

3) With the exception of ground motion displacement records for soil sites, for the General (EHT)-Rayleigh (EHT) distribution, all records pass the Kolmogorov-Smirnov test at the 1, 5, and 10% significance levels.

4) For all ground motion components and all significance levels, for a given EHT probability distribution, a slightly larger percentage of records for rock sites pass the Kolmogorov-Smirnov test than for soil sites.

5) Overall, the level of significance has little influence on the percentage of ground motion records passing the Kolmogorov-Smirnov test. The most noticeable influence is evident for ground motion acceleration records for rock sites whose peaks are modelled by the exponential (EHT) distribution. At the 1% significance level, 85% of the 332 records passed the Kolmogorov-Smirnov test. At the 10% significance level, all records passed the Kolmogorov-Smirnov test. The difference of about 15% between the percentage of records passing at the 1% and 10% significance levels is the greatest effect of the level of significance observed.

In summary, a high percentage of ground motion records passed the Kolmogorov-Smirnov tests when modelled by the exponential (EHT) and Rayleigh (EHT) distributions. These two distributions are shown below in Section 3.4.2 to best predict the largest peaks.

3.4.2 COMPARISONS OF PEAK X(k) vs. PREDICTED PEAK $\bar{X}(k)$

Second, the capability of each probability distribution to minimize the standard error between the observed (actual) peak X(k) and the predicted peak $\bar{X}(k)$ is illustrated for ground motion peaks X(1), X(2), X(5), X(10), and X(20). The objective is to determine if successful prediction of the ground motion peak X(k) depends on the

probability distribution used to model the peaks of the ground motion record. The standard error, E(k), of peak X(k) is given as:

$$E(k) = \left[\frac{\sum_{i=1}^{NREC} \left[\frac{\bar{X}(k)_i - X(k)_i}{X(k)_i} \right]^2}{NREC - 1} \right]^{1/2} \qquad (3.25)$$

where i is summed over the data base of ground motion records in Table 3.2, NREC is equal to the number of records with peak X(k), typically equal to 332, and $X(k)_i$ and $\bar{X}(k)_i$ are the observed and predicted k^{th} largest peaks, respectively, for record i of the data base.

The values of the standard error, E(k), for ground motion acceleration, velocity, and displacement records are shown in Tables 3.12, 3.13, and 3.14, respectively, and are based on all 332 records in the data base regardless of site geology conditions. (The same trends have been observed for the standard error computed separately for soil and rock sites). In Tables 3.12 and 3.13, the standard error, E(k), is computed for peaks X(1), X(2), X(5), X(10), and X(20) for ground motion acceleration and velocity records, respectively. Because a number of ground motion displacement records did not contain peaks X(10) and X(20), the standard error is not computed in Table 3.14 for these peaks. For each peak X(k), the probability distri-

butions are listed in these tables in order of minimum to maximum values of E(k).

The trends noted in Tables 3.12, 3.13, and 3.14, which are discussed below, are aided by the graphical comparisons of the observed peak X(k) vs. the predicted peak $\bar{X}(k)$ in Figures 3.9 through 3.15 for six of the seven probability distributions listed in Table 3.3. Comparison of the observed vs. predicted peaks from the traditional Rayleigh distribution is not graphed in these figures since this distribution was initially observed in this study to predict a given peak X(k) least successfully of all probability distributions considered.

For comparison, also graphed in each figure is the line $\bar{X}(k) = X(k)$. Ideally, $\bar{X}(k)$ and X(k) should plot along this line. However, if for a given probability distribution, the peaks tend to plot below this line, then that distribution underpredicts the observed peak in the ground motion acceleration records. Conversely, if the peaks plot above this line, then the observed peaks are overpredicted by that particular distribution. Figures 3.9, 3.10, 3.11, and 3.12 graph the observed vs. predicted peaks X(1), X(5), X(10), and X(20), respectively, for ground motion acceleration records for both soil and rock records combined. Similar graphs are shown in Figures 3.13 and 3.14 for

ground motion velocity peaks X(1) and X(5), respectively, and in Figure 3.15 for ground motion displacement peak X(1).

For ground motion acceleration records, Table 3.12 indicates that for predicting X(1), i.e., the PGA, the standard error E(1) is comparably minimized by the Rayleigh (EHT), N* Rayleigh (EHT), and General (EHT) distributions. Hence, an interesting result of this investigation is the slight preference of the Rayleigh (EHT) distribution over the General (EHT) distribution to predict X(1). Preference of the prediction of the PGA from the Rayleigh (EHT) distribution, which is based on modelling all the ground motion records of the data base by this distribution, has the advantage of eliminating the need to determine a priori whether the expected acceleration peaks of a given site under investigation will follow an exponential (EHT), Rayleigh (EHT), or Weibull (EHT) distribution as suggested by Deherrera and Zsutty (1982) for their EHT model.

The maximum values of the standard error, E(1), and hence the worst predictors of X(1), are given by the traditional exponential and Rayleigh distributions. This result is expected since these two distributions are based on modelling the entire set of peaks of each ground motion acceleration time history and hence the prediction of the extreme values will not be as accurate. Figure 3.9

illustrates the above conclusions for X(1). While the exponential distribution tends to underpredict X(1) for most records, the remainder of the distributions show very good agreement between X(1) and $\bar{X}(1)$, especially the Rayleigh (EHT) and N* Rayleigh (EHT) distributions, as noted above.

While the Rayleigh (EHT) distribution is preferred over the other probability distributions to predict X(1), the General (EHT) and exponential (EHT) distributions are favored for acceleration peaks X(2), X(5), and X(10). As seen in Table 3.12, the General (EHT) distribution is only a marginally better predictor of these peaks than the exponential (EHT) distribution. Consequently, this study recommends the use of the exponential (EHT) distribution as a simplification to predict these near maximum peaks.

For ground motion acceleration peaks X(5) and X(10), Figures 3.10 and 3.11, respectively, show very good agreement between the observed peaks and the peaks predicted from the General (EHT) and exponential (EHT) distributions. Again, the traditional exponential distribution tends to consistently underpredict these peaks. The tendency of the Rayleigh (EHT) and N* Rayleigh (EHT) distributions to overpredict these peaks is also illustrated in these figures.

Finally, for ground motion acceleration peak X(20), Table 3.12 and Figure 3.12 show that the general (EHT) distribution minimizes E(20). The exponential and exponential (EHT) distributions give the next smallest values of E(20); however, the values of E(20) for these distributions are slightly greater than twice the value of E(20) for the General (EHT) distribution. As observed for peaks X(5) and X(10), the Rayleigh (EHT) and N* Rayleigh (EHT) distributions likewise tend to overpredict X(20).

For the largest peaks of ground motion velocity and displacement time histories, however, the General (EHT) distribution does not always minimize the standard error E(k) between the observed peak X(k) and the predicted peak $\bar{X}(k)$. As shown in Table 3.13 for ground motion velocity, the Rayleigh (EHT) distribution minimizes the standard error, E(1), between the observed peak X(1) and the predicted peak $\bar{X}(1)$. This trend is verified in Figure 3.13 for the PGV. Figure 3.13 shows that the exponential distribution again tends to underpredict the PGV, while the EHT distributions improve the accuracy in prediction of the PGV.

An initially unexpected result of this investigation, as illustrated in Table 3.13, is that while the exponential (EHT) distribution is favored for prediction of the ground motion velocity peak X(2), the lesser ground

motion velocity peaks X(5), X(10), and X(20) favor the traditional exponential distribution over the EHT distributions. This trend is illustrated in Figure 3.14 for ground motion velocity peak X(5).

For ground motion displacement, similar trends are observed for E(k) as for ground motion velocity. As shown in Table 3.14, the error E(1) is minimized for peak X(1), the PGD, by either the Rayleigh (EHT) or General (EHT) distributions. This trend is verified in Figure 3.15. However, for the displacement peaks X(2) and X(5), these peaks are best predicted by the exponential (EHT) and exponential distributions, respectively, which minimize the standard error for these peaks in Table 3.14.

An inspection of Tables 3.12, 3.13, and 3.14 and Figures 3.9 to 3.15 also indicates that the N* EHT distributions can predict the largest peaks reasonably well. The N* Rayleigh (EHT) distribution predicts X(1) quite well; however, this distribution typically overpredicts the lesser peaks X(2), X(5), etc. For these lesser peaks, the N* exponential (EHT) distribution is a better predictor of these peaks than the N* Rayleigh (EHT) distribution.

Table 3.15 summarizes the probability distribution which minimizes E(k) for each ground motion component and each peak X(k). An important result of this study is that for predicting the PGA, PGV, and PGD, the Rayleigh (EHT)

distribution is favored over the other probability distributions, including the General (EHT) and traditional exponential and Rayleigh distributions. However, the exponential (EHT) or traditional exponential distributions are shown to best predict the near maximum peaks X(2), X(5), X(10), and X(20).

Because the Rayleigh (EHT) distribution is derived from squaring the original set of peaks in the ground motion time history, this distribution is strongly influenced by the maximum peak, X(1). Hence, this distribution will not predict the lesser, near maximum peaks as well. The exponential (EHT) and the traditional exponential distributions, however, are derived from the untransformed set of peaks of the time history and therefore give lesser weight to the extreme values than the Rayleigh (EHT) and Rayleigh distributions. Consequently, the two exponential distributions will be more influenced by, and hence, more representative of, the lesser, near maximum peaks.

3.5 RELATIONSHIPS BETWEEN PGA, PGV, PGD AND $1/\lambda$

Also of interest in this study is to determine if there is a direct relationship between the observed peak X(1) and the EHT parameter $1/\lambda$ of a given time history, where λ is the parameter derived for the exponential (EHT) and Rayleigh (EHT) distributions. The parameter $1/\lambda$ will

have units of acceleration, velocity, or displacement if the modelled peaks are from a ground motion acceleration, velocity, or displacement time history, respectively. Figures 3.16, 3.17, and 3.18 graph the relationship between the PGA, PGV, and PGD and $1/\lambda$, respectively, from both the exponential (EHT) and Rayleigh (EHT) distributions for all records irrespective of site geology. For both EHT probability distributions, these graphs show a definite linear relationships between the maximum values (PGA, PGV, and PGD) and $1/\lambda$. For the exponential (EHT) distribution, the PGA, PGV, and PGD are approximately 4 to 5 times greater than the corresponding $1/\lambda$ values. For the Rayleigh (EHT) distribution, the maximum values appear to be about a factor of 2 times greater than $1/\lambda$. The linearity between the maximum values and $1/\lambda$ is most evident for ground displacement.

Hence the parameter $1/\lambda$, which represents the characteristic acceleration, velocity, or displacement, shows a similar relationship to the maximum value as for PGA and the rms acceleration parameter for ground motion. The parameter $1/\lambda$, which is related to the maximum value of the time history, is a parameter characterizing the largest peaks of the time history. This implies that the maximum value, X(1), does contain information on the lesser, near maximum peaks. The linear relationship between the maximum

value of the time history and $1/\lambda$ in Figures 3.16, 3.17, and 3.18 appears to be independent of site geology.

Since the PGA, PGV, and PGD have been shown to attenuate in a number of studies as a function of Richter magnitude and distance from the source, the parameter $1/\lambda$ should also attenuate. Hence if an attenuation relationship for $1/\lambda$ is known and the peaks are assumed to come from a standardized number of peaks N* in Table 3.8, then the expected ground motion peaks $\bar{X}(k)$ can be predicted for a given site. A preliminary attenuation relationship for $1/\lambda$ for the exponential distribution is given by Deherrera and Zsutty (1982).

3.6 SENSITIVITY OF PREDICTED PEAKS TO NUMBER OF PEAKS, N

The ground motion peaks in sections 3.4 and 3.5 have been predicted from equations (3.12) and (3.13) which are dependent on two parameters of the assumed probability distributions: $1/\lambda$ and the number of peaks, N. It was shown in Section 3.3 that the number of peaks N of each ground motion time history can be replaced by a standard number of peaks, N*, given in Table 3.8. From this table, it is evident that ground motion acceleration time histories have the largest number of peaks, and ground motion displacement, the smallest number. This section discusses the sensitivity of the prediction of the peaks from

equations (3.12) and (3.13) to the number of peaks N in the exponential and Rayleigh distributions.

Assuming a unit value of λ, Figures 3.19 and 3.20 graph the magnitudes of $\bar{X}(1)$, $\bar{X}(2)$, $\bar{X}(5)$, $\bar{X}(10)$, and $\bar{X}(20)$ predicted from equation (3.12) for the exponential and Rayleigh distributions, respectively, as a function of the number of peaks N in the distribution. Both figures show that the magnitude of the predicted peaks $\bar{X}(k)$ increases monotonically as N increases. As the number of peaks N in the distribution decreases and approaches the peak number k, the magnitudes are most influenced by changes in N. As N increases with respect to the peak number k, the peaks become less sensitive to changes in N.

The effect of the percent change in N on the magnitudes of the predicted peaks $\bar{X}(k)$ is shown in Table 3.16 for the exponential distribution. The following trends are noted in Table 3.16 for the exponential distribution and would also be observed for the Rayleigh distribution:

- For a given peak $\bar{X}(k)$ and a given number of peaks N, as the percent change in N increases, the magnitude of $\bar{X}(k)$ increases.
- For a given peak $\bar{X}(k)$ and a given percent change in N, as the number of peaks N in the distribution increases, the magnitude of $\bar{X}(k)$ becomes less sensitive to increases in N.
- For a given number of peaks N and a given percent change in N, as the peak number k of $\bar{X}(k)$ increases, the magnitude of $\bar{X}(k)$ becomes more sensitive to changes in N.

Also of interest is a comparison of the relative magnitudes of the predicted peaks $\bar{X}(2)$, $\bar{X}(5)$, $\bar{X}(10)$ and $\bar{X}(20)$ with respect to the maximum peak $\bar{X}(1)$. Figures 3.20 and 3.21 plot the ratio $\bar{X}(k)/\bar{X}(1)$ as a function of the number of peaks N for the exponential and Rayleigh distributions, respectively. The following trends are observed in these two figures:

- The ratio $\bar{X}(k)/\bar{X}(1)$ increases as N increases.
- As observed for $\bar{X}(k)$, the ratio is most sensitive to N for small changes in N as N decreases and approaches the peak number k.

Recall from Table 3.8 that the standardized number of peaks N* is largest for acceleration time histories and smallest for displacement. Hence based on the above observations for $\bar{X}(k)$ as a function of the number of peaks N in the distribution, the magnitudes of the displacement peaks will be the most sensitive of the three ground motion components to changes in N.

3.7 CONCLUSIONS

This chapter demonstrates that the largest peaks of ground motion time histories can be characterized by traditional and modified (EHT) exponential and Rayleigh distributions. Successful prediction of a specific ranked

peak, X(k), however, is shown to depend on the particular probability distribution which models the peaks of the ground motion time history. While the Rayleigh (EHT) distribution best predicts X(1), i.e., the PGA, PGV, and PGD, the near maximum peaks X(2), X(5), X(10), and X(20) are best predicted by either the exponential (EHT) or the traditional exponential distribution.

For ground motion acceleration, velocity, and displacement time histories, the following trends are also observed when the largest peaks are modelled by the exponential (EHT) and Rayleigh (EHT) distributions:

- the EHT parameter $1/\lambda$ is a constant fraction of the maximum value of the time history
- the number of peaks in the time history can be replaced by a standardized number of peaks N*. The resulting N* EHT distributions are shown to adequately model the largest peaks.

In general, site geology is not observed to be a dominant factor for characterization of the probability distributions and prediction of the largest peaks of ground motion time histories.

The following extensions of the ground motion study in this chapter are proposed to improve the characterization of strong ground motion:

1) Develop attenuation formulas for $1/\lambda$ predicted from the exponential (EHT) and Rayleigh (EHT) distributions for ground motion acceleration,

velocity, and displacement time histories. Using the attenuated value of $1/\lambda$ with a standardized number of peaks N*, the expected largest peaks $\bar{X}(k)$ can be predicted at a given site. Also to be investigated is whether $1/\lambda$ is a more stable parameter when attenuated than the maximum value X(1).

2) Empirically attenuate the near maximum ground motion peaks X(2), X(5), X(10), etc., as a function of magnitude, source to site distance, etc.

3) For a given EHT distribution, investigate the relationships among the values of $1/\lambda$ computed for ground motion acceleration, velocity, and displacement. Of interest is whether similar trends would be observed as for empirically derived relationships among PGA, PGV, and PGD.

4) For a given ground motion component (acceleration, velocity, or displacement), investigate the relationship between the values of $1/\lambda$ computed from the exponential (EHT) and Rayleigh (EHT) distributions. Deherrera and Zsutty (1982) have investigated this relationship for acceleration.

5) Investigate the use of $1/\lambda$ as a normalization parameter for seismic design response spectra.

6) Incorporate information on the distribution of the largest peaks to derive more representative, simulated ground motion time histories.

Chapter 4 parallels the characterization of the largest peaks of ground motion time histories by characterizing the largest peaks of linear single-degree-of-freedom oscillator and recorded building response time histories. The traditional and upper-half tail (EHT) distributions are also investigated in Chapter 4 to determine which distribution best predicts the response peaks.

CHAPTER 4

CHARACTERIZATION OF THE AMPLITUDES OF THE LARGEST PEAKS OF RESPONSE TIME HISTORIES

4.1 INTRODUCTION

For seismic design, response spectra are traditionally plotted for the maximum amplitude of the response of a linear, elastic single-degree-of-freedom (SDOF) oscillator subjected to strong earthquake ground motion. Such characterization, however, does not retain information on the amplitudes and the duration of the lesser, but near maximum peaks of the response time history which contribute to the strong motion portion of the response.

Therefore, utilizing the probability distributions investigated in Chapter 3 for ground motion, the objective of this chapter is to characterize explicitly the amplitudes and implicitly the duration of the largest peaks of the response time history of a linear, elastic SDOF oscillator subjected to earthquake excitation and of the building records obtained during the 9 February 1971 San Fernando, CA earthquake. The methodology of this chapter will parallel the characterization of the largest peaks of ground motion time histories in Chapter 3.

The adequacy of the traditional exponential and Rayleigh distributions, as well as the upper half-tail exponential (EHT), Rayleigh (EHT), and Weibull (EHT) distributions, to model and predict the largest peaks of response time histories is addressed. The emphasis of this chapter will focus on characterizing the probability distributions of the largest peaks of the acceleration response time history of a SDOF system subjected to strong ground motion. This characterization avoids the need to derive explicit, empirical relationships for the maximum and near maximum peaks of a response time history as in Perez and Brady (1984) and Prince (1984).

Also investigated in this chapter is which EHT probability distribution (exponential, Rayleigh, or Weibull) best characterizes the largest peaks of building response (acceleration) records obtained from 45 buildings during the San Fernando, CA earthquake of 9 February 1971. The objective is to determine if the largest peaks of building response records follow the same probability distributions as for SDOF oscillator response time histories.

For structural response, a peak is defined in this chapter as the maximum absolute amplitude between two consecutive zero crossings of the acceleration, relative velocity, or relative displacement time history. As shown

in Figure 4.1, the k^{th} largest peak, X(k), of a response time history is the k^{th} peak of the time history when the peaks are ranked in descending order from the largest, X(1), to smallest peak. The peak X(k) then summarizes the amplitude above which there will be k/2 cycles of response exceeding this amplitude.

Section 4.2 presents the methodology used in this chapter to model the probability distributions of the largest peaks of the acceleration response of a SDOF oscillator subjected to strong ground motion. The adequacy of the investigated probability distributions to predict the largest peaks of SDOF oscillator response time histories is verified in Section 4.3. The relationship between peak acceleration and the parameter $1/\lambda$ derived from the exponential (EHT) and Rayleigh (EHT) distributions is illustrated in Section 4.4.

Average $1/\lambda$ acceleration spectra, normalized by peak ground acceleration (PGA), are presented in Section 4.5 for the exponential (EHT) and Rayleigh (EHT) distributions. Together with a standardized number of peaks N*, derived as a function of the oscillator period, and the expected PGA of the site, the value of $1/\lambda$ given by these spectra can be used to predict the largest peaks $\bar{X}(k)$ from equations (3.12) and (3.13) for SDOF oscillator response at that site. Section 4.6 characterizes the EHT probability

distributions of recorded building response. Finally, Section 4.7 reviews the findings of this chapter and suggests future research to characterize structural response.

4.2 INVESTIGATION FOR SDOF OSCILLATOR RESPONSE

Characterization of the largest peaks of response time histories is investigated for a SDOF oscillator subjected to the 112 horizontal ground motion records listed in Table 2.1 which are also used in Chapter 2 for investigation of rms acceleration. Again, as discussed in Chapters 2 and 3, to investigate the effects of site geology conditions on the characterization of the largest response peaks, the soil conditions of the recording stations are divided into the same two site categories: "soil" and "rock".

The response of a SDOF oscillator subjected to strong ground motion is computed, as discussed in Chapter 2, from the numerical procedure outlined in Nigam and Jennings (1968). The response is initially calculated for 2, 5, and 10% of critical damping; however, this chapter will primarily focus on the characterization of the response for 5% of critical damping, which is a representative value of damping for a wide range of structural systems. The response is calculated for forty (40) oscillator periods

between 0.03 second and 30 seconds at approximately 13 equally-spaced oscillator periods for each cycle of the logarithmic scale. Initially, the probability distributions of the largest peaks of acceleration, relative velocity, and relative displacement response are investigated; then, the remainder of the investigation will focus on the characterization of acceleration response.

4.2.1 SELECTION OF PROBABILITY DISTRIBUTION MODELS

The largest peaks of acceleration, relative velocity, and relative displacement response time histories of a SDOF oscillator are modelled by the exponential or exponential-like probability distributions analyzed in Chapter 3. For characterization of response peaks, the largest peaks of the response time history of a SDOF oscillator are modelled by the probability distributions listed in Table 4.1. The first two probability distributions are again the well-known exponential and Rayleigh distributions given by equations (3.6), (3.7), (3.9) and (3.10). These two distributions are derived using the entire set of peaks of each response time history.

As in a ground motion time history, a number of peaks of a response time history, however, will consist of smaller amplitude peaks which do not contribute to the strong motion portion of the record. Consequently,

inclusion of these smaller amplitude peaks in the derivation of the exponential or Rayleigh distributions will greatly reduce the accuracy of prediction of the maximum and near maximum peaks which comprise the strong motion portion of interest. To improve the prediction of the larger peaks, the EHT distributions used in Chapter 3 for ground motion studies will also be used to model only the upper half-tail response peaks without the influence of the smaller peaks.

Initially, all three EHT distributions, i.e., the exponential (EHT), Rayleigh (EHT), and Weibull (EHT) distributions, are considered to model the largest peaks of acceleration, relative velocity, and relative displacement response time histories. However, based on the results described below in a preliminary investigation, only the exponential (EHT) and Rayleigh (EHT) distributions will be investigated in depth to model response peaks.

A preliminary investigation is made to determine if the largest peaks of SDOF oscillator response time histories favor the exponential (EHT), Rayleigh (EHT), or Weibull (EHT) distributions. Table 4.2 shows, as a function of the natural period of a SDOF oscillator with 5% damping subjected to the ground motion in Table 2.1, the fraction of acceleration, relative velocity, and relative displacement response time histories whose largest peaks

are selected by the criterion in equation (3.24) to best be modelled by one of the three EHT distributions. This table combines the response records for both soil and rock sites. The largest peaks in response time histories generally favor either the exponential (EHT) or Rayleigh (EHT) distributions. For periods greater than about 0.1 second, however, the Rayleigh (EHT) distribution is preferred over the exponential (EHT) distribution. Between oscillator periods of 0.1 second and 1 second, typically less than 20% of the response records follow a Weibull (EHT) distribution.

The fraction of relative displacement records following a given EHT distribution is approximately the same as for acceleration; this trend is not observed, however, between relative velocity and acceleration records. For the response records considered separately for soil and rock sites as shown in Tables 4.3 and 4.4, respectively, the favoring of the exponential (EHT) and Rayleigh (EHT) distributions, as discussed above for combined soil and rock records in Table 4.2, is similarly observed.

In addition, the trends noted above for a SDOF oscillator with 5% damping have also been observed for the response of a SDOF oscillator with 2% and 10% of critical damping. For comparison, Table 4.5 shows that as for 5%

damping, the largest peaks of response time histories of a SDOF oscillator with 2% and 10% damping with periods between 0.1 second and 10 seconds also favor the exponential (EHT) and Rayleigh (EHT) distributions. Again, the Rayleigh (EHT) distribution is preferred over the exponential (EHT) distribution. An interesting trend is also noted in Table 4.5. As the oscillator period increases and the percent of critical damping increases, the fraction of response records modelled by the exponential (EHT) and Weibull (EHT) distributions increases, and the fraction modelled by the Rayleigh (EHT) distribution decreases.

In general, the Rayleigh (EHT) distribution is favored over the exponential (EHT) distribution. The preference of the exponential (EHT) and Rayleigh (EHT) distributions for oscillator periods between 0.03 second and 30 seconds is also shown in Tables 4.6 and 4.7 for the response of a SDOF oscillator with 5% damping subjected to two well-known ground motion records: the 1940 El Centro, CA Comp S00E and the 1979 Imperial Valley, CA earthquake, Bond's Corner, Comp 230°, records, respectively.

Consequently, the third and fourth probability distributions considered in this study are the exponential (EHT) and Rayleigh (EHT) distributions, which are Cases 3 and 4, respectively, in Table 4.1. It is assumed that the largest peaks of all response records can be modelled by

these two distributions irrespective of the EHT distribution selected by the criterion of equation (3.24). Hence, the Weibull (EHT) distribution is not considered for SDOF oscillator response studies.

4.2.2 RELATIONSHIP BETWEEN $1/\lambda$ OF ACCELERATION, RELATIVE VELOCITY, AND RELATIVE DISPLACEMENT TIME HISTORIES

The remainder of this study will focus primarily on modelling the probability distributions of the largest peaks of the acceleration response time histories of a SDOF oscillator subjected to strong ground motion. However, the largest peaks of relative velocity and relative displacement time histories can be predicted using the parameter $1/\lambda$ of the EHT distributions of the largest peaks of acceleration time histories. The pseudo-spectral relationships which relate peak absolute acceleration to peak relative velocity or peak relative displacement are shown below to be generally valid for the parameter $1/\lambda$ of the exponential (EHT) and Rayleigh (EHT) distributions.

Let $1/\lambda_a$, $1/\lambda_v$, and $1/\lambda_d$ be equal to the EHT parameter $1/\lambda$ derived for the largest peaks of an acceleration, relative velocity, and relative displacement time history, respectively, for either the exponential (EHT) or Rayleigh (EHT) distribution. If the largest peaks of the acceleration, relative velocity, and relative displacement response time histories are assumed to be modeled by the same EHT

distribution, then investigated below is whether the following "pseudo-spectral" relationships are satisfied:

$$1/\lambda_a = \omega * 1/\lambda_v \qquad (4.1)$$

$$1/\lambda_a = \omega^2 * 1/\lambda_d \qquad (4.2)$$

where ω is the circular frequency of the SDOF oscillator. The frequency ω is related to the natural period, T, of the oscillator by the relationship

$$\omega = 2\pi/T \qquad (4.3)$$

The objective is to determine if the relative velocity and relative displacement peaks could be successfully predicted from equations (3.12) and (3.13) using from $1/\lambda_v$ and $1/\lambda_d$ calculated from $1/\lambda_a$.

For illustration, the relationships in equations (4.1) and (4.2) are graphed in Figures 4.2 through 4.13 for the exponential (EHT) and Rayleigh (EHT) distributions for the response of a SDOF oscillator with 5% damping and oscillator periods of 0.1 second, 1.0 second, and 10 seconds. These periods are selected to represent a range of oscillator periods most frequently encountered in

seismic design. These graphs are plotted irrespective of site conditions.

Figures 4.3, 4.5, 4.7, 4.9, and 4.11 show that equation (4.2), which relates $1/\lambda_a$ to $1/\lambda_d$, is satisfied almost identically at all three oscillator periods for both EHT distributions. Hence the relative displacement peaks can be successfully predicted from the relationship $1/\lambda_d = (1/\lambda_a)/\omega^2$. However, for the relationship between $1/\lambda_a$ and $1/\lambda_v$ given by equation (4.1), Figures 4.2 and 4.4 show that for both the exponential (EHT) and Rayleigh (EHT) distributions, respectively, the parameter $\omega * 1/\lambda_v$ typically is less than $1/\lambda_a$ for oscillator response at a period of 0.1 second. Consequently, to predict the largest peaks of relative velocity time histories from equations (3.12) or (3.13) using the relationship $1/\lambda_v = (1/\lambda_a)/\omega$ would lead to overprediction of the largest peaks of the relative velocity time history.

For an oscillator period of 1 second, equation (4.1) is satisfied almost identically by both the exponential (EHT) and Rayleigh (EHT) distributions as shown in Figures 4.6 and 4.8, respectively. At an oscillator period of 10 seconds, however, Figures 4.10 and 4.12 show that for both the exponential (EHT) and Rayleigh (EHT) distributions, respectively, the parameter $\omega * 1/\lambda_v$ is typically greater

than $1/\lambda_a$. Hence, the relative velocity peaks would be underpredicted from the relationship $1/\lambda_v = (1/\lambda_a)/\omega$.

Therefore, while the relative displacement peaks can be predicted directly from information on the acceleration peaks, successful prediction of the relative velocity peaks is a function of the oscillator period.

4.3 PREDICTION OF THE LARGEST PEAKS

The capability of the traditional and modified (EHT) exponential and Rayleigh distributions listed in Table 4.1 to predict the largest peaks of response time histories is verified in this section as follows:

- Analytically, by computation of the percentage of acceleration response records for oscillator periods of 0.1, 0.5, 1, 2 and 10 seconds passing selected significance levels of the Kolmogorov-Smirnov test;
- Graphically, by comparison of the average actual acceleration spectra computed for response peaks X(1), X(2), X(5), X(10), and X(20) with average acceleration spectra computed for these peaks predicted from the exponential, Rayleigh, exponential (EHT), and Rayleigh (EHT) distributions.

4.3.1 KOLMOGOROV-SMIRNOV TESTS

As in Chapter 3 for ground motion, as a part of model verification, Kolmogorov-Smirnov tests are performed for the probability distributions listed in Table 4.1. The percentage of response records for oscillator periods of

0.1, 0.5, 1, 2, and 10 seconds and with 5% damping passing the 1, 5, and 10% significance levels of the Kolmogorov-Smirnov test are listed in Tables 4.8, 4.9, and 4.10 for acceleration, relative velocity, and relative displacement response, respectively, irrespective of site geology.

The following trends are noted:

- Regardless of response component (acceleration, relative velocity, or relative displacement), none of the records pass the Kolmogorov-Smirnov test at the 1, 5, and 10% significance levels when the peaks are modelled by the traditional exponential and Rayleigh distributions.
- Regardless of the response component, between 80 and 90 percent of the response records pass the Kolmogorov-Smirnov tests at the 1, 5, and 10% significance levels when the peaks are modelled by the exponential (EHT) and Rayleigh (EHT) distributions.
- For both the exponential (EHT) and Rayleigh (EHT) distributions, the percentage of records passing the 1, 5, and 10% significance leveles is almost identical for acceleration, relative velocity, and relative displacement records.

The results of the Kolmogorov-Smirnov tests for response records are consistent with the results obtained in Section 3.4.1 for ground motion records. The traditional exponential and Rayleigh distributions do not pass the Kolmogorov-Smirnov test for both ground motion and response records and generally do not predict the near maximum peaks with reasonably accuracy. The majority of records modelled by the exponential (EHT) and Rayleigh (EHT) distributions, however, do satisfy the Kolmogorov-

Smirnov tests and are generally the best predictors of the largest peaks, especially for ground motion and response acceleration time histories.

4.3.2 AVERAGE ACCELERATION SPECTRA FOR X(k)

The remainder of this chapter is devoted to characterizing the largest peaks of acceleration response time histories for SDOF oscillator response with 5% damping. First, as an initial part of graphical model verification, comparisons are presented in Figures 4.14, 4.15, and 4.16 for combined soil and rock sites to illustrate the adequacy of the probability distributions in Table 4.1 to predict peaks X(1), X(10), and X(20), respectively, of the acceleration response time histories of a SDOF oscillator with 5% critical damping and 1 second period. For aid in comparison, also shown in each graph for X(k) is the line $\bar{X}(k) = X(k)$.

The upper two graphs for acceleration peak X(1) in Figure 4.14, corresponding to the traditional exponential and Rayleigh distributions, show that typically the maximum acceleration peak is underpredicted by these distributions which are derived from the entire set of peaks of each response time history. However, accuracy in the prediction of X(1) is improved by modelling only the largest peaks of the response time history by the exponen-

tial (EHT) and Rayleigh (EHT) distributions as shown in the lower two graphs. The Rayleigh (EHT) distribution predicts X(1) with very good accuracy and with slightly better accuracy than the exponential (EHT) distribution. In Figures 4.15 and 4.16, the near maximum acceleration peaks X(10) and X(20), respectively, are better predicted by the exponential (EHT) distribution than the Rayleigh (EHT) distribution. However, the exponential (EHT) distribution tends to underpredict these peaks. The Rayleigh (EHT) distribution tends to overpredict these peaks.

As a second and more extensive part of graphical model verification, average acceleration spectra computed for actual (observed) peaks X(k) in acceleration response time histories are compared to the average acceleration spectra of these peaks predicted by the four probability distributions listed in Table 4.1. Average actual acceleration spectra computed for peaks X(1), X(2), X(5), X(10), and X(20) of the response of a SDOF oscillator with 5% critical damping and for periods between 0.03 second and 10 seconds are shown separately for soil and rock sites in Figure 4.17. Each peak X(k) has been normalized by the PGA of the input record. The spectra for acceleration peak X(1) is the traditionally plotted maximum acceleration response spectra. Figure 4.17 indicates that for both soil and rock

sites, the average acceleration spectra of the near maximum peaks X(2), X(5), X(10), and X(20) are similar in shape to the traditional average maximum acceleration spectrum for X(1). The spectra of the lesser peaks appear to be a scaling down of the maximum peak spectrum.

The coefficient of variation of the average actual acceleration spectra shown in Figure 4.17 is graphed in Figure 4.18. For both soil and rock sites, Figure 4.18 shows that the coefficient of variation of the average actual acceleration spectra increases with increasing peak number k and with increasing oscillator period. The average actual acceleration spectra computed for the near maximum peaks do not reduce the scatter observed in the spectrum plotted for the maximum acceleration peak. Hence, the uncertainty of the amplitude of X(k) increases as the peak number k increases.

Comparisons of the average actual acceleration spectra for 5% damping for soil vs. rock sites for peaks X(1), X(2), X(5), X(10), and X(20) are shown in Figures 4.19 through 4.23, respectively. For peaks X(1), X(2), X(5), and X(10), the site geology effects are a function of the oscillator period as shown in Figures 4.19 through 4.22. Typically, for periods less than about 0.15 second, the response for soil sites is amplified slightly greater than the response for rock sites. For periods between 0.15

second and about 0.30 second, the spectral amplification for rock sites is slightly greater than for soil sites. For periods greater than about 0.3 second, the spectral amplification is greater for soil sites. For acceleration peak X(20), Figure 4.23 indicates that for all oscillator periods, the spectrum for soil sites has greater amplification than the spectrum for rock sites.

To illustrate the accuracy of the different probability distributions of Table 4.1 to model the largest peaks of acceleration response time histories, Figures 4.24 through 4.28 compare the average actual acceleration spectra graphed in Figure 4.17 with the average acceleration spectra of peaks X(1), X(2), X(5), X(10), and X(20) predicted from the exponential, Rayleigh, exponential (EHT), and Rayleigh (EHT) distributions. The average acceleration spectra for each predicted peak $\bar{X}(k)$ has been computed by normalizing $\bar{X}(k)$ by the PGA. In these figures and in other figures in this chapter, the investigated probability distributions are abbreviated as follows: E, exponential; R, Rayleigh; E-EHT, exponential (EHT); and R-EHT, Rayleigh (EHT).

Figure 4.24 shows that for both soil and rock sites, X(1) is best predicted by the Rayleigh (EHT) distribution, which tends to slightly overpredict X(1) between periods of about 0.1 second and 1 second; otherwise, for all other

periods, the agreement between the actual and the Rayleigh (EHT) spectra is excellent. The exponential (EHT) spectrum tends to overpredict both the actual spectrum and the Rayleigh (EHT) spectrum. Both the traditional exponential and Rayleigh spectra underpredict the actual spectrum by a factor of about 2 to 3. The Rayleigh distribution underpredicts X(1) by the greatest difference.

Comparison of the actual and predicted spectra of X(2) in Figure 4.25 shows that for both soil and rock sites, X(2) is very accurately predicted (slightly overpredicted) by both the exponential (EHT) and Rayleigh (EHT) distributions. The Rayleigh (EHT) spectrum is almost identical to the actual spectrum. As for X(1), the traditional exponential and Rayleigh distributions underpredict X(2) by at least a factor of 2.

However, the actual spectra of X(5), X(10), and X(20) in Figures 4.26, 4.27, and 4.28, respectively, are bounded by the Rayleigh (EHT) spectrum as an upper limit and the exponential (EHT) spectrum as a lower limit. The difference, or deviation, between the actual spectrum and the spectra predicted from the EHT distributions for these peaks is seen to increase with increasing peak number k. As the peak number k increases, the exponential (EHT) spectrum generally becomes a better match to the actual spectrum than the Rayleigh (EHT) spectrum. This is most

clearly illustrated in Figure 4.28 for peak X(20) for both soil and rock sites. Also, the traditional exponential and Rayleigh distributions underpredict X(5), X(10), and X(20), but as the peak number k increases, the exponential distribution, rather than the Rayleigh distribution, becomes the worst predictor of the peaks.

Hence, as also noted for the largest peaks of ground motion time histories, the exponential (EHT) and Rayleigh (EHT) distributions, derived from consideration of only the largest peaks of a response time history, are better predictors of the maximum and near maximum acceleration peaks than the traditional exponential and Rayleigh distributions. Moreover, as illustrated in Figures 4.24 to 4.28, the adequacy of the different probability distributions to model and predict the largest peaks is found to be the same for both soil and rock sites, i.e., site geology is not a factor in characterizing the distributions of the largest peaks.

Also of interest is the variability of the average acceleration spectra of the predicted peaks compared to the variability of the average acceleration spectra of the actual peaks. Consequently, Figures 4.29 to 4.33 compare the coefficient of variation of the average actual acceleration spectra with the coefficient of variation of the average acceleration spectra of the peaks predicted from

the exponential (EHT) and Rayleigh (EHT) distributions in Figures 4.24 to 4.28. The following trends are noted:

- The coefficient of variation of the spectra of the predicted peaks show similar behavior as the coefficient of variation of the actual spectra, i.e., the coefficient of variation increases with increasing oscillator period.

- The coefficient of variation of the spectra of the predicted peaks is very close to the coefficient of variation of the actual spectra. However, as the peak number k increases, the differences between the coefficient of variation of these spectra increases.

- For peak X(1), the minimum value of the coefficient of variation for any oscillator period is given by the actual spectra. For peaks X(2), X(5), X(10), and X(20), the spectra of the predicted peaks are observed to minimize the coefficient of variation for a number of oscillator periods. This is most pronounced for peak X(20) in Figure 4.33.

The scatter of the average acceleration spectra of the predicted peaks is comparable to the scatter observed for the average acceleration spectra of the actual peaks. Consequently, this indicates, along with the comparison of the actual and predicted spectra in Figures 4.24 to 4.28, that the Rayleigh (EHT) and exponential (EHT) distributions can successfully model the largest peaks of acceleration resonse time histories. The Rayleigh (EHT) distribution best predicts the first few largest peaks of the acceleration response time history, e.g., X(1), X(2) and X(5). As the peak number increases, e.g., for peaks X(10) and X(20) however, the exponential (EHT) distribution becomes a better predictor of the peaks (but underpredicts) than

the Rayleigh (EHT) distribution. A similar trend is observed in Section 3.4.2 for ground motion acceleration.

4.4 RELATIONSHIP BETWEEN PEAK ACCELERATION AND $1/\lambda$

As for ground motion, also of interest in this study is to determine if a relationship exists between the observed peak X(1), i.e., the peak acceleration, and the parameter $1/\lambda$ derived from the exponential (EHT) and Rayleigh (EHT) distributions. Recall that the parameter $1/\lambda$ will have units of acceleration. Figures 4.34, 4.35, and 4.36 graph peak acceleration vs. $1/\lambda$ for the response of a SDOF oscillator with 5% damping and oscillator periods of 0.1 second, 1 second, and 10 seconds, respectively, for the exponential (EHT) and Rayleigh (EHT) distributions, as a function of soil and rock sites.

For both EHT distributions, a linear relationship is observed between the peak acceleration and $1/\lambda$. The relationship appears to be a function of the oscillator period and the EHT distribution modelled but independent of the site geology. For the exponential (EHT) distribution, the ratio of peak acceleration to $1/\lambda$ is seen to decrease from about 5 for a period of 0.1 second (Figure 4.34a) to about 3.5 for a period of 10 seconds (Figure 4.36a) for the exponential (EHT) distribution. A similar trend is noted for the Rayleigh (EHT) distribution, but where the

ratio of peak acceleration to $1/\lambda$ is about one-half the value of the exponential (EHT) distribution. Hence, a linear relationship exists between the peak acceleration and $1/\lambda$ which is a function of the oscillator period. The parameter $1/\lambda$ appears to be a scaling down of the peak acceleration of the time history. This trend implies that the peak acceleration does contain information on the lesser peaks of the time history which are summarized by the $1/\lambda$ parameter. Hence for response acceleration, $1/\lambda$ is similar to the rms acceleration parameter for response observed in Chapter 2 in Figures 2.34, 2.35, and 2.36.

4.5 AVERAGE $(1/\lambda)$/PGA ACCELERATION SPECTRA

The advantage of characterizing the largest peaks by the exponential (EHT) and Rayleigh (EHT) distributions is that any specific peak level, X(k), can be predicted from the two parameters, λ and N, of these distributions. Consequently, average $1/\lambda$ acceleration spectra are derived in this section to predict the expected largest response peaks at a given site from the exponential (EHT) or Rayleigh (EHT) distributions. If the expected PGA of a given site is known, for example, from attenuation studies, then from proposed average acceleration spectra computed for $1/\lambda$, which are normalized by the PGA, and for a known standardized number of peaks, N*, derived for each

oscillator period, any specific response peak X(k) can be predicted from equations (3.12) and (3.13).

First, using the same methodology as in Chapter 3, the standardized number of peaks, N*, is derived for SDOF oscillator response with 5% damping as a function of oscillator period for the exponential (EHT) and Rayleigh (EHT) distributions. Because average acceleration spectra are computed for $(1/\lambda)/PGA$, the values of N* for both the exponential (EHT) and Rayleigh (EHT) distributions are calculated from the following two relationships:

$$(1/\lambda)/PGA \text{ vs. } [(1/\lambda * (\ln N)^m]/PGA \qquad (4.4)$$

$$1/\lambda \text{ vs. } 1/\lambda * (\ln N)^m \qquad (4.5)$$

where again m is equal to 1 and 1/2 for the exponential (EHT) and Rayleigh (EHT) distributions, respectively. These EHT distributions have been shown in Section 4.3 to successfully model the largest acceleration peaks. The second relationship is used in Chapter 3 to derive standardized N* values for ground motion time histories.

For both EHT distributions, these two relationships are graphed separately for soil and rock sites in Figures 4.37 through 4.40 for the acceleration response of a SDOF freedom oscillator with 5% damping and 1 second period.

These relationships follow a linear trend as also observed for the second relationship for ground motion acceleration in Figure 3.6. Hence, standardized N* values can also be derived for SDOF oscillator response.

The standardized N* values computed for the acceleration response of a SDOF oscillator with 5% damping are listed in Tables 4.11 and 4.12 for the exponential (EHT) and Rayleigh (EHT) distributions, respectively, as a function of oscillator period for combined soil and rock sites, soil sites, and rock sites. The N* values computed from the relationships in (4.4) and (4.5) are essentially the same. For both EHT distributions, the standardized number of peaks N* reaches a maximum value for oscillator periods around 0.1 second. Beyond 0.1 second, N* decreases and ranges between 7 and 20 for periods greater than 10 seconds.

At oscillator periods of 0.08 second, 0.6 second, and 3.5 seconds for rock sites for the Rayleigh (EHT) distribution, the acceleration response for several ground motion input records listed in Table 4.13 are observed to contain an unusually large number of peaks when modelled by the Rayleigh (EHT) distribution. This resulted in unusually large N* values for these three periods as shown in Table 4.12. However, the large N* values do not appear to be consistent with the trends observed at nearby

oscillator periods or for the exponential (EHT) distribution. Consequently, N* is also computed for these periods with the ground motion records in Table 4.13 removed from the data base in Table 2.1. The revised N* values for these periods are listed in parentheses in Table 4.12 and appear to be more consistent with the N* values obtained for other oscillator periods.

Figures 4.41 and 4.42 graph separately for soil and rock sites, the standardized number of peaks, N*, derived for the exponential (EHT) and Rayleigh (EHT) distributions, respectively. The revised N* values are plotted in Figure 4.42 for rock sites for the Rayleigh (EHT) distribution. These figures indicate that the N* values for the exponential (EHT) distribution are relatively insensitive site geology; however, site effects become more pronounced for the Rayleigh (EHT) distribution.

The sensitivity of the largest peaks predicted by equations (3.12) and (3.13) to the number of peaks N in the exponential and Rayleigh distributions has been addressed in Section 3.6. As seen in Tables 4.11 and 4.12, the N* values are the smallest at the longer oscillator periods. Hence the predicted peaks at these periods will be most sensitive to changes in N.

The average $(1/\lambda)$/PGA spectra derived for SDOF oscillator response with 5% damping are shown in Figures

4.43 and 4.44 as a function of soil and rock sites for the exponential (EHT) and Rayleigh (EHT) distributions, respectively. The spectra shown in these figures are similar in shape and behavior as the average actual acceleration spectra derived for the peaks X(k) in Figure 4.17 and the average rms acceleration spectra for 5% damping developed in Chapter 2 in Figures 2.32 and 2.33. Hence again $1/\lambda$ is observed to be an rms-like parameter. For periods between about 0.15 second and 0.30 second, the $(1/\lambda)$/PGA spectra derived for both the exponential (EHT) and Rayleigh (EHT) distributions for rock sites show slightly greater amplification than the spectra for soil sites. At all other periods, the amplification is greater for soil sites than for rock sites.

The coefficient of variation of the spectra shown in Figures 4.43 and 4.44 is shown in Figures 4.45 and 4.46, respectively. For the average $(1/\lambda)$/PGA spectra derived for both EHT distributions, the coefficient of variation of these spectra increases with increasing oscillator period. The magnitudes and behavior of the coefficient of variation as a function of oscillator period are very similar in shape to the coefficient of variation of the average actual acceleration spectra in Figure 4.18.

The exponential (EHT) probability distribution of the largest peaks characterized by the average $(1/\lambda)$/PGA

spectra from Figure 4.43 and the N* values from Figure 4.41 and Table 4.11 is referred to below as the N* exponential (EHT) distribution. Similarly, the Rayleigh (EHT) probability distribution characterized by the average $(1/\lambda)/PGA$ spectra from Figure 4.44 and the N* values from Figure 4.42 and Table 4.12 is referred to below as the N* Rayleigh (EHT) distribution.

The adequacy of the N* exponential (EHT) and N* Rayleigh (EHT) distributions to predict acceleration peaks X(1), X(10), and X(20) of the response of a SDOF oscillator with 5% damping and 1 second period subjected to the ground motion in Table 2.1 is shown in Figure 4.47. As in Figures 4.14, 4.15, and 4.16 for these same peaks, Figure 4.47 graphs the observed peak X(k) vs. the predicted peak $\bar{X}(k)$. The appropriate N* values for soil and rock sites are used to predict these peaks. For these peaks, both N* EHT distributions are seen to predict X(k) with comparable accuracy when predicted by the exponential (EHT) and Rayleigh (EHT) distributions in Figures 4.14, 4.15, and 4.16.

As further verification, Table 4.14 compares the observed vs. predicted peaks X(1), X(2), X(5), X(10), and X(20) as a function of oscillator period for a SDOF oscillator with 5% damping subjected to the 1940 El Centro, CA record (A001, Comp S00E). An inspection of Table 4.14

indicates that, overall, the acceleration peaks can be predicted reasonably well by the N* EHT distributions.

Consequently, the N* EHT distributions developed in this section can be used to predict the expected largest peaks of SDOF oscillator response at a given site. Such characterization provides a more complete description of the expected response than the traditionally maximum value only predicted from seismic design response spectra.

4.6 INVESTIGATION FOR RECORDED BUILDING RESPONSE

The objective of this section is to determine if the largest peaks of building response records can be modelled by the EHT probability distributions investigated in this chapter for linear, elastic SDOF oscillator response. Specifically investigated is whether the largest peaks of recorded acceleration response also favors the Rayleigh (EHT) distribution as for SDOF oscillator response. Analyzed are the acceleration records obtained at the roof and the base of 45 buildings during the San Fernando, CA earthquake of 9 February 1971. Only very minor structural damage was observed in these buildings due to this earthquake. Using the criterion in equation (3.24), the appropriate EHT distribution of the largest acceleration peaks of each of the two orthogonal, horizontal components

recorded at both the roof and the base of each building is determined.

The records analyzed are from the Volume II records published by the California Institute of Technology (1973) and are listed in Table 4.15 by CalTech EERL number, building name, and address. A brief description of each building is summarized in Table 4.16. A number of the buildings had fundamental earthquake periods greater than 1 second. The soil conditions of the recording stations are again divided into the two site categories used for SDOF oscillator response studies. Four buildings are located on rock and 41 buildings on soil sites. Because only a few buildings are located on rock sites, however, the effects of site geology are not considered.

Figure 4.48 shows an exponential probability plot for the acceleration peaks recorded at the roof of the Holiday Inn Building located at 1640 S. Marengo Street, Comp S52W, during the 1971 San Fernando, CA earthquake. As for the base acceleration records shown in Figure 3.5, the acceleration peaks plot concave upward and hence follow a Rayleigh distribution.

The parameters of the EHT distribution selected by the criterion of equation (3.24) to best model the largest acceleration peaks at the roof and the base of each building are listed in Table 4.17. The heading "D" in

Table 4.17 corresponds to the type of EHT distribution selected: 0, exponential; 1, Rayleigh; and 2, Weibull. Table 4.18, which summarizes the selection of the EHT distributions in Table 4.17, indicates that for the majority of both roof response and the base motion records, the acceleration peaks favor the Rayleigh (EHT) distribution. The Weibull (EHT) distribution is favored the least.

Table 4.19 compares the EHT distributions at the roof and the base of each building. A comparison of the distributions of the two orthogonal components at a given level indicates that the distribution selected is not necessarily the same in both orthogonal directions. In addition, for a given component (direction), the distributions selected to model the roof and base acceleration peaks are not necessarily the same.

To determine if the EHT distribution type selected by equation (3.24) for the roof and the base records is a function of the earthquake period of the building, Table 4.20 summarizes the selected EHT distributions as a function of earthquake period. For acceleration response records at the roof, Table 4.20 indicates that for buildings with fundamental earthquake periods less than or equal to 0.5 second, the exponential (EHT) distribution is preferred. In fact, for this period range, none of the

building records follow the Rayleigh (EHT) distribution. Beyond a period of 0.5 second, the largest peaks of recorded response favor the Rayleigh (EHT) distribution. For the base motion records, the Rayleigh (EHT) distribution is preferred over the other EHT distributions, with the exception of the exponential (EHT) distribution for periods between 0.5 second and 1 second.

Consequently, the largest peaks of recorded building response at the roof and the base are seen to favor the Rayleigh (EHT) distribution over the other EHT distributions. This preference follows the general favoring of the Rayleigh (EHT) distribution observed for linear SDOF oscillator response in Tables 4.2 through 4.5 for 2, 5, and 10% damping.

Finally, comparisons of the observed peak X(1) vs. the predicted peak $\bar{X}(1)$ from the appropriate EHT distribution in Table 4.17 for building response recorded at the roof are shown in Figure 4.49. The agreement between X(1) and $\bar{X}(1)$ is best for the Rayleigh (EHT) distribution, again indicating the preference of this distribution to model structural response. Typically, both the exponential (EHT) and Weibull (EHT) distributions overpredict X(1).

4.7 CONCLUSIONS

Characterzation of the probability distributions of the largest peaks of response time histories facilitates a comprehensive description of the maximum and near maximum response amplitudes and the number of cycles of response over which these amplitudes are sustained. The Rayleigh (EHT) and exponential (EHT) distributions are shown in this chapter to successfully predict the largest acceleration peaks of SDOF oscillator response time histories better than the traditional exponential and Rayleigh distributions. From the parameters of the EHT distributions, the expected amplitude sustained over a given number of cycles can be determined.

The characterization of the acceleration response time histories of a SDOF oscillator with 5% of critical damping can be summarized as follows:

- The average actual acceleration spectra of response peaks X(2), X(5), X(10), and X(20) are similar in shape as the average actual acceleration spectra of X(1).
- The largest peaks of acceleration response time histories are shown to generally favor the Rayleigh (EHT) distribution.
- The maximum and the second largest acceleration response peaks, X(1) and X(2), respectively, can be successfully predicted (slightly overpredicted) by both the Rayleigh (EHT) and exponential (EHT) distributions for both soil and rock sites.

- Prediction of the near maximum acceleration peaks X(5), X(10), and X(20) are bounded by the Rayleigh (EHT) distribution as an upper limit and the exponential (EHT) distribution as a lower limit for both soil and rock sites.

- A standardized number of peaks, N*, which replaces the actual number of peaks N determined for each acceleration response time history, can be derived for SDOF oscillator response as for ground motion and is a function of the EHT distribution, oscillator period, and site conditions.

- Using the derived N* values, any expected peak of acceleration response at a given site can be predicted from the average $(1/\lambda)/PGA$ spectra derived for the exponential (EHT) and Rayleigh (EHT) distributions.

- The parameter $1/\lambda$ of the exponential (EHT) and Rayleigh (EHT) distributions is shown to be linearly related to the peak (maximum) acceleration of the response record. Hence the parameter $1/\lambda$ appears to be a scaling down of the peak acceleration. This relationship is a function of the EHT distribution and the oscillator period. Because the parameter $1/\lambda$ represents a summary of the largest response peaks, the linear relationship between peak acceleration and $1/\lambda$ implies that the peak acceleration does in fact retain information on the lesser, but near maximum peaks.

- Assuming a given EHT distribution, the parameter $1/\lambda_a$ determined for acceleration response is found to be identically related to the parameter $1/\lambda_d$ determined for relative displacement response by the pseudo-spectral relationship

$$1/\lambda_a = \omega^2 * 1/\lambda_d$$

where ω is the circular frequency of the oscillator. This relationship enables the k^{th} largest relative displacement peak to be predicted from information on the distribution of the largest acceleration peaks. The pseudo-spectral relationship

$$1/\lambda_a = \omega * 1/\lambda_v$$

where $1/\lambda_v$ is determined for relative velocity response, v is a function of the oscillator period.

- The largest peaks of acceleration response of building records obtained during the 1971 San Fernando earthquake are generally shown to favor the Rayleigh (EHT) distribution. Hence, the probability distributions which model the largest acceleration peaks of recorded response are consistent with the distributions selected to model the largest acceleration peaks of the response of a SDOF oscillator.

- Site geology conditions do not appear to be a factor in the selection of the probability distribution which best predicts the acceleration response peaks.

Proposed extensions of this study for future research are the following:

1) Investigate the effects of refined soil site categories and other damping values on the characterization of the average $(1/\lambda)$/PGA spectra.

2) Investigate the effects of refined soil site categories and other damping values on the standardized number of peaks N*.

3) Investigate the relationship between $1/\lambda$ determined from the exponential (EHT) distribution and $1/\lambda$ determined from the Rayleigh (EHT) distribution for SDOF oscillator acceleration response.

4) Investigate other normalization parameters for the average $1/\lambda$ spectra.

5) As an alternative method to retain information on specific response peaks, empirically derive from regression analysis the relationship describing the relative magnitudes of all the largest acceleration peaks X(k) for SDOF oscillator resonse as a function of percent of critical damping and oscillator. This methodology will retain information on all the expected largest peaks at a particular oscil-

lator period and avoid the need to derive explicit relationships for X(k).

CHAPTER 5

CONCLUSIONS

This study investigates two methods to characterize the largest amplitudes of ground motion and response time histories. First, rms acceleration is investigated in Chapter 2 as ground motion and response parameters to characterize the strong motion amplitudes sustained over a given duration. The duration required to compute rms acceleration in the time domain is computed from the duration measures defined by Bolt (1973) and Trifunac and Brady (1975). The rms acceleration is found to be dependent on the duration measure.

For ground motion, rms acceleration is found to be linearly related to the PGA. Hence, the PGA does contain information on the lesser peaks of the ground motion time history. For SDOF oscillator response, rms acceleration is similarly shown to be a scaling down of the peak acceleration of the response time history but the scaling is a function of the percent of critical damping, the oscillator period, and the duration measure.

In addition, for ground motion, rms acceleration does not consistently summarize the same number of cycles whose amplitudes will exceed the rms acceleration for each ground motion record and for each duration measure. Similarly for

response, rms acceleration does not consistently summarize the same number of cycles whose amplitudes will exceed the rms acceleration for each damping value, oscillator period, and duration measure. Hence, the rms acceleration paramter does not give consistent information on the number of cycles of the ground motion or response time history whose amplitudes will exceed the magnitude of the rms acceleration. With the exception of the PGA or the peak response acceleration, the rms acceleration representation does not give specific information on any of the expected lesser, but near maximum peaks of a time history.

However, Chapters 3 and 4 present a methodolgy which enables prediction of the expected amplitudes of specific peaks of ground motion and response time histories, respectively. The largest peaks of ground motion records, acceleration time histories of a SDOF oscillator response, and recorded building response can be predicted from the upper half-tail exponential (EHT) and Rayleigh (EHT) distributions proposed by Deherrera and Zsutty (1982).

Overall, the traditional exponential and Rayleigh distributions generally are not successful predictors of the largest peaks of ground motion and acceleration response time histories. In general, the Rayleigh (EHT) distribution is shown to best predict the maximum peak,

X(1), of ground motion (i.e., PGA, PGV, and PGD) and acceleration response time histories. For the lesser peaks of ground motion time histories, i.e., X(2), X(5), X(10), and X(2), either the exponential (EHT) or the traditional exponential distributions are better predictors of these peaks than the Rayleigh (EHT) or the traditional Rayleigh distributions.

For SDOF oscillator response with 5% damping, the Rayleigh (EHT) distribution best predicts X(1), the maximum acceleration of the time history. The second largest peak, X(2), is predicted successfully by both the Rayleigh (EHT) and exponential (EHT) distributions. However, the prediction of the lesser acceleration response peaks X(5), X(10), and X(20) is bounded by the Rayleigh (EHT) distribution as an upper limit and the exponential (EHT) distribution as a lower limit.

For both ground motion and SDOF oscillator response time histories, the parameter $1/\lambda$ of the EHT distributions, which characterize the largest peaks of the time history, is shown to be related to the maximum value of the time history. Hence, the parameter $1/\lambda$ is similar to an rms-like parameter.

This study also shows that the number of peaks N in an earthquake time history can be replaced by a standarized number of peaks N* for prediction of the largest peaks. N*

values are derived for ground motion acceleration, velocity, and displacement time histories and for acceleration response time histories of a SDOF oscillator with 5% damping. For response, the N* values are a function of the oscillator period.

For ground motion, the standarized N* values could be used with attenuation formulas derived for the EHT parameter $1/\lambda$ to predict the expected largest ground motion peaks at a given site. For response, average $(1/\lambda)$/PGA spectra are presented which can be used with the N* values to predict the expected k^{th} largest acceleration response peaks at a given site.

For recorded building response from the 1971 San Fernando, CA earthquake, the largest peaks of the acceleration response records at the roof and the base are shown to favor the Rayleigh (EHT) distribution. This trend is consistent with the favoring of the Rayleigh (EHT) distribution for the acceleration response of a SDOF oscillator.

Extensions of this study for future research have been presented in Sections 3.7 and 4.7 for ground motion and SDOF oscillator response, respectively, which recommend further investigation of the characterization of the largest peaks of ground motion and response time histories. Retaining information on the relative magnitudes of the near maximum peaks as well as the maximum peak of a time

history presents a more comprehensive description of the expected loading demands and response than the traditionally characterized maximum value and rms acceleration parameters of an earthquake time history.

TABLE 2.1

Summary of Records Analyzed

EARTHQUAKE	DATE	RICHTER MAGNITUDE	RECORDING STATION	I.D. NUMBER	SITE[1] CONDITION	EPICENTRAL DIST. (km)	PGA cm/sec/sec
Imperial Valley, CA	5-18-40	7.1	El Centro	A001 S00E	S	11	341.7
Imperial Valley, CA	5-18-40	7.1	El Centro	A001 S90W	S	11	210.1
Kern County, CA	7-21-52	7.7	Pasadena, CIT Athenaeum	A003 S00E	S	127	46.5
Kern County, CA	7-21-52	7.7	Pasadena, CIT Athenaeum	A003 S90W	S	127	52.1
Kern County, CA	7-21-52	7.7	Taft, Lincoln School Tunnel	A004 N21E	R	43	152.7
Kern County, CA	7-21-52	7.7	Taft, Lincoln School Tunnel	A004 S69E	R	43	175.9
Eureka, CA	12-21-54	6.6	Eureka Federal Bldg.	A008 N11W	S	24	164.5
Eureka, CA	12-21-54	6.6	Eureka Federal Bldg.	A008 N79E	S	24	252.7
Eureka, CA	12-21-54	6.6	Ferndale City Hall	A009 N44E	S	40	155.7
Eureka, CA	12-21-54	6.6	Ferndale City Hall	A009 N46W	S	40	197.3
San Francisco, CA	03-22-57	5.3	Alexander Building	A014 N09W	S	15	41.8
San Francisco, CA	03-22-57	5.3	Alexander Building	A014 N81E	S	15	45.4
San Francisco, CA	3-22-57	5.3	Golden Gate Park	A015 N10E	R	12	81.8
San Francisco, CA	3-22-57	5.3	Golden Gate Park	A015 S80E	R	12	102.8
San Francisco, CA	3-22-57	5.3	State Building	A016 S09E	S	14	83.8
San Francisco, CA	3-22-57	5.3	State Building	A016 S81W	S	14	55.1
Lower California	12-30-34	6.5	El Centro	B024 S00W	S	64	156.8
Lower California	12-30-34	6.5	El Centro	B024 S90W	S	64	179.1
Helena, Montana	10-31-35	6.0	Carroll College	B025 S00W	R	7	143.5
Helena, Montana	10-31-35	6.0	Carroll College	B025 S90W	R	7	142.5
Western Washington	4-13-49	7.0	Olympia, Highway Test Lab	B029 N04W	S	16	161.6
Western Washington	4-13-49	7.0	Olympia, Highway Test Lab	B029 N86E	S	16	274.6
Puget Sound, WA	4-29-65	6.5	Olympia, Highway Test Lab	B032 S04E	S	61	134.2
Puget Sound, WA	4-29-65	6.5	Olympia, Highway Test Lab	B032 S86W	S	61	194.3
Parkfield, CA	6-27-66	5.3	Cholame-Shandon, Array 5	B034 N05W	S	5	347.8
Parkfield, CA	6-27-66	5.3	Cholame-Shandon, Array 5	B034 N85E	S	5	425.7
Parkfield, CA	6-27-66	5.3	Temblor, CA. No. 2	B037 N65W	R	6	264.3

TABLE 2.1
(Cont'd.)

EARTHQUAKE	DATE	RICHTER MAGNITUDE	RECORDING STATION	I.D. NUMBER	SITE[1] CONDITION	EPICENTRAL DIST. (km)	PGA cm/sec/sec
Parkfield, CA	6-27-66	5.3	Temblor, CA No. 2	B037 S25W	R	6	340.8
Borrego Mt., CA	4-08-68	6.5	San Onofre, SCE Power Plant	B040 N33E	R	134	40.0
Borrego Mt., CA	4-08-68	6.5	San Onofre, SCE Power Plant	B040 N57W	R	134	45.5
San Fernando, CA	2-09-71	6.4	Pacoima Dam	C041 S16E	R	8	1148.1
San Fernando, CA	2-09-71	6.4	Pacoima Dam	C041 S74W	R	8	1054.9
San Fernando, CA	2-09-71	6.4	Los Angeles, 8244 Orion	C048 N00W	S	20	250.0
San Fernando, CA	2-09-71	6.4	Los Angeles 8244 Orion	C048 S90W	S	20	131.7
San Fernando, CA	2-09-71	6.4	Castaic	D056 N21E	S	29	309.4
San Fernando, CA	2-09-71	6.4	Castaic	D056 N69W	S	29	265.4
San Fernando, CA	2-09-71	6.4	LA, Hollywood Storage	D058 S00W	S	35	167.3
San Fernando, CA	2-09-71	6.4	LA, Hollywood Storage	D058 N90E	S	35	207.0
San Fernando, CA	2-09-71	6.4	LA, 3470 Wilshire	E075 N00E	S	39	133.8
San Fernando, CA	2-09-71	6.4	LA, 3470 Wilshire	E075 S90W	S	39	111.8
San Fernando, CA	2-09-71	6.4	LA, 3407 West Sixth	E083 S00W	S	39	158.2
San Fernando, CA	2-09-71	6.4	LA, 3407 West Sixth	E083 N90E	S	39	161.9
San Fernando, CA	2-09-71	6.4	Pasadena, Seismo-logical Lab	G106 S00W	R	34	87.5
San Fernando, CA	2-09-71	6.4	Pasadena, Seismo-logical Lab	G106 S90W	R	34	188.6
San Fernando, CA	2-09-71	6.4	Pasadena, CIT Athenaeum	G107 N00E	S	37	93.5
San Fernando, CA	2-09-71	6.4	Pasadena, CIT Athenaeum	G107 N90E	S	37	107.3
San Fernando, CA	2-09-71	6.4	Pasadena, CIT Millikan Library	G108 N00E	S	37	198.0
San Fernando, CA	2-09-71	6.4	Pasadena, CIT Millikan Library	G108 N90E	S	37	181.6
San Fernando, CA	2-09-71	6.4	Pasadena, JPL	G110 S82E	S	29	207.8
San Fernando, CA	2-09-71	6.4	Pasadena, JPL	G110 S08W	S	29	139.0
San Fernando, CA	2-09-71	6.4	LA, 15250 Ventura	H115 N11E	S	28	220.6
San Fernando, CA	2-09-71	6.4	LA, 15250 Ventura	H115 N79W	S	28	146.0
San Fernando, CA	2-09-71	6.4	Lake Hughes, No. 4	J142 S69E	R	29	168.2

TABLE 2.1
(Cont'd.)

EARTHQUAKE	DATE	RICHTER MAGNITUDE	RECORDING STATION	I.D. NUMBER	SITE[1] CONDITION	EPICENTRAL DIST. (km)	PGA cm/sec/sec
San Fernando, CA	2-09-71	6.4	Lake Hughes, No. 4	J142 S21W	R	29	143.5
San Fernando, CA	2-09-71	6.4	Lake Hughes, No. 12	J144 N21E	R	25	346.2
San Fernando, CA	2-09-71	6.4	Lake Hughes, No. 12	J144 N69W	R	25	277.9
San Fernando, CA	2-09-71	6.4	LA, 3838 Lankershim	L166 N00E	R	30	164.2
San Fernando, CA	2-09-71	6.4	LA, 3838 Lankershim	L166 S90W	R	30	147.6
San Fernando, CA	2-09-71	6.4	LA, Griffith Park Obsv.	O198 S00W	R	33	176.9
San Fernando, CA	2-09-71	6.4	LA, Griffith Park Obsv.	O198 S90W	R	33	167.4
San Fernando, CA	2-09-71	6.4	LA, 14274 Ventura	Q233 S12W	S	28	243.3
San Fernando, CA	2-09-71	6.4	LA, 14274 Ventura	Q233 N78W	S	28	197.0
San Fernando, CA	2-09-71	6.4	LA, 3550 Wilshire	S266 Nort	S	39	153.6
San Fernando, CA	2-09-71	6.4	LA, 3550 Wilshire	S266 West	S	39	129.7
Northern CA	12-10-67	5.8	Ferndale City Hall	U312 N46W	S	32	103.1
Northern CA	12-10-67	5.8	Ferndale City Hall	U312 S44W	S	32	232.1
Lytle Creek, CA	9-12-70	5.4	Wrightwood, 6074 Park Drive	W334 S65E	R	13	139.0
Lytle Creek, CA	9-12-70	5.4	Wrightwood, 6074 Park Drive	W334 S25W	R	13	194.4
Imperial Valley, CA	10-15-79	6.6	El Centro, Array 1	IV01 230	S	36	136.2
Imperial Valley, CA	10-15-79	6.6	El Centro, Array 1	IV01 140	S	36	139.4
Imperial Valley, CA	10-15-79	6.6	El Centro, Array 2	IV02 230	S	31	405.5
Imperial Valley, CA	10-15-79	6.6	El Centro, Array 2	IV02 140	S	31	309.3
Imperial Valley, CA	10-15-79	6.6	El Centro, Array 3	IV03 230	S	29	218.1
Imperial Valley, CA	10-15-79	6.6	El Centro, Array 3	IV03 140	S	29	261.7
Imperial Valley, CA	10-15-79	6.6	El Centro, Array 4	IV04 230	S	27	349.7
Imperial Valley, CA	10-15-79	6.6	El Centro, Array 4	IV04 140	S	27	483.6
Imperial Valley, CA	10-15-79	6.6	El Centro, Array 5	IV05 230	S	27	367.2
Imperial Valley, CA	10-15-79	6.6	El Centro, Array 5	IV05 140	S	27	517.2
Imperial Valley, CA	10-15-79	6.6	El Centro, Array 6	IV06 230	S	27	428.1
Imperial Valley, CA	10-15-79	6.6	El Centro, Array 6	IV06 140	S	27	368.7
Imperial Valley, CA	10-15-79	6.6	El Centro, Array 7	IV07 230	S	27	453.7
Imperial Valley, CA	10-15-79	6.6	El Centro, Array 7	IV07 140	S	27	326.8
Imperial Valley, CA	10-15-79	6.6	El Centro, Array 8	IV08 230	S	27	457.4
Imperial Valley, CA	10-15-79	6.6	El Centro, Array 8	IV08 140	S	27	598.3
Imperial Valley, CA	10-15-79	6.6	El Centro, Diff. Array	IV09 360	S	27	477.1
Imperial Valley, CA	10-15-79	6.6	El Centro, Diff. Array	IV09 270	S	27	344.9
Imperial Valley, CA	10-15-79	6.6	El Centro, Array 10	IV10 50	S	27	168.2
Imperial Valley, CA	10-15-79	6.6	El Centro, Array 10	IV10 320	S	27	221.7

TABLE 2.1
(Cont'd.)

EARTHQUAKE	DATE	RICHTER MAGNITUDE	RECORDING STATION	I.D. NUMBER	SITE[1] CONDITION	EPICENTRAL DIST. (km)	PGA cm/sec/sec
Imperial Valley, CA	10-15-79	6.6	El Centro, Array 11	IV11 230	S	28	374.5
Imperial Valley, CA	10-15-79	6.6	El Centro, Array 11	IV11 140	S	28	355.4
Imperial Valley, CA	10-15-79	6.6	El Centro, Array 12	IV12 230	S	30	113.4
Imperial Valley, CA	10-15-79	6.6	El Centro, Array 12	IV12 140	S	30	138.7
Imperial Valley, CA	10-15-79	6.6	El Centro, Array 13	IV13 230	S	34	136.2
Imperial Valley, CA	10-15-79	6.6	El Centro, Array 13	IV13 140	S	34	114.6
Imperial Valley, CA	10-15-79	6.6	Parachute Test Facility	IV14 315	S	47	200.2
Imperial Valley, CA	10-15-79	6.6	Parachute Test Facility	IV14 225	S	47	106.9
Imperial Valley, CA	10-15-79	6.6	Calipatria, Fire Station	IV15 315	S	57	77.0
Imperial Valley, CA	10-15-79	6.6	Calipatria, Fire Station	IV15 225	S	57	125.7
Imperial Valley, CA	10-15-79	6.6	Superstition Mt.	IV16 135	R	58	189.2
Imperial Valley, CA	10-15-79	6.6	Superstition Mt.	IV16 45	R	58	108.0
Imperial Valley, CA	10-15-79	6.6	Plaster City Storehouse	IV17 135	S	52	55.5
Imperial Valley, CA	10-15-79	6.6	Plaster City Storehouse	IV17 45	S	52	41.9
Imperial Valley, CA	10-15-79	6.6	Coachella Canal #4	IV18 135	S	84	125.7
Imperial Valley, CA	10-15-79	6.6	Coachella Canal #4	IV18 45	S	84	113.6
Imperial Valley, CA	10-15-79	6.6	Bond's Corner	IV19 230	S	6	770.4
Imperial Valley, CA	10-15-79	6.6	Bond's Corner	IV19 140	S	6	575.7
Imperial Valley, CA	10-15-79	6.6	Brawley Airport	IV20 315	S	42	216.5
Imperial Valley, CA	10-15-79	6.6	Brawley Airport	IV20 225	S	42	162.2
Imperial Valley, CA	10-15-79	6.6	Holtville Post Office	IV21 315	S	20	213.2
Imperial Valley, CA	10-15-79	6.6	Holtville Post Office	IV21 225	S	20	246.2
Imperial Valley, CA	10-15-79	6.6	Calexico Fire Station	IV22 315	S	15	196.9
Imperial Valley, CA	10-15-79	6.6	Calexico Fire Station	IV22 225	S	15	269.6

[1] S - Soil Site
R - Rock Site

TABLE 2.2
Summary of RMS Acceleration Parameters

Record	PGA (cm/sec/sec)	Duration (sec)		RMS (cm/sec/sec)		PGA/RMS		Peak No. of RMS Acceleration	
		Bolt	T - B	Bolt	T - B	Bolt	T - B	Bolt	T - B
A001 S00E	341.70	29.30	24.40	61.65	64.75	5.54	5.28	74	69
A001 S90W	210.10	26.38	24.52	54.26	54.40	3.87	3.86	90	90
A003 S00E	46.50	.00	29.98	.00	11.05	.00	4.21	0	53
A003 S90W	52.10	.14	29.72	54.74	14.70	.95	3.54	1	44
A004 N21E	152.70	19.58	30.52	38.51	31.70	3.97	4.82	66	80
A004 S69E	175.90	15.56	28.84	44.66	33.96	3.94	5.18	59	83
A008 N11W	164.50	4.32	14.16	63.65	36.69	2.58	4.48	15	19
A008 N79E	252.70	6.10	9.92	80.96	63.43	3.12	3.98	15	17
A009 N44E	155.70	10.56	17.94	52.04	41.38	2.99	3.76	14	21
A009 N46W	197.30	8.50	19.52	47.94	32.95	4.12	5.99	12	23
A014 N09W	41.80	.00	27.92	.00	5.70	.00	7.33	0	57
A014 N81E	45.40	.00	28.46	.00	5.27	.00	8.62	0	66
A015 N10E	81.80	.38	3.64	48.24	20.90	1.70	3.91	5	15
A015 S80E	102.80	1.60	3.22	40.78	29.70	2.52	3.46	12	14
A016 S09E	83.80	1.40	27.46	37.72	10.43	2.22	8.03	10	50
A016 S81W	55.10	1.26	27.70	26.15	8.31	2.11	6.63	14	51
B024 S00W	156.80	16.86	21.08	42.64	38.27	3.68	4.10	70	75
B024 S90W	179.10	18.12	20.26	44.61	41.57	4.02	4.31	70	76
B025 S00W	143.50	1.72	2.22	48.03	43.17	2.99	3.32	12	13
B025 S90W	142.50	1.56	2.00	63.83	57.17	2.23	2.49	8	9
B029 N04W	161.60	22.30	25.78	44.27	40.51	3.65	3.99	100	108
B029 N86E	274.60	21.12	18.06	55.99	59.22	4.90	4.64	88	85
B032 S04E	134.20	10.34	24.96	38.31	26.14	3.50	5.13	65	97
B032 S86W	194.30	11.76	20.84	44.71	34.90	4.35	5.57	68	90
B034 N05W	347.80	7.88	7.48	67.75	68.50	5.13	5.08	22	22
B034 N85E	425.70	7.30	6.72	82.85	84.34	5.14	5.05	20	20
B037 N65W	264.30	3.70	5.60	67.37	55.41	3.92	4.77	11	12
B037 S25W	340.80	3.46	4.48	86.39	75.25	3.95	4.53	8	10
B040 N33E	40.00	.00	31.32	.00	7.11	.00	5.63	0	92
B040 N57W	45.50	.00	30.00	.00	8.18	.00	5.56	0	91
C041 S16E	1148.10	33.66	7.02	124.93	259.83	9.19	4.42	54	29
C041 S74W	1054.90	33.60	7.26	119.71	244.57	8.81	4.31	65	28
C048 N00W	250.00	18.66	16.56	63.65	65.89	3.93	3.79	46	44
C048 S90W	131.70	17.94	21.66	45.96	41.92	2.87	3.14	51	53
D056 N21E	309.40	14.90	15.90	51.89	49.57	5.96	6.24	40	42
D056 N69W	265.40	19.64	16.94	55.02	57.89	4.82	4.58	52	50
D058 S00W	167.30	8.50	13.84	50.67	40.98	3.30	4.08	48	61
D058 N90E	207.00	9.26	13.20	62.55	52.45	3.31	3.95	36	45
E075 N00E	133.80	12.82	15.30	38.90	35.98	3.44	3.72	35	39
E075 S90W	111.80	10.56	15.56	34.83	30.11	3.21	3.71	33	38
E083 S00W	158.20	12.32	12.90	46.26	44.58	3.42	3.55	41	42
E083 N90E	161.90	12.60	13.24	40.45	38.95	4.00	4.16	49	51
G106 S00W	87.50	5.16	14.62	30.05	20.95	2.91	4.18	44	66
G106 S90W	188.60	6.72	7.42	54.17	51.01	3.48	3.70	30	34
G107 N00E	93.50	6.42	15.36	31.11	22.07	3.01	4.24	33	48
G107 N90E	107.30	8.14	12.78	36.73	30.72	2.92	3.49	27	34
G108 N00E	198.00	10.34	13.10	45.13	40.30	4.39	4.91	33	39
G108 N90E	181.60	10.76	17.46	41.73	33.56	4.35	5.41	32	40
G110 S82E	207.80	5.60	9.66	58.12	45.14	3.58	4.60	22	33
G110 S08W	139.00	7.92	12.32	35.55	29.39	3.91	4.73	38	44
H115 N11E	220.60	16.82	18.42	55.75	52.75	3.96	4.18	56	58
H115 N79W	146.00	18.16	24.52	40.88	36.45	3.57	4.01	59	67
J142 S69E	168.20	5.68	12.64	44.06	31.14	3.82	5.40	41	66
J142 S21W	143.50	4.32	12.58	45.50	29.21	3.15	4.91	27	62
J144 N21E	346.20	14.12	10.72	61.87	68.23	5.60	5.07	52	47
J144 N69W	277.90	14.50	12.04	56.34	59.60	4.93	4.66	52	49

TABLE 2.2
(Cont'd.)

Record	PGA (cm/sec/sec)	Duration (sec)		RMS (cm/sec/sec)		PGA/RMS		Peak No. of RMS Acceleration	
		Bolt	T - B	Bolt	T - B	Bolt	T - B	Bolt	T - B
L166 N00E	164.20	6.68	11.98	38.05	30.17	4.31	5.44	35	42
L166 S90W	147.60	6.22	11.96	50.35	37.27	2.93	3.96	29	35
0198 S00W	176.90	6.76	10.08	53.30	44.79	3.32	3.95	24	34
0198 S90W	167.40	9.60	10.34	55.05	52.75	3.04	3.17	43	44
Q233 S12W	243.30	17.56	16.38	61.92	62.49	3.93	3.89	46	46
Q233 N78W	197.00	23.08	22.52	43.32	43.14	4.55	4.57	86	86
S266 NORTH	153.60	12.88	15.08	36.73	34.28	4.18	4.48	43	44
S266 WEST	129.70	10.42	14.26	38.13	33.76	3.40	3.84	33	35
U312 N46W	103.10	.36	24.98	74.90	12.98	1.38	7.94	2	44
U312 S44W	232.10	.70	16.44	75.01	18.99	3.09	12.22	3	21
W334 S65E	139.00	2.78	3.16	52.26	48.91	2.66	2.84	15	16
W334 S25W	194.40	2.06	2.66	62.38	55.55	3.12	3.50	11	12
IU11 230	374.54	12.01	7.98	89.87	106.74	4.17	3.51	36	31
IU11 140	355.41	11.57	9.00	101.70	111.59	3.49	3.18	42	40
IU03 230	218.13	10.80	14.16	60.15	52.50	3.63	4.16	57	65
IU03 140	261.74	12.59	11.69	73.28	74.20	3.57	3.53	39	38
IU14 315	200.17	5.37	17.66	42.40	26.66	4.72	7.51	28	64
IU14 225	106.86	7.72	18.61	35.16	24.81	3.04	4.31	38	61
IU02 230	405.49	13.08	11.74	67.19	69.29	6.03	5.85	53	52
IU02 140	309.30	12.16	8.91	79.21	89.83	3.90	3.44	40	33
IU12 230	113.36	16.05	19.79	33.88	30.63	3.35	3.70	68	75
IU12 140	138.68	**17.94**	**19.83**	35.12	33.42	3.95	4.15	68	73
IU15 315	77.00	**1.12**	**25.41**	38.46	15.03	2.00	5.12	10	72
IU15 225	125.65	**1.91**	**26.69**	43.57	17.75	2.88	7.08	10	84
IU13 230	136.22	**12.48**	**22.26**	33.04	25.94	4.12	5.25	59	79
IU13 140	114.63	**8.82**	**21.50**	37.72	26.66	3.04	4.30	56	80
IU01 230	136.23	8.63	20.73	34.79	24.36	3.92	5.59	84	124
IU01 140	139.35	10.44	15.14	38.14	32.17	3.65	4.33	78	92
IU16 135	189.21	4.33	6.66	49.38	41.66	3.83	4.54	23	32
IU16 45	107.97	4.73	11.80	27.62	20.42	3.91	5.29	48	66
IU17 135	55.49	2.18	11.36	22.97	16.78	2.42	3.31	38	60
IU17 45	41.93	.00	12.07	.00	12.07	.00	3.47	0	68
IU18 135	125.74	4.79	10.37	45.72	33.19	2.75	3.79	13	18
IU18 45	113.58	3.87	11.34	35.31	24.12	3.22	4.71	13	24
IU07 230	453.65	10.36	4.78	100.46	142.11	4.52	3.19	7	5
IU07 140	326.78	8.03	6.80	79.60	84.47	4.11	3.87	13	12
IU06 230	428.09	10.53	8.32	100.80	109.70	4.25	3.90	32	28
IU06 140	368.67	11.87	11.47	86.65	85.67	4.25	4.30	42	43
IU19 230	770.42	18.87	9.76	140.20	185.85	5.50	4.15	41	35
IU19 140	575.73	18.97	9.70	112.24	150.17	5.13	3.83	50	42
IU08 230	457.37	9.61	5.83	97.25	120.32	4.70	3.80	35	31
IU08 140	598.25	11.80	6.77	90.70	115.31	6.60	5.19	35	27
IU05 230	367.21	15.44	9.47	81.51	100.09	4.51	3.67	30	23
IU05 140	517.19	36.09	8.26	53.47	106.30	9.67	4.87	58	21
IU09 360	477.14	11.54	6.57	105.81	134.64	4.51	3.54	25	18
IU09 270	344.90	13.13	7.06	89.41	117.44	3.86	2.94	42	33
IU04 230	349.65	12.29	10.25	67.50	71.93	5.18	4.86	21	19
IU04 140	483.64	11.14	6.64	84.92	106.20	5.70	4.55	24	20
IU20 315	216.52	11.55	14.48	46.69	41.58	4.64	5.21	31	34
IU20 225	162.17	11.63	15.03	37.94	33.83	4.27	4.79	40	48
IU21 315	213.06	14.02	13.11	59.75	60.24	3.57	3.54	42	42
IU21 225	246.19	11.67	11.88	66.19	64.42	3.72	3.82	37	40
IU10 50	168.21	11.03	13.11	53.85	49.48	3.12	3.40	33	37
IU10 320	221.69	10.21	12.03	62.23	56.92	3.56	3.89	26	32
IU22 315	196.86	13.70	15.40	56.14	52.21	3.51	3.77	70	75
IU22 225	269.61	12.98	11.07	62.54	65.95	4.31	4.09	49	49

TABLE 3.1

SUMMARY OF EARTHQUAKES INVESTIGATED

EQ. ID. NO.	DATE	LOCATION	RICHTER MAGNITUDE[1]	NUMBER OF RECORDS
1	03-10-33	Long Beach, CA	6.3	2
2	10-02-33	Southern California	5.4	2
3	07-06-34	Eureka, CA	-	2
4	12-30-34	Lower California	6.5	2
5	10-31-35	Helena, Montana	6.0	4
6	11-28-35	Helena, Montana	-	2
7	02-06-37	Humboldt Bay, CA	5.75	2
8	09-11-38	Northwest California	5.5	2
9	05-18-40	Imperial Valley, CA	7.1	2
10	02-09-41	Northwest California	6.6	2
11	10-03-41	Northern California	6.4	2
12	10-21-42	Borrego Valley, CA	6.5	2
13	04-13-49	Western Washington	7.0	2
14	01-23-51	Imperial Valley, CA	5.6	2
15	10-07-51	Northwest California	6.0	2
16	07-21-52	Kern County, CA	7.7	8
17	09-22-52	Northern California	5.4	2
18	11-21-52	Southern California	6+	2
19	06-13-53	Imperial Valley, CA	5.5	2
20	01-12-54	Wheeler Ridge, CA	5.9	2
21	11-12-54	Lower California	6.3	2
22	12-21-54	Eureka, CA	6.6	4
23	02-09-56	El Alamo, Baja, CA	6.8	2
24	03-18-57	Southern California	5.0	2
25	03-22-57	San Francisco, CA	5.3	8
26	06-05-60	Northern California	5.7	2
27	09-04-62	Northern California	5.0	2
28	04-29-65	Puget Sound, WA	6.5	4
29	07-15-65	Southern California	4.5	2
30	06-27-66	Parkfield, CA	5.3	8
31	12-10-67	Northern California	5.8	4
32	04-08-68	Borrego Mountain, CA	6.5	16
33	09-12-70	Lytle Creek, CA	5.4	10
34	02-09-71	San Fernando, CA	6.4	176
35	10-15-79	Imperial Valley, CA	6.6	44

[1]Per McGuire and Barnhard (1977), Murphy, Steinbrugge, and Martin (1973), Chavez et al. (1982).

TABLE 3.2

RECORDS ANALYZED IN INVESTIGATION

ID. NO.[4]	RECORDING STATION LOCATION	EQ. ID. NO.[1]	R.M.[2]	SITE[3]	EPI. DIST. (km)	REFERENCE FOR EPI. DIST.
A001	El Centro Imperial Valley	9	7.1	S	11	1
A002	Ferndale City Hall	15	6.0	S	53	1
A003	Pasadena, C.I.T., Athenaeum	16	7.7	S	127	1
A004	Taft, Lincoln School Tunnel	16	7.7	R	43	1
A006	LA, Hollywood Storage Building, Bsmt.	16	7.7	S	119	1
A007	LA, Hollywood Storage Building, PE Lot	16	7.7	S	119	1
A008	Eureka Federal Building	22	6.6	S	24	1
A009	Ferndale City Hall	22	6.6	S	40	1
A011	El Centro, Imperial Valley	23	6.8	S	119	1
A014	San Francisco, Alexander Bldg. Bsmt.	25	5.3	S	15	1
A015	San Francisco, Golden Gate Park	25	5.3	R	12	1
A016	San Francisco, State Building	25	5.3	S	14	1
A017	Oakland City Hall	25	5.3	S	24	1
A019	El Centro, Imperial Valley	31	6.5	S	64	1
B021	Vernon CMD Building	1	6.3	S	53	1
B023	LA, Hollywood Storage Building, Bsmt.	2	5.4	S	38	1
B024	El Centro, Imperial Valley	4	6.5	S	64	1
B025	Helena, Montana Carroll College	5	6.0	R	7	1
B026	Ferndale City Hall	8	5.5	S	55	1
B027	Ferndale City Hall	10	6.6	S	104	1
B029	Olympia, WA, Highway Test Lab	13	7.0	S	16	1
B030	Ferndale City Hall	17	5.4	S	43	1
B031	Taft, Lincoln School Tunnel	20	5.9	R	43	1
B032	Olympia, WA, Highway Test Lab	28	6.5	S	61	1
B034	Cholame-Shandon, Array #5	30	5.3	S	5	1
B037	Temblor, Cal. No. 2	30	5.3	R	6	1
B038	San Luis Obispo, Recreation Building	30	5.3	R	77	1
B039	Eureka City Hall	31	5.8	S	51	1
B040	San Onofre SCE Power Plant	32	6.5	R	134	1
C048	Los Angeles, 8244 Orion	34	6.4	S	20	2
C054	Los Angeles, 445 S. Figueroa	34	6.4	R	41	2
D056	Castaic	34	6.4	S	29	2
D057	LA, Hollywood Storage	34	6.4	S	35	2
D058	LA, Hollywood Storage	34	6.4	S	35	2
D059	LA, 1901 Avenue of Stars	34	6.4	S	38	2
D062	LA, 1640 Marengo	34	6.4	S	42	2
D065	LA, 3710 Wilshire	34	6.4	S	39	2
D068	LA, 7080 Hollywood	34	6.4	S	34	2

TABLE 3.2 (Cont'd.)

ID. NO.	RECORDING STATION LOCATION	EQ. ID. NO.	R.M.	SITE	EPI. DIST. (km)	REFERENCE FOR EPI. DIST.
E072	LA, 4680 Wilshire	34	6.4	S	38	2
E075	LA, 3470 Wilshire	34	6.4	S	39	2
E078	LA, Water and Power Building	34	6.4	R	41	2
E083	LA, 3407 West Sixth	34	6.4	S	39	2
F086	Vernon	34	6.4	S	46	2
F087	Santa Ana	34	6.4	S	86	2
F088	Glendale, 633 East Broadway	34	6.4	S	32	2
F089	Los Angeles, 808 S. Olive	34	6.4	S	42	2
F092	Los Angeles, 2011 Zonal	34	6.4	R	42	2
F095	Los Angeles, 120 Robertson	34	6.4	S	36	2
F098	Los Angeles, 646 South Olive	34	6.4	S	42	2
F101	Colton	34	6.4	S	104	2
F102	Tejon	34	6.4	R	71	2
F103	Pearblossom	34	6.4	S	46	2
F105	Los Angeles, U.C.L.A.	34	6.4	S	37	2
G106	Pasadena, Seismological Laboratory	34	6.4	R	34	2
G107	Pasadena, C.I.T., Athenaeum	34	6.4	S	37	2
G108	Pasadena, C.I.T., Millikan Library	34	6.4	S	37	2
G110	Pasadena, Jet Propulsion Laboratory	34	6.4	S	29	2
G112	Los Angeles, 611 West Sixth	34	6.4	S	41	2
G114	Palmdale	34	6.4	S	33	2
H115	Los Angeles, 15250 Ventura	34	6.4	S	28	2
H118	Los Angeles, 8639 Lincoln	34	6.4	S	48	2
H121	Alhambra, 900 South Fremont	34	6.4	S	42	2
H124	Fullerton, 2600 Nutwood	34	6.4	S	74	2
I137	Los Angeles, 15910 Ventura	34	6.4	S	28	2
J141	Lake Hughes, No. 1	34	6.4	R	31	2
J142	Lake Hughes, No. 4	34	6.4	R	29	2
J143	Lake Hughes, No. 9	34	6.4	R	29	2
J144	Lake Hughes, No. 12	34	6.4	R	25	2
J145	Los Angeles, 15107 Vanowen	34	6.4	S	24	2
J148	LA, 616 South Normandie	34	6.4	S	39	2
K157	LA, 420 South Grand	34	6.4	R	41	2
L166	LA, 3838 Lankershim	34	6.4	R	30	2
L171	San Onofre	34	6.4	S	135	2
M176	LA, 1150 South Hill	34	6.4	S	42	2
M179	Grapevine, Techachapi Pumping Plant	34	6.4	S	73	2
M180	Orange, 4000 West Chapman	34	6.4	S	83	2
M183	Wrightwood	34	6.4	R	70	2
M184	Wrightwood	34	6.4	R	70	2

TABLE 3.2 (Cont'd.)

ID. NO.	RECORDING STATION LOCATION	EQ. ID. NO.	R.M.	SITE	EPI. DIST. (km)	REFERENCE FOR EPI. DIST.
N185	Carbon Canyon Dam	34	6.4	S	74	2
N186	Whittier, Narrows Dam	34	6.4	S	52	2
N187	San Antonio Dam	34	6.4	S	71	2
N188	LA, 1880 Century Park East	34	6.4	S	38	2
N191	Palos Verdes Estates	34	6.4	S	67	2
N192	LA, 2500 Wilshire	34	6.4	S	40	2
N195	San Juan Capistrano	34	6.4	S	120	2
N196	Long Beach, State College	34	6.4	S	73	2
N197	Anza	34	6.4	S	178	2
O198	LA, Griffith Park Observatory	34	6.4	R	33	2
O199	LA, 1625 Olympic	34	6.4	S	41	2
O204	Long Beach, Utility Building	34	6.4	S	72	2
O205	Long Beach, Terminal Island	34	6.4	S	71	2
O206	San Bernadino	34	6.4	S	104	2
O207	Fairmont Reservoir	34	6.4	R	36	2
O210	Hemet	34	6.4	S	139	2
P214	LA, 4867 Sunset	34	6.4	S	35	2
P217	LA, 3345 Wilshire	34	6.4	S	39	2
P220	Costa Mesa	34	6.4	S	96	2
P221	Santa Anita Dam	34	6.4	R	42	2
P222	Port Hueneme	34	6.4	S	78	2
P223	Puddingstone Dam	34	6.4	R	62	2
P231	LA, 9841 Airport Boulevard	34	6.4	S	49	2
Q233	LA, 14724 Ventura	34	6.4	S	28	2
Q236	LA, 1760 North Orchid	34	6.4	S	34	2
Q239	Beverly Hills, 9100 Wilshire	34	6.4	S	37	2
Q241	LA, 800 West First	34	6.4	R	41	2
R244	LA, 222 South Figueroa	34	6.4	S	41	2
R246	LA, 6464 Sunset	34	6.4	S	34	2
R249	LA, 1900 Avenue of Stars	34	6.4	S	38	2
R251	LA, 234 South Figueroa	34	6.4	S	41	2
R253	LA, 533 South Fremont	34	6.4	S	41	2
S255	LA, 6200 Wilshire	34	6.4	S	38	2
S258	LA, 3440 University, U.S.C.	34	6.4	S	42	2
S262	LA, 5900 Wilshire	34	6.4	S	38	2
S265	LA, 3411 Wilshire	34	6.4	R	39	2
S266	LA, 3550 Wilshire	34	6.4	S	39	2
S267	LA, 5260 Century	34	6.4	S	49	2
T286	El Centro, Imperial Valley	12	6.5	S	48	1
T287	El Centro, Imperial Valley	14	5.6	S	30	1
T288	El Centro, Imperial Valley	19	5.5	S	11	1
T289	El Centro, Imperial Valley	21	6.3	S	150	1

TABLE 3.2 (Cont'd.)

ID. NO.	RECORDING STATION LOCATION	EQ. ID. NO.	R.M.	SITE	EPI. DIST. (km)	REFERENCE FOR EPI. DIST.
U294	Ferndale City Hall	03	Offshore	S	128	1
U295	Helena, Montana, Federal Building	05	6.0	R	3-8	1
U297	Helena, Montana, Federal Building	06	-	R	3-8	1
U298	Ferndale City Hall	07	5.75	S	80	1
U300	Ferndale City Hall	11	6.4	S	50	1
U308	Ferndale City Hall	26	5.7	S	59	1
U310	Seattle, Washington, Federal Building	28	6.5	S	22	1
U311	Taft Lincoln School Tunnel	30	5.3	R	131	1
U312	Ferndale City Hall	31	5.8	S	32	1
V319	San Luis Obispo, City Recreation Building	18	6+	R	77	1
V329	Port Nueneme Navy Research Laboratory	24	5.0	S	6	1
V330	Eureka Federal Building	27	5.0	S	19	1
V331	Castaic Old Ridge Route	29	4.5	S	18	1
W334	Wrightwood, 6074 Park Drive	33	5.4	R	13	1
W335	Cedar Springs, Allen Ranch	33	5.4	R	19	1
W338	San Bernadino, Hall of Records	33	5.4	S	18	1
W342	Pasadena, C.I.T., Library	33	5.4	S	56	1
W344	Pasadena, C.I.T., J.P.L.	33	5.4	S	59	1
Y371	Santa Ana, Orange County Eng. Building	32	6.5	S	174	1
Y373	Pasadena, C.I.T., J.P.L.	32	6.5	S	219	1
Y375	Pasadena, C.I.T., Library	32	6.5	S	214	1
Y376	Pasadena, C.I.T., Athenaeum	32	6.5	S	214	1
Y379	Vernon, CMD Building	32	6.5	S	214	1
Y380	Hollywood Storage, P.E. Lot	32	6.5	S	223	1
IV01[5]	El Centro Array 1, Borchard Ranches	35	6.6	S	36	3
IV02	El Centro Array 2, Keystone Road	35	6.6	S	31	3
IV03	El Centro Array 3, Pine Union School	35	6.6	S	29	3
IV04	El Centro Array 4, 2905 Anderson Road	35	6.6	S	27	3
IV05	El Centro Array 5, 2801 James Road	35	6.6	S	27	3
IV06	El Centro Array 6, 551 Huston Road	35	6.6	S	27	3
IV07	El Centro Array 7, Imperial Valley College	35	6.6	S	27	3
IV08	El Centro Array 8, 95 E. Cruickshank Road	35	6.6	S	27	3
IV09	El Centro Array 9, 302 Commercial Avenue	35	6.6	S	27	3
IV10	El Centro Array 10, Community Hospital	35	6.6	S	27	3
IV11	El Centro Array 11, McCabe School	35	6.6	S	28	3
IV12	El Centro Array 12, 907 Brockman Road	35	6.6	S	30	3
IV13	El Centro Array 13, Strobel Residence	35	6.6	S	34	3
IV14	Parachute Test Site, Imler Road	35	6.6	S	47	3
IV15	Calipatria, Fire Station	35	6.6	S	57	3
IV16	Superstition Mountain	35	6.6	R	58	3
IV17	Plaster City, Storehouse	35	6.6	S	52	3
IV18	Coachella Canal, Station 4	35	6.6	S	84	3

TABLE 3.2 (Cont'd.)

I.D. NO.	RECORDING STATION LOCATION	EQ. ID. NO.	R.M.	SITE	EPI. DIST. (km)	REFERENCE FOR EPI. DIST.
IV19	Bonds Corner, Highways 98 & 115	35	6.6	S	6	3
IV20	Brawley Municipal Airport	35	6.6	S	42	3
IV21	Holtville Post Office	35	6.6	S	20	3
IV22	Calexico, Fire Station	35	6.6	S	15	3

FOOTNOTES

[1] Per Table 3.1

[2] Richter Magnitude per Table 3.1

[3] R - Rock Site
S - Soil Site

[4] Caltech EERL No.

[5] 15 October 1979 Imperial Valley Earthquake ID No.

REFERENCES

1. McGuire and Barnhard (1977)

2. Maley and Cloud (1973)

3. Porcella, Matthiesen, and Maley (1982)

TABLE 3.3

Probability Distributions Analyzed in Investigation

CASE NUMBER	PROBABILITY DISTRIBUTION
1	Exponential
2	Rayleigh
3	Exponential (EHT)
4	Rayleigh (EHT)
5	General (EHT)[1] Exponential (EHT) Rayleigh (EHT) Weibull (EHT)
6	N* Exponential (EHT)[2]
7	N* Rayleigh (EHT)[3]

[1]Model selects the appropriate distribution from the three listed.

[2]Same as Case 3 but assumes a standardized number of peaks, N*.

[3]Same as Case 4 but assumes a standardized number of peaks, N*.

TABLE 3.4

Summary of EHT Probability Distributions
for Ground Motion Time Histories

Ground Motion Record	Acceleration			Velocity			Displacement		
	Dist.[1]	N/2	1/λ	Dist.	N/2	1/λ	Dist.	N/2	1/λ
A001 S00E	0	137	54.609	1	12	16.446	1	12	6.005
A001 S90W	0	154	38.662	0	28	7.985	1	5	11.099
A002 S44W	0	72	17.123	0	57	1.029	1	4	1.293
A002 N46W	0	50	20.286	0	50	1.352	1	4	1.513
A003 S00E	0	100	8.562	1	22	3.040	1	11	1.520
A003 S90W	1	31	25.186	1	16	4.420	1	11	1.654
A004 N21E	0	153	27.258	0	56	2.921	1	11	3.657
A004 S69E	0	160	27.587	0	48	3.446	1	8	4.914
A006 S00W	1	50	21.891	1	23	3.172	0	20	1.118
A006 N90E	1	48	19.582	1	21	4.412	0	18	1.621
A007 S00W	1	62	22.137	1	29	3.138	1	13	2.054
A007 N90E	1	54	19.723	1	18	4.363	1	9	3.326
A008 N11W	1	14	80.782	2	56	.904	0	18	2.783
A008 N79E	1	9	142.407	2	65	1.077	1	3	8.035
A009 N44E	2	112	6.133	2	55	1.515	2	17	.912
A009 N46W	2	120	5.207	2	44	1.317	0	14	2.256
A011 S00W	1	54	15.186	1	37	1.994	1	15	1.216
A011 S90W	1	40	22.823	1	30	3.274	0	31	.892
A014 N09W	2	296	1.132	2	57	.125	1	5	.711
A014 N81E	2	265	1.138	2	93	.091	1	6	.553
A015 N10E	1	8	43.611	1	3	2.848	1	2	1.376
A015 S80E	1	11	53.725	2	56	.166	1	7	.424
A016 S09E	2	220	2.308	2	71	.208	1	4	.651
A016 S81W	1	17	28.467	2	74	.173	1	7	.505
A017 N26E	2	187	1.033	1	27	.793	1	8	.818
A017 S64E	0	66	4.823	1	18	.599	1	5	.619
A019 S00W	2	230	3.126	2	53	1.272	1	12	6.250
A019 S90W	1	45	24.107	1	17	6.908	1	8	5.819
B021 S08W	0	55	26.448	2	67	.861	2	19	1.072
B021 N82W	2	209	3.841	2	50	.779	1	4	10.327
B023 N00E	0	74	5.067	0	44	.432	1	6	.426
B023 N90W	0	80	4.746	0	58	.422	1	14	.219
B024 S00W	1	49	66.808	2	125	.637	1	11	2.238
B024 S90W	0	100	35.160	1	23	5.608	1	12	1.955
B025 S00W	2	320	2.413	2	43	.267	2	14	.093
B025 S90W	0	18	38.883	0	4	4.593	1	2	2.283
B026 N45E	2	183	3.328	1	11	3.292	1	2	2.384
B026 S45E	2	195	2.966	2	117	.219	2	31	.067
B027 N45E	0	59	11.283	1	21	1.735	1	11	1.061
B027 S45E	1	27	19.241	1	43	1.334	1	11	1.029
B029 N04W	1	69	69.367	0	49	3.831	2	28	.507
B029 N86E	0	144	40.982	1	16	9.149	2	33	.518
B030 N44E	2	200	1.995	2	64	.322	1	9	1.026
B030 S46E	2	214	2.068	1	16	2.294	1	9	1.023
B031 N21E	2	237	1.775	2	82	.215	1	9	.907
B031 S69E	0	66	12.161	0	63	.661	1	12	.566
B032 S04E	0	142	25.739	0	69	1.687	1	8	1.487
B032 S86W	0	137	30.791	2	120	.523	1	8	1.963

TABLE 3.4
(Cont'd.)

Ground Motion Record	Acceleration			Velocity			Displacement		
	Dist.	N/2	1/λ	Dist.	N/2	1/λ	Dist.	N/2	1/λ
B034 N05W	2	222	7.017	2	61	.863	1	8	2.980
B034 N85E	2	176	9.164	1	10	11.978	0	10	1.982
B037 N65W	0	23	55.507	2	46	.680	1	4	2.572
B037 S25W	0	12	80.983	2	51	.781	0	4	1.801
B038 N36W	0	117	2.604	1	17	.575	1	5	.663
B038 S54W	0	136	2.017	1	20	.390	1	6	.313
B039 S11E	1	11	10.131	0	23	.522	1	9	.470
B039 N79E	1	13	9.105	0	19	.628	1	5	.768
B040 N33E	0	151	6.179	0	50	.723	1	8	.910
B040 N57W	0	133	7.107	1	21	1.946	1	6	1.552
C048 N00W	1	33	104.189	1	13	15.383	1	12	7.007
C048 S90W	1	41	65.771	1	13	12.820	1	8	7.462
C054 N52W	2	230	3.456	1	6	10.026	0	10	3.182
C054 S38W	1	32	50.137	2	46	.886	1	4	6.556
D056 N21E	2	340	6.594	0	42	3.174	1	7	2.195
D056 N69W	0	81	47.167	2	96	1.021	1	4	5.090
D057 S00W	1	28	49.134	0	25	3.799	1	5	4.679
D057 N90E	1	25	68.241	1	11	10.034	2	35	.562
D058 S00W	1	32	80.013	2	70	.604	1	4	4.607
D058 N90E	1	23	103.450	1	12	10.532	1	4	8.288
D059 N46W	0	64	26.128	1	16	4.629	2	28	.395
D059 S44W	0	68	31.423	0	25	3.728	2	24	.716
D062 N38W	0	64	25.553	2	51	.785	0	4	3.956
D062 S52W	1	28	66.653	1	9	8.873	0	9	1.937
D065 S00W	0	51	25.755	2	39	.972	1	4	5.785
D065 S90W	1	23	70.997	1	8	11.255	1	5	7.591
D068 N00E	1	23	42.029	2	49	.469	0	6	2.226
D068 N90E	0	56	20.435	1	9	6.642	1	4	4.315
E072 N75W	1	23	41.552	1	7	11.012	1	5	8.328
E072 N15E	1	27	54.514	0	12	5.744	1	4	6.534
E075 N00E	0	58	29.806	2	45	1.172	0	11	2.818
E075 S90W	1	27	53.259	1	7	10.202	1	5	6.935
E078 N50W	0	52	24.874	0	15	5.453	2	19	.708
E078 S40W	2	318	4.054	2	49	.817	2	23	.476
E083 S00W	1	25	80.717	2	54	.988	0	13	2.279
E083 N90E	1	26	76.243	1	15	8.118	0	9	2.984
F086 N83W	0	60	19.844	2	54	.912	1	5	7.800
F086 S07W	1	32	35.334	2	67	.577	2	26	.525
F087 S04E	1	76	10.853	1	30	2.328	1	15	1.894
F087 S86W	1	57	12.785	0	44	1.446	1	14	2.706
F088 S70E	1	17	127.008	0	19	8.353	1	2	6.763
F088 S20W	1	25	93.947	1	10	11.727	2	35	.306
F089 S53E	0	61	29.559	1	7	11.361	1	4	8.309
F089 S37W	0	60	26.212	2	51	.892	2	25	.647
F092 S62E	0	55	14.834	1	6	7.537	2	12	.668
F092 S28W	0	61	16.692	0	20	2.768	1	5	3.422
F095 S88E	1	22	42.880	2	54	.819	2	27	.521
F095 S02W	1	26	42.528	2	54	.718	2	22	.661
F098 S53E	2	323	5.846	1	9	10.621	1	5	7.384
F098 S37W	0	60	37.473	0	26	4.166	2	18	.769

TABLE 3.4
(Cont'd.)

Ground Motion Record	Acceleration			Velocity			Displacement		
	Dist.[1]	N/2	1/λ	Dist.	N/2	1/λ	Dist.	N/2	1/λ
F101 S00W	1	36	17.528	1	14	1.270	1	4	.640
F101 N90E	1	38	13.384	1	15	1.132	1	3	.798
F102 N00E	0	92	4.603	1	8	.772	1	3	.477
F102 N90E	1	50	9.185	0	22	.331	1	5	.448
F103 N00E	1	54	39.084	1	27	2.056	1	5	1.427
F103 N90W	1	53	50.892	1	28	2.376	1	4	1.446
F105 S00W	1	33	37.721	2	61	.393	0	15	1.081
F105 N90E	1	35	33.213	1	10	4.475	0	18	1.277
G106 S00W	0	116	17.101	2	119	.221	0	33	.338
G106 S90W	0	57	37.377	0	26	2.778	2	33	.243
G107 N00E	0	82	18.551	1	17	4.115	1	10	1.412
G107 N90E	1	24	48.768	0	24	3.333	1	5	3.875
G108 N00E	2	384	4.393	1	17	5.120	1	10	1.490
G108 N90E	2	301	4.148	2	100	.643	2	36	.309
G110 S82E	0	48	39.217	2	101	.483	0	18	1.226
G110 S08W	0	70	25.663	2	91	.379	2	39	.158
G112 N38E	0	55	21.678	2	39	.847	0	9	3.149
G112 N52W	1	36	35.350	2	37	.925	0	13	2.374
G114 S60E	1	45	52.722	0	33	3.351	1	9	2.063
G114 S30W	0	94	24.334	1	25	4.267	1	15	1.328
H115 N11E	1	41	91.853	0	37	6.198	1	6	7.757
H115 N79W	1	40	66.772	1	15	11.003	1	12	5.042
H118 S45E	1	43	15.466	0	31	3.065	0	27	2.207
H118 S45W	1	50	14.721	0	35	2.349	0	30	1.768
H121 S90W	0	76	23.785	1	8	8.794	0	10	2.369
H121 S00W	1	29	54.326	1	11	5.774	1	6	2.338
H124 S90W	1	62	12.764	1	12	2.275	1	8	1.220
H124 S00W	1	44	15.465	1	11	2.829	1	8	1.511
I137 S81E	0	108	24.285	1	19	7.883	1	10	3.669
I137 S09W	1	41	57.150	0	32	5.662	0	19	2.286
J141 N21E	2	315	2.920	2	102	.540	0	12	.995
J141 S69E	0	112	17.328	2	88	.500	1	8	1.628
J142 S69E	0	149	25.413	0	46	1.172	1	6	.670
J142 S21W	2	409	4.105	2	52	.426	0	14	.508
J143 N21E	0	69	23.352	1	15	2.352	1	7	1.089
J143 N69W	0	81	22.331	1	16	2.132	1	5	1.373
J144 N21E	2	274	10.009	2	99	.560	1	7	1.000
J144 N69W	2	313	8.624	0	30	3.053	1	4	4.899
J145 S00W	1	38	55.979	1	12	15.198	1	10	8.532
J145 S90W	1	29	54.272	1	11	14.597	2	42	.785
J148 N00E	1	35	50.692	1	8	8.685	1	4	4.082
J148 S90W	1	34	53.011	1	11	9.059	1	4	6.322
K157 S53E	2	282	3.992	1	7	9.789	0	22	2.253
K157 S37W	0	63	22.611	1	8	8.546	2	36	.409
L166 N00E	2	309	3.905	2	63	.570	2	23	.296
L166 S90W	0	55	32.973	2	69	.583	2	31	.261
L171 N33E	1	51	5.314	1	24	.916	1	7	1.058
L171 N57W	0	103	2.830	0	26	.621	1	8	1.127
M176 N37E	1	30	39.383	2	58	.915	2	30	.654
M176 S53E	0	60	21.850	2	56	.857	1	5	7.669

TABLE 3.4
(Cont'd.)

Ground Motion Record	Acceleration			Velocity			Displacement		
	Dist.	N/2	1/λ	Dist.	N/2	1/λ	Dist.	N/2	1/λ
M179 S00W	0	117	3.279	1	7	.612	1	3	.425
M179 N90E	1	19	23.242	2	38	.127	1	4	.539
M180 S00W	1	64	11.088	1	31	2.243	1	16	1.748
M180 S90W	1	59	12.010	1	16	4.185	1	15	3.278
M183 N65W	0	144	7.384	1	12	1.765	1	5	.713
M183 N25E	0	119	9.267	1	22	1.322	1	6	.506
M184 S65E	0	169	7.219	2	53	.217	1	8	.646
M184 S25W	0	133	9.196	1	21	1.385	1	9	.376
N185 S50E	1	70	26.690	1	25	1.745	1	10	.966
N185 S40W	1	58	30.362	1	30	2.017	1	11	.995
N186 S37E	0	99	17.036	0	43	1.720	2	30	.298
N186 S53W	0	115	19.616	1	14	4.486	0	23	1.194
N187 N15E	0	142	10.286	0	60	.623	1	9	.389
N187 N75W	1	46	34.496	1	34	1.558	1	7	.418
N188 N54E	1	30	47.908	0	22	3.568	1	5	5.825
N188 N36W	1	31	64.971	0	40	2.514	0	19	1.314
N191 N65E	1	59	11.136	1	20	2.122	1	17	1.250
N191 S25E	0	124	6.020	1	24	2.244	1	11	1.660
N192 N29E	1	40	43.543	1	7	8.090	1	5	4.265
N192 N61W	1	31	47.223	1	7	10.256	1	5	4.715
N195 N33E	0	119	7.731	1	26	1.910	0	31	.497
N195 N57W	0	128	6.528	0	66	.875	1	17	1.175
N196 N76W	1	45	17.304	1	13	4.705	0	12	2.214
N196 S14W	1	47	15.604	1	17	4.573	1	12	3.337
N197 N45E	0	113	4.404	1	21	.955	1	5	.659
N197 N45W	0	93	6.855	0	60	.510	1	9	.549
0198 S00W	2	254	5.175	2	45	.976	1	4	4.249
0198 S90W	1	35	76.695	1	14	7.456	0	14	1.522
0199 N28E	1	28	63.702	0	23	4.407	0	13	2.510
0199 N62W	2	267	6.375	1	9	11.499	1	6	5.943
0204 N00E	1	60	10.589	1	17	4.099	1	15	2.928
0204 N90E	1	59	9.371	1	11	5.131	1	10	4.218
0205 N21W	1	69	11.177	1	20	3.766	1	19	3.031
0205 S69W	1	75	11.909	1	15	4.894	1	12	4.222
0206 N00E	0	124	6.676	0	52	.676	1	12	.740
0206 N90E	0	121	6.569	1	35	1.250	1	14	.499
0207 N56E	2	414	1.561	2	74	.188	1	12	.628
0207 N34W	2	347	2.004	2	58	.258	1	7	.864
0210 S45E	0	122	6.131	0	40	.604	0	16	.425
0210 S45W	0	123	7.329	1	26	1.343	1	11	.680
P214 S89W	1	20	77.595	2	41	1.132	1	5	4.647
P214 S01E	1	26	76.049	1	10	8.377	1	5	4.320
P217 S00W	0	55	23.728	0	28	3.536	1	4	5.492
P217 N90E	1	21	42.385	1	7	8.964	1	4	5.549
P220 S00W	1	73	9.770	0	31	1.545	1	7	3.524
P220 N90E	0	109	6.613	1	22	2.998	1	12	3.255
P221 N03E	0	145	25.827	1	18	2.466	1	6	1.728
P221 N87W	0	122	29.720	1	15	3.235	1	3	3.405
P222 S00W	1	53	12.517	1	24	3.267	1	13	2.387
P222 S90W	1	72	10.475	0	52	1.187	2	27	.282

TABLE 3.4
(Cont'd.)

Ground Motion Record	Acceleration			Velocity			Displacement		
	Dist.	N/2	1/λ	Dist.	N/2	1/λ	Dist.	N/2	1/λ
P223 N55E	0	94	11.912	1	11	2.341	1	5	1.195
P223 N35W	0	112	9.998	0	35	.853	1	5	1.074
P231 N00E	1	40	17.076	1	12	5.378	1	5	4.776
P231 S90W	1	39	17.211	0	25	3.400	1	6	6.034
Q233 S12W	1	22	131.572	0	31	6.609	0	13	4.548
Q233 N78W	1	39	90.943	1	18	9.199	1	14	4.525
Q236 SOUTH	0	86	32.136	1	10	7.202	1	9	3.291
Q236 EAST	0	126	21.735	2	58	.451	2	21	.334
Q239 SOUTH	1	34	58.655	1	11	8.333	1	5	5.452
Q239 EAST	0	84	26.956	2	51	.945	1	6	6.490
Q241 N37E	1	38	44.197	2	50	.897	2	18	.597
Q241 N53W	2	241	3.652	0	20	4.643	0	15	2.561
R244 N53W	2	263	3.636	2	37	1.047	1	5	5.528
R244 S37W	0	55	25.683	2	49	.881	0	11	2.491
R246 SOUTH	0	78	22.694	2	46	.809	2	22	.469
R246 EAST	1	37	50.337	0	16	4.966	2	19	.656
R249 N44E	0	87	17.834	1	9	8.288	0	13	2.767
R249 S46E	1	31	39.985	1	13	5.169	0	15	1.728
R251 N37E	1	26	82.443	1	11	8.425	1	4	5.455
R251 S53E	2	188	5.226	2	51	1.024	1	3	5.899
R253 N30W	2	234	6.461	0	15	5.479	1	4	6.511
R253 S60W	0	58	39.920	0	22	4.489	1	3	7.399
S255 N08E	1	24	62.258	0	21	5.481	0	10	4.499
S255 N82W	0	70	22.521	2	39	1.017	0	20	2.464
S258 N29E	1	27	28.296	2	34	.910	0	11	2.826
S258 S61E	0	65	15.407	1	11	9.398	1	7	5.759
S262 N83W	1	17	35.343	0	15	6.466	1	6	9.349
S262 S07W	0	39	20.039	1	5	15.158	1	5	7.426
S265 SOUTH	1	28	51.222	1	5	9.714	1	5	4.584
S265 WEST	1	35	54.036	0	13	4.713	1	3	7.231
S266 NORTH	0	64	31.392	0	26	4.057	1	9	4.099
S266 WEST	1	28	58.537	2	36	1.226	1	5	6.234
S267 NORTH	1	38	24.626	0	22	3.188	1	7	4.764
S267 EAST	0	99	11.556	1	11	7.315	1	7	5.371
T286 NORTH	0	165	10.308	1	32	3.134	1	17	2.341
T286 EAST	1	65	18.259	1	26	2.734	1	15	1.968
T287 NORTH	0	128	5.766	1	23	1.390	1	6	1.077
T287 EAST	0	130	5.224	1	24	1.456	1	17	.522
T288 NORTH	0	311	.810	1	8	.692	1	10	.640
T288 EAST	0	213	5.553	2	120	.186	1	16	.719
T289 NORTH	0	231	2.966	2	124	.130	1	14	.530
T289 EAST	0	167	3.624	0	79	.577	2	29	.103
U294 N45W	1	41	7.407	1	28	.658	1	7	.624
U294 S45W	0	103	2.510	1	24	.532	1	6	.708
U295 NORTH	0	14	6.605	1	7	.271	1	4	.179
U295 EAST	0	18	4.809	0	13	.085	1	5	.097
U297 NORTH	0	50	14.502	2	53	.103	1	6	.489
U297 EAST	0	38	17.676	1	5	2.063	1	3	.575

TABLE 3.4
(Cont'd.)

Ground Motion Record	Acceleration			Velocity			Displacement		
	Dist.	N/2	1/λ	Dist.	N/2	1/λ	Dist.	N/2	1/λ
U298 N45W	2	196	1.396	0	78	.542	1	12	.471
U298 S45W	2	212	1.175	0	74	.456	1	11	.542
U300 N45W	2	190	2.963	0	68	1.250	1	7	1.664
U300 S45W	2	211	3.070	0	75	1.053	1	9	1.180
U308 N46W	2	221	1.660	0	83	.566	1	9	.618
U308 S44W	2	201	1.979	0	66	.650	1	12	.672
U310 S32E	1	32	26.219	0	57	1.050	0	24	.565
U310 S58W	0	69	16.289	2	105	.368	2	27	.237
U311 N21E	1	35	3.756	1	14	1.109	0	17	.594
U311 S69E	0	59	2.270	0	40	.444	1	11	.727
U312 N46W	2	187	2.275	2	110	.270	0	29	.338
U312 S44W	2	176	3.069	2	117	.257	0	22	.328
U319 N36W	0	39	11.327	1	17	1.556	1	8	.433
U319 S54W	1	20	17.961	1	17	1.499	0	16	.344
U329 SOUTH	0	11	40.186	2	52	.374	1	4	2.341
U329 WEST	2	198	1.205	0	16	1.777	1	4	1.524
U330 N79E	2	274	.871	2	67	.143	1	9	.930
U330 S11E	2	244	.879	2	66	.127	1	11	.626
U331 SOUTH	1	11	19.681	1	5	1.206	1	3	.556
U331 EAST	2	77	1.547	1	10	.546	1	3	.240
W334 S65E	1	15	65.098	0	20	2.055	1	3	1.241
W334 S25W	2	131	5.459	2	35	.438	1	5	.615
W335 S85E	0	21	21.043	0	4	1.647	1	4	1.322
W335 S05W	1	13	29.036	1	10	.987	1	5	1.140
W338 NORTH	1	9	57.078	0	25	1.112	1	6	.977
W338 EAST	1	19	30.093	0	38	.654	1	5	.936
W342 NORTH	1	45	8.332	1	17	.744	1	4	.957
W342 EAST	0	82	3.916	0	16	.372	1	5	.693
W344 S82E	0	114	2.503	1	12	.568	1	4	.570
W344 S08W	2	188	.704	1	5	1.179	1	4	1.345
Y371 S04E	0	120	2.397	1	13	2.296	1	12	1.852
Y371 S86W	1	60	4.939	0	42	.733	0	22	.606
Y373 S82E	0	77	1.472	0	43	.249	1	7	.294
Y373 S08W	0	77	1.481	0	26	.305	1	7	.390
Y375 NORTH	1	46	4.290	1	26	1.054	0	16	.390
Y375 EAST	1	43	4.765	1	19	1.208	1	9	.989
Y376 SOUTH	0	96	1.483	1	20	.928	1	6	1.045
Y376 WEST	0	94	1.853	0	37	.527	1	7	.835
Y379 N83W	0	89	3.295	1	27	1.906	1	12	1.256
Y379 S07W	0	83	3.410	1	17	2.090	1	12	1.302
Y380 SOUTH	0	93	2.169	1	12	1.312	1	5	1.274
Y380 EAST	0	83	2.396	1	12	1.547	1	11	.756
IV01 230	0	165	22.153	0	31	2.176	1	8	2.416
IV01 140	1	58	60.228	0	19	3.213	1	9	3.155
IV02 230	2	248	11.441	2	41	1.362	1	4	7.502
IV02 140	1	21	157.502	1	11	15.011	1	8	5.147
IV03 230	1	38	95.771	2	26	1.803	0	8	5.013
IV03 140	1	24	131.639	2	40	1.840	0	12	3.802
IV04 230	2	197	8.114	0	8	22.920	1	3	27.648
IV04 140	2	215	9.899	0	17	9.872	1	7	6.559

TABLE 3.4
(Cont'd.)

Ground Motion Record	Acceleration			Velocity			Displacement		
	Dist.	N/2	1/λ	Dist.	N/2	1/λ	Dist.	N/2	1/λ
IU05 230	2	185	12.374	0	6	26.892	0	8	13.755
IU05 140	2	226	12.204	0	21	12.108	1	5	12.091
IU06 230	2	204	13.289	0	4	36.310	0	15	14.397
IU06 140	0	72	69.920	0	7	19.308	1	3	15.620
IU07 230	0	47	74.628	0	23	26.256	0	5	13.895
IU07 140	2	197	6.727	0	8	13.878	0	7	5.454
IU08 230	0	54	91.841	0	8	14.177	1	4	16.216
IU08 140	2	234	13.464	1	4	30.152	2	17	1.302
IU09 360	0	42	105.096	0	10	13.483	1	7	7.199
IU09 270	1	23	179.701	0	9	17.547	1	3	19.806
IU10 50	0	80	33.988	1	4	24.540	1	5	14.361
IU10 320	0	69	41.315	2	30	2.085	2	18	1.028
IU11 230	1	19	176.948	2	45	1.886	0	11	3.792
IU11 140	1	33	165.737	0	26	7.638	1	7	7.571
IU12 230	1	53	51.888	0	26	4.076	1	9	4.632
IU12 140	1	48	57.677	1	12	9.506	1	9	4.848
IU13 230	0	115	23.784	0	36	2.900	1	10	3.207
IU13 140	1	47	51.483	0	37	2.957	1	7	3.024
IU14 315	2	248	4.597	2	46	.736	0	12	1.962
IU14 225	0	122	19.563	0	18	4.209	1	9	4.493
IU15 315	0	116	12.485	1	13	5.907	1	12	2.664
IU15 228	0	112	16.185	0	22	3.210	1	11	3.463
IU16 135	2	224	5.680	2	62	.407	1	6	1.034
IU16 45	0	105	17.418	0	46	.961	1	7	1.069
IU17 135	1	48	25.190	0	31	1.161	1	6	.967
IU17 45	1	40	19.921	1	12	1.702	1	5	.824
IU18 135	2	119	4.605	2	56	.664	2	22	.172
IU18 45	2	151	3.244	2	49	.544	1	8	1.217
IU19 230	0	49	160.172	1	14	22.846	2	25	.788
IU19 140	0	55	128.746	1	12	21.473	0	8	3.525
IU20 315	2	249	5.701	2	27	1.652	1	9	5.086
IU20 225	2	244	5.320	2	24	1.859	0	11	4.474
IU21 315	1	28	105.040	0	11	11.572	1	4	12.384
IU21 225	1	28	106.531	1	3	26.355	0	5	8.072
IU22 315	1	45	88.680	1	16	8.464	1	11	3.689
IU22 225	0	66	51.823	0	37	4.335	1	6	3.178

[1] 0 - Exponential (EHT) Distribution
1 - Rayleigh (EHT) Distribution
2 - Weibull (EHT) Distribution

TABLE 3.5

Percentage of Ground Motion Records on Soil and Rock Sites
Whose Largest Peaks Follow A Given EHT Probability Distribution
(332 Records from 35 Earthquakes)

Ground Motion Component		EXPONENTIAL-HALF-TAIL DISTRIBUTION		
		Exponential	Rayleigh	Weibull
Acceleration:	Soil	36%	46%	18%
	Rock	57%	18%	25%
Velocity:	Soil	31%	45%	24%
	Rock	30%	38%	32%
Displacement:	Soil	19%	70%	11%
	Rock	15%	72%	13%

TABLE 3.6

Percentage of Ground Motion Records on Soil and Rock Sites
Whose Largest Peaks Follow A Given EHT Probability Distribution
from the 9 February 1971 San Fernando, CA Earthquake
(176 records: 138 soil sites, 38 rock sites)

Ground Motion Component		Exponential Half-Tail Distribution		
		Exponential	Rayleigh	Weibull
Acceleration:	Soil	35%	58%	7%
	Rock	53%	18%	29%
Velocity:	Soil	26%	51%	23%
	Rock	24%	42%	34%
Displacement:	Soil	21%	66%	13%
	Rock	16%	63%	21%

TABLE 3.7

Percentage of Ground Motion Records on Soil and Rock Sites
Whose Largest Peaks Follow A Given EHT Probability Distribution
from the 15 October 1979 Imperial Valley, CA Earthquake
(44 records: 42 soil sites, 2 rock sites)

		Exponential Half-Tail Distribution		
Ground Motion Component		Exponential	Rayleigh	Weibull
Acceleration:	Soil	33%	36%	31%
	Rock[1]	50%	0%	50%
Velocity:	Soil	52%	24%	24%
	Rock[1]	50%	0%	50%
Displacement:	Soil	26%	64%	10%
	Rock[1]	0%	100%	0%

[1]Based on records from only 2 rock sites.

TABLE 3.8

Standardized Number of Peaks N* in Ground Motion Records for the Exponential (EHT) and Rayleigh (EHT) Distributions

Ground Motion Component	PROBABILITY DISTRIBUTION	
	Exponential (EHT)	Rayleigh (EHT)
Acceleration		
Soil	128	47
Rock	121	52
Soil and Rock	127	48
Velocity		
Soil	36	26
Rock	41	21
Soil and Rock	37	25
Displacement		
Soil	21	14
Rock	16	13
Soil and Rock	20	14

TABLE 3.9

Percentage of Ground Motion Acceleration Records
Passing Selected Significance Levels of
the Kolmogorov-Smirnov Test

DISTRIBUTION	SIGNIFICANCE LEVELS 1%	5%	10%
Soil (266 records)			
Exponential	0	0	0
Rayleigh	0	0	0
Exponential (EHT)	82	85	91
Rayleigh (EHT)	86	87	89
General (EHT)			
Exponential (EHT)	91	96	98
Rayleigh (EHT)	100	100	100
Weibull (EHT)	0	0	0
Rock (66 records)			
Exponential	0	0	0
Rayleigh	0	0	0
Exponential (EHT)	85	92	100
Rayleigh (EHT)	90	93	94
General (EHT)			
Exponential (EHT)	100	100	100
Rayleigh (EHT)	100	100	100
Weibull (EHT)	0	0	0
Soil and Rock (332 records)			
Exponential	0	0	0
Rayleigh	0	0	0
Exponential (EHT)	84	88	96
Rayleigh (EHT)	88	90	92
General (EHT)			
Exponential (EHT)	96	97	99
Rayleigh (EHT)	100	100	100
Weibull (EHT)	0	0	0

TABLE 3.10

Percentage of Ground Motion Velocity Records
Passing Selected Significance Levels of
the Kolmogorov-Smirnov Test

DISTRIBUTION	SIGNIFICANCE LEVELS 1%	5%	10%
Soil (266 records)			
Exponential	0	0	0
Rayleigh	0	0	0
Exponential (EHT)	91	96	97
Rayleigh (EHT)	86	87	87
General (EHT)			
Exponential (EHT)	95	97	97
Rayleigh (EHT)	100	100	100
Weibull (EHT)	0	0	0
Rock (66 records)			
Exponential	0	0	0
Rayleigh	0	0	0
Exponential (EHT)	96	97	99
Rayleigh (EHT)	91	92	92
General (EHT)			
Exponential (EHT)	100	100	100
Rayleigh (EHT)	100	100	100
Weibull (EHT)	0	0	0
Soil and Rock (332 records)			
Exponential	0	0	0
Rayleigh	0	0	0
Exponential (EHT)	94	97	98
Rayleigh (EHT)	89	89	90
General (EHT)			
Exponential (EHT)	97	99	99
Rayleigh (EHT)	100	100	100
Weibull (EHT)	0	0	0

Table 3.11

Percentage of Ground Motion Displacement Records
Passing Selected Significance Levels of
the Kolmogorov-Smirnov Test

DISTRIBUTION	SIGNIFICANCE LEVELS 1%	5%	10%
Soil (266 records)			
Exponential	0	0	0
Rayleigh	0	0	0
Exponential (EHT)	96	96	97
Rayleigh (EHT)	82	82	82
General (EHT)			
Exponential (EHT)	93	93	93
Rayleigh (EHT)	93	98	98
Weibull (EHT)	0	0	0
Rock (66 records)			
Exponential	0	0	0
Rayleigh	0	0	0
Exponential (EHT)	100	100	100
Rayleigh (EHT)	90	92	92
General (EHT)			
Exponential (EHT)	95	95	95
Rayleigh (EHT)	100	100	100
Weibull (EHT)	0	0	0
Soil and Rock (332 records)			
Exponential	0	0	0
Rayleigh	0	0	0
Exponential (EHT)	98	98	98
Rayleigh (EHT)	86	87	87
General (EHT)			
Exponential (EHT)	94	94	94
Rayleigh (EHT)	96	99	99
Weibull (EHT)	0	0	0

TABLE 3.12

Standard Error, E(k), Between Observed X(k) and Predicted $\bar{X}(k)$ Peaks in Ground Motion Acceleration Records (Soil and Rock Records Combined)

PEAK	PROBABILITY DISTRIBUTION	E(k)
X(1)	Rayleigh (EHT)	0.09
	N* Rayleigh (EHT)	0.11
	General (EHT)	0.14
	Exponential (EHT)	0.19
	N* Exponential (EHT)	0.19
	Rayleigh	0.29
	Exponential	0.39
X(2)	General (EHT)	0.12
	Exponential (EHT)	0.13
	N* Exponential (EHT)	0.15
	Rayleigh (EHT)	0.18
	N* Rayleigh (EHT)	0.23
	Rayleigh	0.26
	Exponential	0.37
X(5)	General (EHT)	0.10
	Exponential (EHT)	0.12
	N* Exponential (EHT)	0.23
	Exponential	0.33
	Rayleigh (EHT)	0.46
	N* Rayleigh (EHT)	0.47
	Rayleigh	0.68
X(10)	General (EHT)	0.11
	Exponential (EHT)	0.15
	Exponential	0.30
	N* Exponential (EHT)	0.34
	N* Rayleigh (EHT)	0.70
	Rayleigh (EHT)	0.72
	Rayleigh	0.88
X(20)	General (EHT)	0.11
	Exponential	0.24
	Exponential (EHT)	0.24
	N* Exponential (EHT)	0.59
	N* Rayleigh (EHT)	1.20
	Rayleigh (EHT)	1.37
	Rayleigh	1.82

TABLE 3.13

Standard Error, E(k), Between Observed X(k) and Predicted $\bar{X}(k)$ Peaks in Ground Motion Velocity Records (Soil and Rock Records Combined)

PEAK	PROBABILITY DISTRIBUTION	E(k)
X(1)	Rayleigh (EHT)	0.09
	N* Rayleigh (EHT)	0.13
	Exponential (EHT)	0.15
	General (EHT)	0.16
	N* Exponential (EHT)	0.16
	Rayleigh	0.28
	Exponential	0.33
X(2)	Exponential (EHT)	0.13
	General (EHT)	0.14
	N* Exponential (EHT)	0.20
	Rayleigh (EHT)	0.27
	Exponential (EHT)	0.28
	Rayleigh	0.29
	N* Rayleigh (EHT)	0.31
X(5)	Exponential	0.20
	General (EHT)	0.21
	Exponential (EHT)	0.42
	N* Exponential (EHT)	0.53
	Rayleigh	0.92
	Rayleigh (EHT)	0.98
	N* Rayleigh (EHT)	1.11
X(10)	Exponential	0.21
	General (EHT)	0.43
	Exponential (EHT)	0.61
	N* Exponential (EHT)	0.82
	N* Rayleigh (EHT)	1.78
	Rayleigh (EHT)	1.97
	Rayleigh	2.72
X(20)	Exponential	0.42
	General (EHT)	0.68
	N* Exponential (EHT)	1.21
	Exponential (EHT)	1.25
	N* Rayleigh (EHT)	4.31
	Rayleigh (EHT)	4.72
	Rayleigh	5.31

TABLE 3.14

Standard Error, E(k), Between Observed X(k) and Predicted $\bar{X}(k)$ Peaks in Ground Motion Displacement Time Histories (Soil and Rock Records Combined)

PEAK	PROBABILITY DISTRIBUTION	E(k)
X(1)	Rayleigh (EHT)	0.08
	General (EHT)	0.08
	N* Rayleigh (EHT)	0.10
	Exponential (EHT)	0.13
	N* Exponential (EHT)	0.14
	Rayleigh	0.27
	Exponential	0.39
X(2)	Exponential (EHT)	0.06
	General (EHT)	0.14
	Rayleigh (EHT)	0.17
	N* Rayleigh (EHT)	0.18
	N* Exponential (EHT)	0.19
	Exponential	0.26
	Rayleigh	0.26
X(5)	Exponential	0.43
	Rayleigh	0.61
	Exponential (EHT)	0.82
	General (EHT)	1.70
	Rayleigh (EHT)	1.72
	N* Rayleigh (EHT)	1.72
	N* Exponential (EHT)	1.91

TABLE 3.15

Summary of Probability Distributions Which Minimize the Standard Error, E(k), Between the Observed and Predicted Peaks of Ground Motion Acceleration, Velocity, and Displacement Time Histories[1]

	GROUND MOTION COMPONENT		
PEAK	ACCELERATION	VELOCITY	DISPLACEMENT
X(1)	Rayleigh (EHT)	Rayleigh (EHT)	Rayleigh (EHT)
X(2)	Exponential (EHT)[2]	Exponential (EHT)	Exponential (EHT)
X(5)	Exponential (EHT)[2]	Exponential	Exponential
X(10)	Exponential (EHT)[2]	Exponential	--
X(20)	Exponential[2]	Exponential	--

[1] Summary of Tables 3.12, 3.13, and 3.14

[2] General (EHT) distribution excluded for ground motion acceleration since E(K) of the above distributions is comparable.

TABLE 3.16

Percent Change in Magnitude of Predicted Peaks $\bar{X}(k)$ Due to Percent Exponential Change in Number of Peaks N in the Distribution

	N	Percent Change in N			
		10	50	100	200
$\bar{X}(1)$:	10	3	14	24	38
	20	3	11	19	31
	50	2	9	15	24
	100	2	8	13	21
	200	2	7	12	19
	300	2	6	11	17
$\bar{X}(2)$:	10	4	18	30	48
	20	3	14	23	37
	50	2	10	18	28
	100	2	9	15	24
	200	2	8	13	21
	300	2	7	12	20
$\bar{X}(5)$:	10	10	44	76	120
	20	6	25	43	68
	50	4	16	27	43
	100	3	13	22	34
	200	2	10	18	28
	300	2	9	16	25
$\bar{X}(10)$:	10	90	385	658	1043
	20	12	51	87	138
	50	6	24	40	64
	100	4	17	29	46
	200	3	13	22	35
	300	3	12	20	31
$\bar{X}(20)$:	10	-	-	-	-
	20	186	790	1351	2142
	50	10	42	72	114
	100	6	24	42	66
	200	4	17	29	47
	300	3	15	25	40

TABLE 4.1

Probability Distributions Analyzed for
SDOF Oscillator Response

Case Number	Probability Distribution
1	Exponential
2	Rayleigh
3	Exponential (EHT)
4	Rayleigh (EHT)

TABLE 4.2

Fraction of SDOF Oscillator Response (5% Critical Damping) Records Whose Largest Peaks Follow Exponential, Rayleigh, and Weibull EHT Distributions (112 Soil and Rock Sites)

Period (Sec)	ACCELERATION			RELATIVE VELOCITY			RELATIVE DISPLACEMENT		
	Exponential	Rayleigh	Weibull	Exponential	Rayleigh	Weibull	Exponential	Rayleigh	Weibull
0.03	0.37	0.34	0.29	0.44	0.30	0.26	0.30	0.28	0.42
0.04	0.32	0.37	0.31	0.51	0.25	0.24	0.28	0.28	0.44
0.05	0.39	0.33	0.28	0.57	0.28	0.15	0.38	0.31	0.31
0.06	0.44	0.35	0.21	0.52	0.33	0.15	0.40	0.27	0.33
0.07	0.42	0.36	0.22	0.45	0.40	0.15	0.35	0.31	0.34
0.08	0.50	0.32	0.18	0.51	0.40	0.09	0.46	0.30	0.24
0.10	0.41	0.44	0.15	0.49	0.42	0.09	0.45	0.39	0.16
0.125	0.39	0.47	0.14	0.39	0.55	0.06	0.41	0.46	0.13
0.15	0.34	0.52	0.14	0.33	0.60	0.07	0.35	0.50	0.15
0.175	0.42	0.46	0.12	0.45	0.45	0.10	0.52	0.26	0.22
0.20	0.32	0.51	0.17	0.32	0.57	0.11	0.33	0.50	0.17
0.30	0.32	0.55	0.13	0.32	0.56	0.12	0.30	0.56	0.14
0.40	0.37	0.47	0.16	0.37	0.52	0.11	0.35	0.48	0.17
0.50	0.28	0.57	0.15	0.23	0.59	0.18	0.27	0.58	0.15
0.60	0.37	0.49	0.14	0.31	0.50	0.19	0.36	0.48	0.16
0.70	0.31	0.50	0.19	0.30	0.53	0.17	0.29	0.53	0.18
0.80	0.23	0.62	0.15	0.29	0.59	0.12	0.24	0.61	0.15
1.00	0.32	0.53	0.15	0.35	0.53	0.12	0.31	0.53	0.16
1.25	0.22	0.68	0.10	0.36	0.54	0.10	0.22	0.68	0.10
1.50	0.25	0.62	0.13	0.30	0.52	0.18	0.25	0.62	0.13
1.75	0.29	0.59	0.12	0.38	0.47	0.15	0.29	0.58	0.13
2.00	0.25	0.60	0.15	0.35	0.46	0.19	0.24	0.60	0.16
2.50	0.26	0.65	0.09	0.24	0.60	0.16	0.26	0.66	0.08
3.00	0.21	0.74	0.05	0.23	0.61	0.16	0.18	0.77	0.05
4.00	0.15	0.84	0.01	0.21	0.66	0.13	0.16	0.83	0.01
5.00	0.08	0.90	0.02	0.23	0.66	0.11	0.07	0.91	0.02
6.00	0.15	0.81	0.04	0.28	0.55	0.17	0.11	0.86	0.03
7.00	0.08	0.88	0.04	0.24	0.59	0.17	0.11	0.86	0.03
8.00	0.13	0.83	0.04	0.33	0.47	0.20	0.13	0.84	0.03
10.00	0.07	0.86	0.07	0.27	0.44	0.29	0.08	0.85	0.07
12.50	0.16	0.77	0.07	0.30	0.36	0.34	0.12	0.83	0.05
15.00	0.25	0.69	0.06	0.38	0.33	0.29	0.21	0.75	0.04
17.50	0.26	0.66	0.08	0.38	0.29	0.33	0.24	0.73	0.03
20.00	0.30	0.55	0.15	0.36	0.28	0.36	0.20	0.78	0.02
25.00	0.22	0.60	0.18	0.37	0.25	0.38	0.12	0.84	0.04
30.00	0.27	0.53	0.20	0.34	0.25	0.41	0.12	0.79	0.09

TABLE 4.3

Fraction of SDOF Oscillator Response (5% Critical Damping) Records Whose Largest Peaks Follow Exponential, Rayleigh, and Weibull EHT Distributions (86 Soil Sites)

Period (Sec)	ACCELERATION			RELATIVE VELOCITY			RELATIVE DISPLACEMENT		
	Exponential	Rayleigh	Weibull	Exponential	Rayleigh	Weibull	Exponential	Rayleigh	Weibull
0.03	0.34	0.39	0.27	0.43	0.30	0.27	0.30	0.33	0.37
0.05	0.35	0.38	0.27	0.55	0.30	0.15	0.34	0.36	0.30
0.10	0.40	0.44	0.16	0.54	0.38	0.08	0.44	0.38	0.18
0.15	0.26	0.66	0.08	0.39	0.33	0.28	0.25	0.70	0.05
0.20	0.31	0.50	0.19	0.32	0.59	0.09	0.30	0.51	0.19
0.30	0.33	0.53	0.14	0.30	0.60	0.10	0.30	0.55	0.15
0.40	0.38	0.47	0.15	0.37	0.54	0.09	0.35	0.49	0.16
0.50	0.28	0.58	0.14	0.21	0.63	0.16	0.29	0.57	0.14
0.60	0.36	0.49	0.15	0.31	0.51	0.18	0.35	0.49	0.16
0.70	0.31	0.50	0.19	0.28	0.53	0.19	0.30	0.51	0.19
0.80	0.24	0.61	0.15	0.30	0.58	0.12	0.27	0.58	0.15
1.00	0.36	0.50	0.14	0.35	0.55	0.10	0.34	0.51	0.15
1.25	0.21	0.70	0.09	0.37	0.55	0.08	0.21	0.70	0.09
1.50	0.25	0.66	0.09	0.34	0.55	0.11	0.25	0.66	0.09
1.75	0.29	0.56	0.15	0.38	0.49	0.13	0.29	0.56	0.15
2.00	0.22	0.62	0.16	0.31	0.51	0.18	0.21	0.62	0.17
2.50	0.25	0.66	0.09	0.26	0.60	0.14	0.26	0.66	0.08
3.00	0.21	0.73	0.06	0.24	0.63	0.13	0.16	0.77	0.07
4.00	0.15	0.85	0.00	0.21	0.66	0.13	0.16	0.84	0.00
5.00	0.07	0.92	0.01	0.24	0.66	0.10	0.07	0.92	0.01
6.00	0.14	0.84	0.02	0.23	0.60	0.17	0.11	0.87	0.02
7.00	0.06	0.88	0.06	0.21	0.60	0.19	0.10	0.86	0.04
8.00	0.14	0.84	0.02	0.27	0.53	0.20	0.14	0.84	0.02
10.00	0.07	0.86	0.07	0.25	0.49	0.26	0.08	0.86	0.06
15.00	0.26	0.66	0.08	0.39	0.33	0.28	0.25	0.70	0.05
20.00	0.29	0.55	0.16	0.36	0.30	0.34	0.20	0.78	0.02
30.00	0.26	0.53	0.21	0.35	0.26	0.39	0.12	0.80	0.08

TABLE 4.4

Fraction of SDOF Oscillator Response (5% Critical Damping) Records Whose Largest Peaks Follow Exponential, Rayleigh, and Weibull EHT Distributions (26 Rock Sites)

Period (Sec)	ACCELERATION			RELATIVE VELOCITY			RELATIVE DISPLACEMENT		
	Exponential	Rayleigh	Weibull	Exponential	Rayleigh	Weibull	Exponential	Rayleigh	Weibull
0.03	0.50	0.15	0.35	0.46	0.31	0.23	0.31	0.11	0.58
0.05	0.54	0.15	0.31	0.66	0.19	0.15	0.50	0.15	0.35
0.10	0.46	0.42	0.12	0.35	0.54	0.11	0.46	0.42	0.12
0.15	0.42	0.46	0.12	0.23	0.62	0.15	0.50	0.38	0.12
0.20	0.35	0.54	0.11	0.35	0.50	0.15	0.42	0.46	0.12
0.30	0.31	0.58	0.11	0.39	0.46	0.15	0.27	0.62	0.11
0.40	0.31	0.50	0.19	0.39	0.46	0.15	0.35	0.46	0.19
0.50	0.27	0.54	0.19	0.31	0.46	0.23	0.19	0.62	0.19
0.60	0.38	0.50	0.12	0.31	0.46	0.23	0.39	0.46	0.15
0.70	0.31	0.50	0.19	0.38	0.50	0.12	0.27	0.58	0.15
0.80	0.19	0.66	0.15	0.23	0.62	0.15	0.15	0.70	0.15
1.00	0.19	0.62	0.19	0.35	0.46	0.19	0.23	0.58	0.19
1.25	0.27	0.62	0.11	0.31	0.54	0.15	0.27	0.62	0.11
1.50	0.27	0.46	0.27	0.19	0.42	0.39	0.27	0.46	0.27
1.75	0.27	0.69	0.04	0.38	0.39	0.23	0.27	0.65	0.08
2.00	0.35	0.54	0.11	0.46	0.31	0.23	0.35	0.54	0.11
2.50	0.31	0.61	0.08	0.19	0.58	0.23	0.27	0.65	0.08
3.00	0.23	0.77	0.00	0.19	0.54	0.27	0.23	0.77	0.00
4.00	0.15	0.81	0.04	0.20	0.65	0.15	0.15	0.81	0.04
5.00	0.11	0.85	0.04	0.23	0.65	0.12	0.08	0.88	0.04
6.00	0.19	0.73	0.08	0.42	0.42	0.16	0.15	0.81	0.04
7.00	0.15	0.85	0.00	0.35	0.54	0.11	0.12	0.88	0.00
8.00	0.08	0.81	0.11	0.54	0.27	0.19	0.11	0.85	0.04
10.00	0.08	0.84	0.08	0.31	0.27	0.42	0.08	0.81	0.11
15.00	0.23	0.77	0.00	0.35	0.35	0.30	0.08	0.92	0.00
20.00	0.35	0.54	0.11	0.35	0.19	0.46	0.19	0.81	0.00
30.00	0.31	0.50	0.19	0.31	0.23	0.46	0.12	0.77	0.11

TABLE 4.5

Fraction of SDOF Oscillator Response Records Whose Largest Peaks Follow Exponential, Rayleigh, and Weibull EHT Distributions as a Function of Damping (112 Soil and Rock Records)

Period (sec) and % Critical Damping	ACCELERATION			RELATIVE VELOCITY			RELATIVE DISPLACEMENT		
	Exponential	Rayleigh	Weibull	Exponential	Rayleigh	Weibull	Exponential	Rayleigh	Weibull
0.1 second									
2%	0.39	0.52	0.09	0.31	0.66	0.03	0.37	0.54	0.09
5%	0.41	0.44	0.15	0.49	0.42	0.09	0.45	0.39	0.16
10%	0.44	0.35	0.21	0.54	0.34	0.12	0.47	0.32	0.21
0.5 second									
2%	0.19	0.75	0.06	0.17	0.76	0.07	0.18	0.75	0.07
5%	0.28	0.57	0.15	0.23	0.59	0.18	0.27	0.58	0.15
10%	0.39	0.45	0.16	0.36	0.46	0.18	0.38	0.43	0.19
1.0 second									
2%	0.34	0.59	0.07	0.29	0.67	0.04	0.39	0.49	0.12
5%	0.32	0.53	0.15	0.35	0.53	0.12	0.31	0.53	0.16
10%	0.33	0.43	0.24	0.33	0.39	0.28	0.36	0.41	0.23
1.5 seconds									
2%	0.22	0.77	0.01	0.28	0.69	0.03	0.22	0.77	0.01
5%	0.25	0.62	0.13	0.30	0.52	0.18	0.25	0.62	0.13
10%	0.31	0.42	0.27	0.35	0.37	0.28	0.33	0.40	0.27
2.0 seconds									
2%	0.15	0.80	0.05	0.27	0.69	0.04	0.15	0.80	0.05
5%	0.25	0.60	0.15	0.35	0.46	0.19	0.24	0.60	0.16
10%	0.27	0.39	0.34	0.33	0.29	0.38	0.27	0.41	0.32
2.5 seconds									
2%	0.10	0.88	0.02	0.17	0.76	0.07	0.11	0.88	0.01
5%	0.26	0.65	0.09	0.24	0.60	0.16	0.26	0.66	0.08
10%	0.28	0.48	0.24	0.31	0.39	0.30	0.27	0.52	0.21
3.0 seconds									
2%	0.08	0.92	0.00	0.24	0.71	0.05	0.08	0.92	0.00
5%	0.21	0.74	0.05	0.23	0.61	0.16	0.18	0.77	0.05
10%	0.29	0.55	0.16	0.30	0.43	0.27	0.25	0.63	0.12
5.0 seconds									
2%	0.03	0.97	0.00	0.20	0.73	0.07	0.12	0.86	0.02
5%	0.08	0.90	0.02	0.23	0.66	0.11	0.07	0.91	0.02
10%	0.19	0.78	0.03	0.27	0.53	0.20	0.13	0.83	0.04
10 seconds									
2%	0.13	0.82	0.05	0.24	0.49	0.27	0.13	0.82	0.05
5%	0.07	0.86	0.07	0.27	0.44	0.29	0.08	0.85	0.07
10%	0.15	0.70	0.15	0.27	0.43	0.30	0.18	0.76	0.06

TABLE 4.6

EHT Distributions Selected to Model the Largest Peaks in Acceleration Response of SDOF Oscillator with 5% Damping Subjected to 18 May 1940 El Centro, CA, Comp S00E, Record

Period (Sec)	EHT DISTRIBUTION[1]		
	Acceleration	Relative Velocity	Relative Displacement
0.00	E	R	R
0.03	E	R	E
0.035	E	W	W
0.04	E	R	E
0.05	E	R	R
0.06	R	R	W
0.07	E	E	W
0.08	E	W	E
0.10	E	E	E
0.125	R	E	R
0.15	E	E	E
0.175	E	E	E
0.20	R	R	R
0.25	E	E	E
0.30	E	E	E
0.35	R	E	R
0.40	R	E	R
0.50	E	E	E
0.60	E	E	E
0.70	R	R	R
0.80	E	E	E
1.00	W	W	W
1.25	R	R	R
1.50	R	R	R
1.75	R	R	R
2.00	R	E	R
2.50	R	R	R
3.00	R	R	R
3.50	E	E	E
4.00	E	E	E
5.00	R	R	R
6.00	R	R	R
7.00	R	R	R
8.00	R	R	R
10.00	R	R	R
12.50	R	R	R
15.00	R	R	R
17.50	R	E	R
20.00	R	E	R
25.00	R	E	R
30.00	R	E	R

[1] E - Exponential
R - Rayleigh
W - Weibull

TABLE 4.7

EHT Distributions Selected to Model the Largest Peaks in Acceleration Response of SDOF Oscillator with 5% Damping Subjected to 15 October 1979 Imperial Valley Earthquake, Bond's Corner, Comp 230°, Record

Period (Sec)	EHT DISTRIBUTION[1]		
	Acceleration	Relative Velocity	Relative Displacement
0.00	E	R	W
0.03	R	E	R
0.035	R	E	R
0.04	R	E	R
0.05	R	E	R
0.06	R	E	R
0.07	E	E	E
0.08	E	R	E
0.10	E	E	E
0.125	R	R	R
0.150	E	E	E
0.075	E	W	E
0.20	E	E	E
0.25	E	E	E
0.30	W	E	W
0.35	W	E	W
0.40	W	E	W
0.50	R	R	R
0.60	R	E	R
0.70	R	R	R
0.80	R	R	R
1.00	R	R	R
1.25	R	R	R
1.50	R	R	R
1.75	R	R	R
2.00	R	R	R
2.50	R	R	R
3.00	R	R	R
3.50	R	R	R
4.00	R	R	R
5.00	R	R	R
6.00	R	R	R
7.00	R	R	R
8.00	R	R	R
10.00	W	R	W
12.50	R	R	R
15.00	E	R	R
17.5	E	R	R
20.0	R	R	R
25.0	R	R	R
30.0	R	R	R

[1] E - Exponential
R - Rayleigh
W - Weibull

TABLE 4.8

Percentage of Acceleration Response Records of SDOF Oscillator with 5% Damping Passing Selected Significance Levels of the Kolmogorov-Smirnov Test
(112 Input Records)

Distribution and Osillator Period	Significance Level		
	1%	5%	10%
Exponential			
0.1 sec	0	0	0
0.5 sec	0	0	0
1.0 sec	0	0	0
2.0 sec	0	0	0
10.0 sec	0	0	0
Rayleigh			
0.1 sec	0	0	0
0.5 sec	0	0	0
1.0 sec	0	0	0
2.0 sec	0	0	0
10.0 sec	0	0	0
Exponential (EHT)			
0.1 sec	82	84	84
0.5 sec	83	84	84
1.0 sec	84	84	84
2.0 sec	86	88	88
10.0 sec	81	81	82
Rayleigh (EHT)			
0.1 sec	80	80	82
0.5 sec	84	86	86
1.0 sec	86	88	88
2.0 sec	88	90	90
10.0 sec	83	85	85

TABLE 4.9

Percentage of Relative Velocity Records of SDOF Oscillator with 5% Damping Passing Selected Significance Levels of the Kolmogorov-Smirnov Test
(112 Input Records)

Distribution and Oscillator Period	Significance Level		
	1%	5%	10%
Exponential			
0.1 sec	0	0	0
0.5 sec	0	0	0
1.0 sec	0	0	0
2.0 sec	0	0	0
10.0 sec	0	0	0
Rayleigh			
0.1 sec	0	0	0
0.5 sec	0	0	0
1.0 sec	0	0	0
2.0 sec	0	0	0
10.0 sec	0	0	0
Exponential (EHT)			
0.1 sec	84	84	84
0.5 sec	85	85	86
1.0 sec	86	86	87
2.0 sec	88	90	90
10.0 sec	83	84	84
Rayleigh (EHT)			
0.1 sec	84	86	86
0.5 sec	86	87	87
1.0 sec	87	88	88
2.0 sec	88	88	88
10.0 sec	84	86	86

TABLE 4.10

Percentage of Relative Displacement Records of SDOF Oscillator Response with 5% Damping Passing Selected Significance Levels of the Kolmogorov-Smirnov Test
(112 Input Records)

Distribution and Oscillator Period	Significance Level		
	1%	5%	10%
Exponential			
0.1 sec	0	0	0
0.5 sec	0	0	0
1.0 sec	0	0	0
2.0 sec	0	0	0
10.0 sec	0	0	0
Rayleigh			
0.1 sec	0	0	0
0.5 sec	0	0	0
1.0 sec	0	0	0
2.0 sec	0	0	0
10.0 sec	0	0	0
Exponential (EHT)			
0.1 sec	82	84	84
0.5 sec	83	84	84
1.0 sec	84	84	84
2.0 sec	86	88	88
10.0 sec	81	82	82
Rayleigh (EHT)			
0.1 sec	80	80	82
0.5 sec	84	86	86
1.0 sec	86	88	88
2.0 sec	88	90	90
10.0 sec	83	85	85

TABLE 4.11

Standardized Number of Peaks, N*, for Exponential (EHT) Distribution for SDOF Response with 5% Damping

PERIOD	SOIL & ROCK		SOIL		ROCK	
(Sec)	N1[1]	N2[2]	N1[1]	N2[2]	N1[1]	N2[2]
0.030	115	123	120	125	103	112
0.040	124	133	135	137	103	111
0.050	158	160	176	169	123	128
0.060	175	187	177	177	168	184
0.070	197	212	198	197	195	209
0.080	206	232	211	208	194	205
0.100	202	227	203	219	199	207
0.125	186	197	181	182	203	231
0.150	157	164	158	168	157	173
0.175	153	160	152	158	154	173
0.200	131	142	131	138	131	130
0.250	101	109	105	109	92	120
0.300	88	91	89	92	84	107
0.400	73	44	78	89	62	71
0.500	62	74	63	61	62	61
0.600	59	73	61	62	50	45
0.700	55	70	54	51	60	57
0.800	49	66	48	47	50	45
1.000	42	57	42	47	41	40
1.250	36	49	41	46	26	23
1.500	38	51	41	42	32	30
1.750	37	48	39	45	32	31
2.000	28	41	29	32	23	22
2.500	33	38	33	33	35	33
3.000	27	32	27	28	25	23
3.500	26	29	26	26	28	25
4.000	27	28	27	29	24	22
5.000	25	26	25	26	27	26
6.000	23	23	23	23	25	26
7.000	20	22	20	21	26	26
8.000	20	20	20	21	23	22
10.000	16	18	16	17	20	20
12.500	13	16	12	12	21	19
15.000	13	16	12	13	18	17
17.500	13	16	13	13	16	13
20.000	13	16	13	13	11	9
25.000	13	16	13	13	16	16
30.000	14	16	14	13	15	15

[1]N1 - Standardized N* from $1/\lambda$ vs. $(1/\lambda) * (\ln N)$
[2]N2 - Standardized N* from $(1/\lambda)/PGA$ vs. $(1/\lambda)*(\ln N)/PGA$

TABLE 4.12

Standardized Number of Peaks, N*, for Rayleigh (EHT) Distribution for SDOF Oscillator Response with 5% Damping

PERIOD	SOIL & ROCK		SOIL		ROCK	
(Sec)	N1[1]	N2[2]	N1[1]	N2[2]	N1[1]	N2[2]
0.030	36	52	35	46	37	32
0.040	40	53	50	61	27	28
0.050	58	71	80	79	32	30
0.060	55	69	60	69	46	42
0.070	65	85	74	58	49	40
0.080	93(66)	88(75)	66	70	205(57)	234(60)
0.100	71	89	75	74	60	62
0.125	60	69	57	53	74	96
0.150	67	90	65	95	73	64
0.175	65	60	73	53	51	59
0.200	53	57	50	65	60	71
0.250	49	59	52	66	43	58
0.300	50	62	49	83	51	62
0.400	51	51	78	55	28	25
0.500	33	45	39	38	25	22
0.600	41(36)	42(41)	37	43	95(28)	133(28)
0.700	49	42	52	65	32	25
0.800	35	37	35	47	33	28
1.000	28	34	34	35	19	18
1.250	20	27	24	25	13	12
1.500	20	27	22	23	17	16
1.750	21	24	21	21	20	19
2.000	21	23	22	25	14	14
2.500	18	19	18	18	18	17
3.000	16	19	16	17	18	17
3.500	15(15)	17(17)	15	16	40(19)	50(20)
4.000	17	19	17	17	17	16
5.000	16	17	16	15	18	18
6.000	14	14	14	13	14	14
7.000	14	15	14	14	12	12
8.000	15	15	15	15	16	16
10.000	10	13	10	11	15	14
12.500	13	14	13	16	8	7
15.000	18	17	20	22	8	7
17.500	13	14	14	13	8	7
20.000	11	12	11	10	9	8
25.000	13	11	13	14	8	7
30.000	15	14	16	15	8	7

[1]N1 - Standardized N* from $1/\lambda$ vs. $(1/\lambda) * \sqrt{\ln N}$.

[2]N2 - Standardized N* from $(1/\lambda)/PGA$ vs. $(1/\lambda) * \sqrt{\ln N}/PGA$.

[3]Number in ( ) is standardized N* excluding rock records listed in Table 4.13.

TABLE 4.13

Rock Records Excluded from Standardized N* Calculations for the Rayleigh (EHT) Distribution

Period (Sec)	Record
0.08	A015 S18E
	B025 S00W
	B025 S90W
	B037 S25W
	C041 S74W
	G106 S90W
0.60	A015 S80E
	B025 S00W
	B025 S90W
	B040 N33E
	C041 S74W
3.50	C041 S16E
	C041 S74W
	L166 S90W

TABLE 4.14

Comparison of Observed vs. Predicted Acceleration Peaks from the N* Exponential (EHT) and N* Rayleigh (EHT) Distributions for SDOF Oscillator Response with 5% Damping Subjected to A001 Comp S00E (Soil Site)

Peak and Period (Sec)		ACTUAL	N* Exponential (EHT)	N* Rayleigh (EHT)
X(1):	0.1 sec	555.4	543.6	564.5
	0.5 sec	819.3	773.1	896.1
	1.0 sec	507.7	710.7	642.3
	2.0 sec	175.1	202.0	194.4
	5.0 sec	29.7	37.5	32.7
	10.0 sec	15.0	16.7	14.9
X(2):	0.1 sec	494.3	461.0	511.5
	0.5 sec	809.6	630.4	800.3
	1.0 sec	456.9	568.9	571.6
	2.0 sec	159.9	158.5	170.7
	5.0 sec	25.2	29.2	28.4
	10.0 sec	13.4	12.6	12.6
X(5):	0.1 sec	394.8	371.6	447.1
	0.5 sec	517.8	475.8	681.5
	1.0 sec	403.0	415.4	483.4
	2.0 sec	135.7	111.4	140.7
	5.0 sec	23.2	20.2	22.8
	10.0 sec	9.0	8.1	9.6
X(10):	0.1 sec	322.9	310.0	396.8
	0.5 sec	415.9	369.4	585.8
	1.0 sec	199.5	309.7	411.8
	2.0 sec	89.8	79.0	115.5
	5.0 sec	8.9	13.9	18.0
	10.0 sec	5.9	5.1	6.9
X(20):	0.1 sec	250.0	250.7	341.2
	0.5 sec	308.8	266.8	475.8
	1.0 sec	99.3	207.8	328.5
	2.0 sec	44.7	47.7	84.4
	5.0 sec	4.8	7.9	11.6
	10.0 sec	-	-	-

Table 4.15

Locations of Accelerographs Recordings

Building No.	EERL No. Near Base	EERL No. Near Roof	Building Name	Address	Accelerograph Locations Near Base	Accelerograph Locations Near Roof
1	C048	C050	Holiday Inn	8244 Orion Blvd.	1st Floor	8th Floor
2	C051	C053	Kajima Building	250 E. First St.	Basement	17th Floor
3	C054	C055	Union Bank Square	445 Figueroa St.	Sub-Basement	19th Floor
4	D059	D061	1901 Ave of the Stars	1901 Ave of the Stars	Sub-Basement	21st Floor
5	D062	D064	Holiday Inn	1640 S. Marengo St.	1st Floor	8th Floor
6	D065	D067	Beneficial Plaza	3710 Wilshire Blvd.	Basement	10th Floor
7	E075	E077	Tishman Plaza	3470 Wilshire Blvd.	Sub-Basement	11th Floor
8	E083	E085	Mutual Building	3407 W. Sixth St.	Basement	Penthouse
9	F089	F091	AMPCO Auto Park Ramp	808 S. Olive	Street Level	8th Level
10	F095	F097	Robertson Plaza	120 N.Robertson Blvd.	Sub-Basement	9th Floor
11	F098	F100	Los Angeles Athletic Club, Parking Ramp	646 S. Olive Ave.	Basement	Roof
12	G108	G109	Millikan Library	Cal.Inst.of Tech.	Basement	10th Floor
13	G110	G111	Jet Propulsion Lab	Cal.Inst.of Tech.	Basement	9th Floor
14	G112	G113	Crockers Bank Pl.	611 W. Sixth St.	Basement	42nd Floor
15	H115	H117	Bank of California	15250 Ventura Blvd.	Basement	Roof
16	H118	H120	Airport Marina Hotel	8639 Lincoln Ave.	Basement	12th Floor
17	H124	H126	Hunt Wessons Bldg.	2600 Nutwood Ave.	Basement	Penthouse
18	I128	I130	Beverly Oakhurst Apartments	435 N. Oakhurst Ave.	Basement	Roof
19	I131	I133	450 Company	450 N. Roxbury Dr.	1st Floor	10th Floor
20	I134	I136	Northrop	1800 Century Park E.	Basement P-3	Penthouse W.
21	I137	I139	Ventura Gloria Building	15910 Ventura Blvd.	Basement	19th Floor
22	J145	J147	Valley Presb.Hosp.	15107 Vanowen St.	Basement	Roof
23	J148	J150	Wilshire Christian	616 S. Normandie Ave.	Basement	Roof

Table 4.15
(Cont'd.)

Building No.	EERL No. Near Base	EERL No. Near Roof	Building Name	Address	Accelerograph Locations Near Base	Accelerograph Locations Near Roof
24	K157	K158	Pacific Telephone	420 S. Grand Ave.	2nd Floor	17th Floor
25	L166	L168	Sheraton-Universal	3838 Lankershim Blvd	Basement	21st Floor
26	M176	M178	Occidental Center	1150 S. Hill St.	Sub-Basement	10th Floor
27	M180	M182	The City Center	4000 W. Chapman Ave.	Basement	19th Floor
28	N188	N190	Property Research	1880 Century Park E.	1st Level Parking	Penthouse
29	N192	N194	Wilshire-Coronado	2500 Wilshire Blvd	Basement	Roof
30	O199	O201	1625 Olympic	1625 Olympic Blvd	Ground Floor	10th Floor
31	P214	P216	Kaiser Hospital	4867 Sunset Blvd	Basement	7th Floor
32	P217	P219	Wilshire Square	3345 Wilshire Blvd	Basement	12th Floor
33	Q233	Q235	Certified Life Tower	14724 Ventura Blvd	1st Floor	Penthouse
34	Q236	Q238	Holiday Inn	1760 N. Orchid Ave	Ground Floor	23rd Floor
35	Q239	Q240	Wilshire Doheny Pl.	9100 Wilshire Blvd	Basement	5th Floor
36	Q241	Q243	Bunker Hill, Central Tower	800 W. First St.	1st Floor	33rd Floor
37	R244	R245	Bunker Hill, West Tower	222 W. Figueroa St.	1st Floor	20th Floor
38	R246	R247	6464 Sunset Blvd.	6464 Sunset Blvd.	Basement	12th Floor
39	R249	R250	1900 Ave. of the Stars	1900 Ave. of the Stars	Basement	29th Floor
40	R251	R252	Bunker Hill, South Tower	234 Figueroa St.	Basement	Roof
41	R253	R254	Coldwell-Banker	533 S. Fremont Ave.	Basement	6th Floor
42	S255	S257	6200 Wilshire Medical	6200 Wilshire Blvd.	Ground Floor	17th Floor
43	S258	S260	Phillips Hall, USC	3440 University Ave.	Basement	Roof
44	S262	S264	Mutual Benefit Life Plaza	5900 Wilshire Blvd.	B Parking Lot	Penthouse
45	S267	S269	Airport Freeway Center	5260 Century Blvd.	1st Floor	Roof

Table 4.16
Descriptions of Buildings

Bldg. No.	Type of Frame[1]	Total Stories Above/Below Grade[1]	Total Height Above/Below Grade[1] (feet)	Epicentral Distance (km)[2]	Soil Site[3]	Direction Component	Earthquake Period[1] Pre (Seconds)	During (Seconds)	Post (Seconds)
1	RC(FP)	7/0	66/0	20	S	N00W	0.48	1.60	0.68
						S90W	0.53	1.24	0.72
2	St(MR)	15/1	190/17	41	S	N36E	1.32	2.90	2.10
						N54W	1.88	2.80	2.15
3	St(MR)	39/4	495/40	41	R	S38W	3.29	-	3.70
						N52W	2.84	-	4.10
4	St(Br)	20/4	270/45	38	S	N46W	2.63	3.50	2.80
						S44W	2.45	3.60	2.72
5	RC(FP)	7/0	66/0	42	S	N38W	0.53	1.00	0.64
						S52W	0.49	1.20	0.63
6	RC(SW)	11/3	160/37	39	S	N90E	0.76	1.10	0.85
						S00W	0.98	1.20	1.06
7	RC(FP,SW)	12/1	148/10	39	S	N00E	0.93	1.60	1.27
						N90E	0.71	1.30	0.97
8	St(MR)	9/0	6/0	39	S	S00W	1.03	1.60	1.20
						N90E	1.05	1.40	1.24
9	RC(BW)	7/0	76/0	42	S	S53E	0.22	0.40	0.28
						S37W	0.40	0.60	0.46
10	RC(SW)	9/2	118/19	36	S	S88E	0.46	0.60	0.49
						S02W	0.63	0.80	0.70
11	RC(SW)	7/0	75/4	42	S	S53E	0.24	0.30	0.25
						S37W	0.51	0.60	0.51
12	RC	9	128	37	S	N00E	0.54	0.60	0.54
						N90E	0.68	1.00	0.79
13	St(MR)	9	114	29	S	S08W	0.99	1.40	1.16
						S82E	0.93	1.30	1.01
14	St(MR)	42/5	601/53	41	S	N38E	4.70	6.00	5.30
						N52W	4.50	5.60	5.30
15	RC(MR)	12/0	159/0	28	S	N79W	-	3.00	1.60
						N11E	-	2.20	1.70
16	RC(SW)	12/1	122/-	48	S	S45E	-	-	-
						S45W	-	-	-

Table 4.16
(Cont'd.)

Bldg. No.	Type of Frame[1]	Total Stories Above/Below Grade[1]	Total Height Above/Below Grade[1] (feet)	Epicentral Distance (km)[2]	Soil Site[3]	Direction Component	Earthquake Period[1] Pre	During (Seconds)	Post
17	RC(SW)	10	-	74	S	S90W	-	0.70	0.59
						S00W	-	0.70	0.59
18	RC(SW)	10	-	36	S	S90W	-	0.60	0.46
						N00E	-	0.40	0.33
19	RC	10	-	37	S	N40W	-	0.80	0.70
						N50E	-	0.50	0.47
20	RC(MR,D)	16/3	224/37	38	S	S36E	-	1.10	0.95
						N54E	-	1.60	1.30
21	St(MR)	15/1	212/12	28	S	S09W	-	3.20	2.37
						S81E	-	2.80	2.27
22	RC	7	-	24	S	S90W	-	0.90	0.60
						S00W	-	1.00	0.72
23	RC(MR)	16/1	152/0	39	S	S90W	-	1.80	1.17
						N00E	-	1.10	0.85
24	St(Br)	17	248	41	R	S37W	0.69	1.00	0.85
						S53E	0.68	1.00	0.88
25	RC(MR,D)	19/1	184/15	30	R	S90W	1.26	2.20	1.50
						N00E	1.22	2.30	1.40
26	St(MR)	10/2	161/34	42	S	S53E	-	2.50	1.66
						N37E	-	2.60	1.90
27	RC	19	-	83	S	S00W	-	2.04	1.94
						S90W	-	1.14	1.05
28	St(MR)	15/3	207/32	38	S	N36W	-	2.90	2.20
						N54E	-	3.50	2.60
29	RC	13/1	166/10	40	S	N29E	-	2.30	1.64
						N61W	-	1.90	1.48
30	RC	10	-	41	S	N28E	-	1.30	1.05
						N62W	-	1.40	1.21
31	RC(SW & Columns)	8/1	86/16	35	S	S89W	0.28	0.50	0.30
						S01E	0.18	0.40	0.22
32	RC(T)	12/3	165/29	39	S	N00W	0.84	1.20	0.99
						N90E	0.68	1.00	0.80
33	RC	14/0	-	28	S	N78W	0.88	1.20	0.96

Table 4.16
(Cont'd.)

Bldg. No.	Type of Frame[1]	Total Stories Above/Below Grade[1]	Total Height Above/Below Grade[1] (feet)	Epicentral Distance (km)[2]	Soil Site[3]	Direction Component	Earthquake Period[1] Pre	During	Post
							(Seconds)		
34	RC	22	-	34	S	South	1.41	2.00	1.58
						East	1.31	2.00	1.50
35	RC	10	-	37	S	South	1.09	1.70	1.26
						East	1.09	1.80	1.23
36	St(MR)	32/0	327/0	41	R	N53W	-	3.30	2.58
						N37E	-	3.40	2.62
37	RC	17	-	41	S	S37W	-	0.60	0.54
						N53W	-	1.10	0.91
38	St	11	-	34	S	South	-	2.30	1.50
						East	-	2.70	1.75
39	St(MR)	27/4	371/46	38	S	S46E	3.30	-	3.60
						N44E	3.30	-	3.60
40	RC	17	-	41	S	N37E	-	1.20	0.89
						S53E	-	0.70	0.57
41	RC(MR)	9/1	119/12	41	S	N30W	0.63	1.10	0.88
						S60W	0.36	0.70	0.49
42	RC	15/0	164/0	38	S	N82W	1.06	1.50	1.20
						N08E	1.26	1.70	1.36
43	RC(SW)	11/1	132/17	42	S	S61E	0.66	0.90	0.86
						N29E	0.71	1.00	0.86
44	St	30/3	409/34	38	S	S07W	-	5.00	4.60
						N83W	-	5.00	4.55
45	St(MR)	7/0	99/0	49	S	N	1.23	2.10	1.33
						E	1.24	1.80	1.25

[1]Per Mulhern and Maley (1973), RC - Reinforced Concrete, St - Steel, MR - Moment Resisting Frame, Br - Braced, SW - Shear Wall, D - Ductile, FP - Flat Plate, BW - Block Wall, T - Tubular Structure.

[2]Per Maley and Cloud (1973).

[3]S - Soil Site
R - Rock Site

Table 4.17

EHT Distribution Parameters of Building Acceleration Response REcorded at the Roof and the Base

Bldg. No.	EERL No.	Acceleration		
		D^1	N/2	$1/\lambda^2$
1	C048 N00W	1	33	104.189
	C048 S90W	1	41	65.771
	C050 N00W	1	18	188.008
	C050 S90W	1	32	144.238
2	C051 N36E	1	36	45.302
	C051 N54W	1	27	51.677
	C053 N36E	1	18	78.270
	C053 N54W	1	34	80.405
3	C054 S38W	1	32	50.137
	C054 N52W	2	230	3.456
	C055 S38W	1	34	49.986
	C055 N52W	2	121	7.510
4	D059 N46W	0	64	26.128
	D059 S44W	0	68	31.423
	D061 N46W	1	19	46.184
	D061 S44W	1	18	46.172
5	D062 N38W	0	64	25.553
	D062 S52W	1	28	66.653
	D064 N38W	1	20	114.224
	D064 S52W	1	19	190.551
6	D065 N90E	1	23	70.997
	D065 S00W	0	51	25.755
	D067 N90E	1	15	175.999
	D067 S00W	1	20	102.849
7	E075 N00E	0	58	29.806
	E075 S90W	1	27	53.259
	E077 N00E	1	28	114.776
	E077 N90E	1	29	108.832
8	E083 S00W	1	25	80.717
	E083 N90E	1	26	76.243
	E085 S00W	0	52	50.012
	E085 N90E	1	14	106.865
9	F089 S53E	0	61	29.559
	F089 S37W	0	60	26.212
	F091 S53E	0	62	87.605
	F091 S37W	1	29	102.444
10	F095 S88E	1	22	42.880
	F095 S02W	1	26	42.528
	F097 S88E	1	23	118.139
	F097 S02W	0	60	61.329
11	F098 S53E	2	323	5.846
	F098 S37W	0	60	37.473
	F100 S53E	2	352	11.285
	F100 S37W	1	25	159.102
12	G108 N00E	2	384	4.393

TABLE 4.17
(Cont'd.)

Bldg. No.	EERL No.	Acceleration		
		D_L	N/2	$1/\lambda^2$
	G108 N90E	2	301	4.148
	G109 N00E	1	46	126.319
	G109 N90E	1	28	173.750
13	G110 S08W	0	70	25.663
	G110 S82E	0	48	39.217
	G111 S08W	0	50	45.594
	G111 S82E	0	53	68.814
14	G112 N38E	0	55	21.678
	G112 N52W	1	36	35.350
	G113 N38E	1	18	77.742
	G113 N52W	1	15	54.507
15	H115 N79W	1	40	66.772
	H115 N11E	1	41	91.853
	H117 N79W	1	42	92.244
	H117 N11E	1	34	136.993
16	H118 S45E	1	43	15.466
	H118 S45W	1	50	14.721
	H120 S45E	1	29	56.115
	H120 S45W	0	73	29.216
17	H124 S90W	1	62	12.764
	H124 S00W	1	44	15.465
	H126 S90W	1	35	48.591
	H126 S00W	0	63	29.764
18	I128 S90W	0	79	15.528
	I128 N00E	1	31	28.558
	I130 S90W	1	32	122.751
	I130 N00E	0	51	63.005
19	I131 N40W	0	83	27.775
	I131 N50E	1	32	75.510
	I133 N40W	1	29	106.493
	I133 N50E	0	43	77.464
20	I134 S36E	1	41	35.732
	I134 N54E	1	21	49.511
	I136 S36E	1	17	146.325
	I136 N54E	0	59	60.943
21	I137 S09W	1	41	57.150
	I137 S81E	0	108	24.285
	I139 S09W	1	25	102.274
	I139 S81E	1	25	98.131
22	J145 S90W	1	29	54.272
	J145 S00W	1	38	55.979
	J147 S90W	1	27	158.609
	J147 S00W	1	31	189.376
23	J148 S90W	1	34	53.011
	J148 N00E	1	35	50.692
	J150 S90W	1	20	101.818
	J150 N00E	1	26	154.030
24	K157 S37W	0	63	22.611
	K157 S53E	2	282	3.992
	K158 S37W	1	15	118.730
	K158 S53E	0	28	75.945

Table 4.17
(Cont'd.)

Bldg. No.	EERL No.	Acceleration D1	N/2	$1/\lambda^2$
25	L166 S90W	0	55	32.973
	L166 N00E	2	309	3.905
	L168 S90W	1	20	92.410
	L168 N00E	1	23	47.203
26	M176 S53E	0	60	21.850
	M176 N37E	1	30	39.383
	M178 S53E	0	51	25.208
	M178 N37E	1	20	61.389
27	M180 S00W	1	64	11.088
	M180 S90W	1	59	12.010
	M182 S00W	1	70	27.129
	M182 S90W	1	56	34.294
28	N188 N36W	1	31	64.971
	N188 N54E	1	30	47.908
	N190 N36W	1	35	61.049
	N190 N54E	1	34	46.663
29	N192 N29E	1	40	43.543
	N192 N61W	1	31	47.223
	N194 N29E	1	28	98.385
	N194 N61W	0	34	39.498
30	O199 N28E	1	28	63.702
	O199 N62W	2	267	6.375
	O201 N28E	1	16	114.542
	O201 N62W	2	94	9.911
31	P214 S89W	1	20	77.595
	P214 S01E	1	26	76.049
	P216 S89W	0	48	106.855
	P216 S01E	0	55	92.148
32	P217 S00W	0	55	23.728
	P217 N90E	1	21	42.385
	P219 S00W	1	24	96.291
	P219 N90E	1	25	126.088
33	Q233 N78W	1	39	90.943
	Q233 S12W	1	22	131.572
	Q235 N78W	1	59	110.451
	Q235 S12W	0	98	76.719
34	Q236 SOUTH	0	86	32.136
	Q236 EAST	0	126	21.735
	Q238 SOUTH	1	28	51.438
	Q238 EAST	2	127	6.807
35	Q239 SOUTH	1	34	58.655
	Q239 EAST	0	84	26.956
	Q240 SOUTH	0	44	30.052
	Q240 EAST	1	16	70.157
36	Q241 N53W	2	241	3.652
	Q241 N37E	1	38	44.197
	Q243 N53W	1	25	135.891
	Q243 N37E	1	30	88.659

Table 4.17
(Cont'd.)

Bldg. No.	EERL No.	Acceleration D[1]	N/2	$1/\lambda^2$
37	R244 S37W	0	55	25.683
	R244 N53W	2	263	3.636
	R245 S37W	0	71	70.390
	R245 N53W	0	44	90.877
38	R246 SOUTH	0	78	22.694
	R246 EAST	1	37	50.337
	R247 SOUTH	1	21	110.600
	R247 EAST	2	97	9.765
39	R249 S46E	1	31	39.985
	R249 N44E	0	87	17.834
	R250 S46E	1	33	49.754
	R250 N44E	1	15	70.355
40	R251 N37E	1	26	82.443
	R251 S53E	2	188	5.226
	R252 N37E	0	73	85.403
	R252 S53E	0	66	85.131
41	R253 N30W	2	234	6.461
	R253 S60W	0	58	39.920
	R254 N30W	1	33	136.344
	R254 S60W	2	299	7.061
42	S255 N82W	0	70	22.521
	S255 N08E	1	24	62.258
	S257 N82W	1	46	92.039
	S257 N08E	0	51	58.813
43	S258 S61E	0	65	15.407
	S258 N29E	1	27	28.296
	S260 S61E	1	23	113.462
	S260 N29E	0	31	55.302
44	S262 S07W	0	39	20.039
	S262 N83W	1	17	35.343
	S264 S07W	1	9	77.777
	S264 N83W	2	53	7.520
45	S267 NORTH	1	38	24.626
	S267 EAST	0	99	11.556
	S269 NORTH	1	28	28.352
	S269 EAST	1	30	39.986

[1]D-Distribution Type: 0-Exponential, 1-Rayleigh, 2-Weibull

[2]Units are cm/sec/sec

TABLE 4.18

Number of Building Acceleration Records at Roof and Base Whose Largest Peaks Follow A Given EHT Distribution

EHT Distribution	Component	
	Roof	Base
Exponential	23	29
Rayleigh	60	50
Weibull	7	11

TABLE 4.19

Comparison of EHT Distributions Selected to Model the Largest Peaks in Building Roof and Base Acceleration Records

Building Number	Building Roof Record	Base Record	Direction	Earthquake[1] Building Period (Sec)	EHT DISTRIBUTION	
					Building Roof	Base
1	C050	C048	N00W	1.60	R	R
	C050	C048	S90W	1.24	R	R
2	C053	C051	N36E	2.90	R	R
	C053	C051	N54W	2.80	R	R
3	C055	C054	S38W	-	R	R
	C055	C054	N52W	-	W	W
4	D061	D059	N46W	3.50	R	E
	D061	D059	S44W	3.60	R	E
5	D064	D062	N38W	1.00	R	E
	D064	D062	S52W	1.20	R	R
6	D067	D065	N90E	1.10	R	R
	D067	D065	S00W	1.20	R	E
7	E077	E075	N00E	1.60	R	E
	E077	E075	N90E	1.30	R	R
8	E085	E083	S00W	1.60	E	R
	E085	E083	N90E	1.40	R	R
9	F091	F089	S53E	0.40	E	E
	F091	F089	S37W	0.60	R	E
10	F097	F095	S88E	0.60	R	R
	F097	F089	S02W	0.80	E	R
11	F100	F098	S53E	0.30	W	W
	F100	F098	S37W	0.60	R	E

TABLE 4.19 (Cont'd.)

Building Number	Roof Record	Base Record	Direction	Earthquake Building Period (Sec)	EHT DISTRIBUTION	
					Building Roof	Base
12	G109	G108	N00E	0.60	R	W
	G109	G108	N90E	1.00	R	W
13	G111	G110	S08W	1.40	E	E
	G111	G110	S82E	1.30	E	E
14	G113	G112	N38E	6.00	R	E
	G113	G112	N52W	5.60	R	R
15	H117	H115	N79W	3.00	R	R
	H117	H115	N11E	2.20	R	R
16	H120	H118	S45E	-	R	R
	H120	H118	S45E	-	E	R
17	H126	H124	S90W	0.70	R	R
	H126	H124	S00W	0.70	E	R
18	I130	I128	S90W	0.60	R	E
	I130	I128	N00E	0.40	E	R
19	I133	I131	N40W	0.80	R	E
	I133	I131	N50E	0.50	E	R
20	I136	I134	S36E	1.10	R	R
	I136	I134	N54E	1.60	E	R
21	I139	I137	S09W	3.20	R	R
	I139	I137	S81E	2.80	R	E
22	J147	J145	S90W	0.90	R	R
	J147	J145	S00W	1.00	R	R
23	J150	J148	S90W	1.80	R	R
	J150	J148	N00E	1.10	R	R
24	K158	K157	S37W	1.00	R	E
	K158	K157	S53E	1.00	E	W

TABLE 4.19 (Cont'd.)

Building Number	Roof Record	Base Record	Direction	Earthquake Building Period (Sec)	EHT DISTRIBUTION	
					Building Roof	Base
25	L168	L166	S90W	2.20	R	E
	L168	L166	N00E	2.30	R	W
26	M178	M176	S53E	2.50	E	E
	M178	M176	N37E	2.60	R	R
27	M182	M180	S00W	2.04	R	R
	M182	M180	S90W	1.14	R	R
28	N190	N188	N36W	2.90	R	R
	N190	N188	N54E	3.50	R	R
29	N194	N192	N29E	2.30	R	R
	N194	N192	N61W	1.90	E	R
30	O201	O199	N28E	1.30	R	R
	O201	O199	N62W	1.40	W	W
31	P216	P214	S89W	0.50	E	R
	P216	P214	S01E	0.40	E	R
32	P219	P217	N00W	1.20	R	E
	P219	P217	N90E	1.00	R	R
33	Q235	Q233	N78W	1.20	R	R
	Q235	Q233	S12W	1.10	E	R
34	Q238	Q236	South	2.00	R	E
	Q238	Q236	East	2.00	W	E
35	Q240	Q239	South	1.70	E	R
	Q240	Q239	East	1.80	R	E
36	Q243	Q241	N53W	3.30	R	W
	Q243	Q241	N37E	3.40	R	R
37	R245	R244	S37W	0.60	E	E
	R245	R244	N53W	1.10	E	W

TABLE 4.19 (Cont'd.)

Building Number	Roof Record	Base Record	Direction	Earthquake Building Period (Sec)	EHT DISTRIBUTION	
					Building Roof	Base
38	R247	R246	South	2.30	R	E
	R247	R246	East	2.70	W	R
39	R250	R249	S46E	-	R	R
	R250	R249	N44E	-	R	E
40	R252	R251	N37E	1.20	E	R
	R252	R251	S53E	0.70	E	W
41	R254	R253	N30W	1.10	R	W
	R254	R253	S60W	0.70	W	E
42	S257	S255	N82W	1.50	R	E
	S257	S255	N08E	1.70	E	R
43	S260	S258	S61E	0.90	R	E
	S260	S258	N29E	1.00	E	R
44	S264	S262	S07W	5.00	R	E
	S264	S262	N83W	5.00	W	R
45	S269	S267	North	2.10	R	R
	S269	S267	East	1.80	R	E

[1] Per Table 5.2

[2] E - Exponential Distribution
R - Rayleigh Distribution
W - Weibull Distribution

TABLE 4.20

Number of Building Acceleration Records Following a Given EHT Distribution as A Function of Buiiding Period, T[1]

Distribution	Component	
	Roof	Base
$T \leq 0.5$		
Exponential (EHT)	5	1
Rayleigh (EHT)	0	4
Weibull (EHT)	1	1
$0.5 < T \leq 1$		
Exponential (EHT)	6	9
Rayleigh (EHT)	14	8
Weibull (EHT)	1	4
$1 < T \leq 2$		
Exponential (EHT)	10	10
Rayleigh (EHT)	20	19
Weibull (EHT)	2	3
$2 < T \leq 3$		
Exponential (EHT)	1	4
Rayleigh (EHT)	13	10
Weibull (EHT)	1	1
$3 < T$		
Exponential (EHT)	0	4
Rayleigh (EHT)	9	5
Weibull (EHT)	1	1

[1]For three buildings, earthquake period is not known. Therefore, only 84 records are considered.

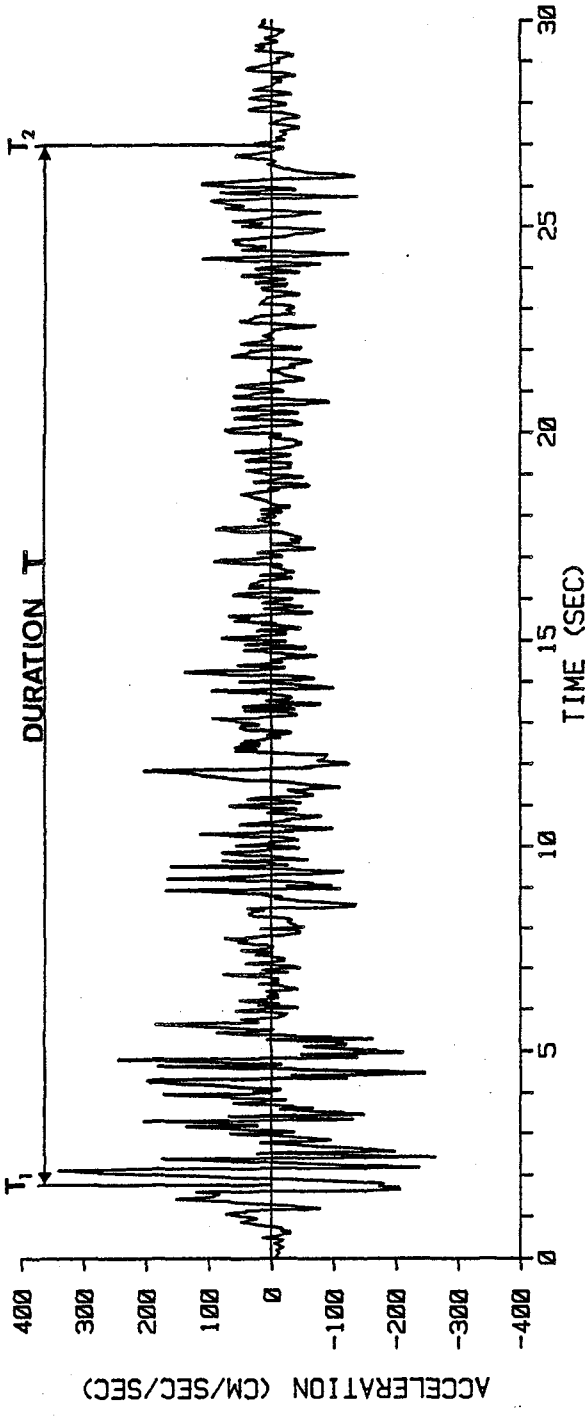

Figure 1.1 Definition of strong ground motion duration: $T = T_2 - T_1$

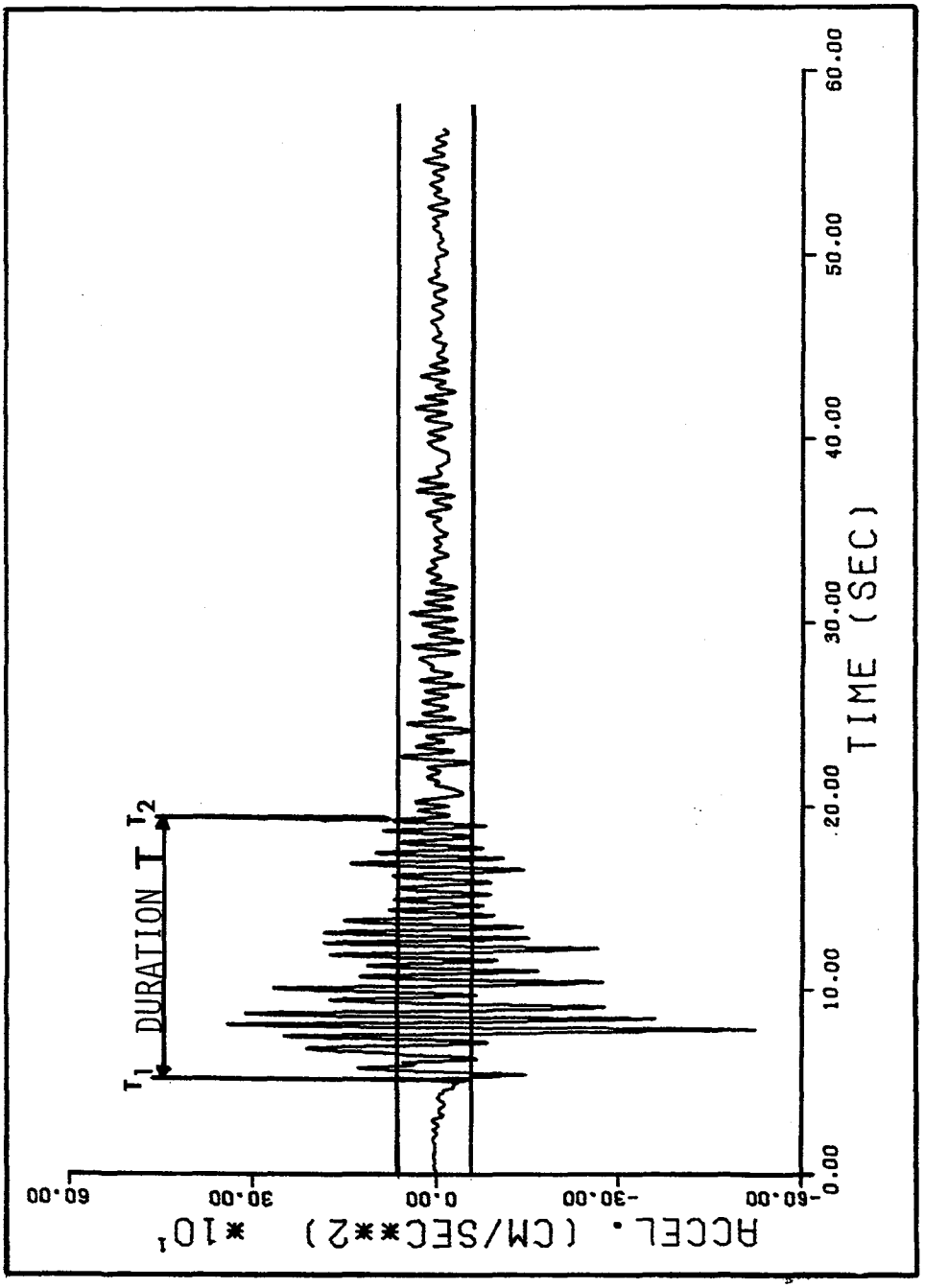

Figure 1.2 Definition of strong ground motion duration per Bolt (1973)

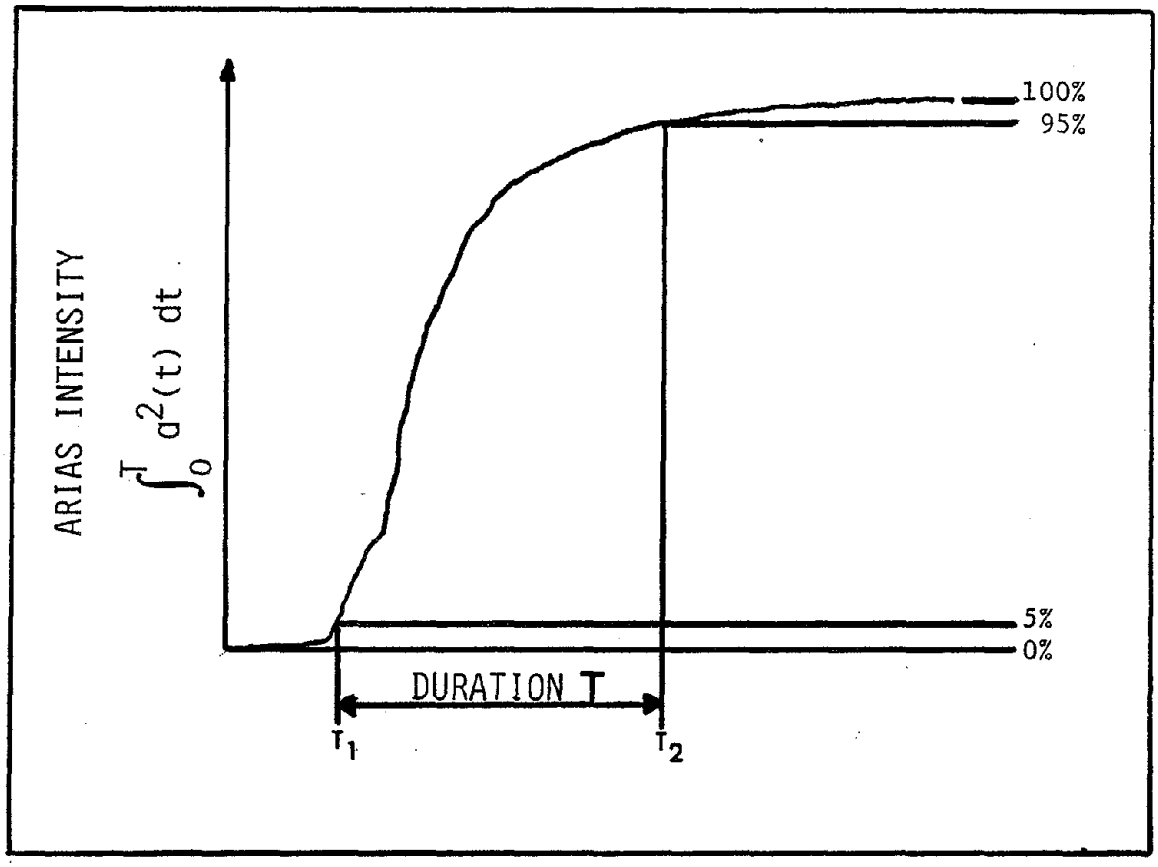

Figure 1.3 Definition of strong ground motion per Trifunac and Brady (1975)

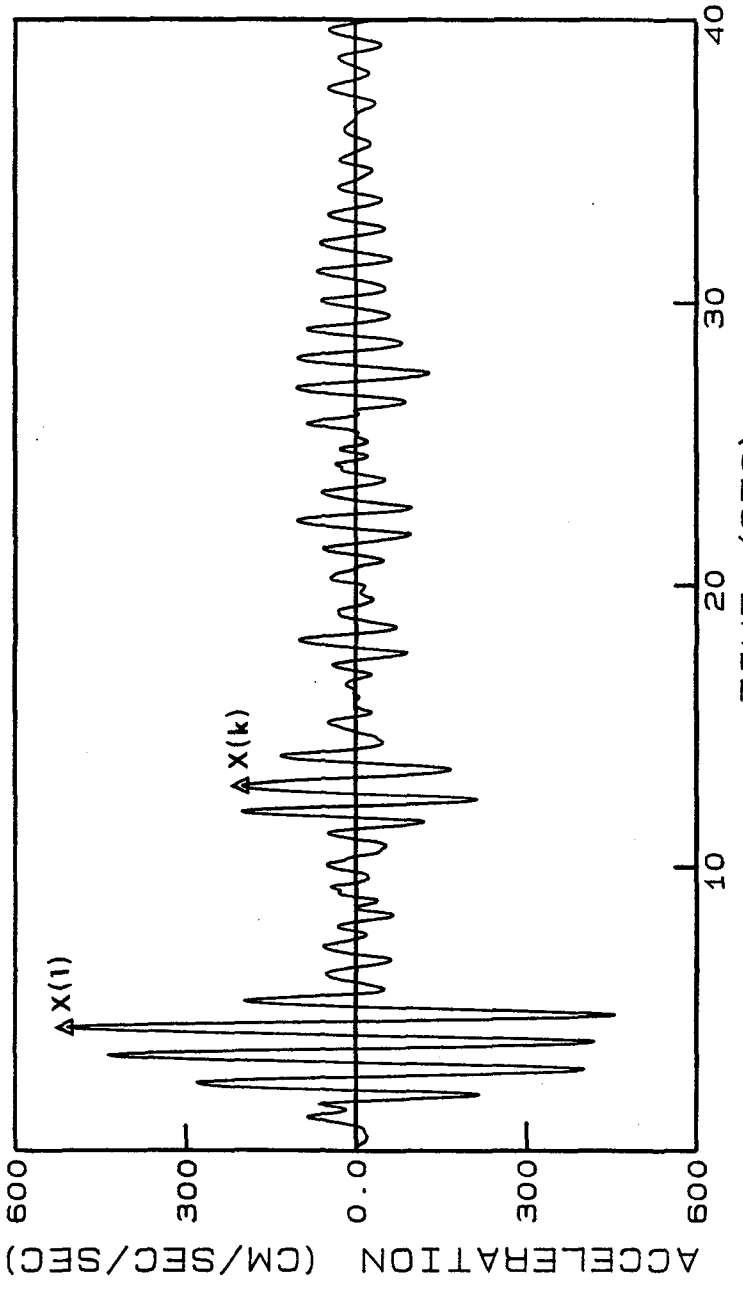

Figure 1.4 Definition of maximum peak X(1), and kth largest peak, X(k) in an acceleration time history.

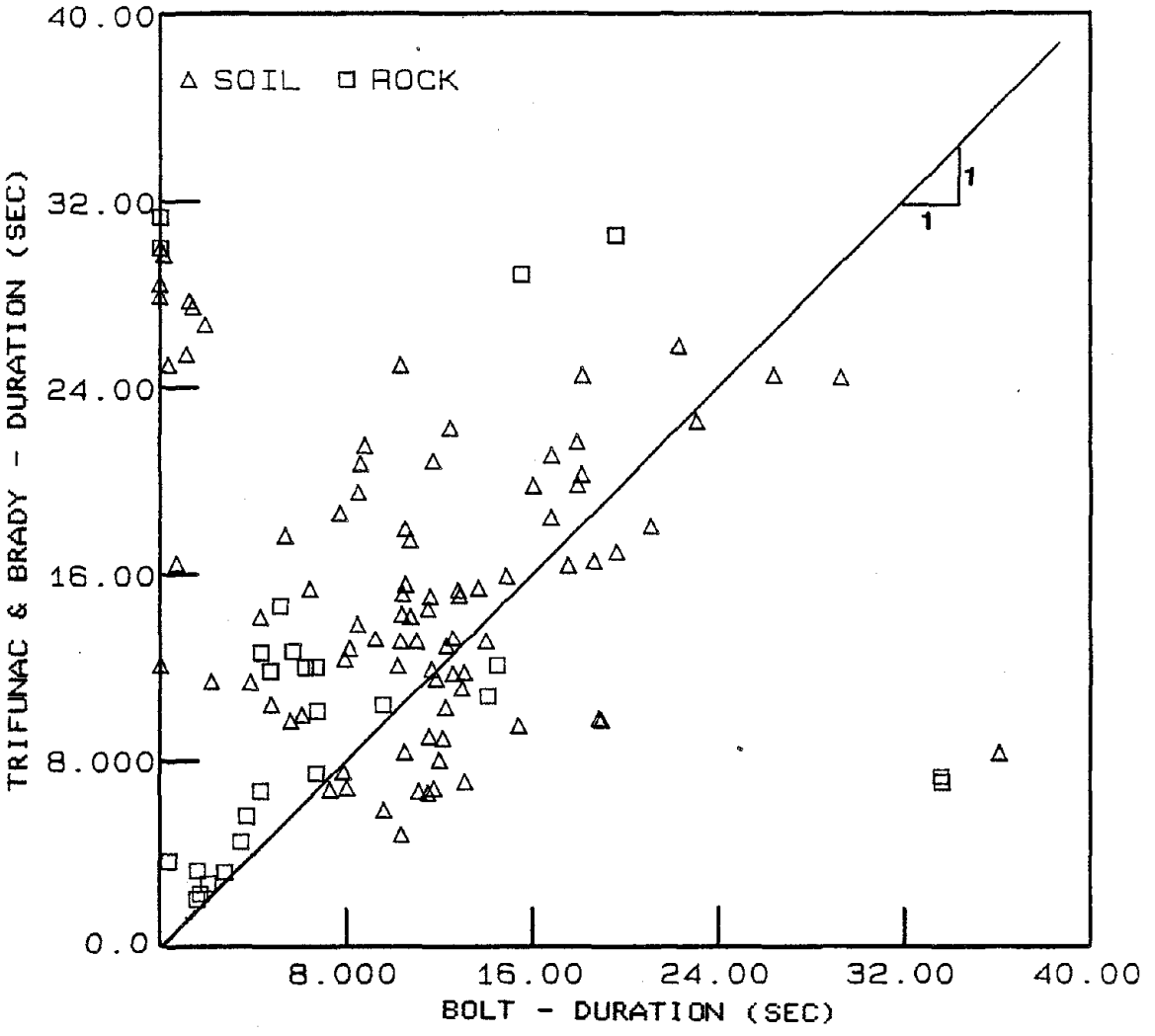

Figure 2.1 Bolt (1973) duration vs. Trifunac and Brady (1975) duration for soil and rock sites.

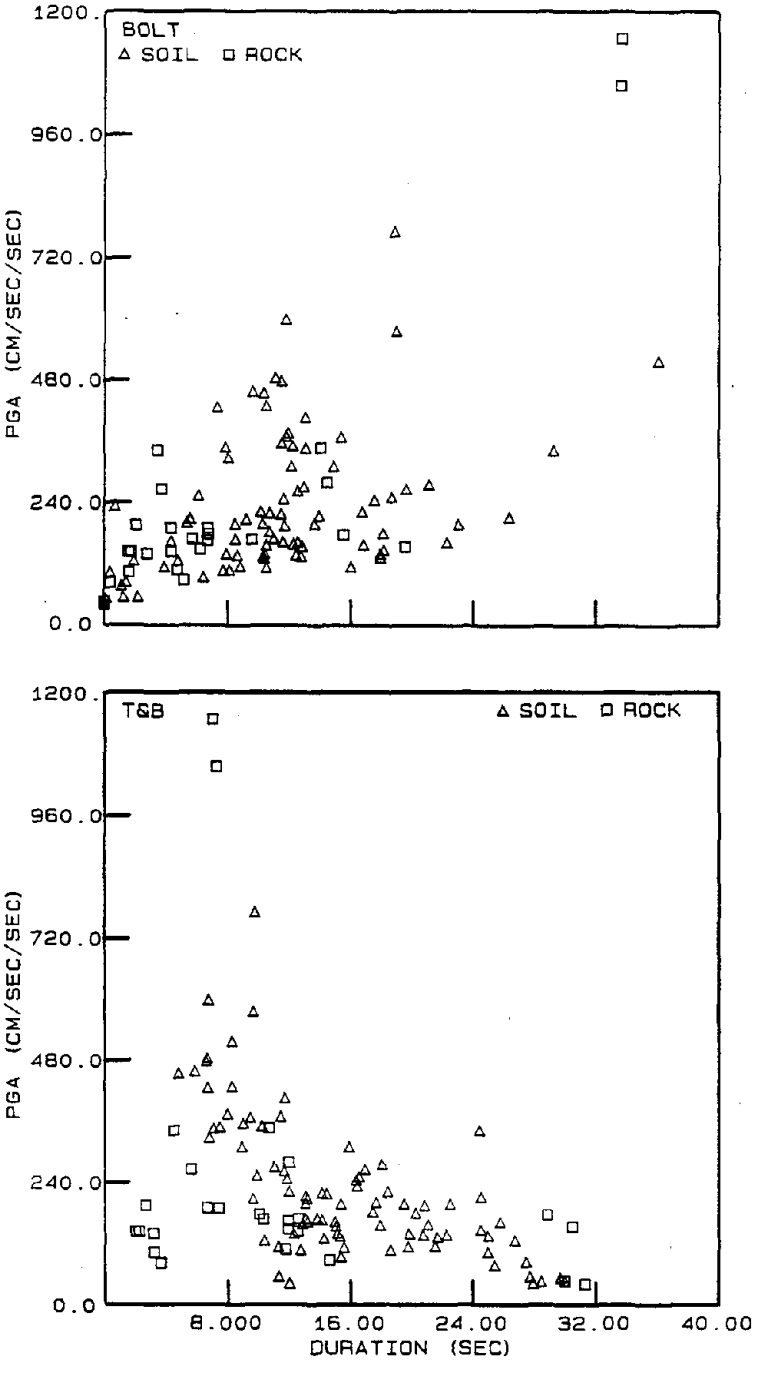

Figure 2.2 PGA vs. duration for soil and rock sites: Bolt (1973) and Trifunac and Brady (1975) durations.

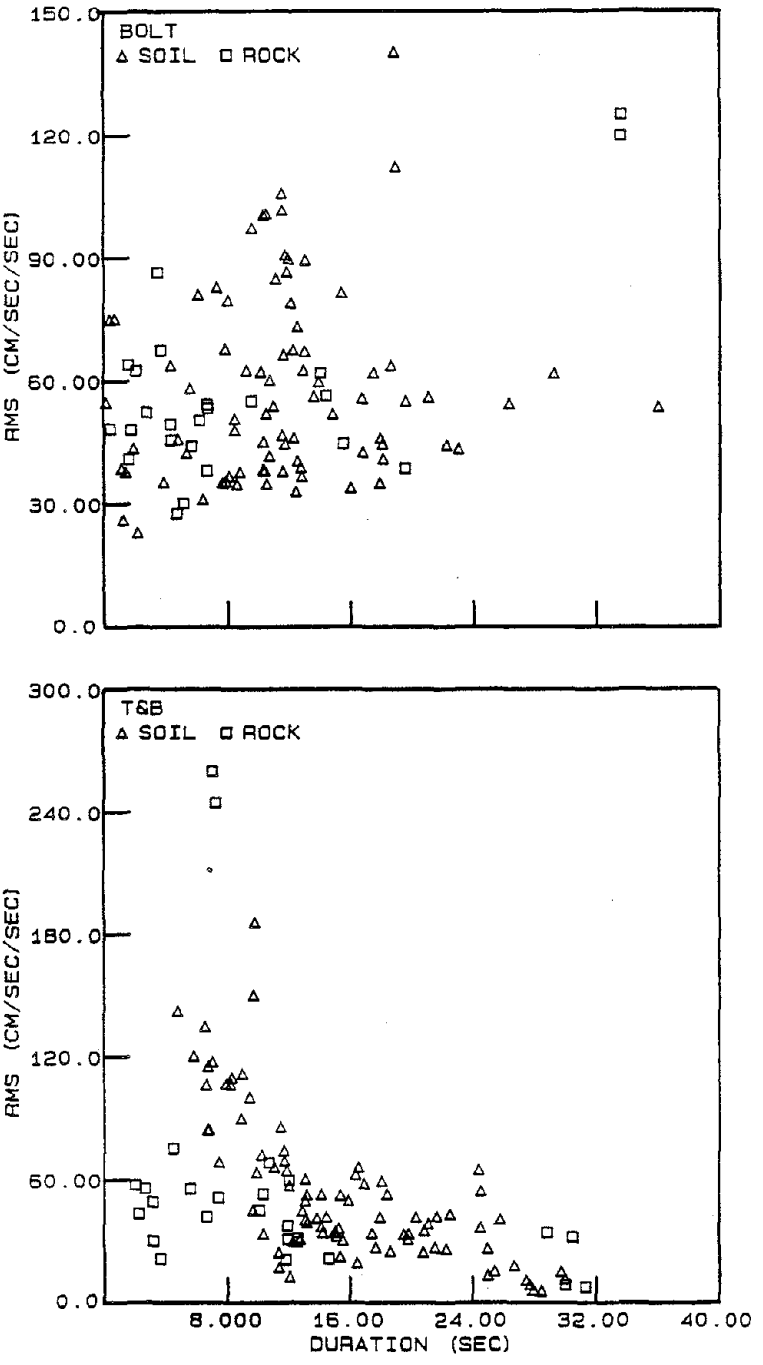

Figure 2.3 RMS acceleration vs. duration for soil and rock sites: Bolt (1973) and Trifunac and Brady (1975) durations.

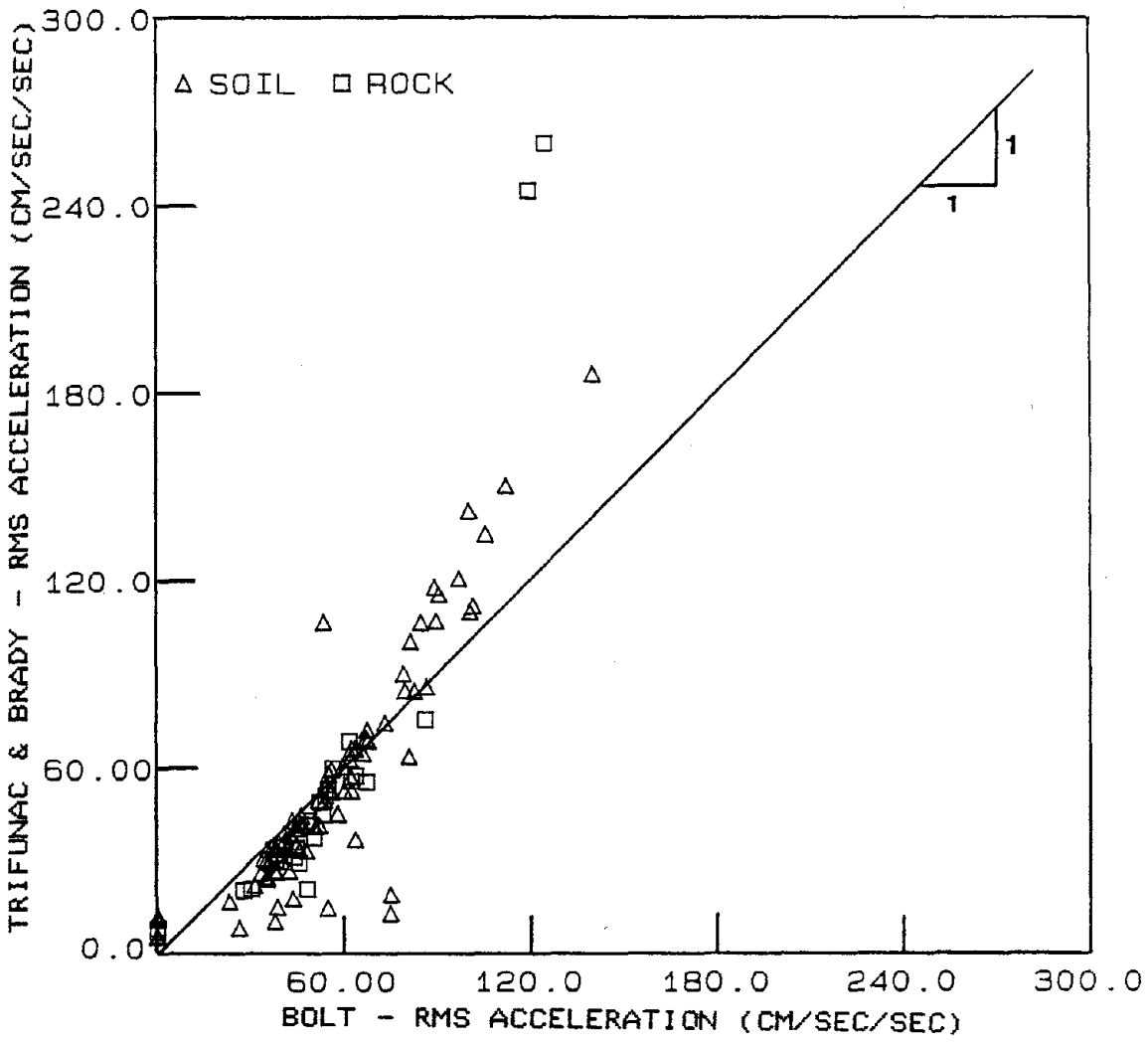

Figure 2.4 RMS acceleration per Bolt (1973) duration vs. RMS acceleration per Trifunac and Brady (1975) duration for soil and rock sites.

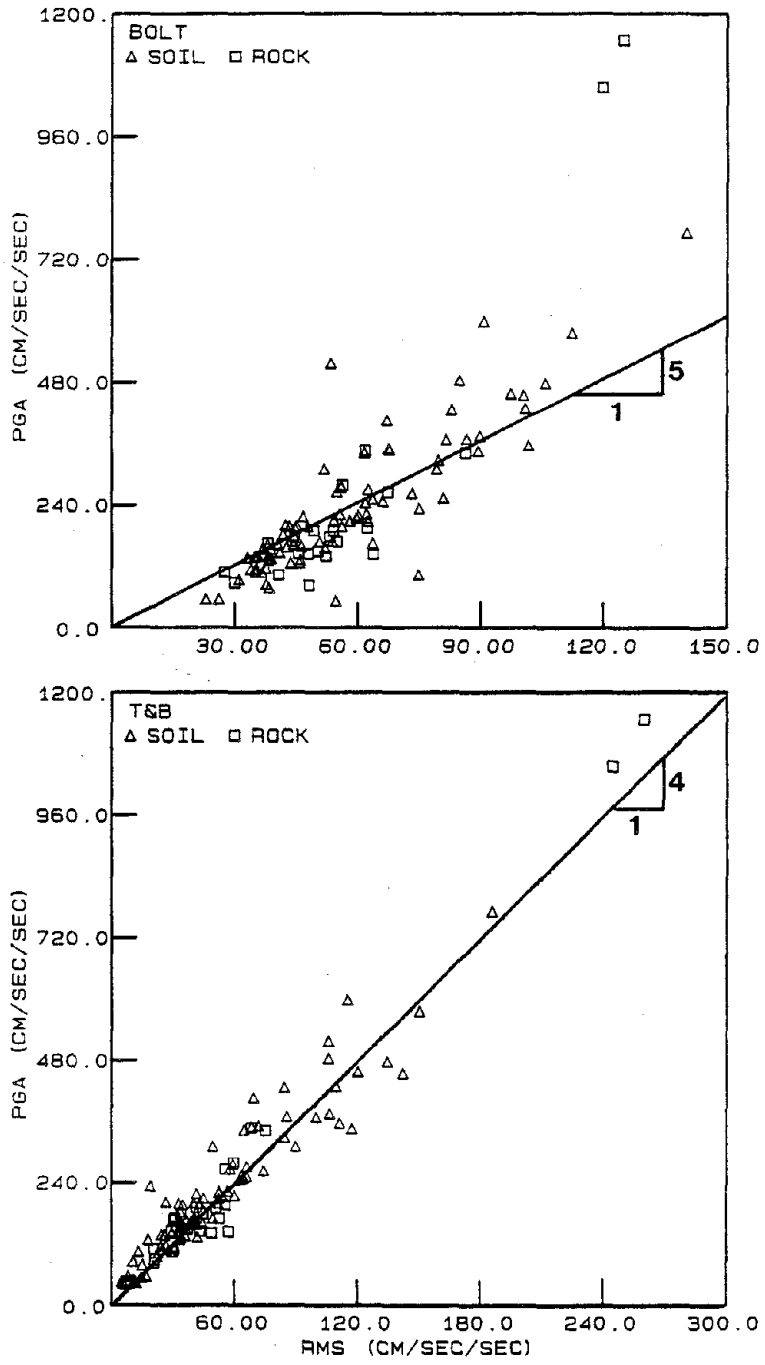

Figure 2.5 PGA vs. RMS acceleration for soil and rock sites for RMS acceleration computed from Bolt (1973) and Trifunac and Brady (1975) duration. (Lines shown are for reference only).

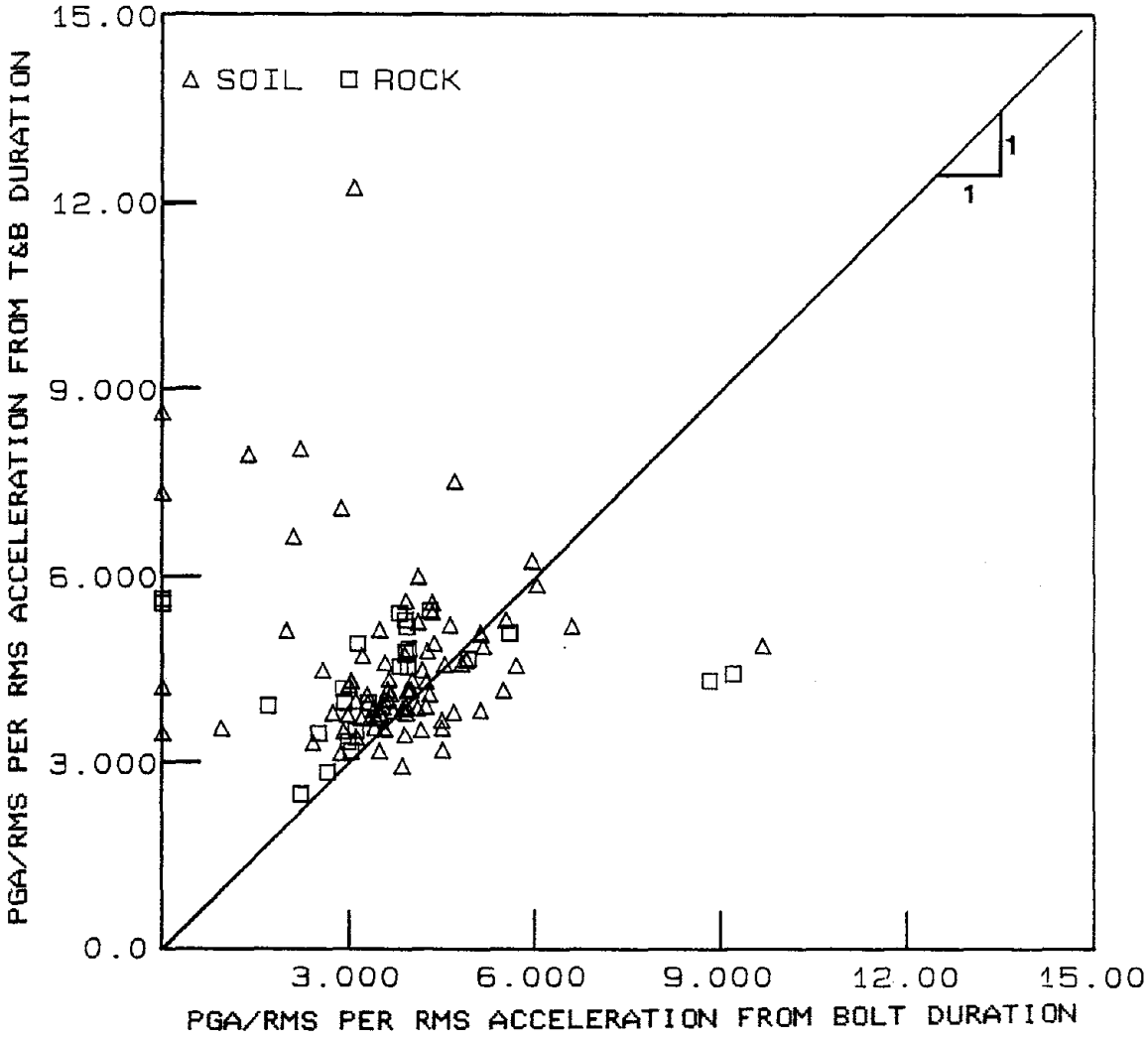

Figure 2.6 PGA/RMS per Bolt (1973) duration vs. PGA/RMS per Trifunac and Brady (1975) duration for soil and rock sites.

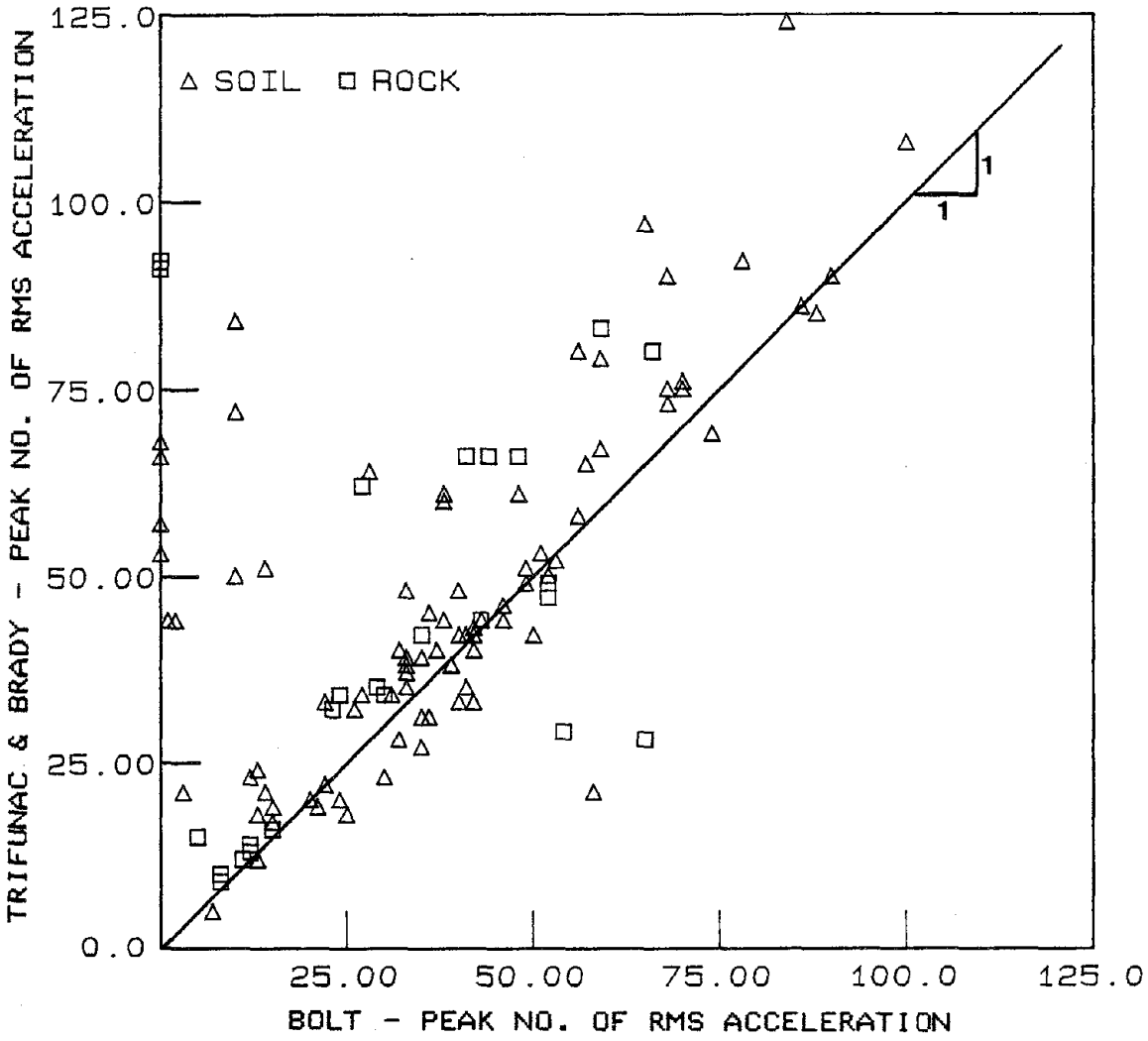

Figure. 2.7 Peak number of RMS acceleration per Bolt (1973) duration vs. peak number of RMS acceleration per Trifunac and Brady (1975) duration for soil and rock sites.

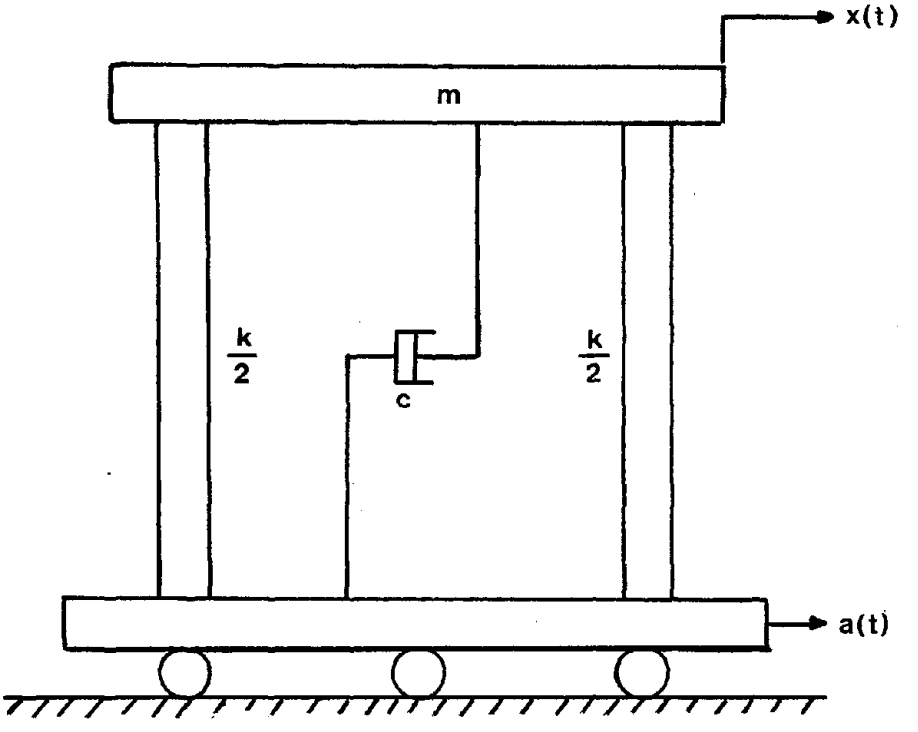

Figure 2.8 Linear, elastic single-degree-of-freedom oscillator.

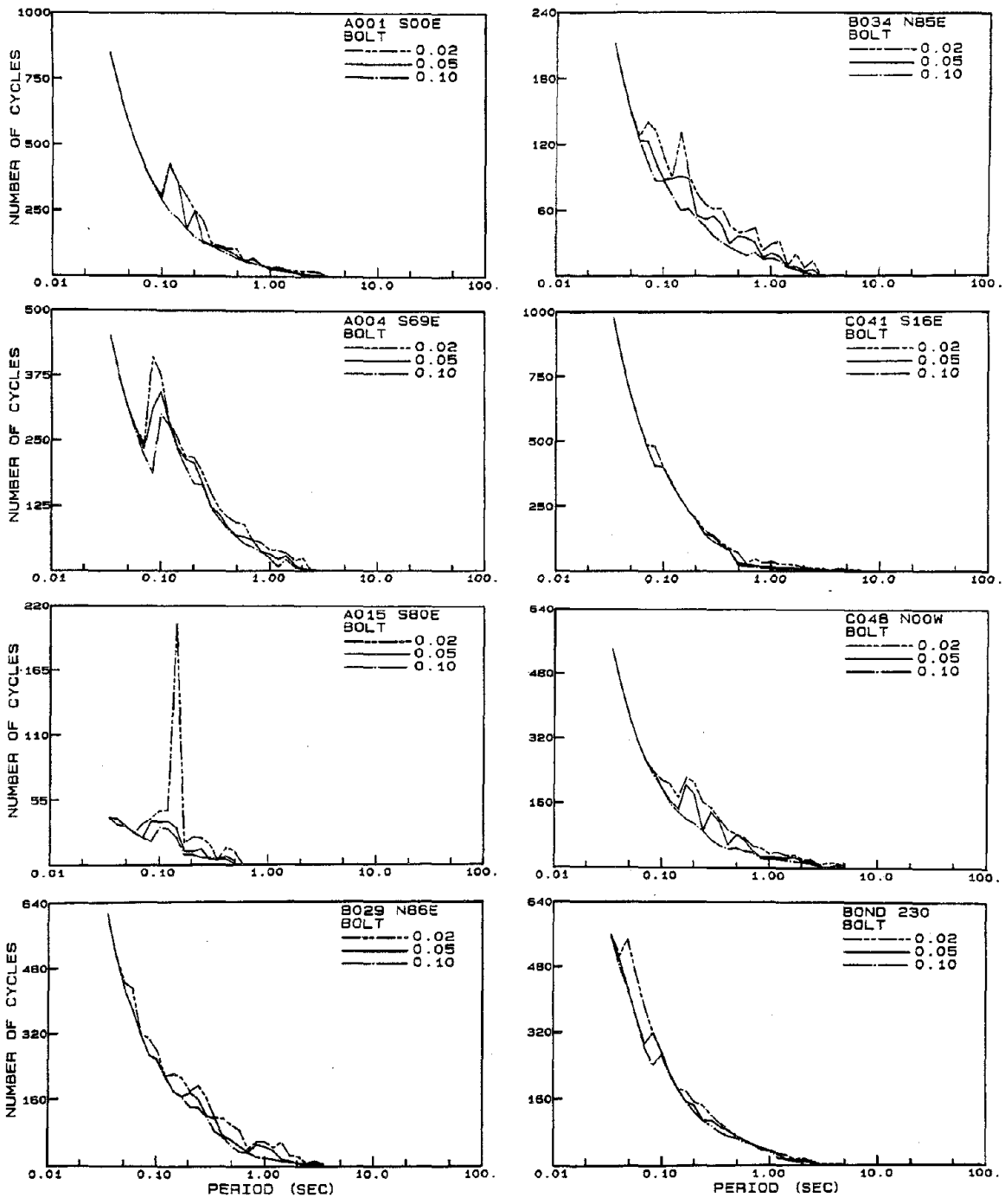

Figure 2.9 Number of cycles from Bolt (1973) duration vs. period for SDOF oscillator with 2, 5, and 10% damping.

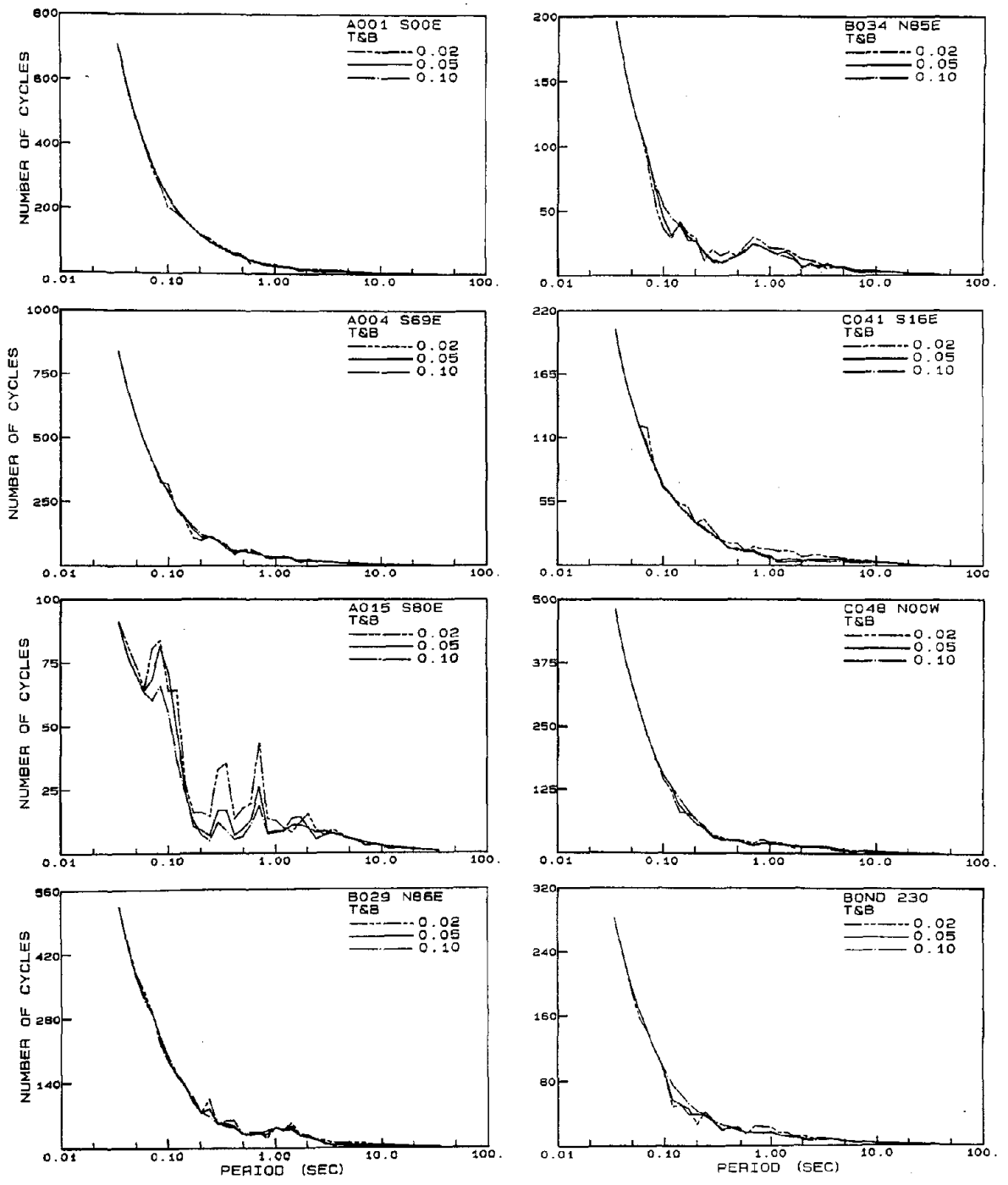

Figure 2.10 Number of cycles from Trifunac and Brady (1975) duration vs. period for SDOF oscillator with 2, 5, and 10% damping.

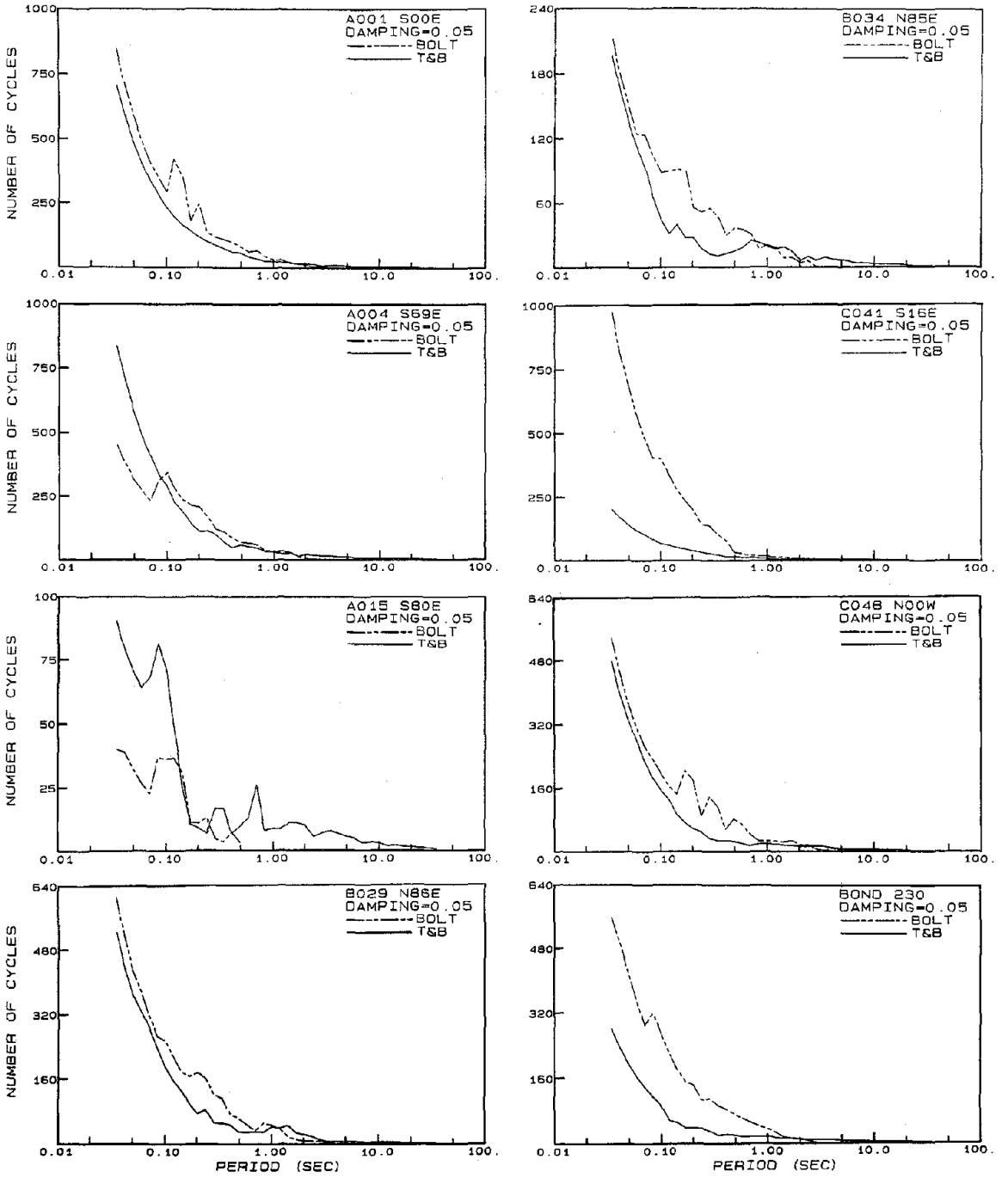

Figure 2.11 Comparison of number of cycles per Bolt (1973) and Trifunac and Brady (1975) durations vs. period for SDOF oscillator with 5% damping.

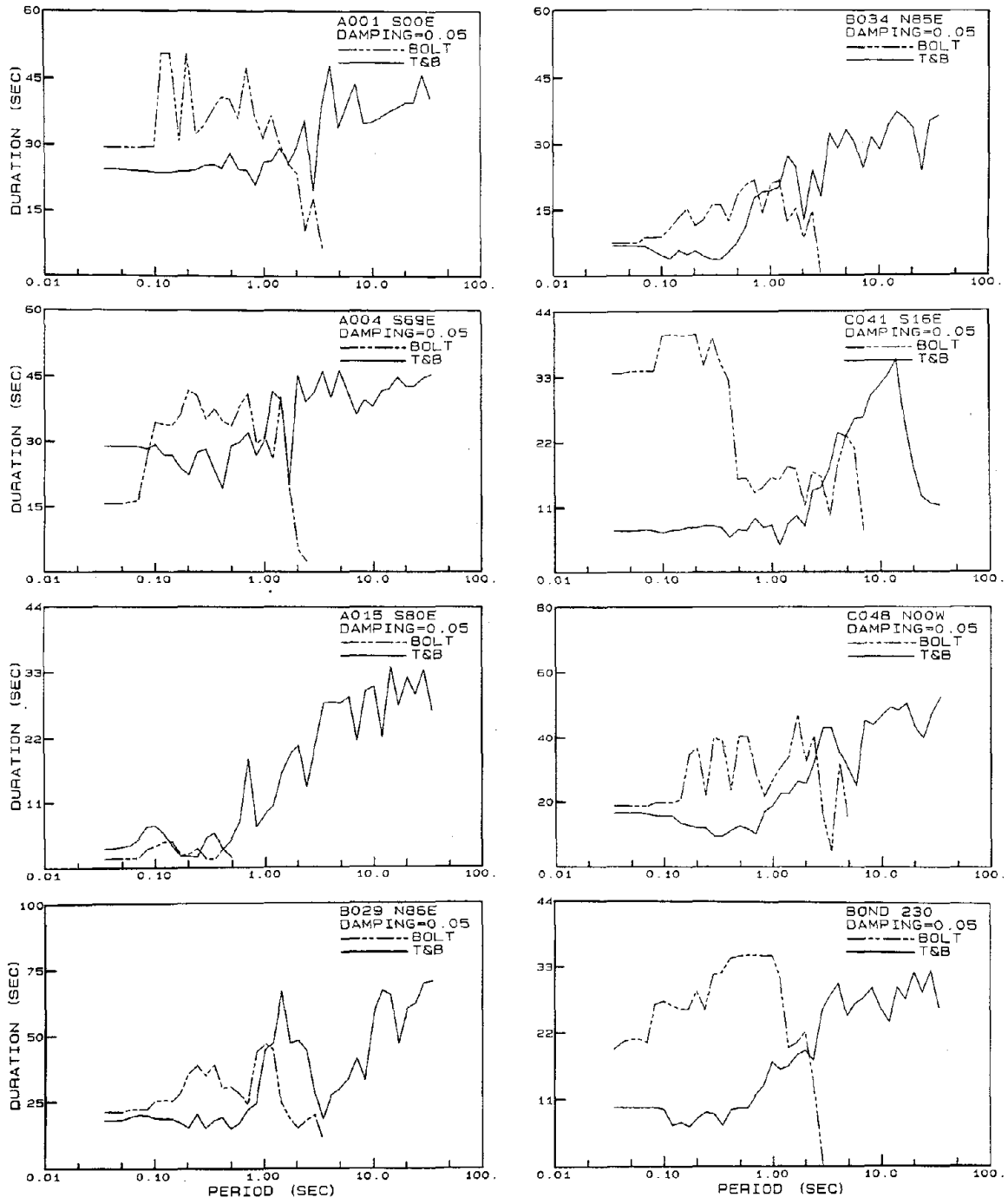

Figure 2.12 Comparison of duration spectra from Bolt (1973) and Trifunac and Brady (1975) durations for response of SDOF oscillator with 5% damping.

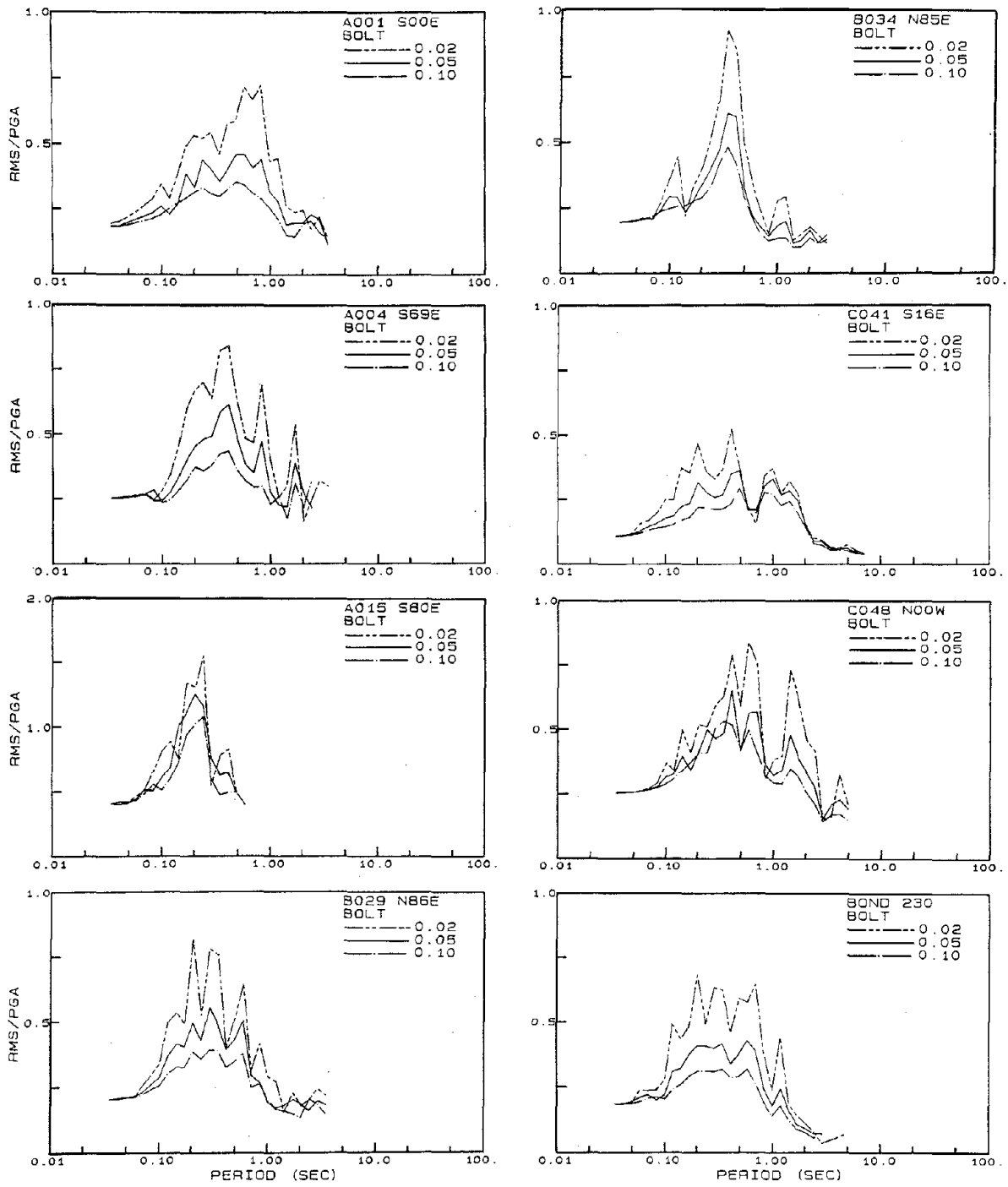

Figure 2.13 RMS acceleration/PGA spectra for SDOF oscillator with 2, 5, and 10% damping for RMS acceleration based on Bolt (1973) duration.

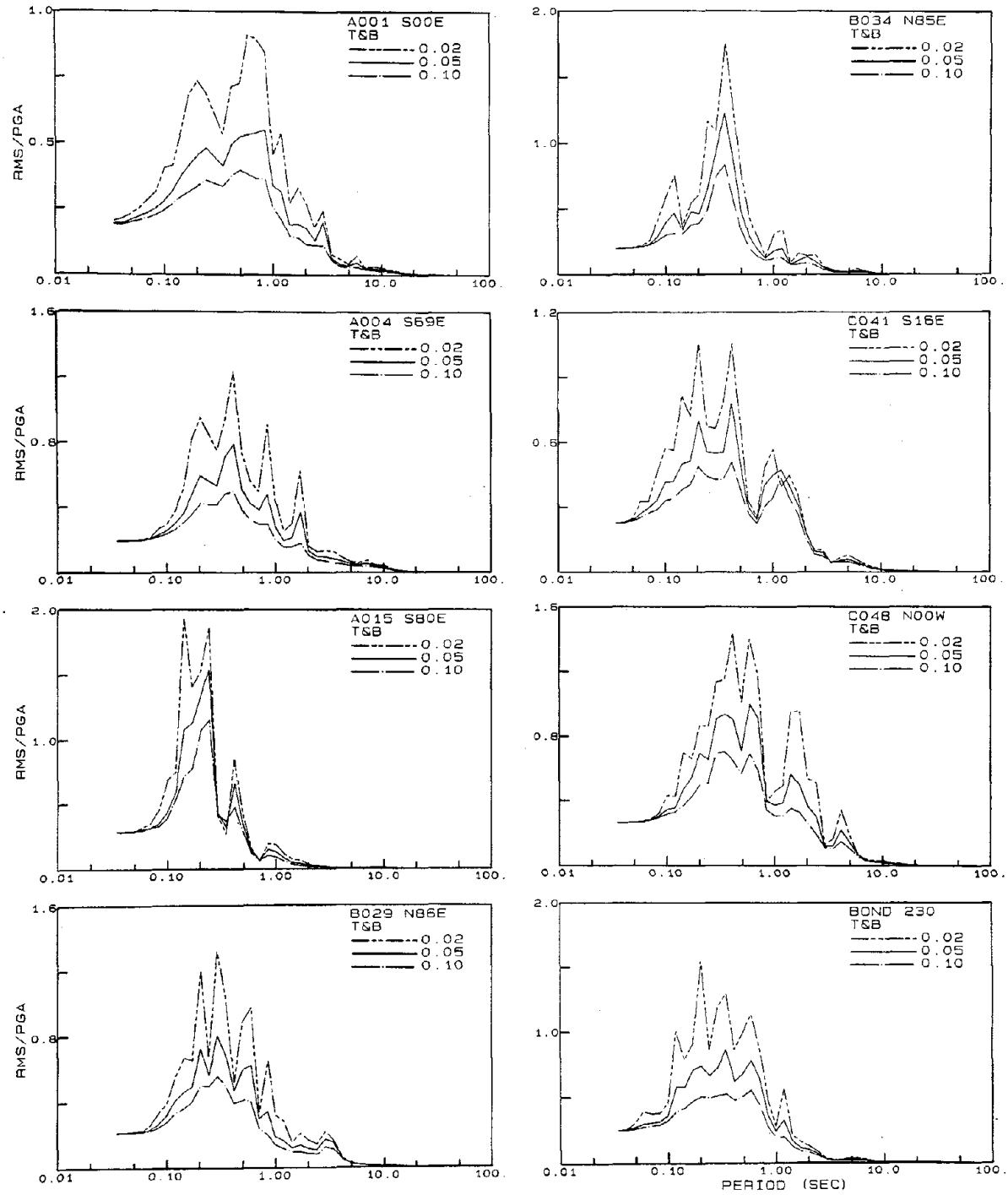

Figure 2.14 RMS acceleration/PGA spectra for SDOF oscillator with 2, 5, and 10% damping for RMS acceleration based on Trifunac and Brady (1975) duration.

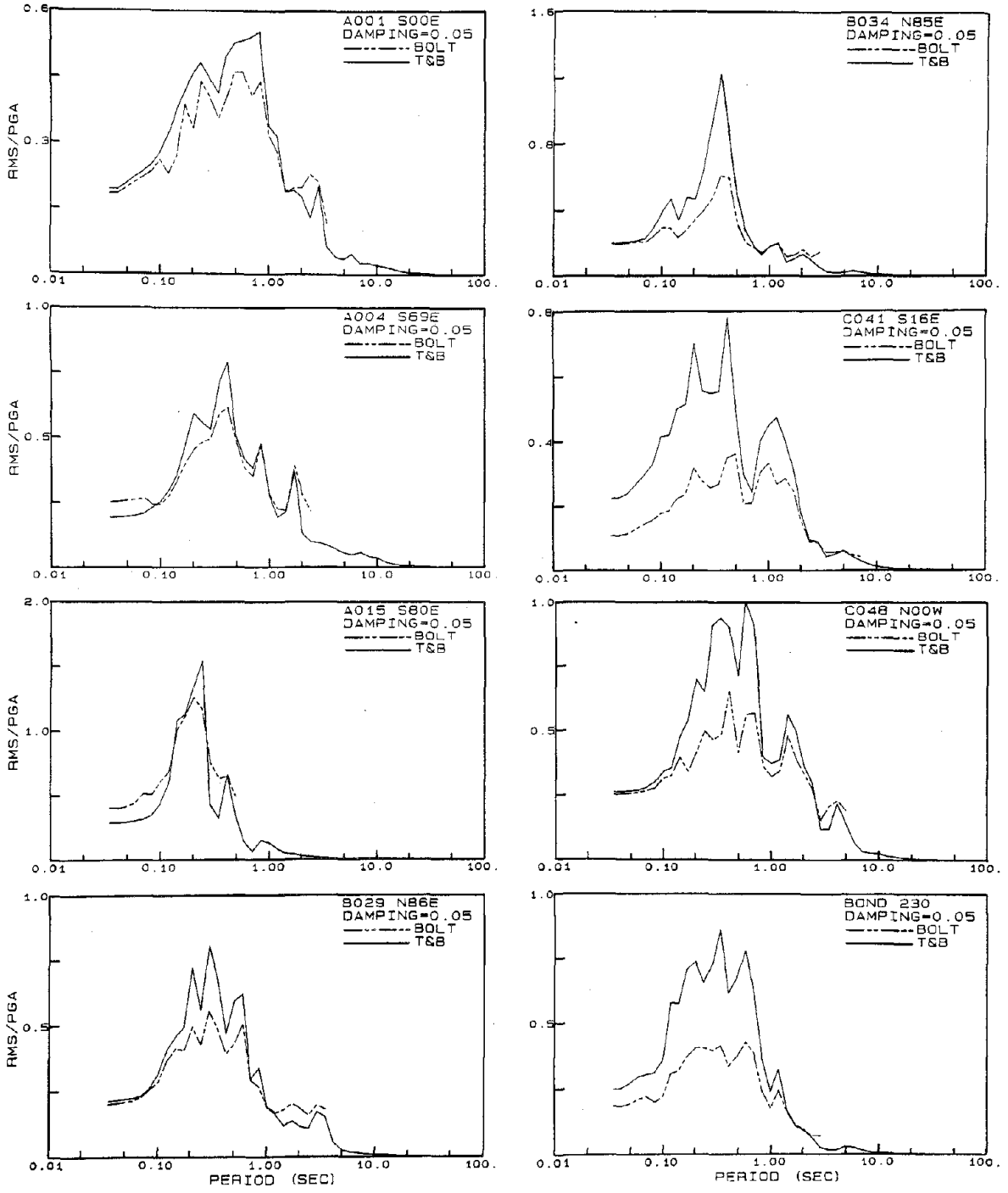

Figure 2.15 Comparison of RMS acceleration/PGA spectra for SDOF oscillator with 5% damping for RMS acceleration based on Bolt (1973) and Trifunac and Brady (1975) durations.

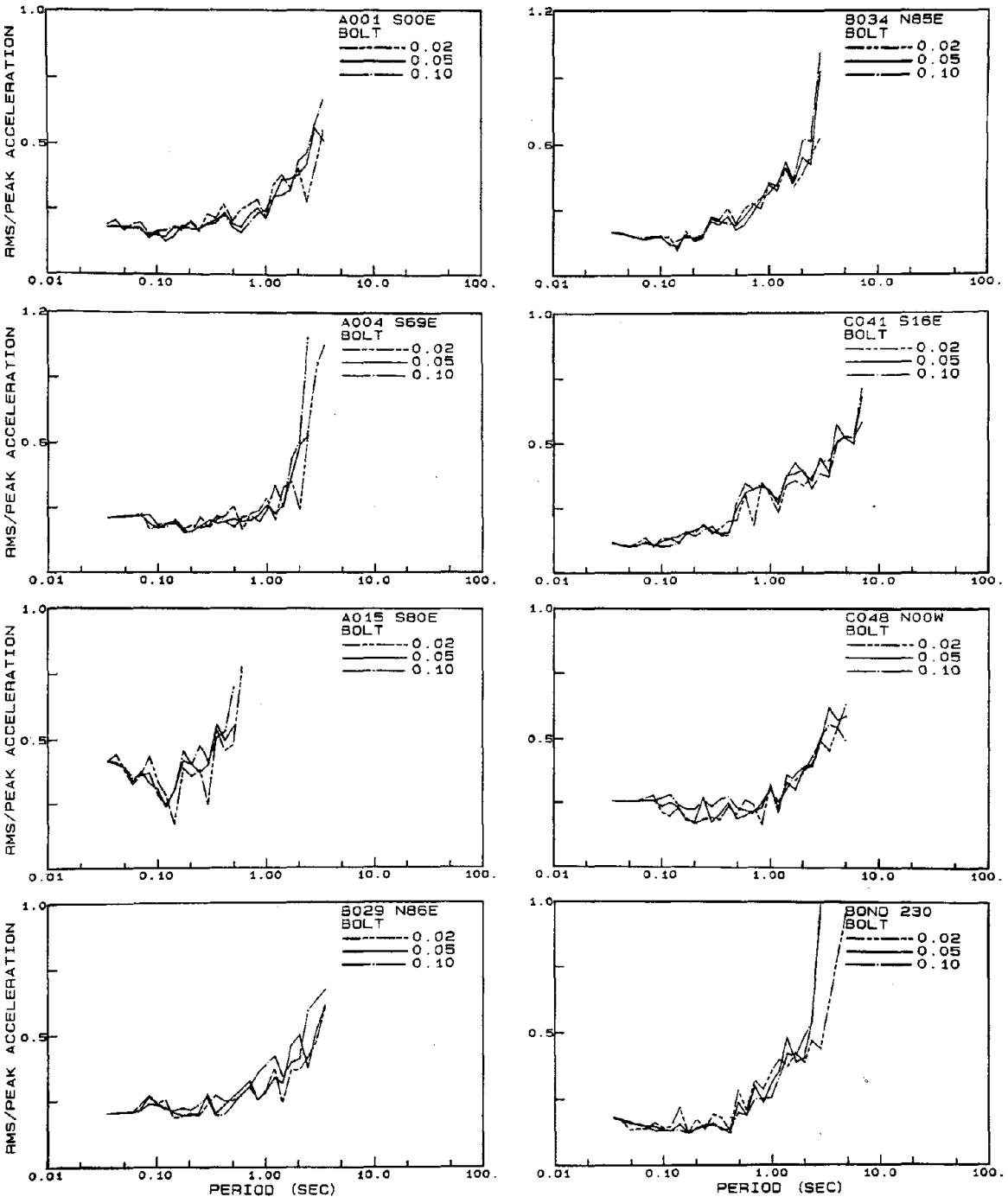

Figure 2.16 RMS acceleration/peak acceleration spectra for SDOF oscillator with 2, 5, and 10% damping for RMS acceleration based on Bolt (1973) duration.

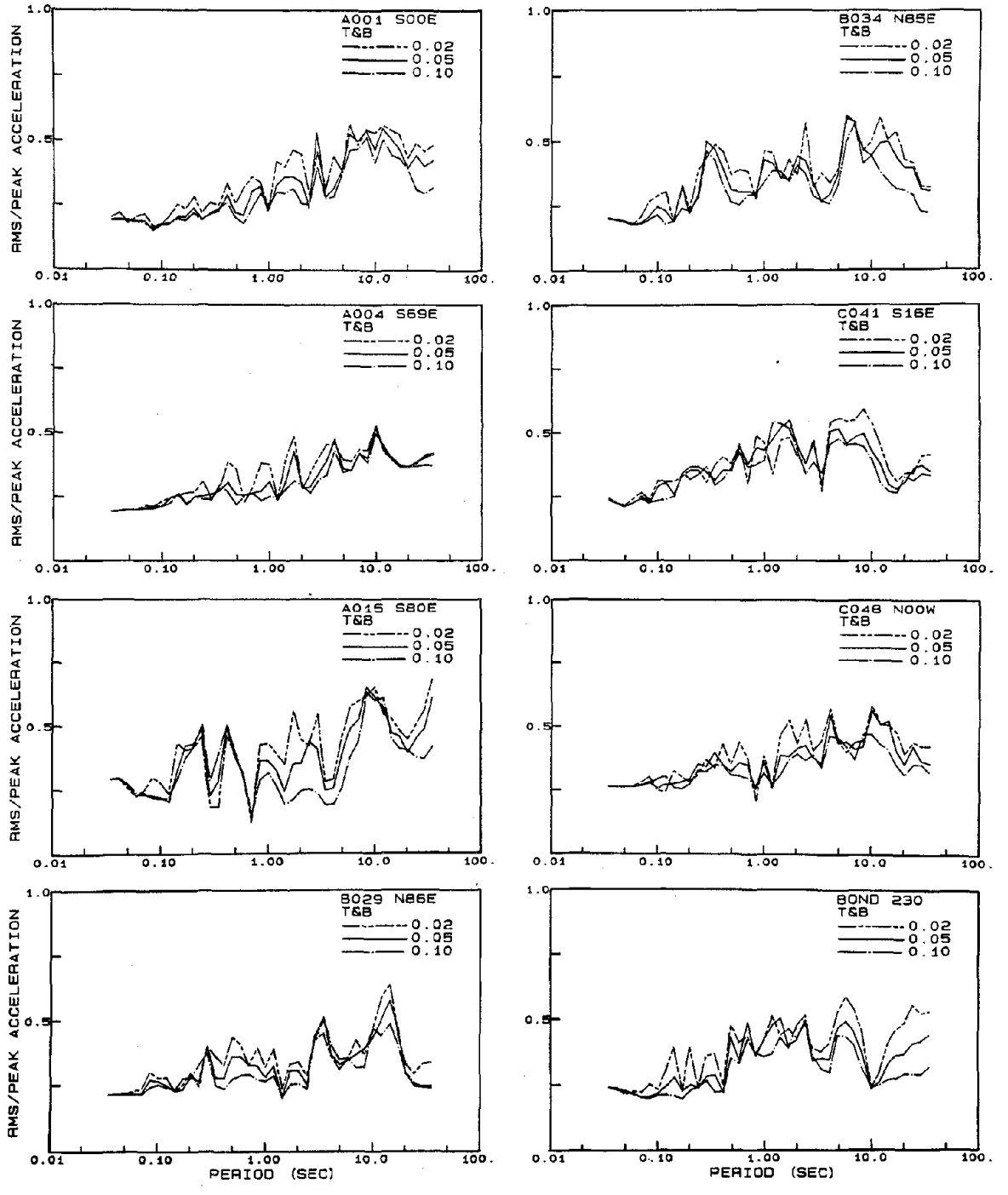

Figure 2.17 RMS acceleration/peak acceleration spectra for SDOF oscillator with 2, 5, and 10% damping for RMS acceleration based on Trifunac and Brady (1975) duration.

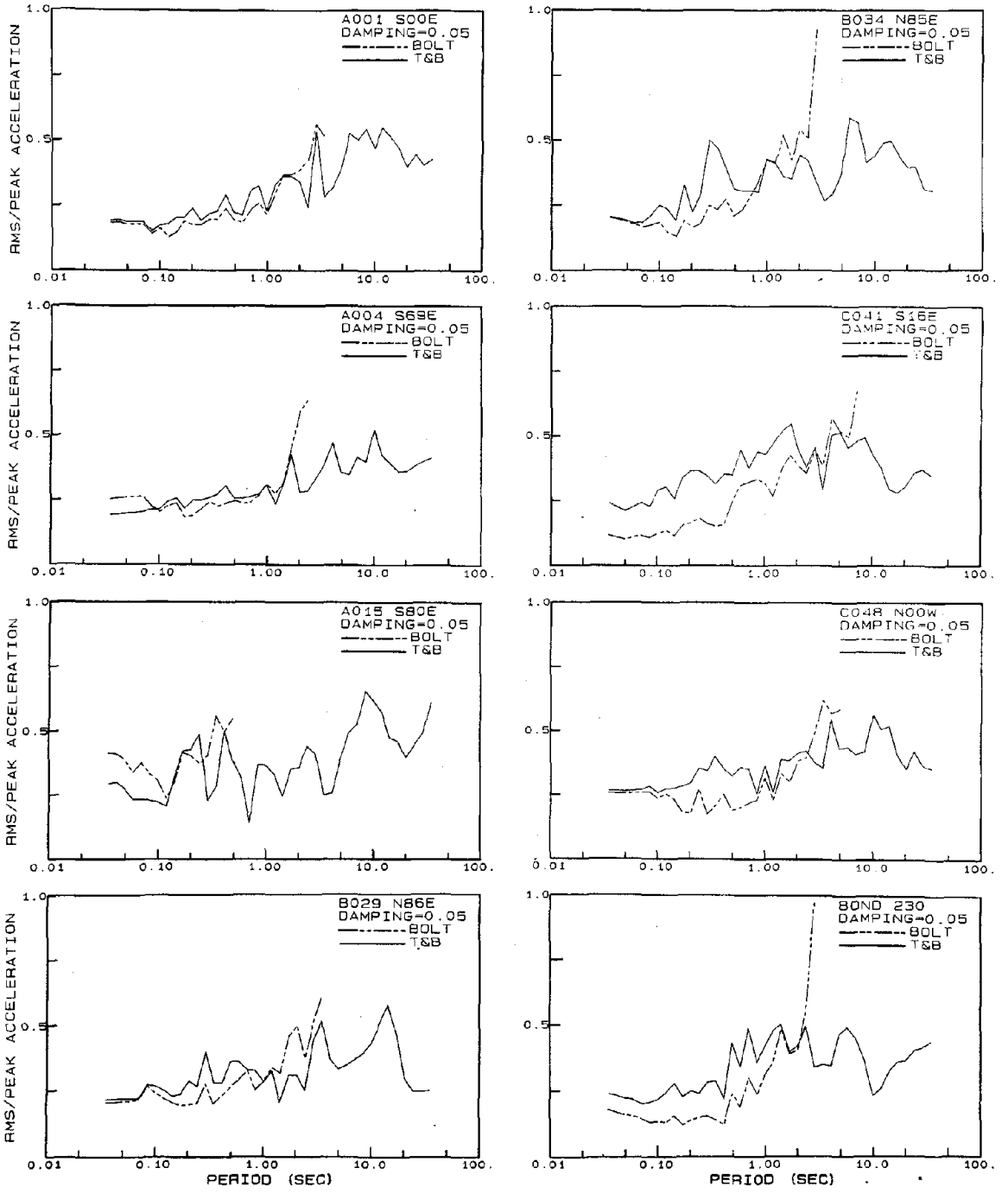

Figure 2.18 Comparison of RMS acceleration/peak acceleration spectra for SDOF oscillator with 5% damping for RMS acceleration based on Bolt (1973) and Trifunac and Brady (1975) durations.

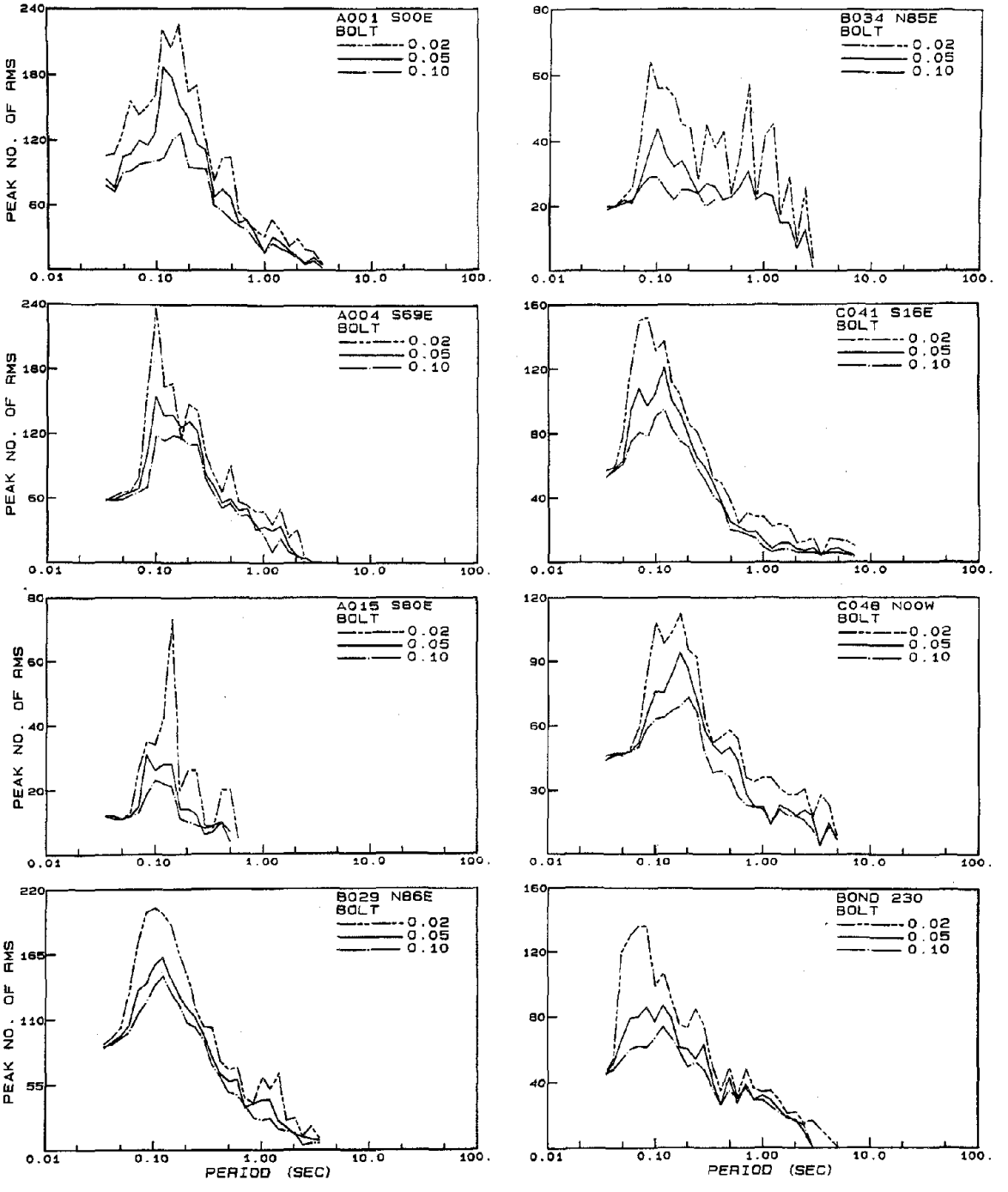

Figure 2.19 Number of kth largest peak in response time history corresponding to RMS acceleration vs. period of response of SDOF oscillator with 2, 5, and 10% damping for RMS acceleration based on Bolt (1973) duration.

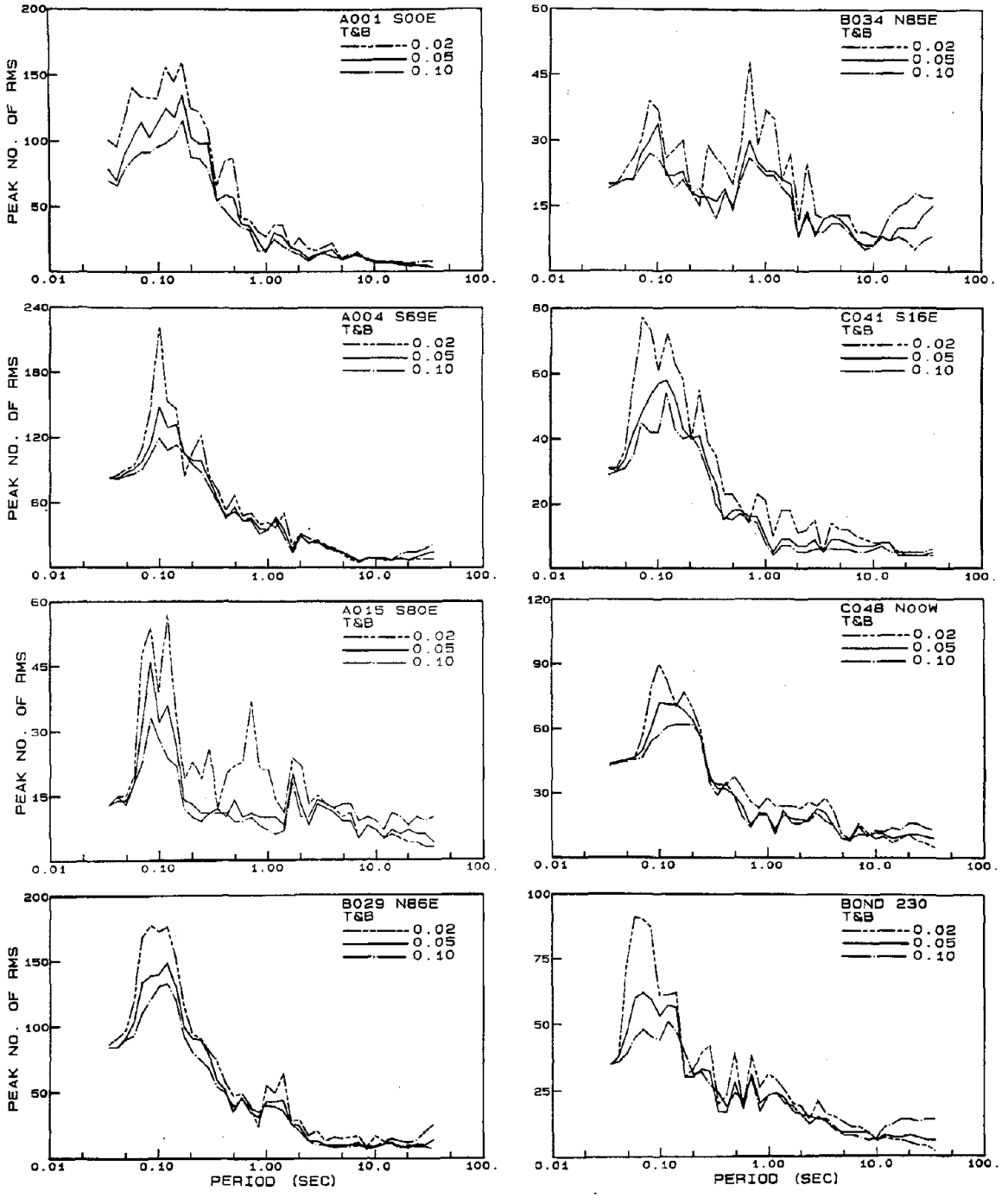

Figure 2.20 Number of kth largest peak in response time history corresponding to RMS acceleration vs. period of response of SDOF oscillator with 2, 5, and 10% damping for RMS acceleration based on Trifunac and Brady (1975) duration.

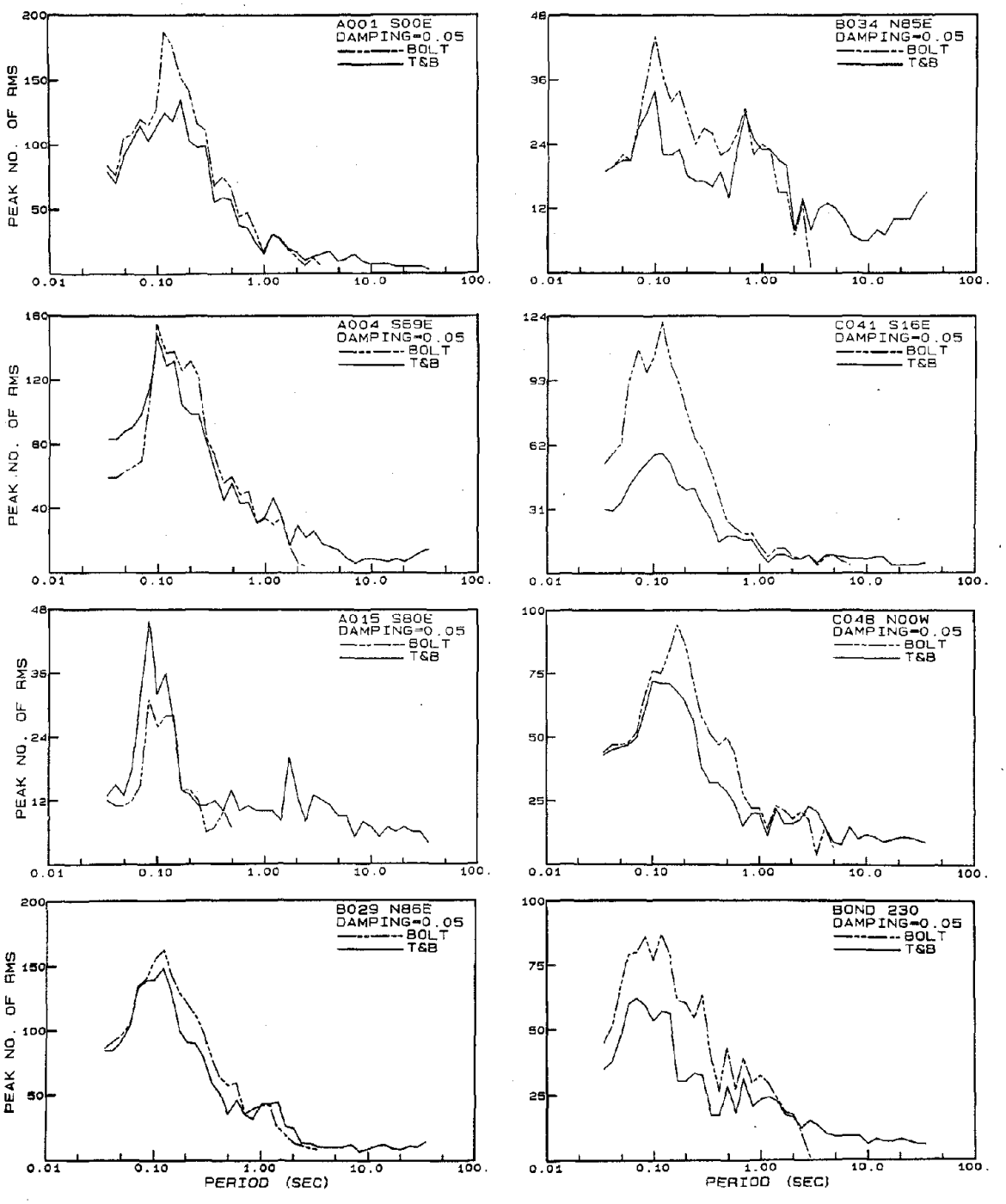

Figure 2.21 Comparison of the number of kth largest peak in response time history corresponding to RMS acceleration vs. period of response of SDOF oscillator with 5% damping for RMS acceleration based on Bolt (1973) and Trifunac and Brady (1975) durations.

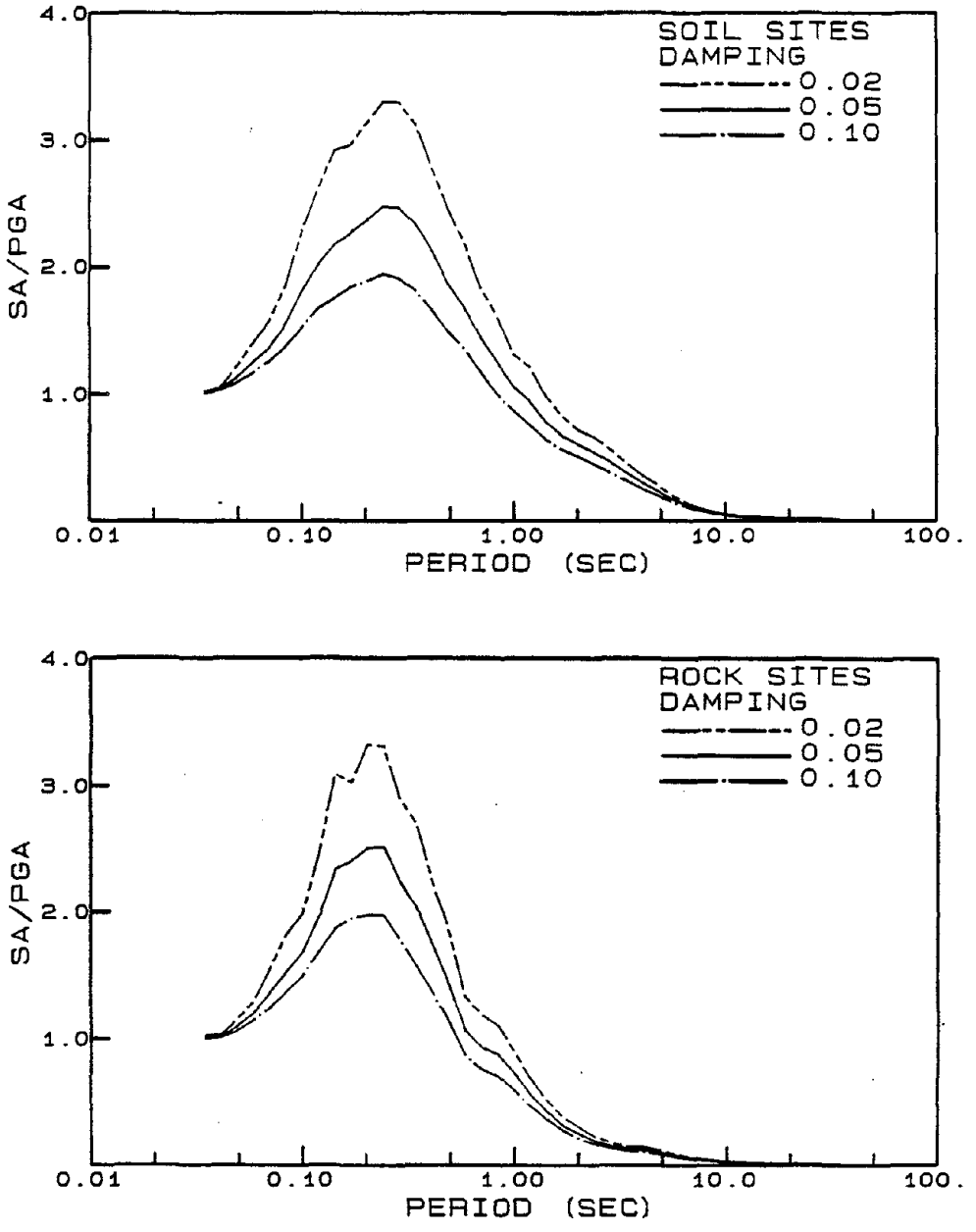

Figure 2.22 Average peak acceleration spectra for soil and rock sites for 2, 5, and 10% damping.

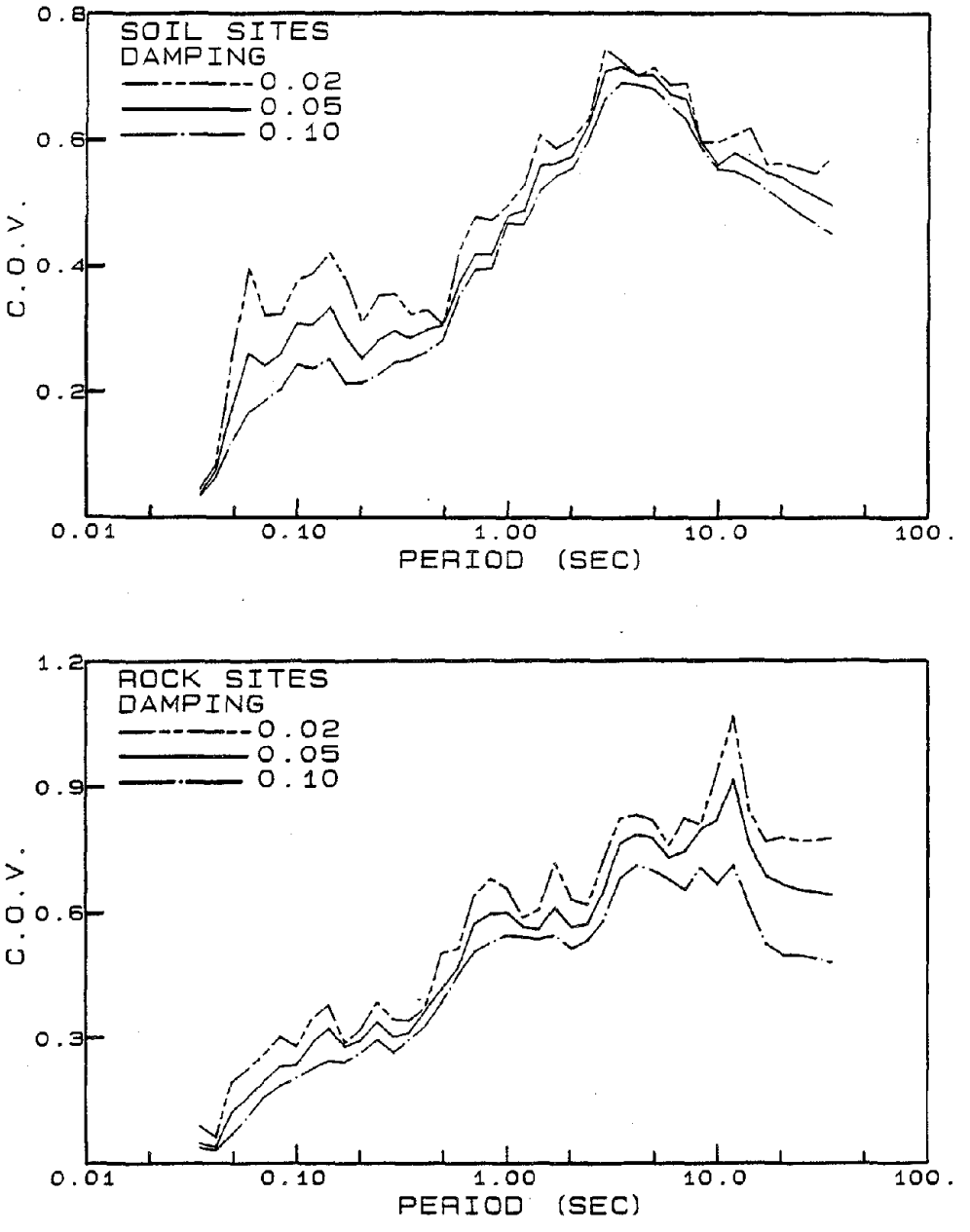

Figure 2.23 Coefficient of variation (C.O.V.) of peak acceleration spectra for rock and soil sites for 2, 5, and 10% damping.

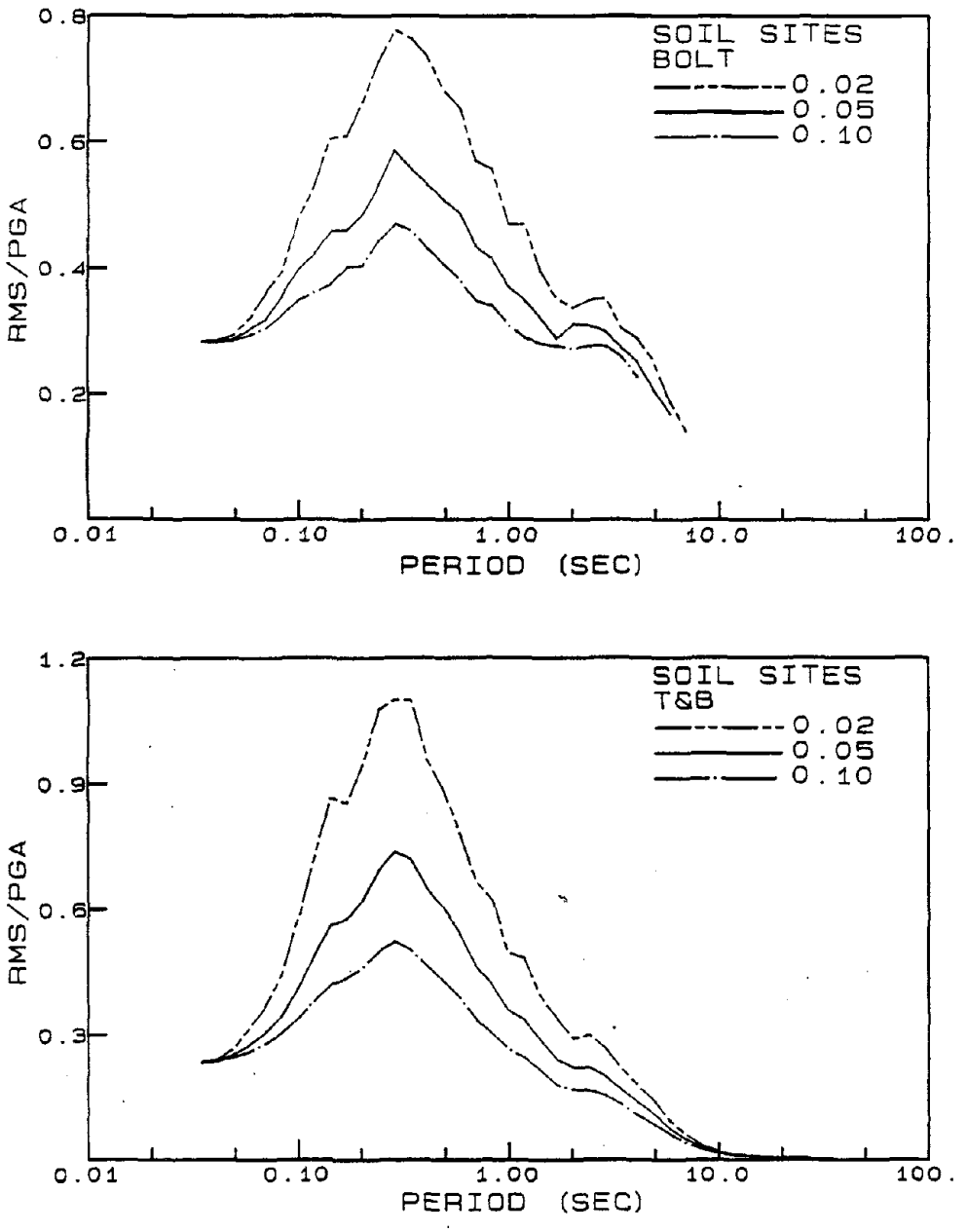

Figure 2.24 Average RMS acceleration spectra for soil and rock sites for 2, 5, and 10% damping.

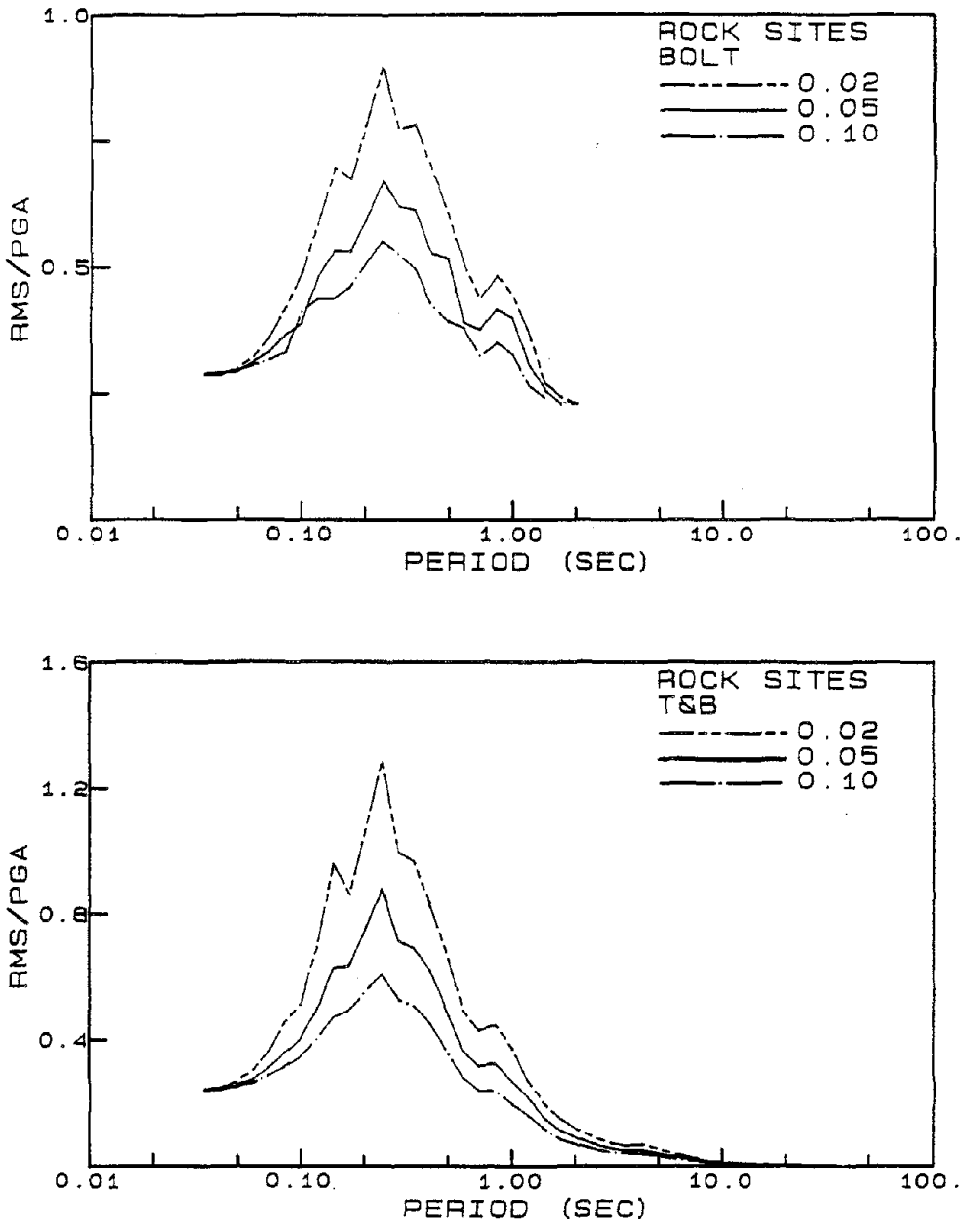

Figure 2.25 Average RMS acceleration spectra for rock sites for 2, 5, and 10% damping based on RMS acceleration computed from Bolt (1973) and Trifunac and Brady (1975) durations.

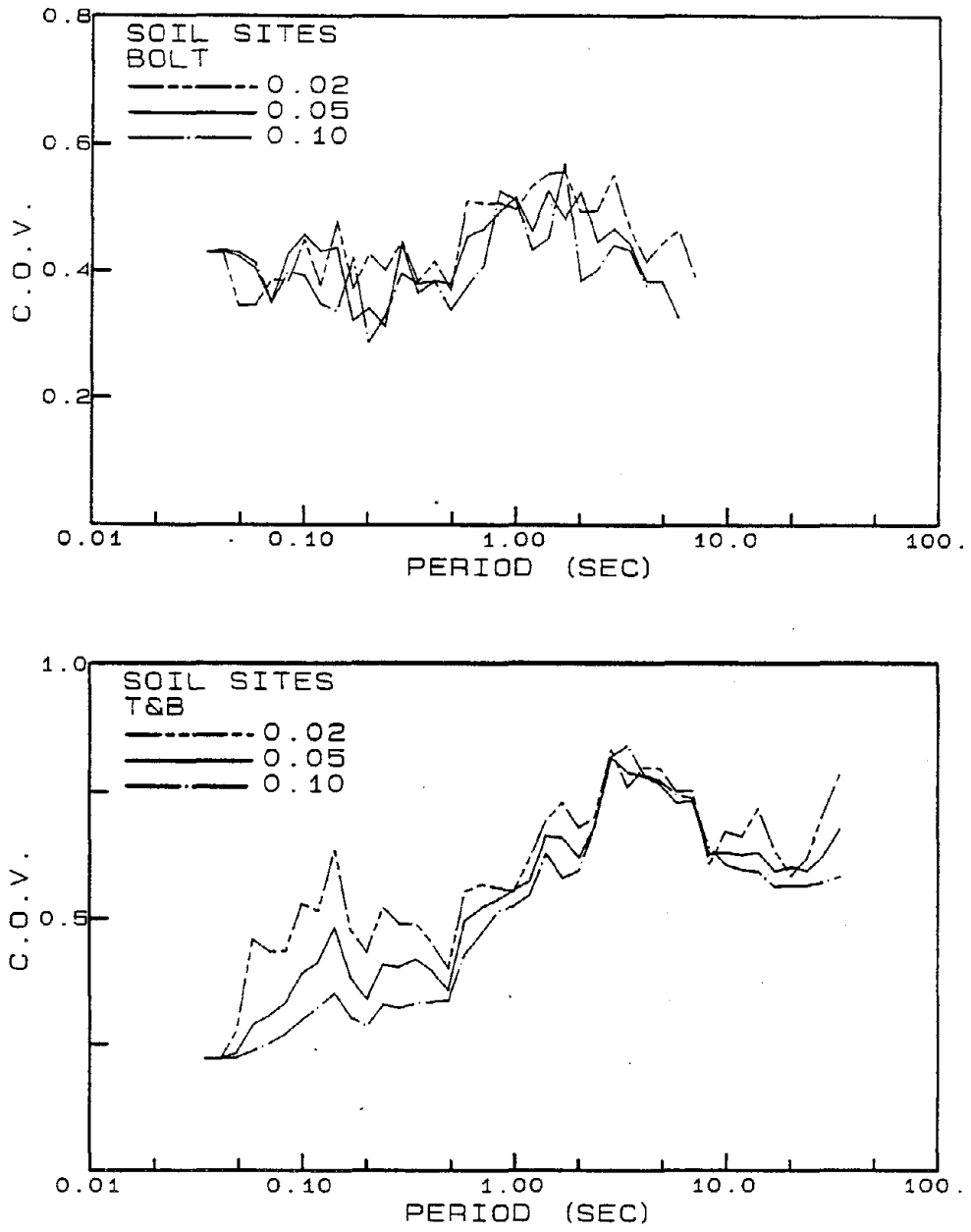

Figure 2.26 Coefficient of variation (C.O.V.) of RMS acceleration spectra for soil sites for 2, 5, and 10% damping for RMS acceleration computed from Bolt (1973) and Trifunac and Brady (1975) durations.

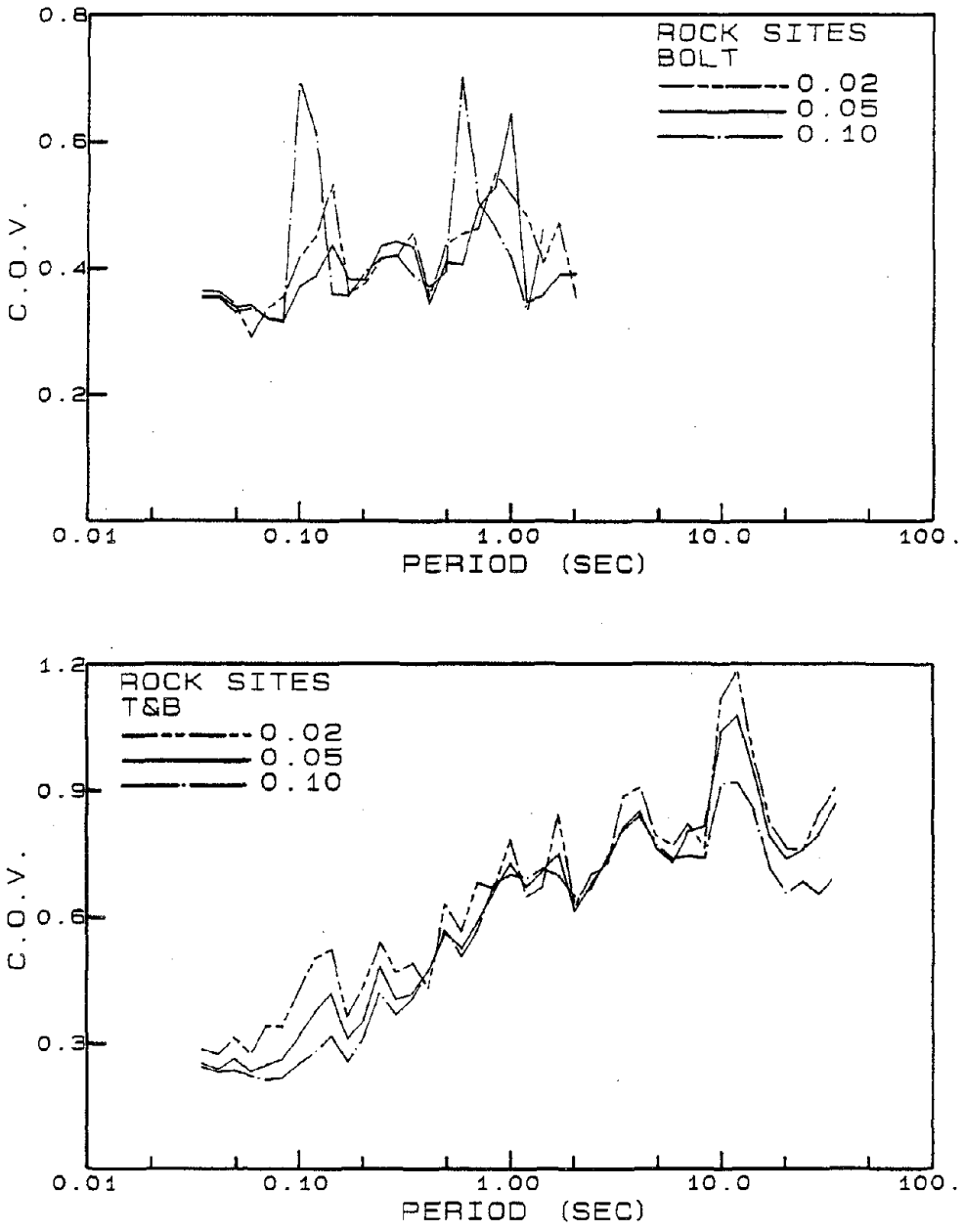

Figure 2.27 Coefficient of variation (C.O.V.) of RMS acceleration spectra for rock sites for 2, 5, and 10% damping for RMS acceleration computed from Bolt (1973) and Trifunac and Brady (1975) durations.

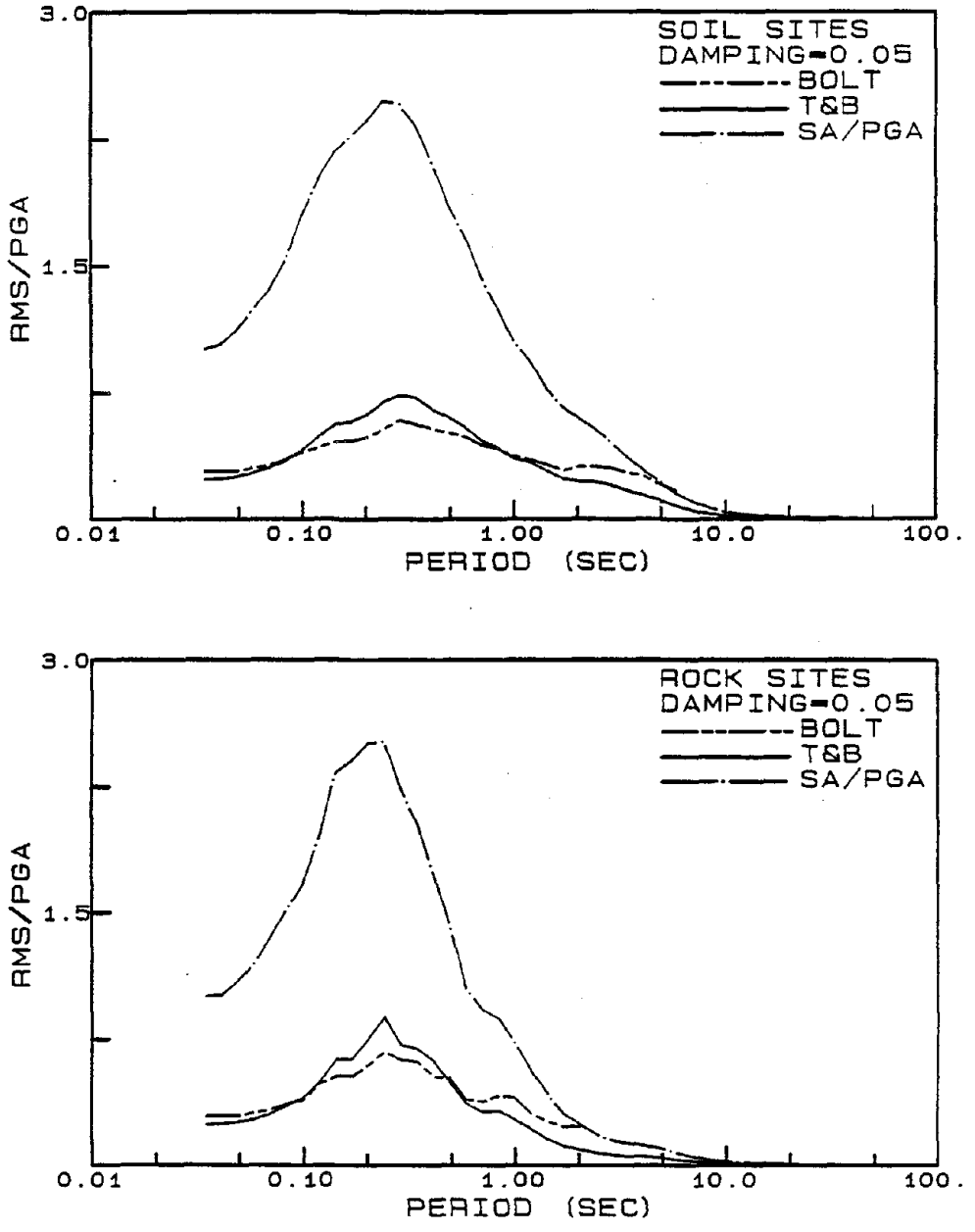

Figure 2.28 Comparison of average peak acceleration (SA/PGA) and average RMS acceleration spectra for soil and rock sites for 5% damping.

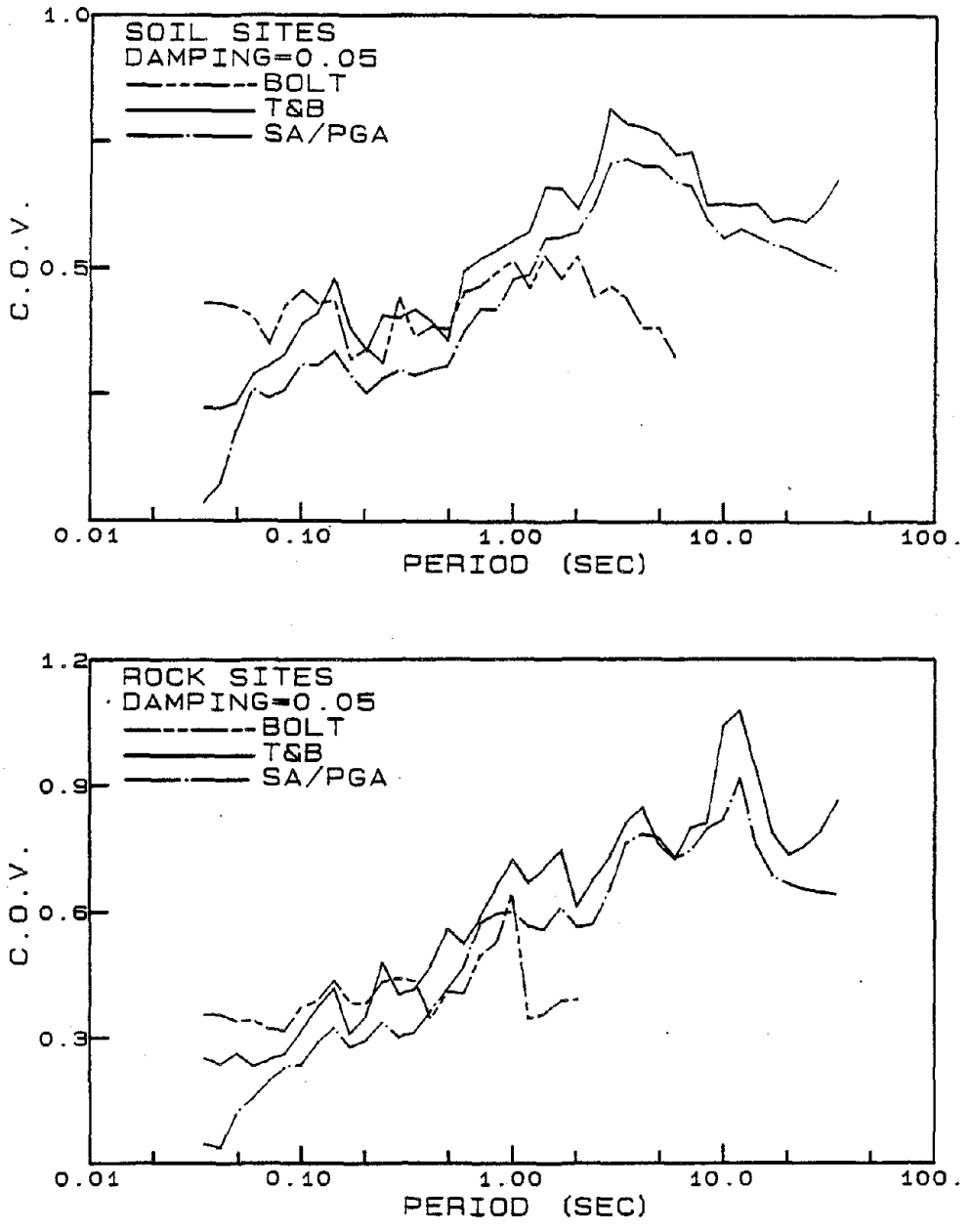

Figure 2.29 Coefficient of variation (C.O.V.) of average peak acceleration (SA/PGA) and average RMS acceleration spectra for soil and rock sites for 5% damping.

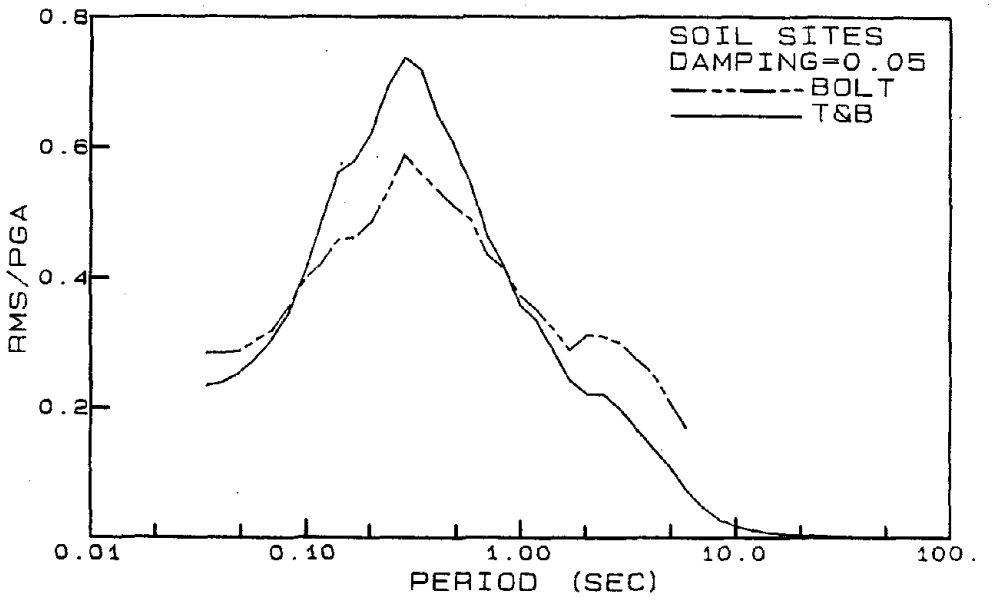

Figure 2.30 Comparison of average RMS acceleration spectra for soil sites for 5% damping for RMS acceleration based on Bolt (1973) and Trifunac and Brady (1975) durations.

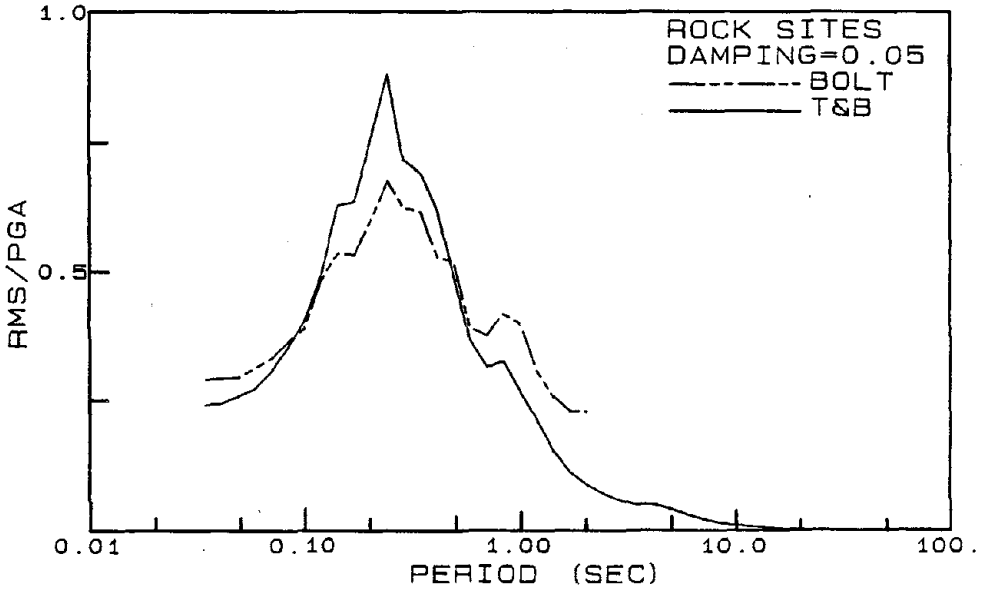

Figure 2.31 Comparison of average RMS acceleration spectra for rock sites for 5% damping for RMS acceleration based on Bolt (1973) and Trifunac and Brady (1975) durations.

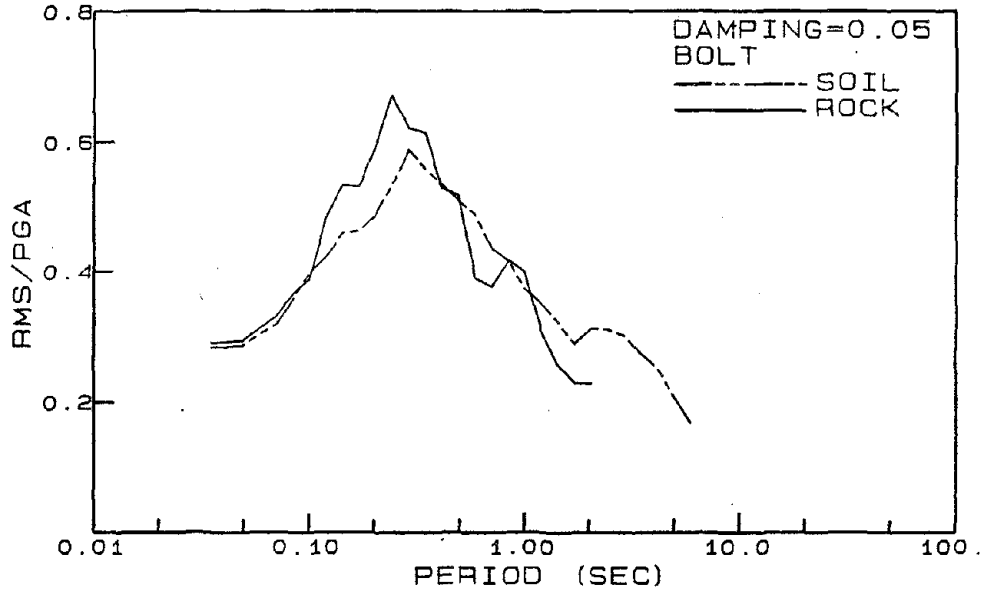

Figure 2.32 Comparison of average RMS acceleration spectra for soil and rock sites for 5% damping for RMS acceleration based on Bolt (1973) duration.

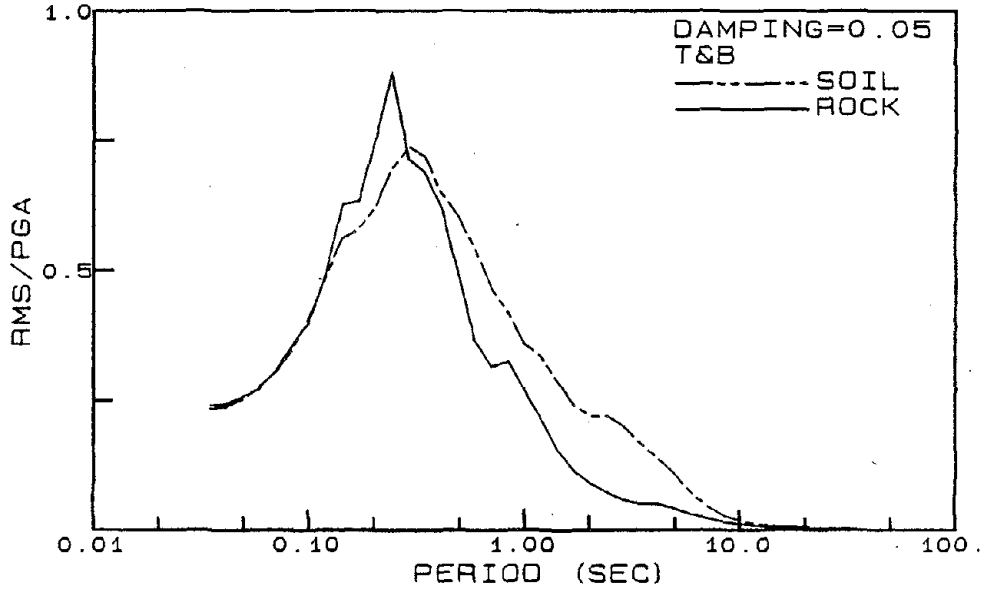

Figure 2.33 Comparison of average RMS acceleration spectra for soil and rock sites for 5% damping based on Trifunac-Brady (1975) duration.

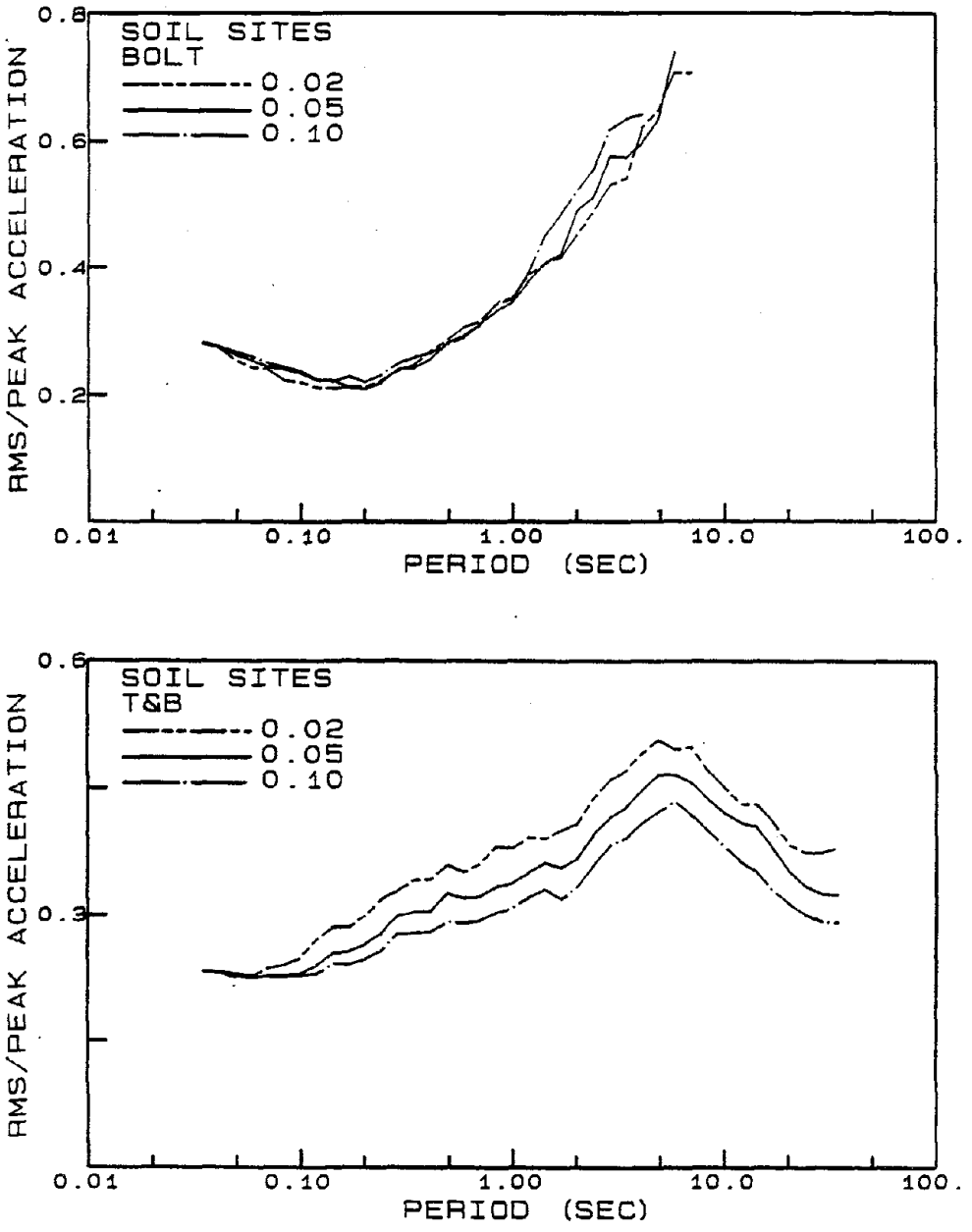

Figure 2.34 Average RMS acceleration/peak acceleration spectra for soil sites for 2, 5, and 10% damping based on RMS acceleration computed from Bolt (1973) and Trifunac and Brady (1975) durations.

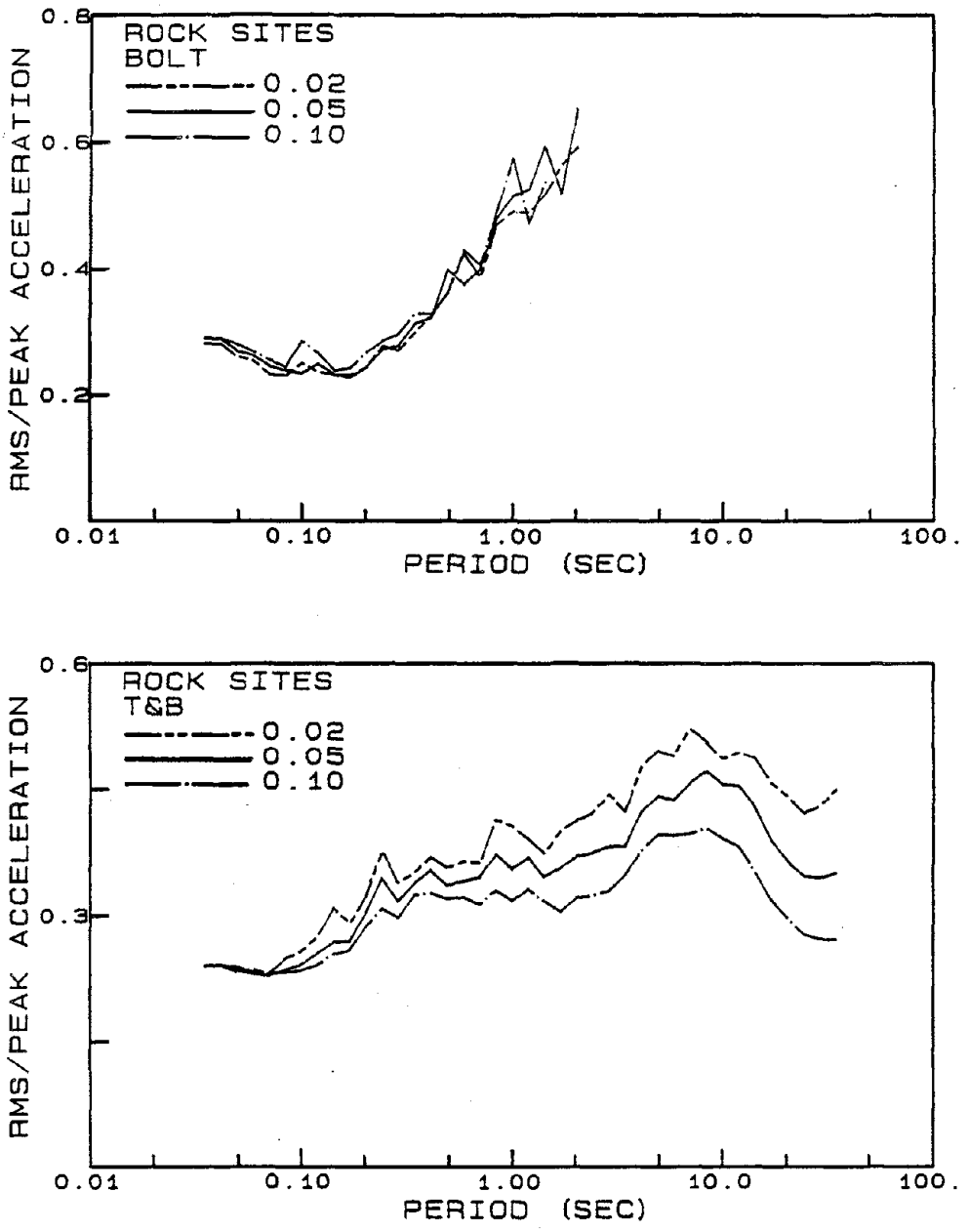

Figure 2.35 Average RMS acceleration/peak acceleration spectra for rock sites for 2, 5, and 10% damping based on RMS accelerations computed from Bolt (1973) and Trifunac and Brady (1975) durations.

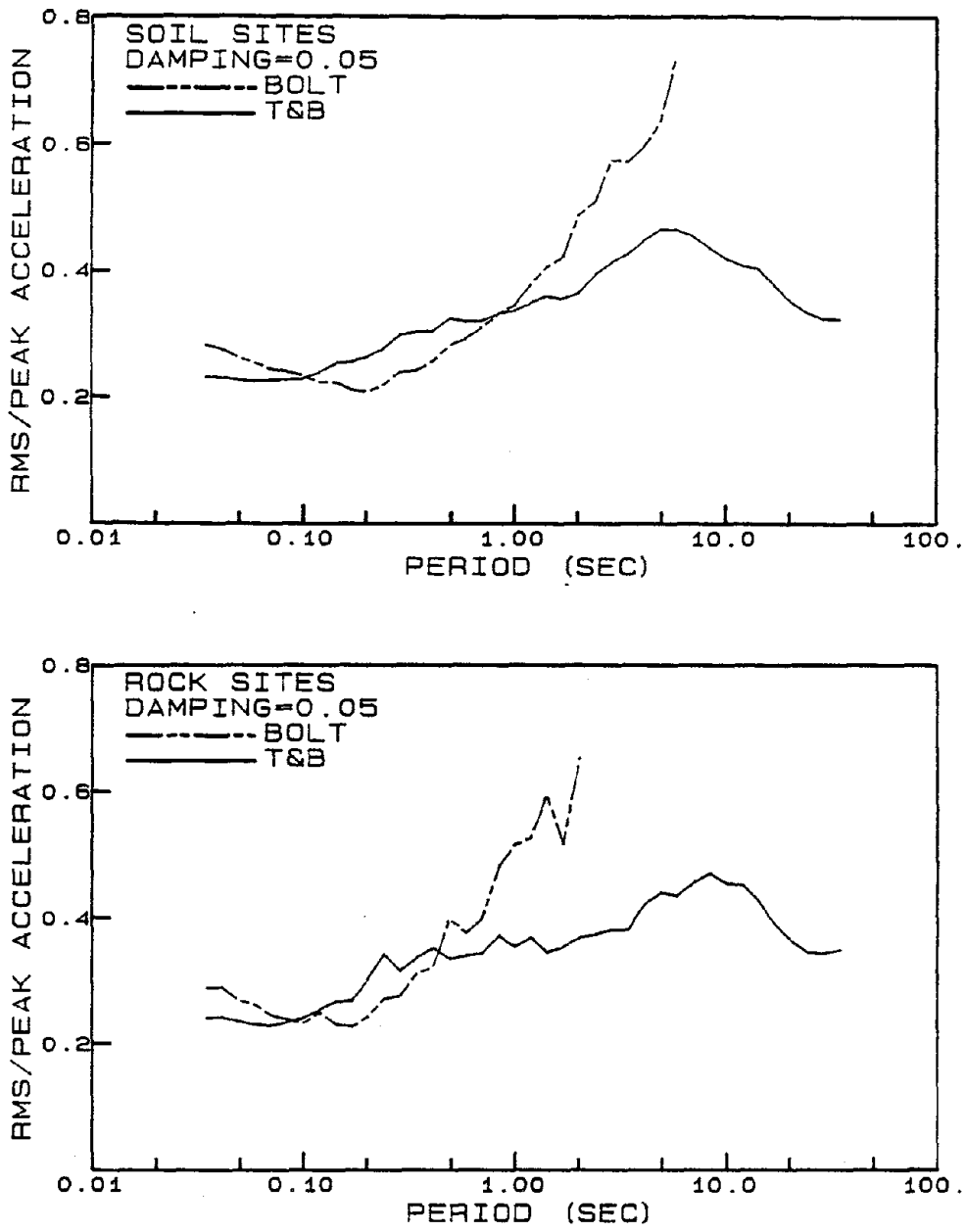

Figure 2.36 Comparison of average RMS acceleration/peak acceleration spectra for 5% damping for RMS acceleration based on Bolt (1973) and Trifunac and Brady (1975) durations for soil and rock sites.

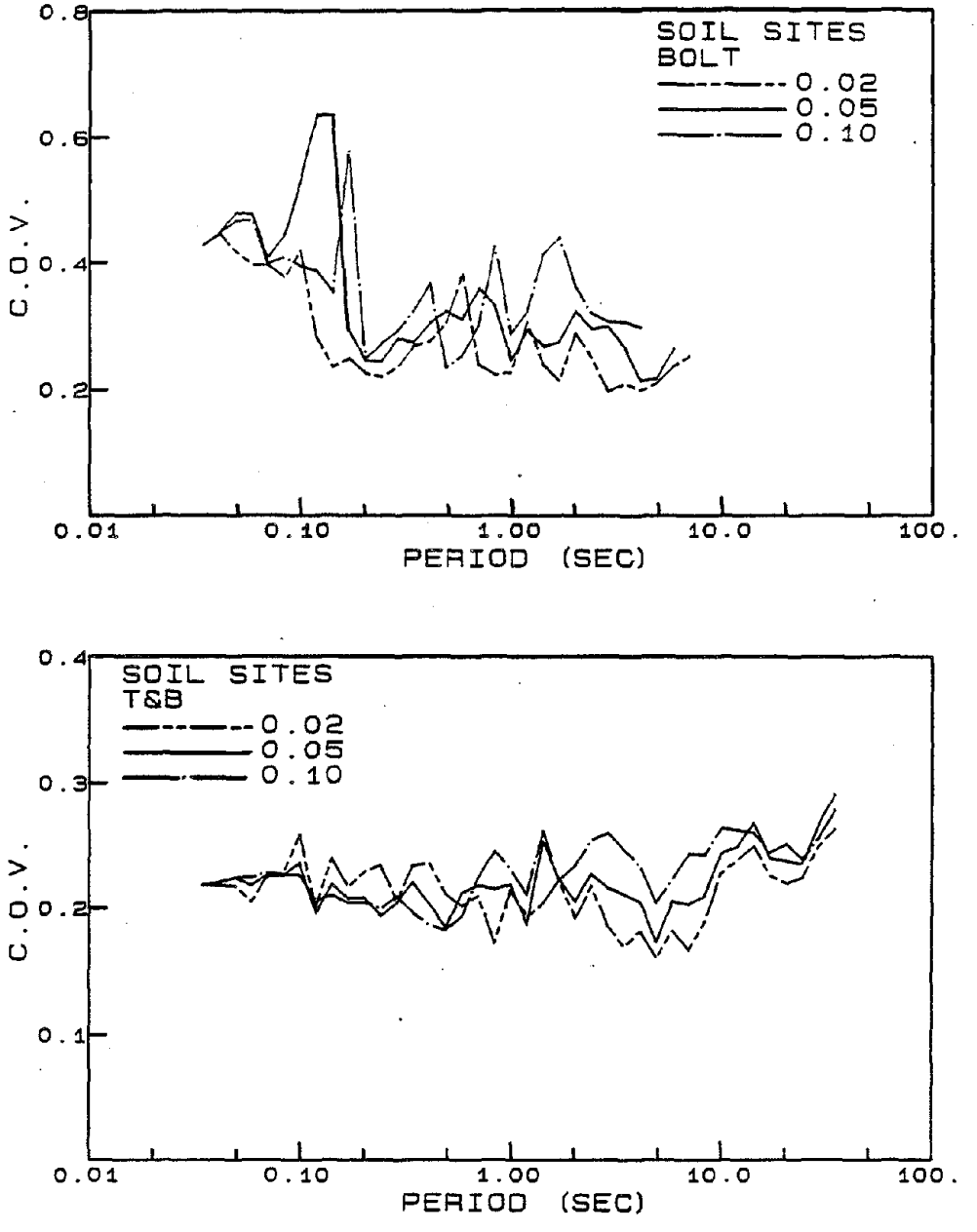

Figure 2.37 Coefficient of variation (C.O.V.) of average RMS acceleration/peak acceleration spectra for soil sites for 2, 5, and 10% damping based on RMS accelerations computed from Bolt (1973) and Trifunac and Brady (1975) durations.

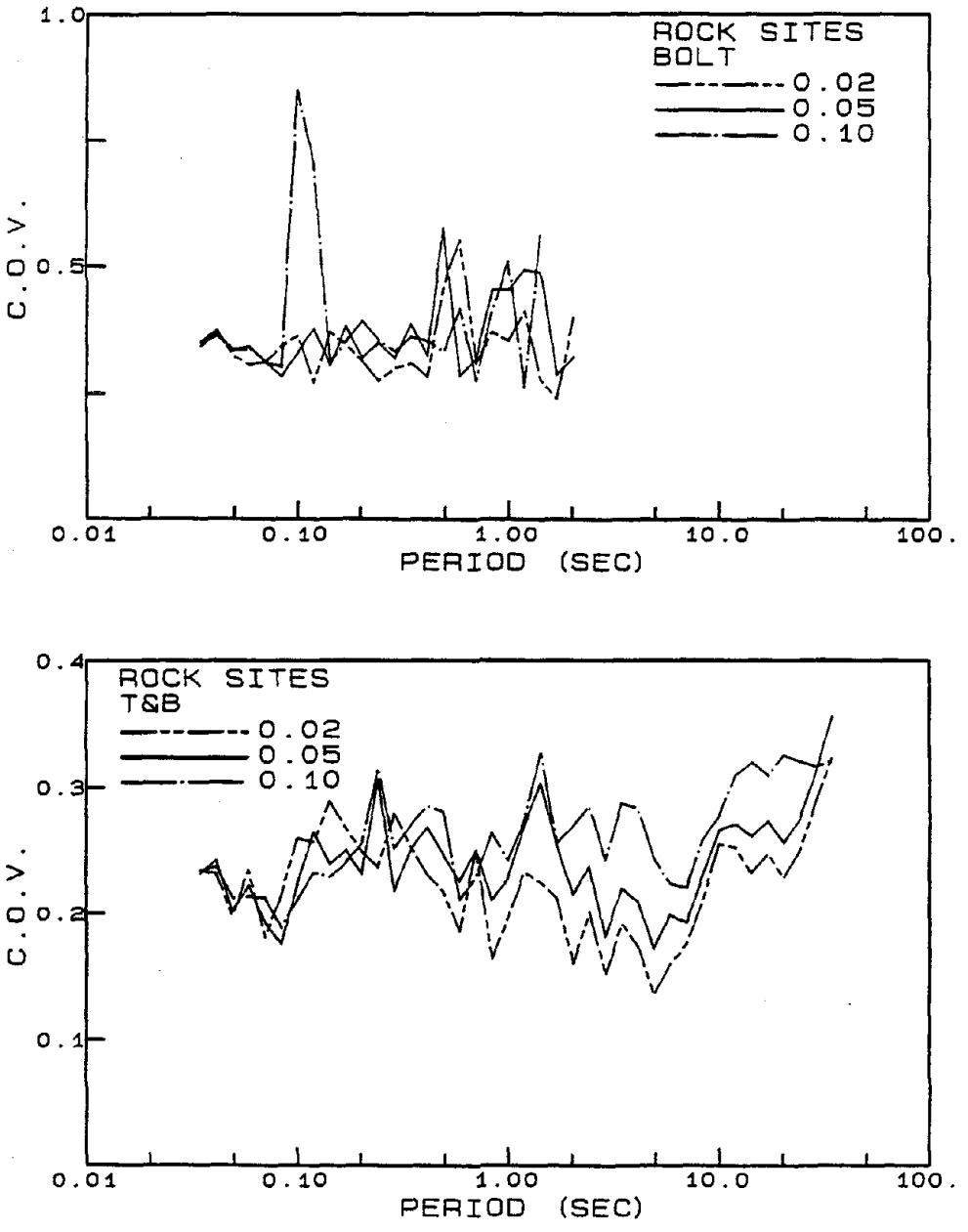

Figure 2.38 Coefficient of variation (C.O.V.) of average RMS acceleration/peak acceleration spectra for rock sites for 2, 5, and 10% damping based on RMS accelerations computed from Bolt (1973) and Trifunac and Brady (1975) durations.

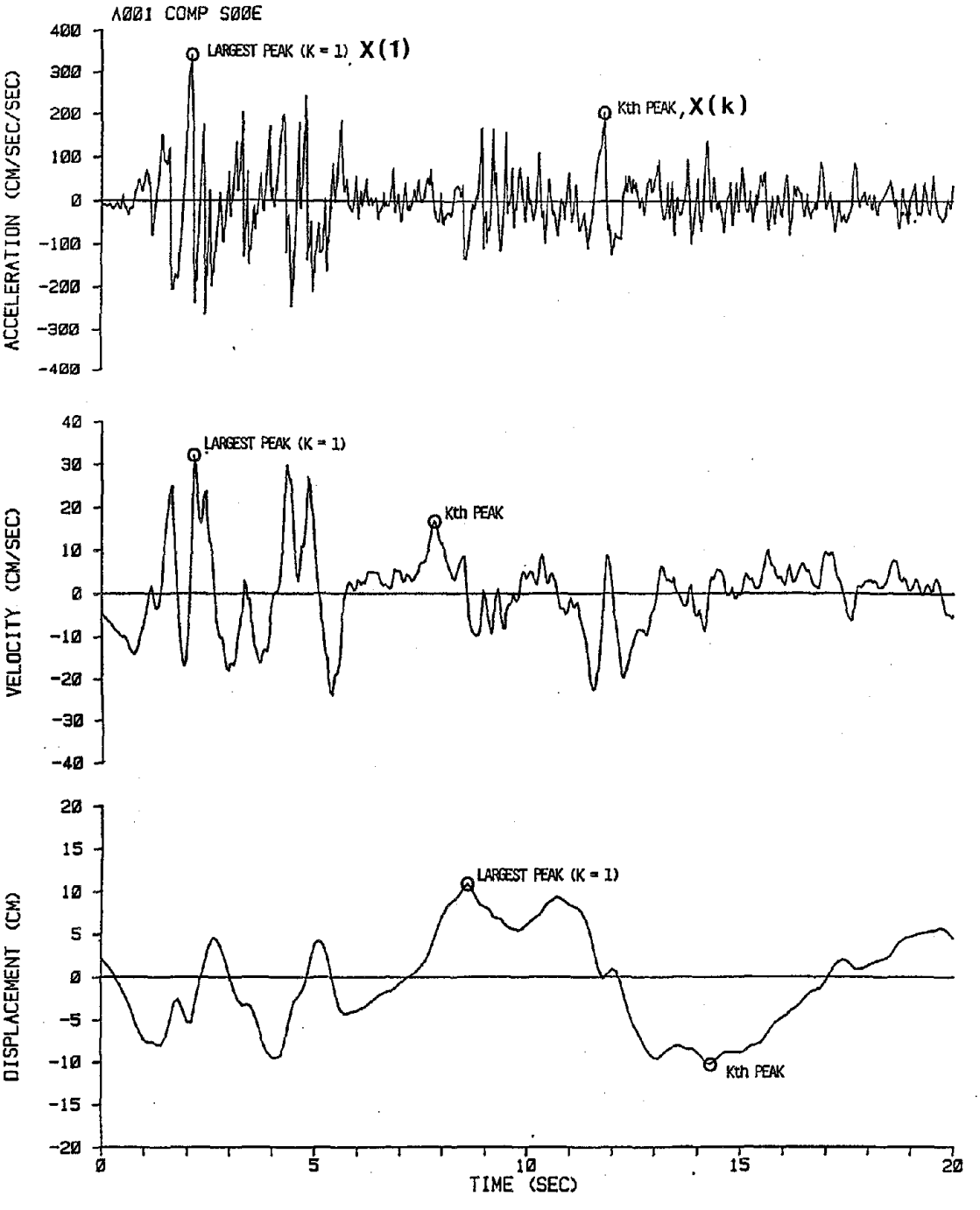

Figure 3.1 Definition of the kth largest peak in ground motion acceleration, velocity, and displacement time histories.

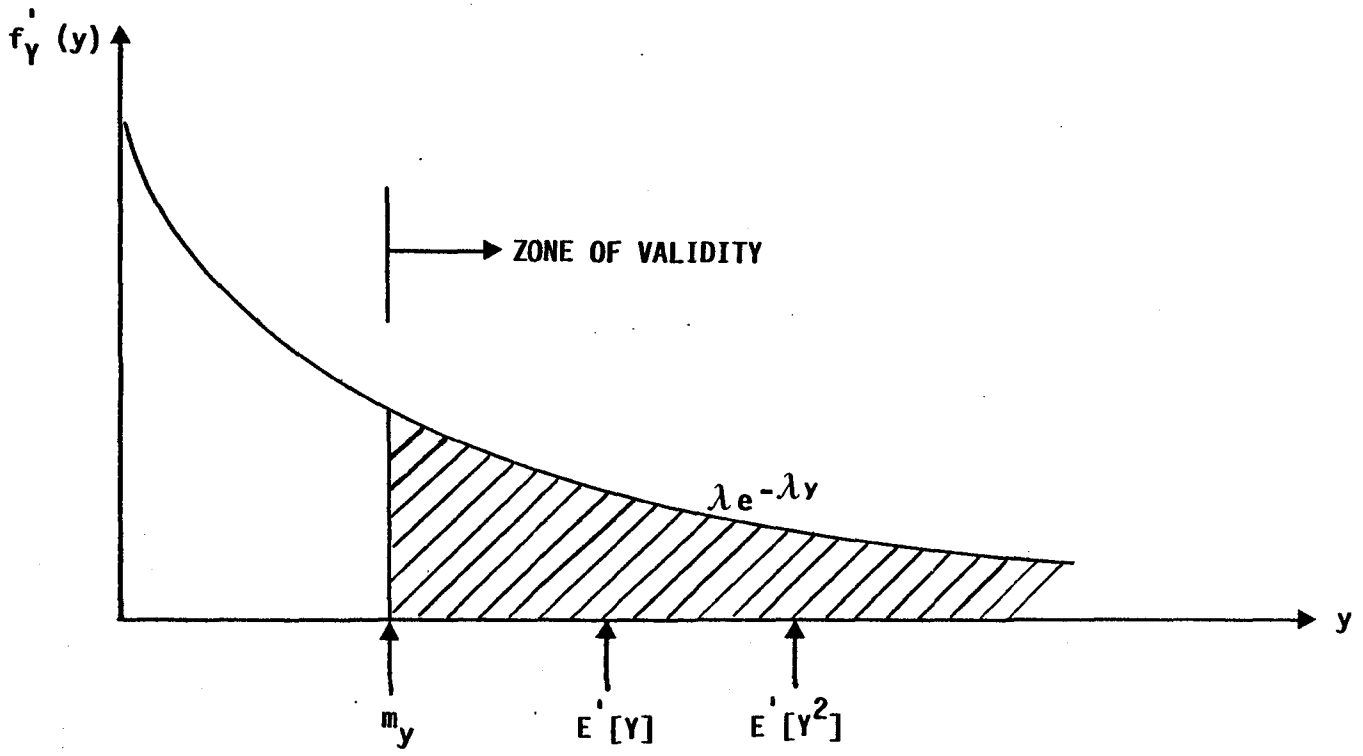

Figure 3.2 Definition of terms associated with exponential half-tail model.

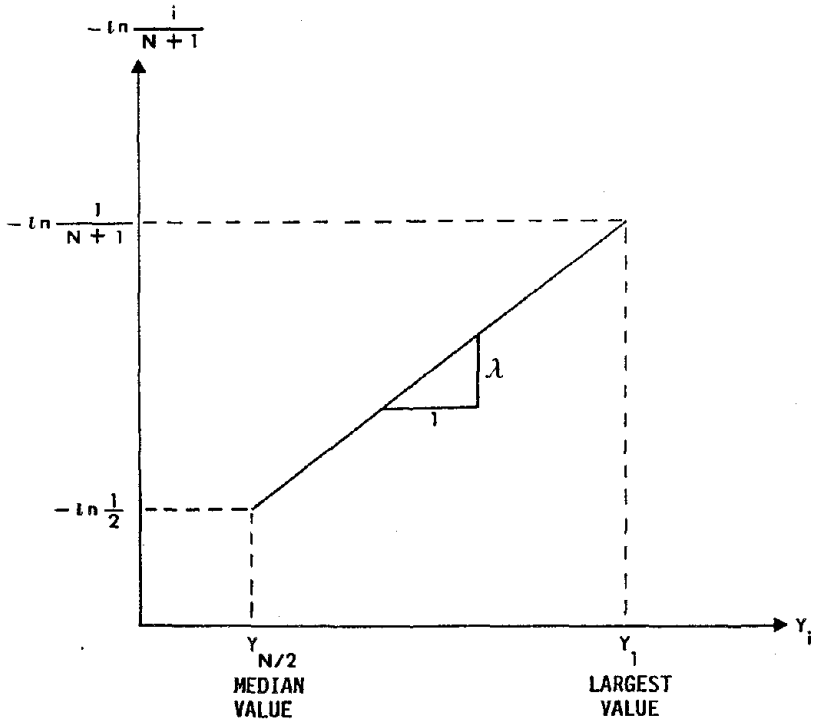

Figure 3.3 Probability paper for the exponential half-tail model.

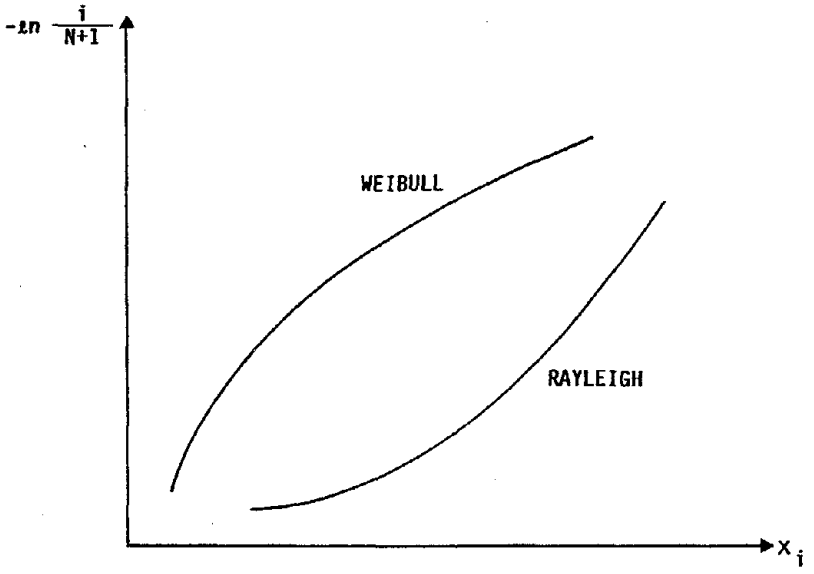

Figure 3.4 General trend of nonexponential data on exponential probability paper.

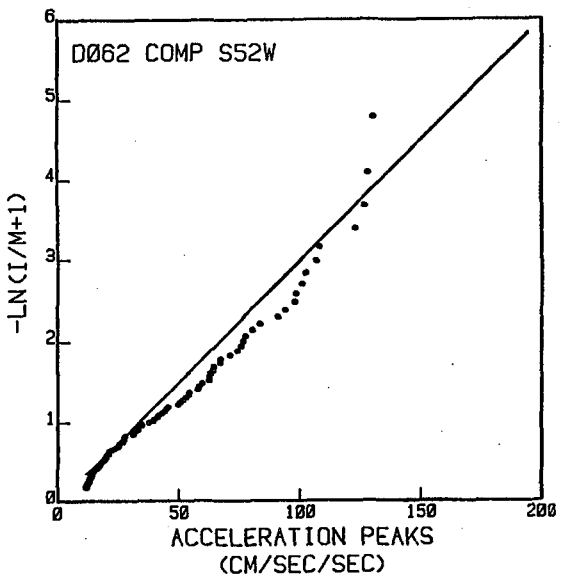

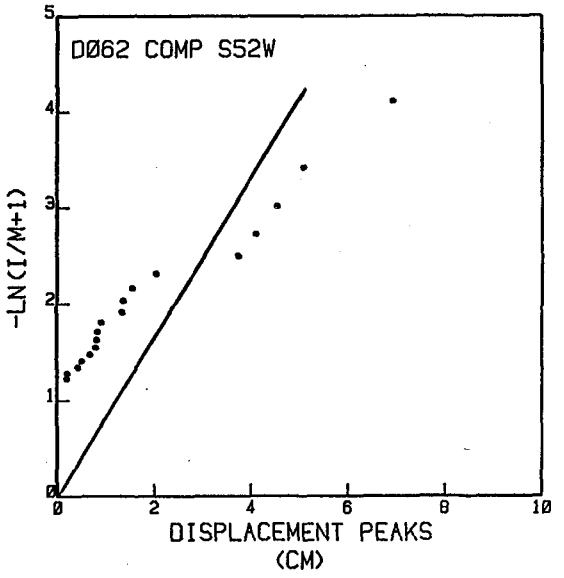

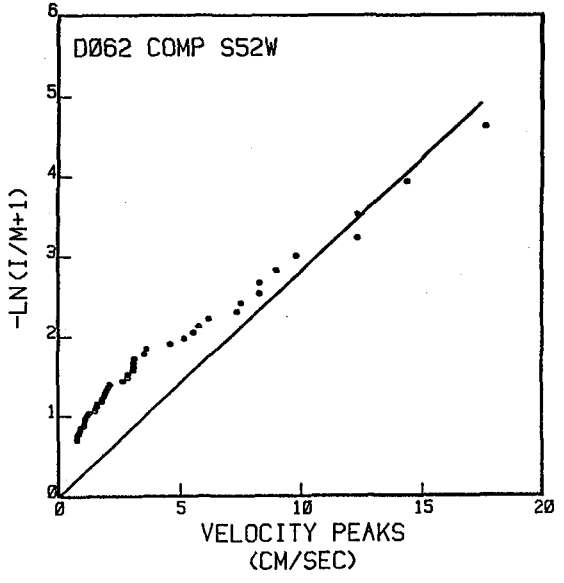

Figure 3.5 Exponential probability plots for acceleration, velocity, and displacement peaks recorded at the base of the Holiday Inn Building, 1640 S. Marengo Street, during the San Fernando, CA earthquake of 9 February 1971.

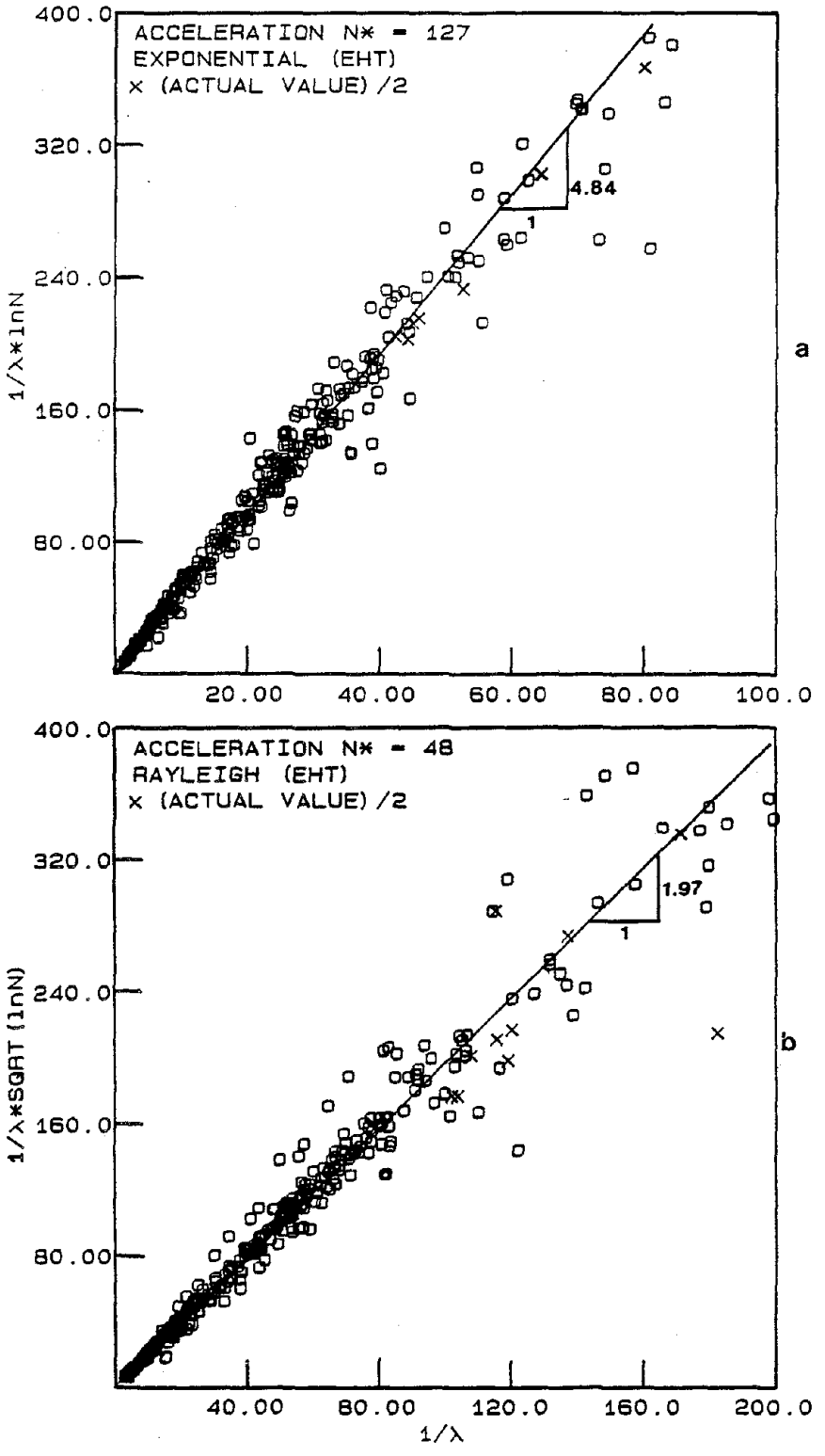

Figure 3.6 Standardized number of peaks, N*, for ground acceleration modelled by (a) exponential (EHT) distribution (slope of line is ln N*), (b) Rayleigh (EHT) distribution (slope of line is $\sqrt{\ln N^*}$).

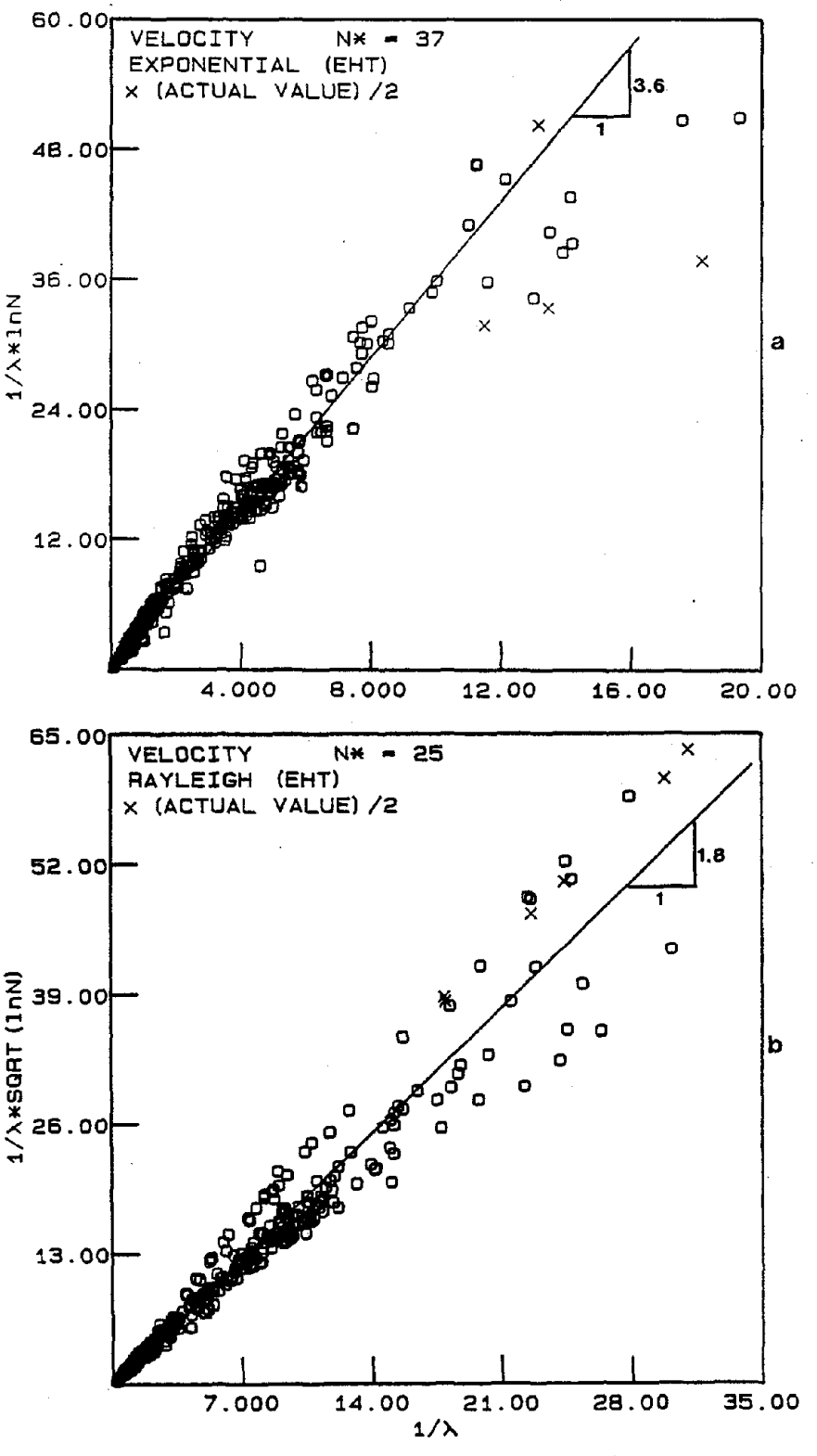

Figure 3.7 Standardized number of peaks, N*, for ground velocity modelled by (a) exponential (EHT) distribution (slope of line is ln N*), (b) Rayleigh (EHT) distribution (slope of line is $\sqrt{\ln N^*}$).

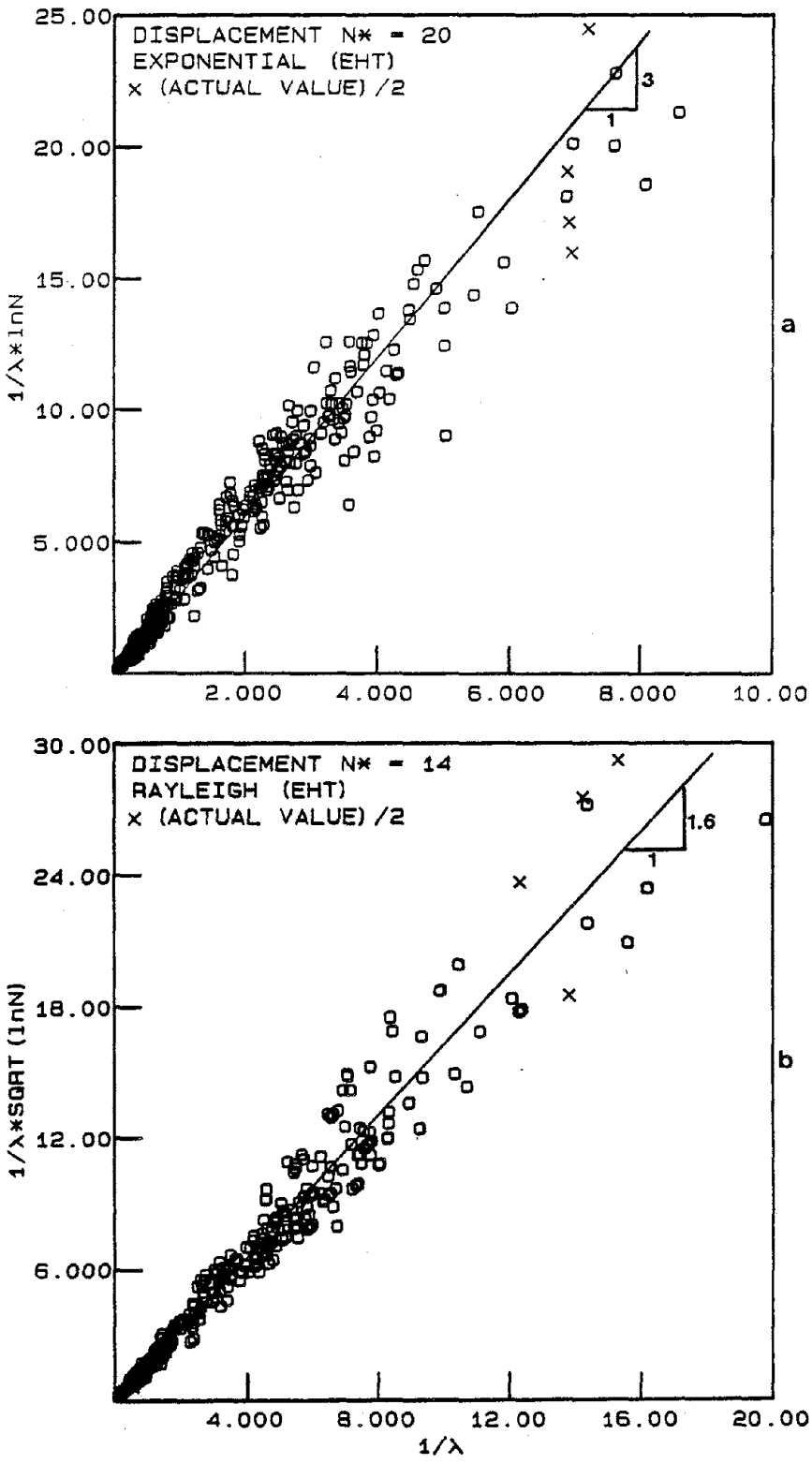

Figure 3.8 Standardized number of peaks, N*, for ground displacement modelled by (a) exponential (EHT) distribution (slope of line is ln N*), (b) Rayleigh (EHT) distribution (slope of line is $\sqrt{\ln N^*}$).

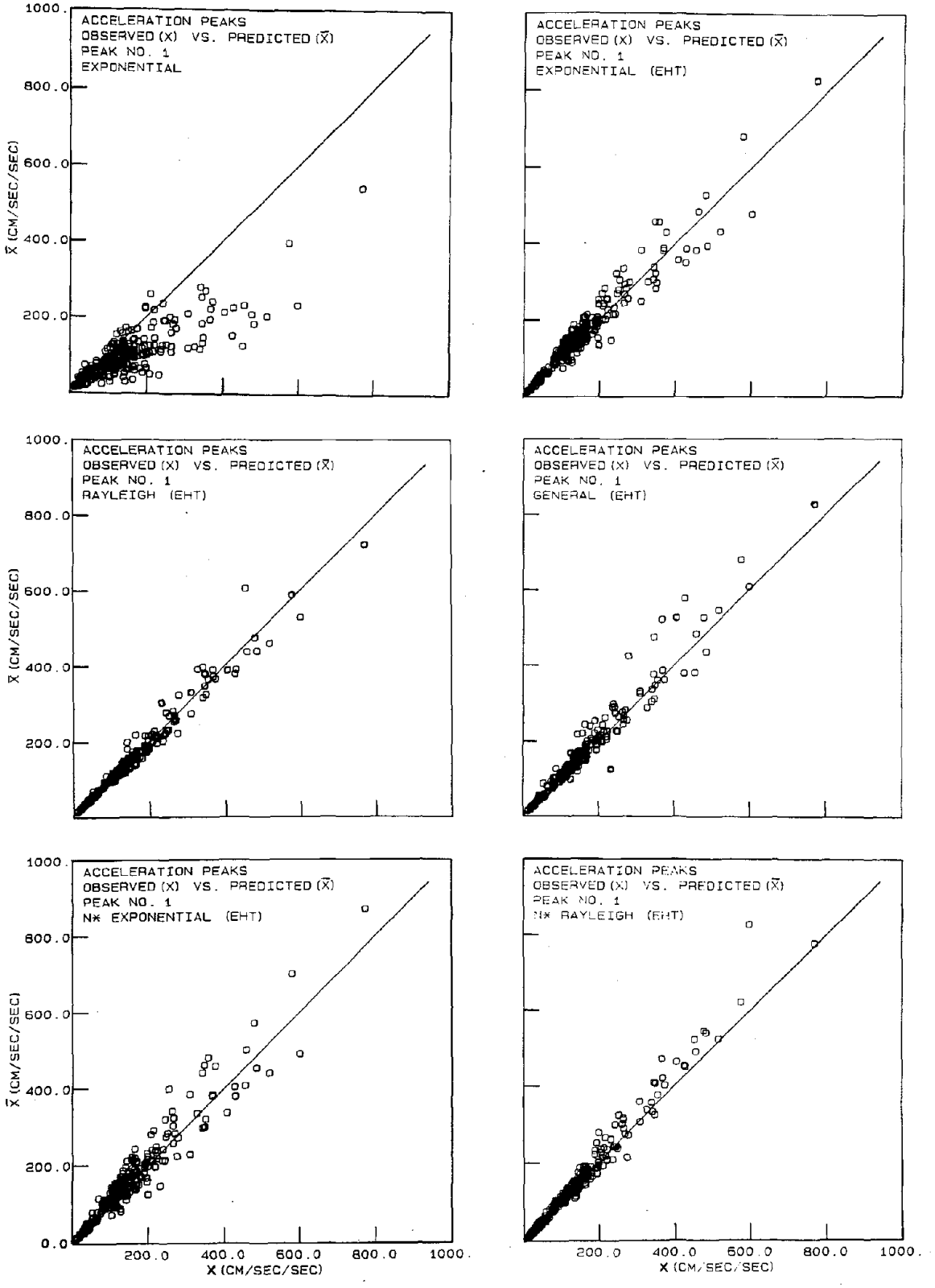

Figure 3.9 Observed X(1) vs. predicted $\bar{X}$(1) peak ground acceleration (PGA) from 6 probability distributions.

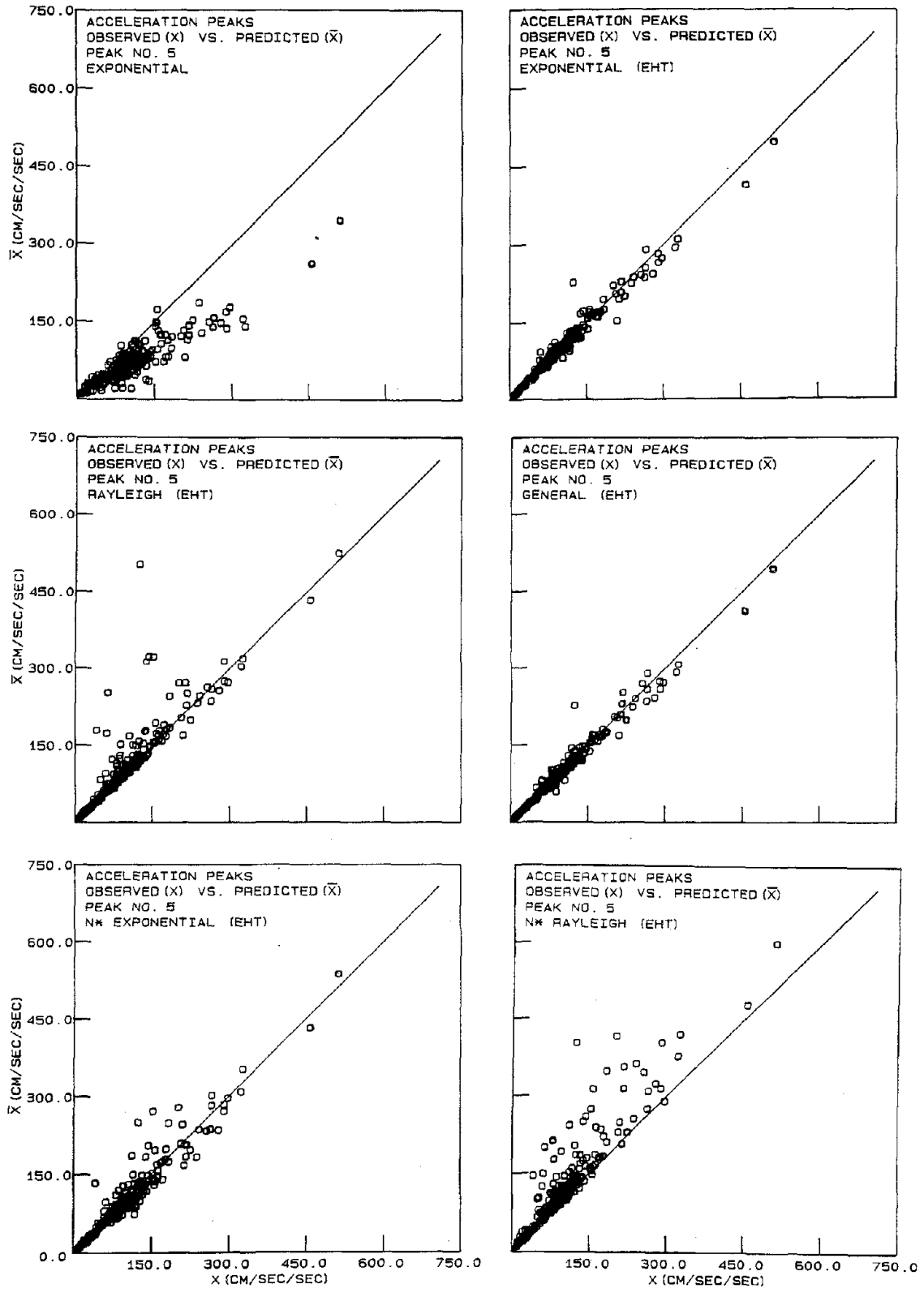

Figure 3.10 Observed X(5) vs. predicted $\bar{X}$(5) ground acceleration peak from 6 probability distributions.

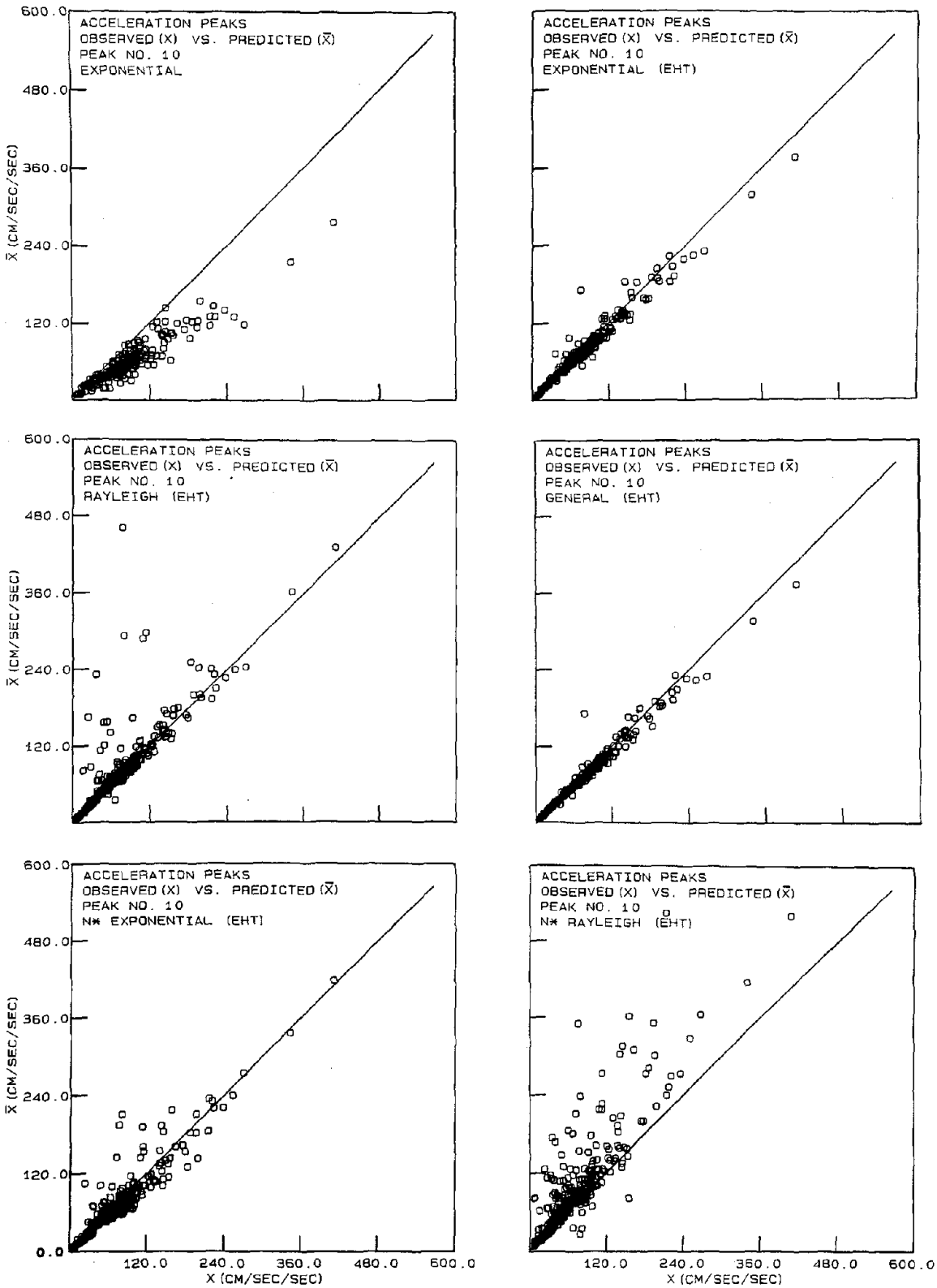

Figure 3.11 Observed X(10) vs. predicted $\bar{X}$(10) ground acceleration peak from 6 probability distributions.

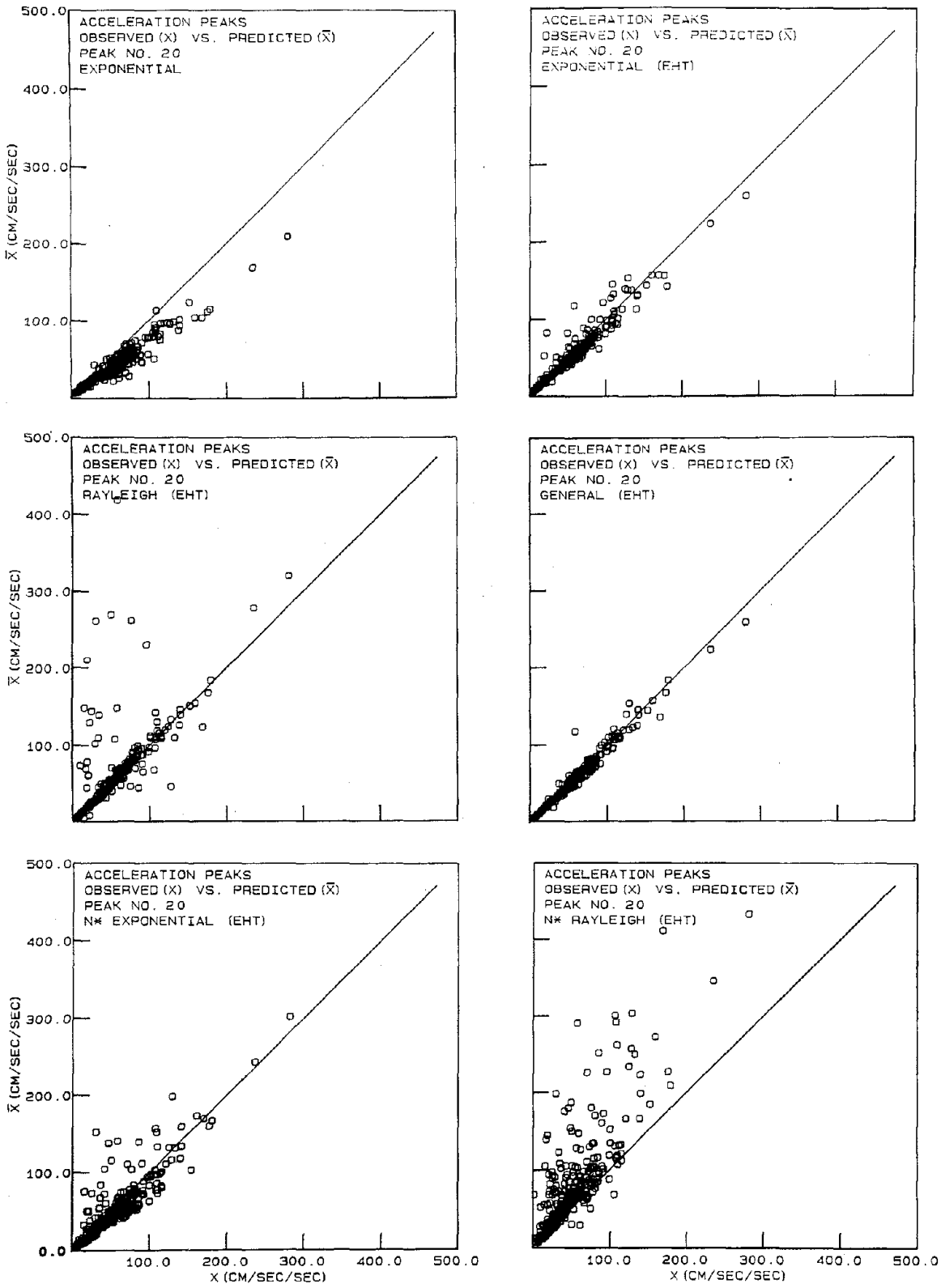

Figure 3.12 Observed X(20) vs. predicted $\bar{X}$(20) ground acceleration peak from 6 probability distributions.

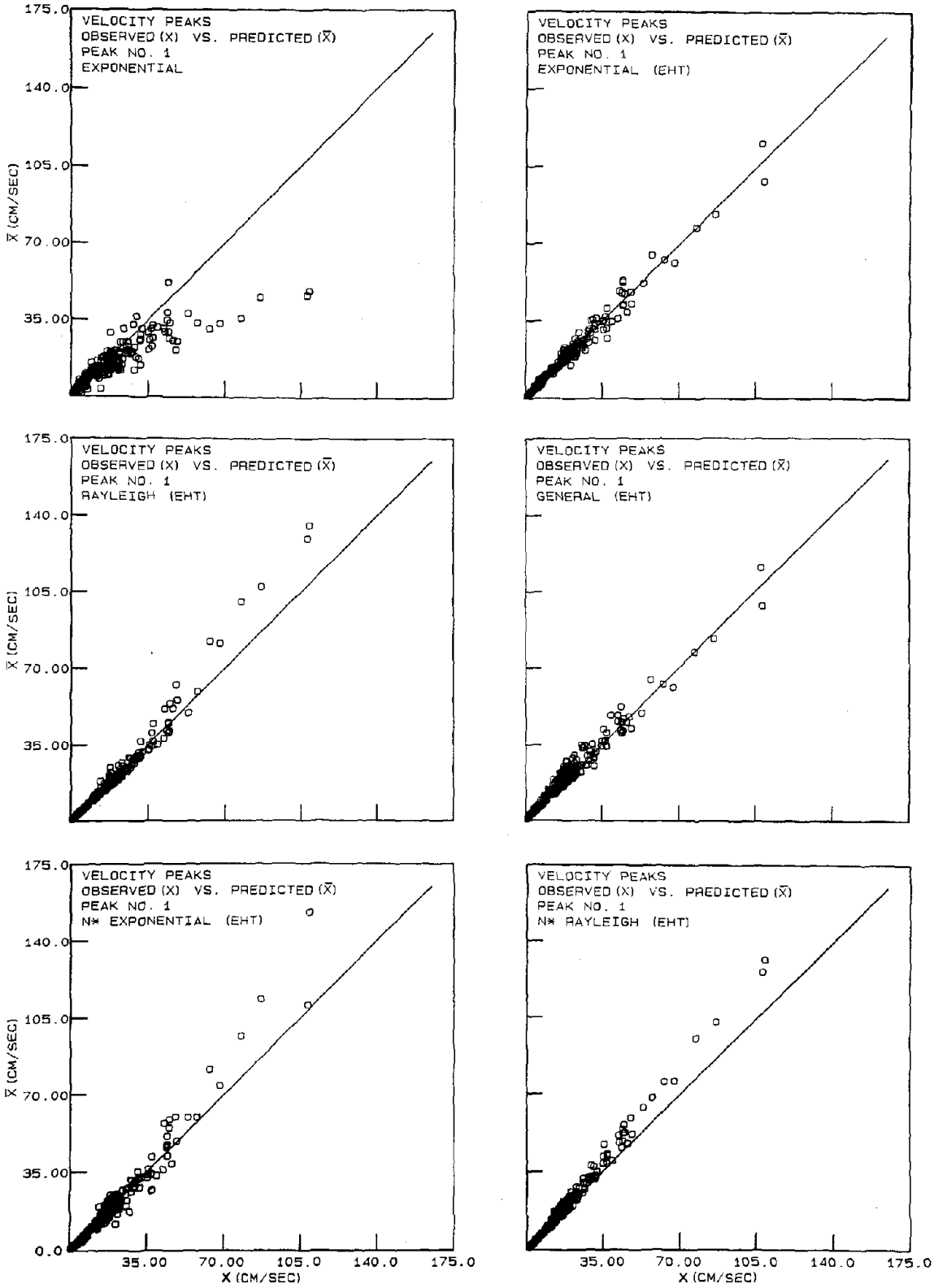

Figure 3.13 Observed X(1) vs. predicted $\bar{X}$(1) peak ground velocity (PGV) from 6 probability distributions.

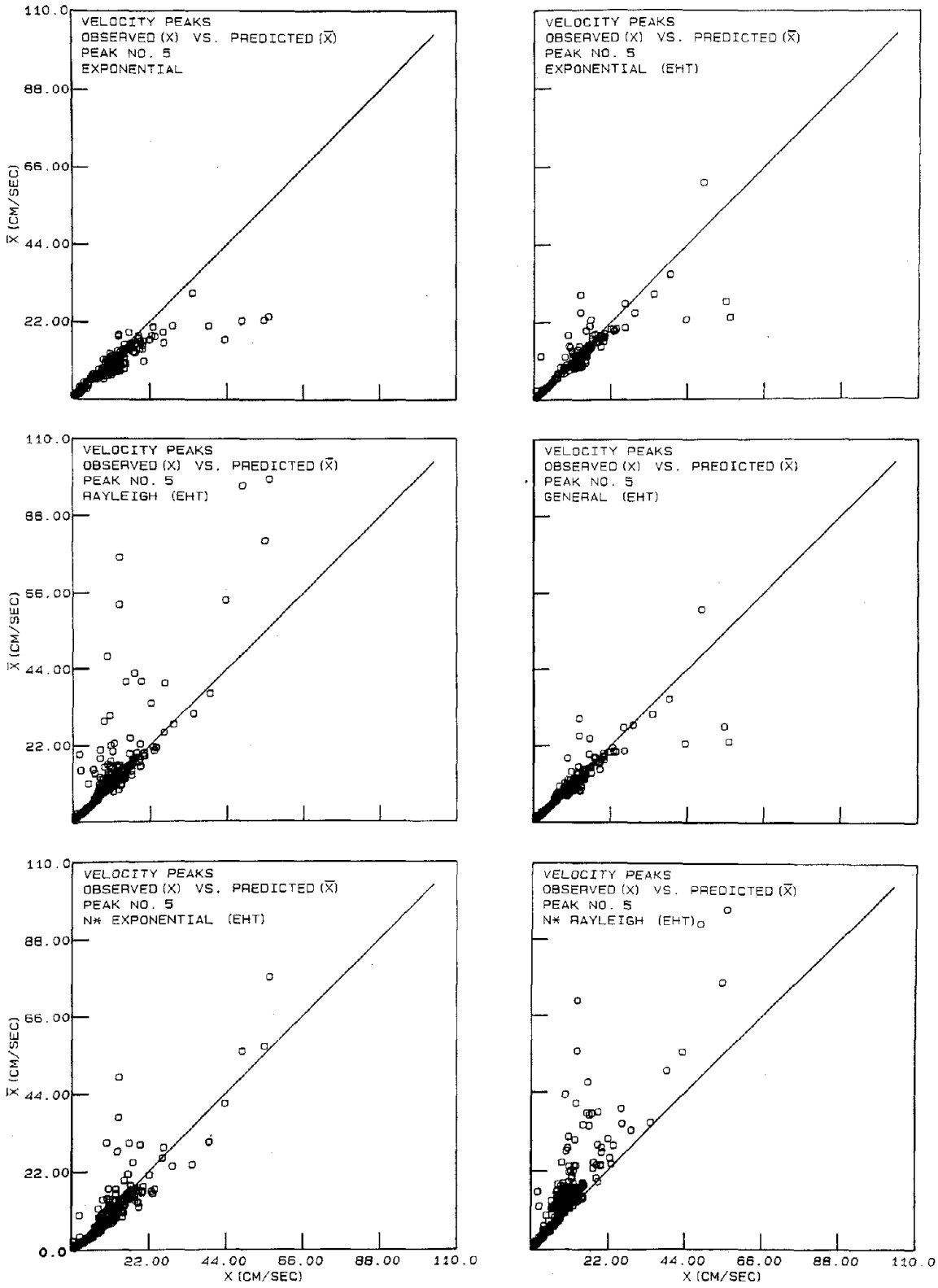

Figure 3.14 Observed X(5) vs. predicted $\bar{X}$(5) ground velocity peak from 6 probability distributions.

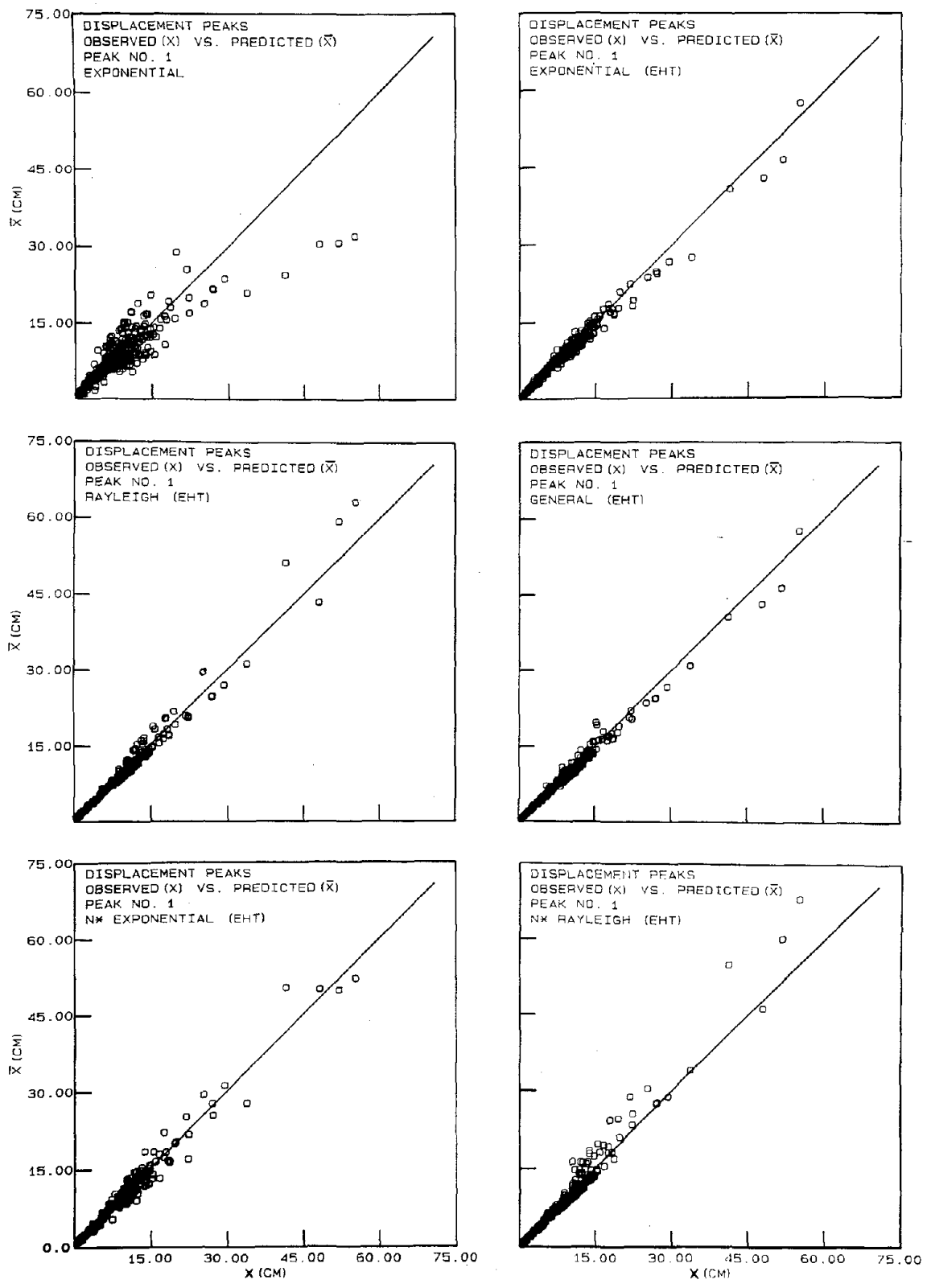

Figure 3.15 Observed X(1) vs. predicted $\bar{X}$(1) peak ground displacement (PGD) from 6 probability distributions.

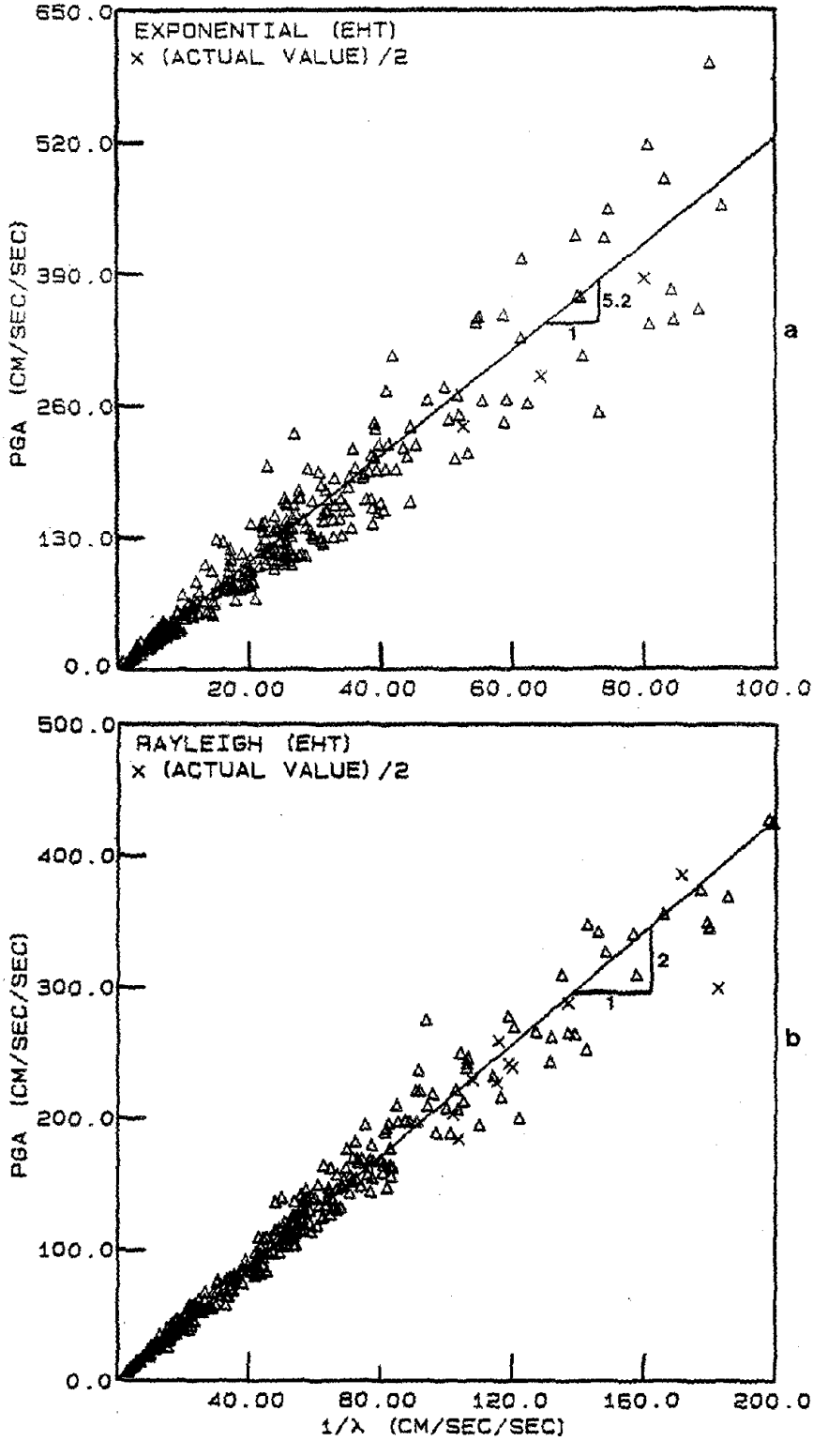

Figure 3.16 PGA vs. $1/\lambda$ for ground acceleration for (a) exponential (EHT) and (b) Rayleigh (EHT) distribution. Lines shown are for reference only.

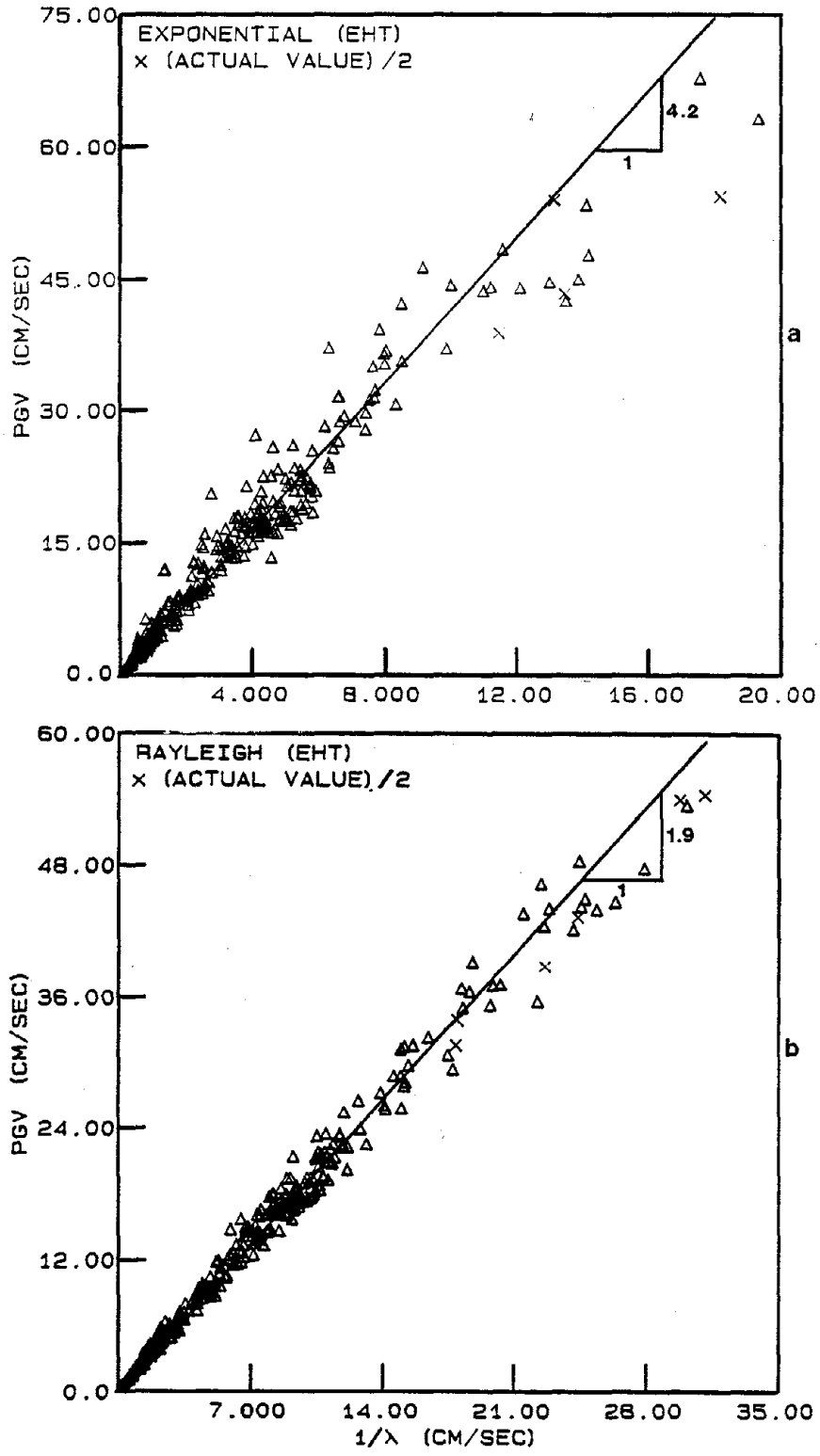

Figure 3.17 PGV vs. $1/\lambda$ for ground velocity for (a) exponential (EHT) and (b) Rayleigh (EHT) distributions. Lines shown are for reference only.

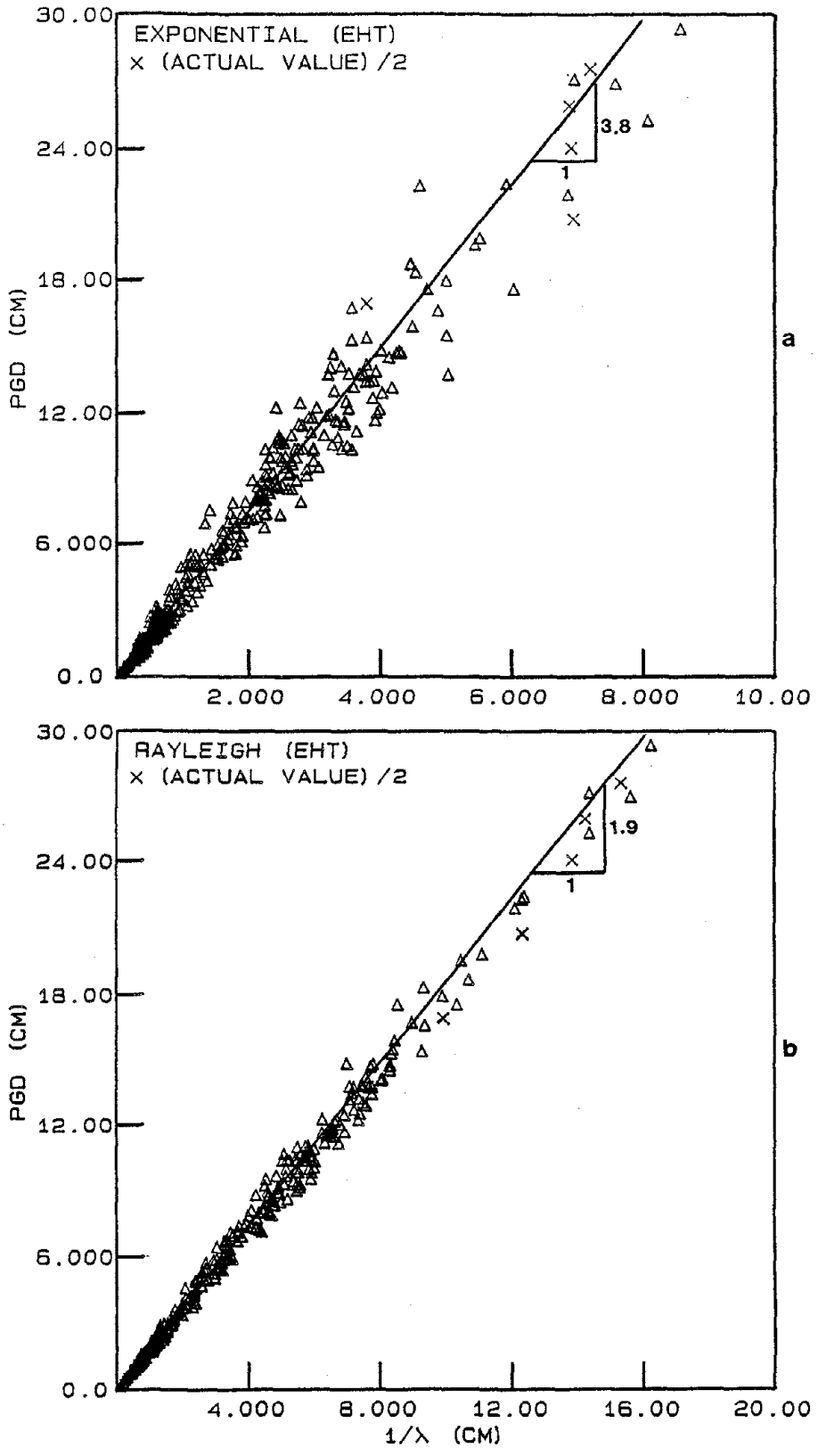

Figure 3.18 PGD vs. $1/\lambda$ for ground displacement for (a) exponential (EHT) and (b) Rayleigh (EHT) distributions. Lines shown are for reference only.

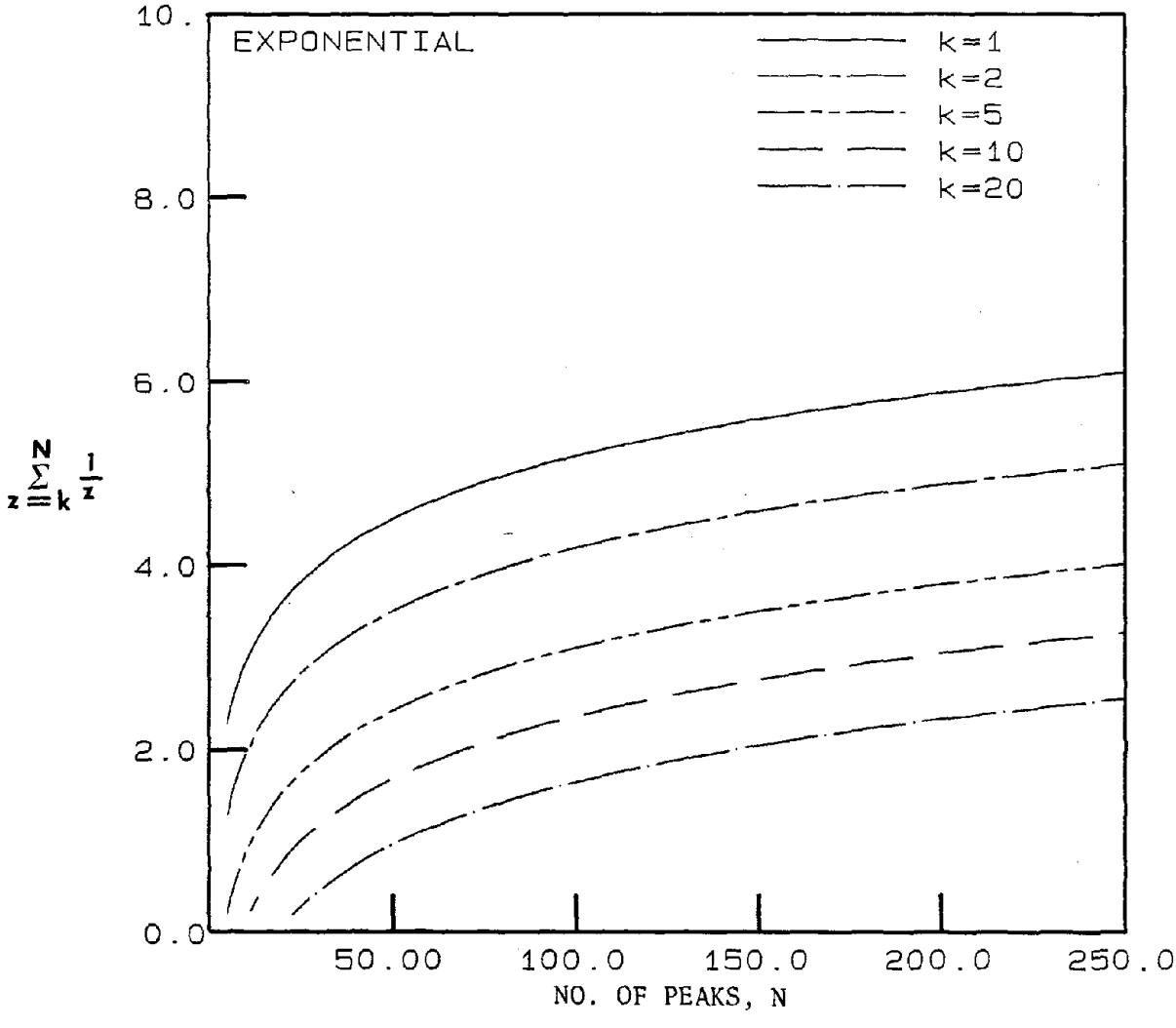

Figure 3.19 Comparison of the relative magnitudes of the expected peaks $\bar{X}(1)$, $\bar{X}(2)$, $\bar{X}(5)$, $\bar{X}(10)$, and $\bar{X}(20)$ predicted from the exponential distribution as a function of the number of peaks, N, for a unit value of λ.

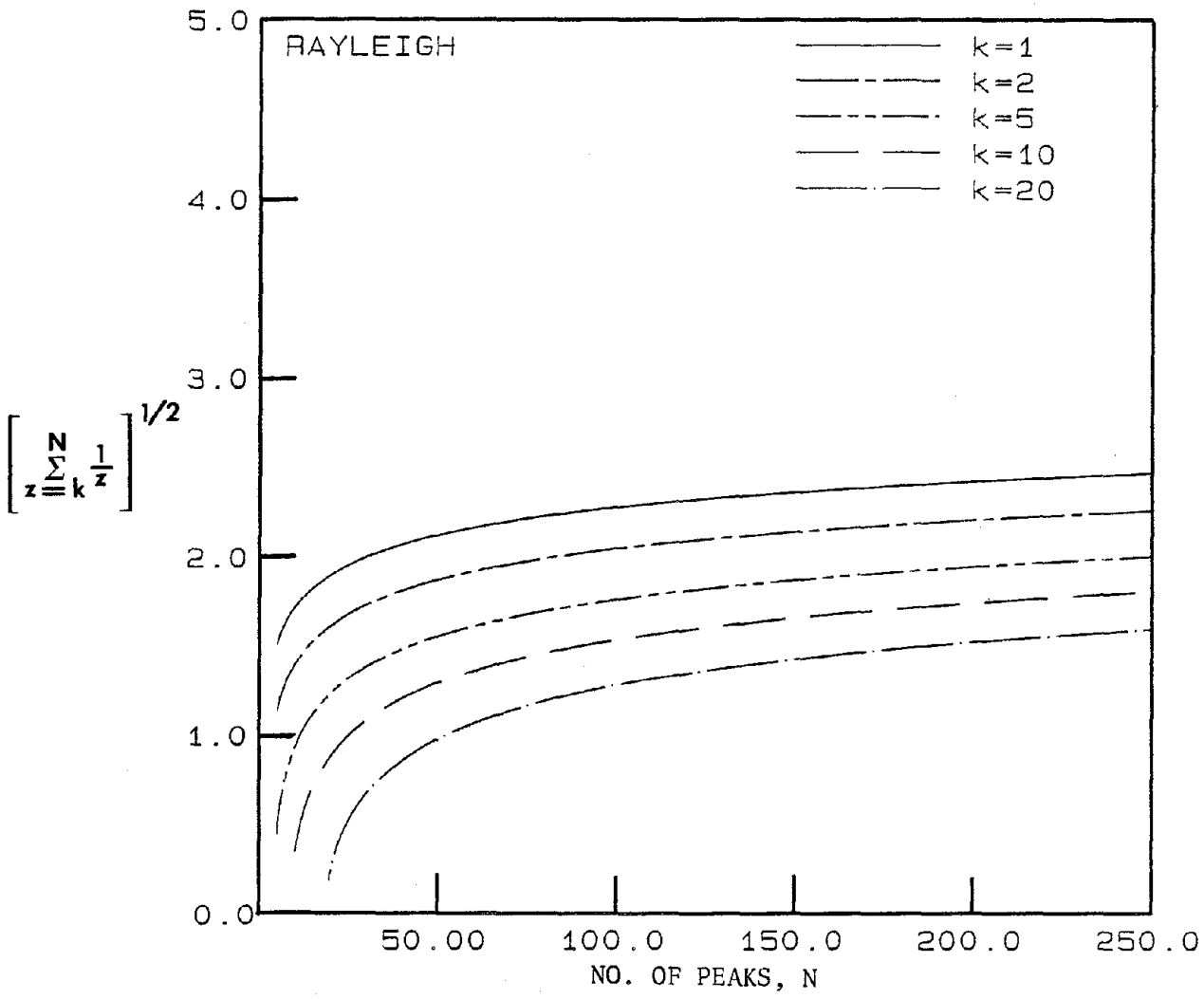

Figure 3.20 Comparison of the relative magnitudes of the expected peaks $\bar{X}(1)$, $\bar{X}(2)$, $\bar{X}(5)$, $\bar{X}(10)$, and $\bar{X}(20)$ predicted from the Rayleigh distributions as a function of the number of peaks, N, for a unit value of λ.

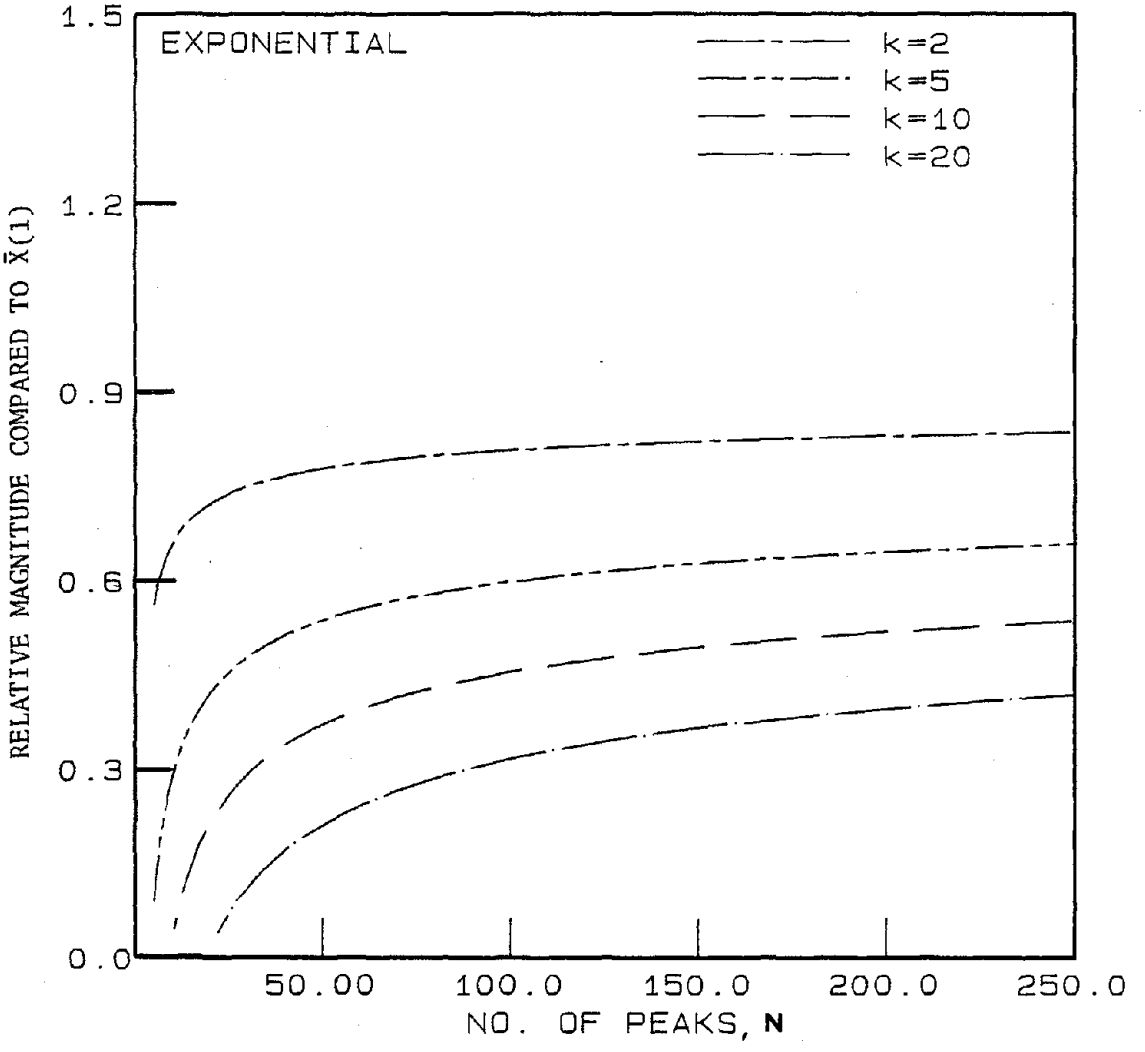

Figure 3.21 Relative magnitudes of the expected peaks $\bar{X}(2)$, $\bar{X}(5)$, $\bar{X}(10)$, and $\bar{X}(20)$ compared to $\bar{X}(1)$ predicted from the exponential distribution as a function of the number of peaks, N, for a unit value of λ.

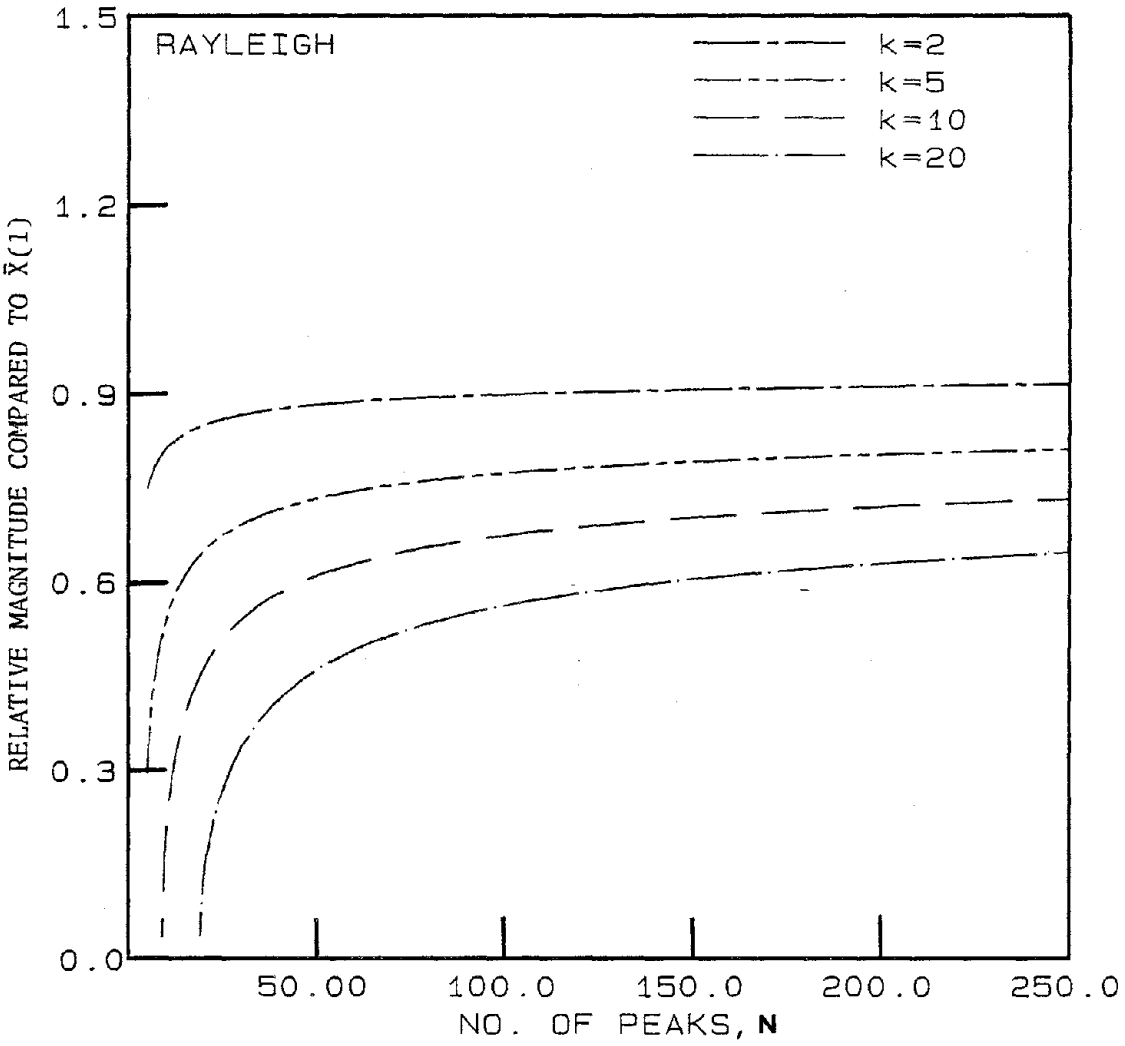

Figure 3.22 Relative magnitudes of the expected peaks $\bar{X}(2)$, $\bar{X}(5)$, $\bar{X}(10)$, and $\bar{X}(20)$ compared to $\bar{X}(1)$ predicted from the Rayleigh distribution as a function of the number of peaks, N, for a unit value of λ.

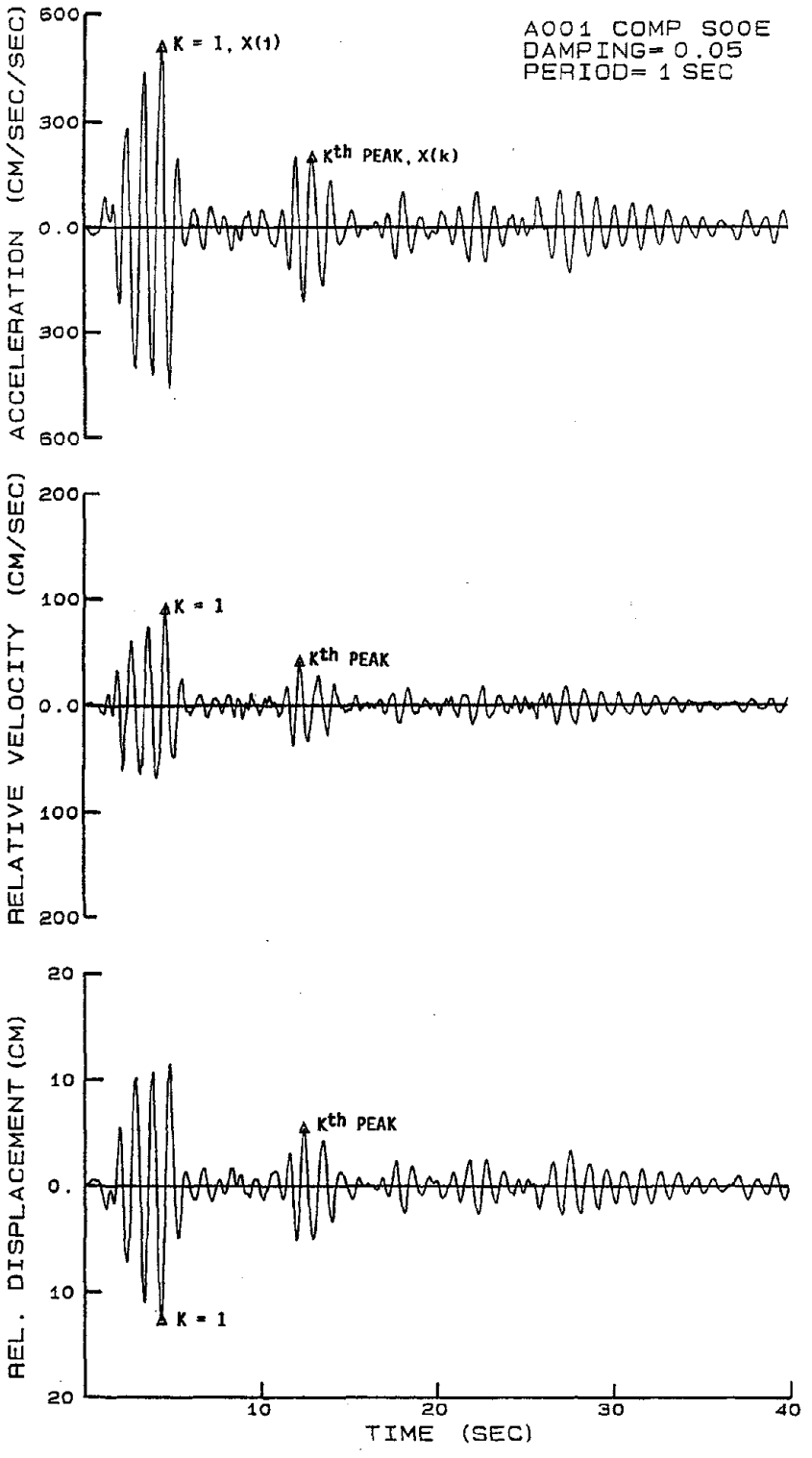

Figure 4.1 Definition of kth largest peak in acceleration, relative velocity, and relative displacement time histories of a SDOF oscillator.

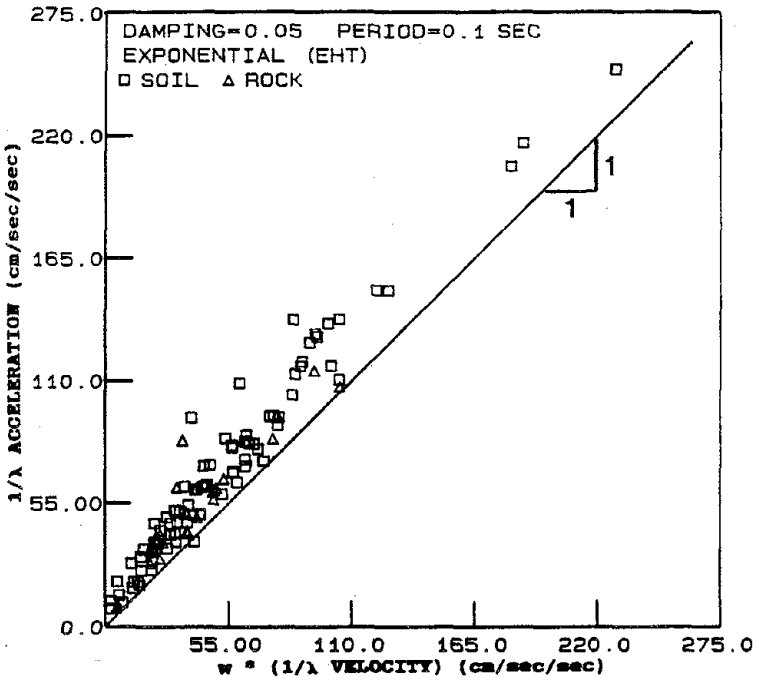

Figure 4.2 1/λ acceleration vs. ω x (1/λ velocity) for exponential (EHT) distribution for SDOF oscillator with 5% damping and 0.1 second period.

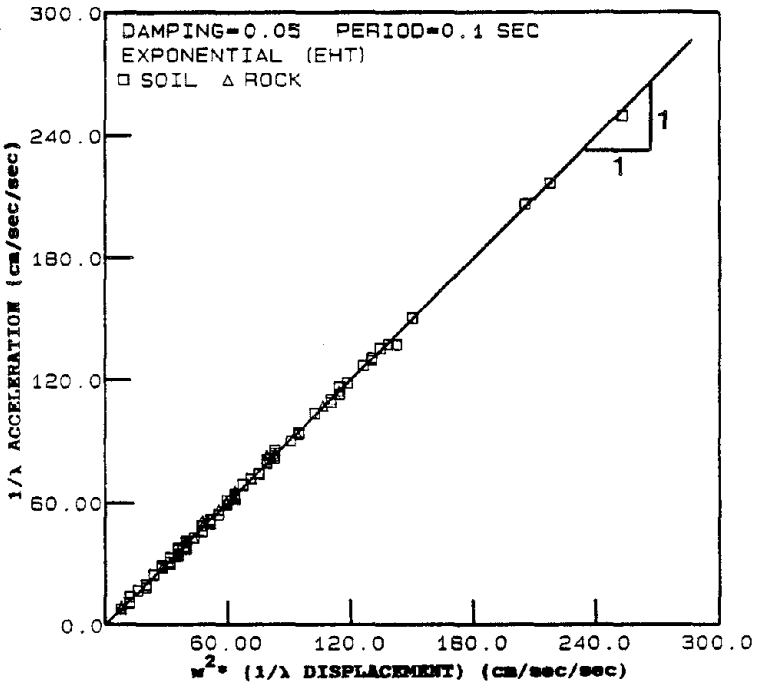

Figure 4.3 1/λ acceleration vs. ω^2 x (1/λ) displacement for exponential (EHT) distribution for SDOF oscillator with 5% damping and 0.1 second period.

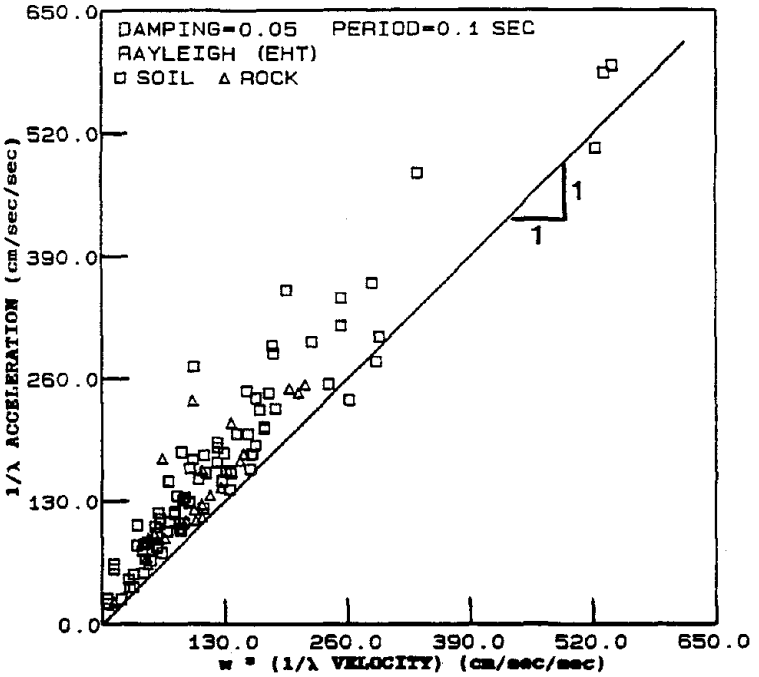

Figure 4.4 $1/\lambda$ acceleration vs. ω x ($1/\lambda$ velocity) for Rayleigh (EHT) distribution with 5% damping and 0.1 second period.

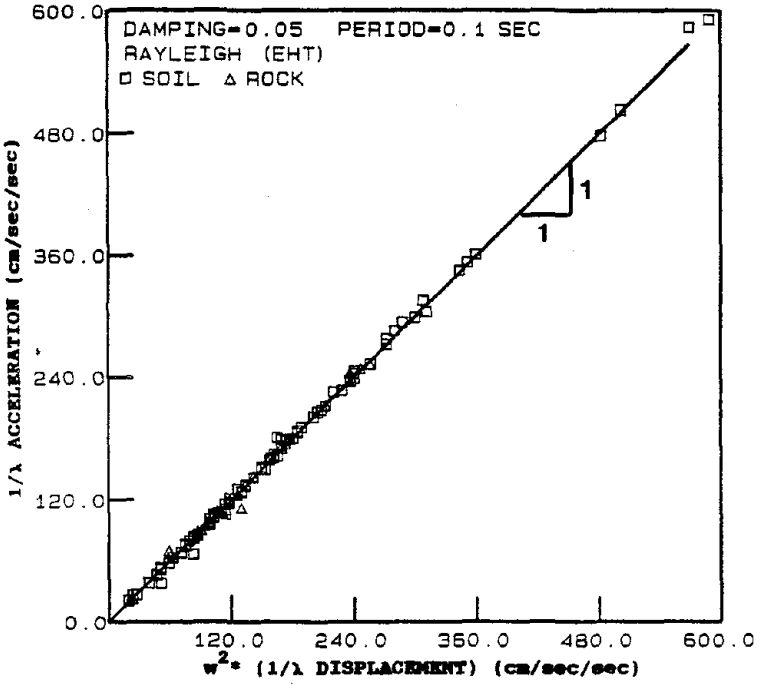

Figure 4.5 $1/\lambda$ acceleration vs. ω^2 x ($1/\lambda$ displacement) for Rayleigh (EHT) distribution with 5% damping and 0.1 second period.

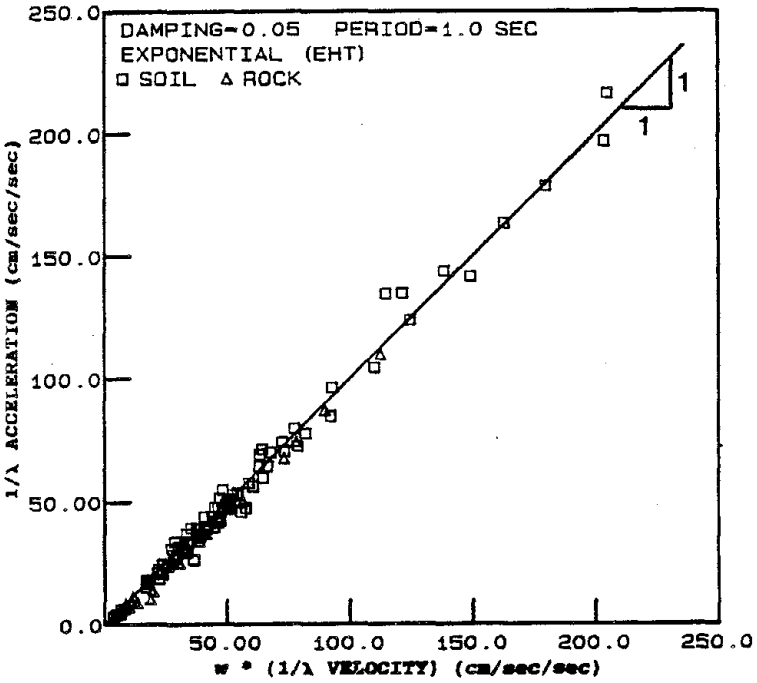

Figure 4.6 $1/\lambda$ acceleration vs. ω x ($1/\lambda$ velocity) for exponential (EHT) distribution for SDOF oscillator with 5% damping and 1.0 second period.

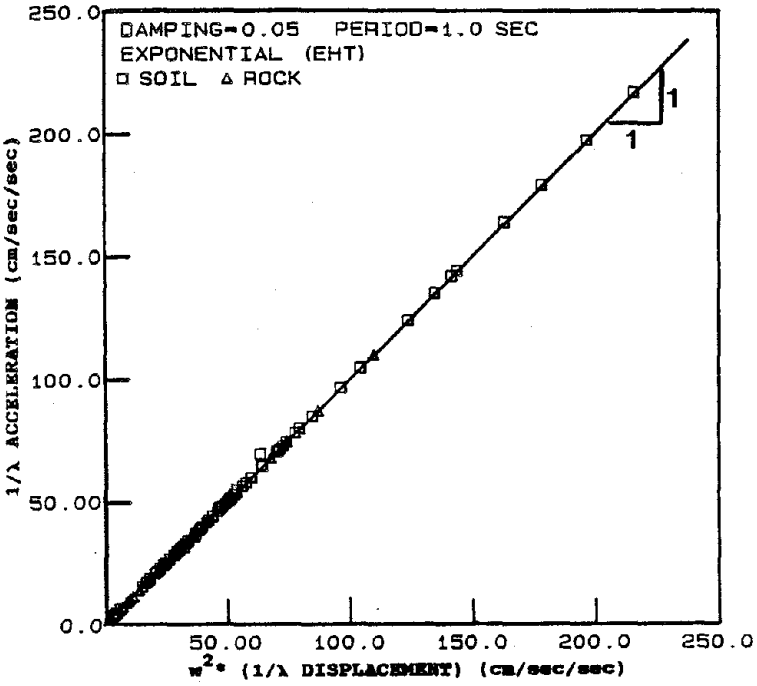

Figure 4.7 $1/\lambda$ acceleration vs. ω^2 x ($1/\lambda$) displacement for exponential (EHT) distribution for SDOF oscillator with 5% damping and 1.0 second period.

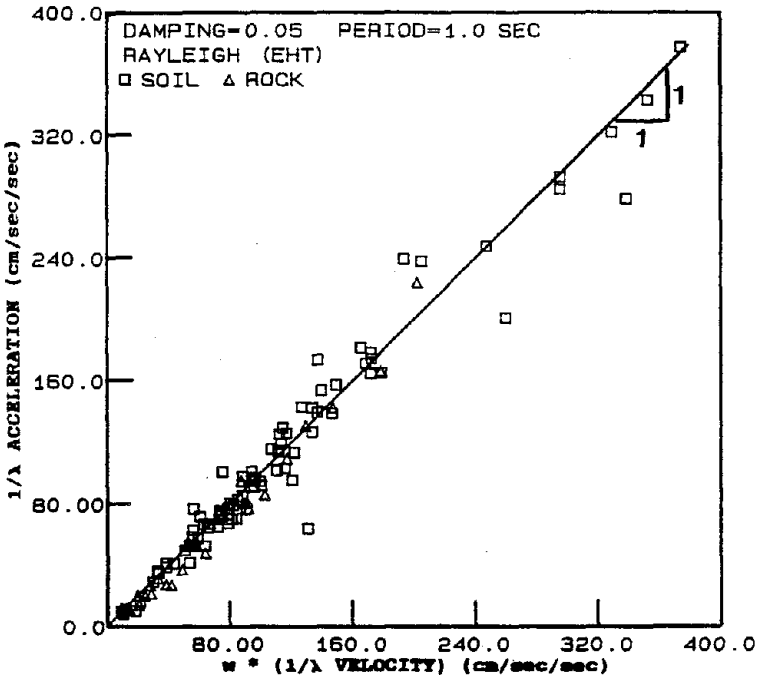

Figure 4.8 $1/\lambda$ acceleration vs. ω x ($1/\lambda$ velocity) for Rayleigh (EHT) distribution with 5% damping and 1.0 second period.

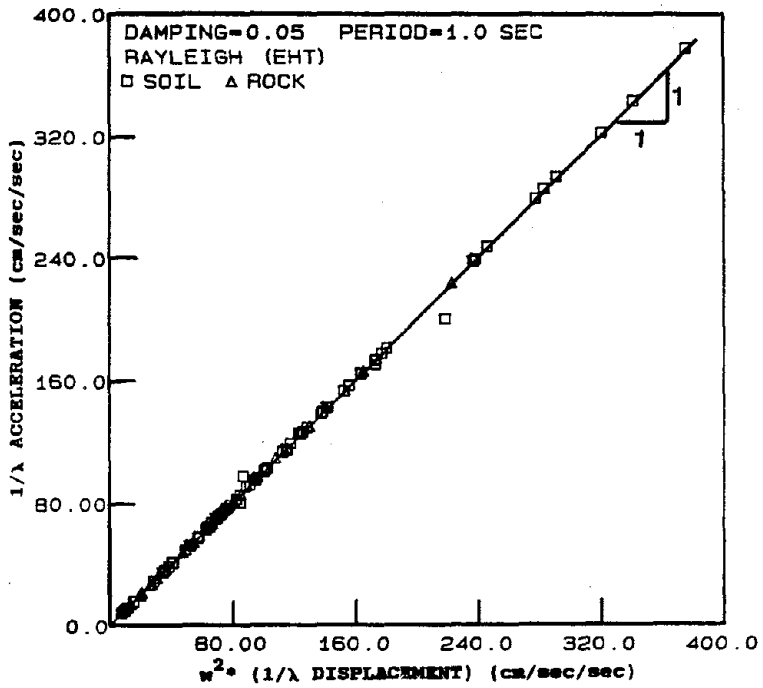

Figure 4.9 $1/\lambda$ acceleration vs. ω^2 x ($1/\lambda$ displacement) for Rayleigh (EHT) distribution with 5% damping and 1.0 second period.

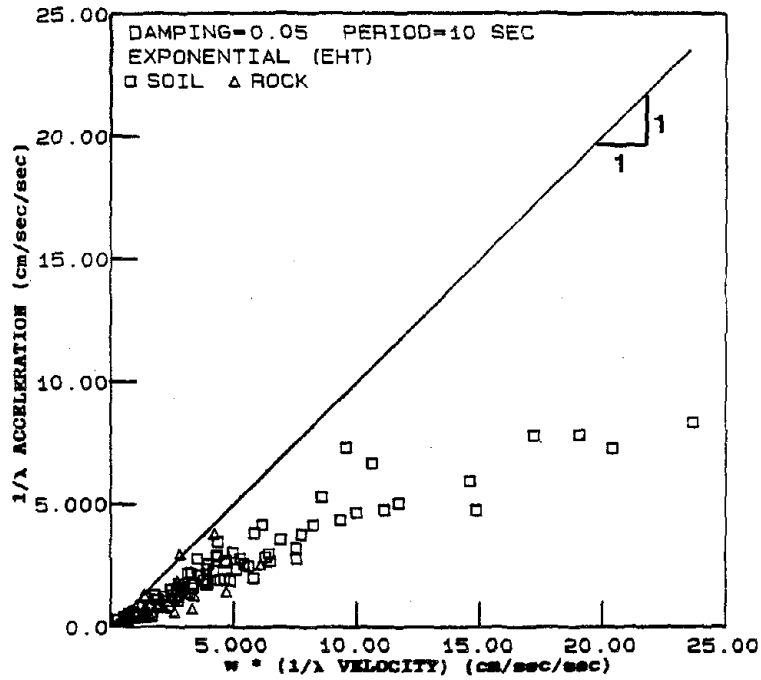

Figure 4.10 $1/\lambda$ acceleration vs. ω x ($1/\lambda$ velocity) for exponential (EHT) distribution for SDOF oscillator with 5% damping and 10 second period.

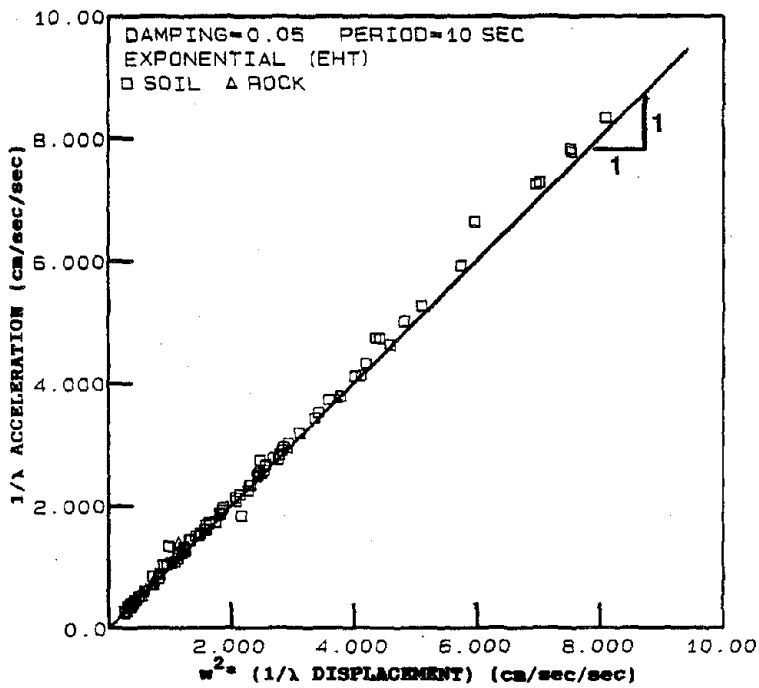

Figure 4.11 $1/\lambda$ acceleration vs. ω^2 x ($1/\lambda$) displacement for exponential (EHT) distribution for SDOF oscillator with 5% damping and 10 second period.

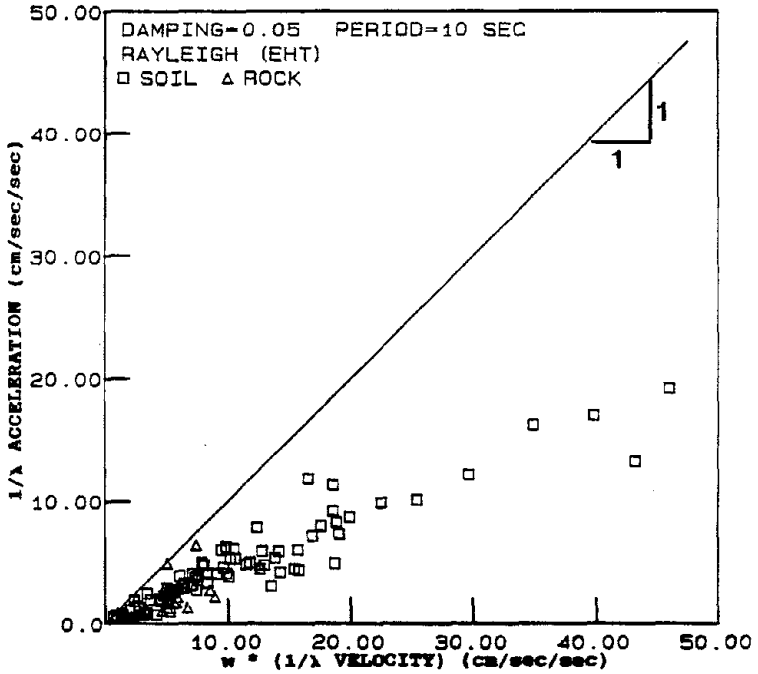

Figure 4.12 $1/\lambda$ acceleration vs. ω x ($1/\lambda$ velocity) for Rayleigh (EHT) distribution with 5% damping and 10 second period.

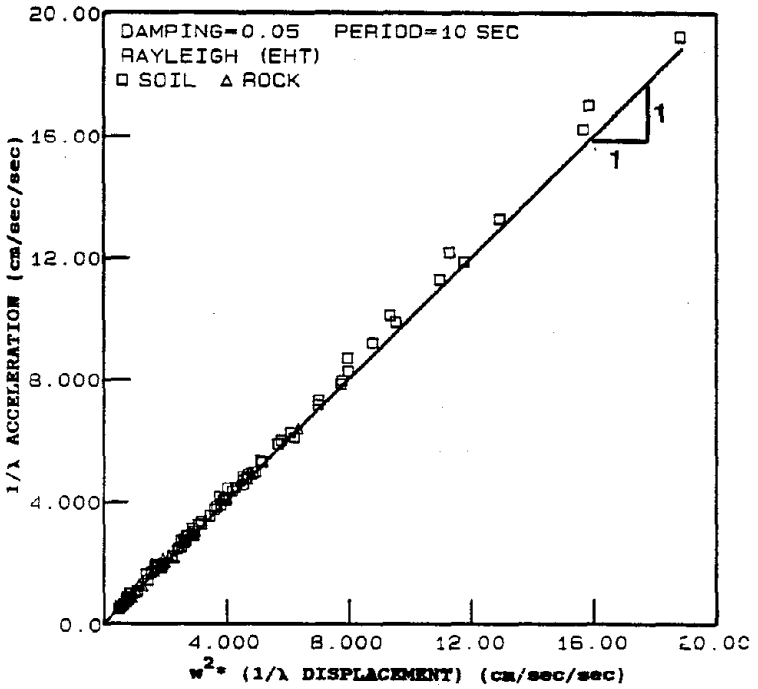

Figure 4.13 $1/\lambda$ acceleration vs. ω^2 x ($1/\lambda$ displacement) for Rayleigh (EHT) distribution with 5% damping and 10 second period.

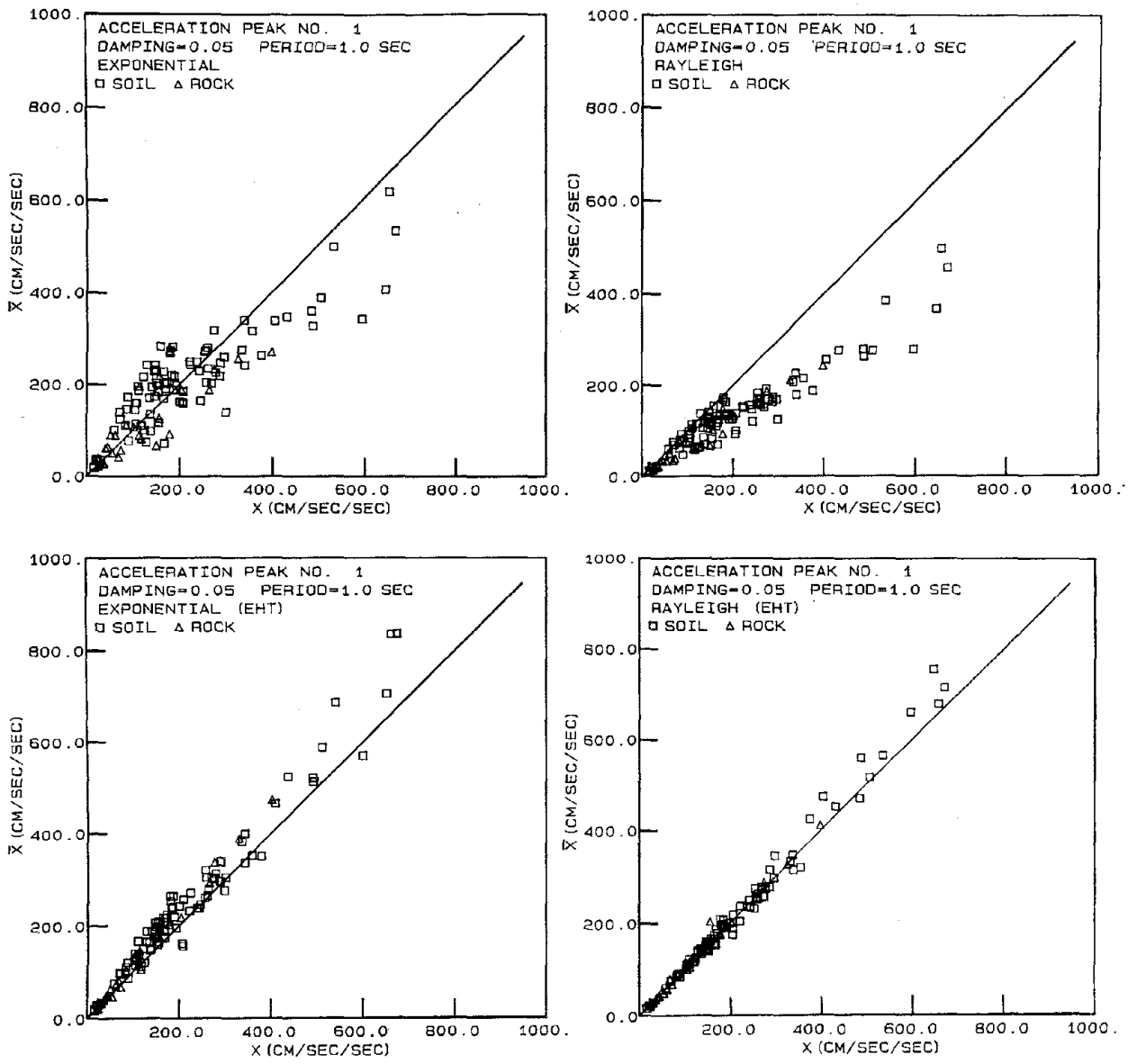

Figure 4.14 Observed X(1) vs. predicted $\bar{X}(1)$ acceleration peak from exponential, Rayleigh, exponential (EHT), and Rayleigh (EHT) distributions for SDOF oscillator with 5% damping and 1.0 second period subjected to 112 ground motion records.

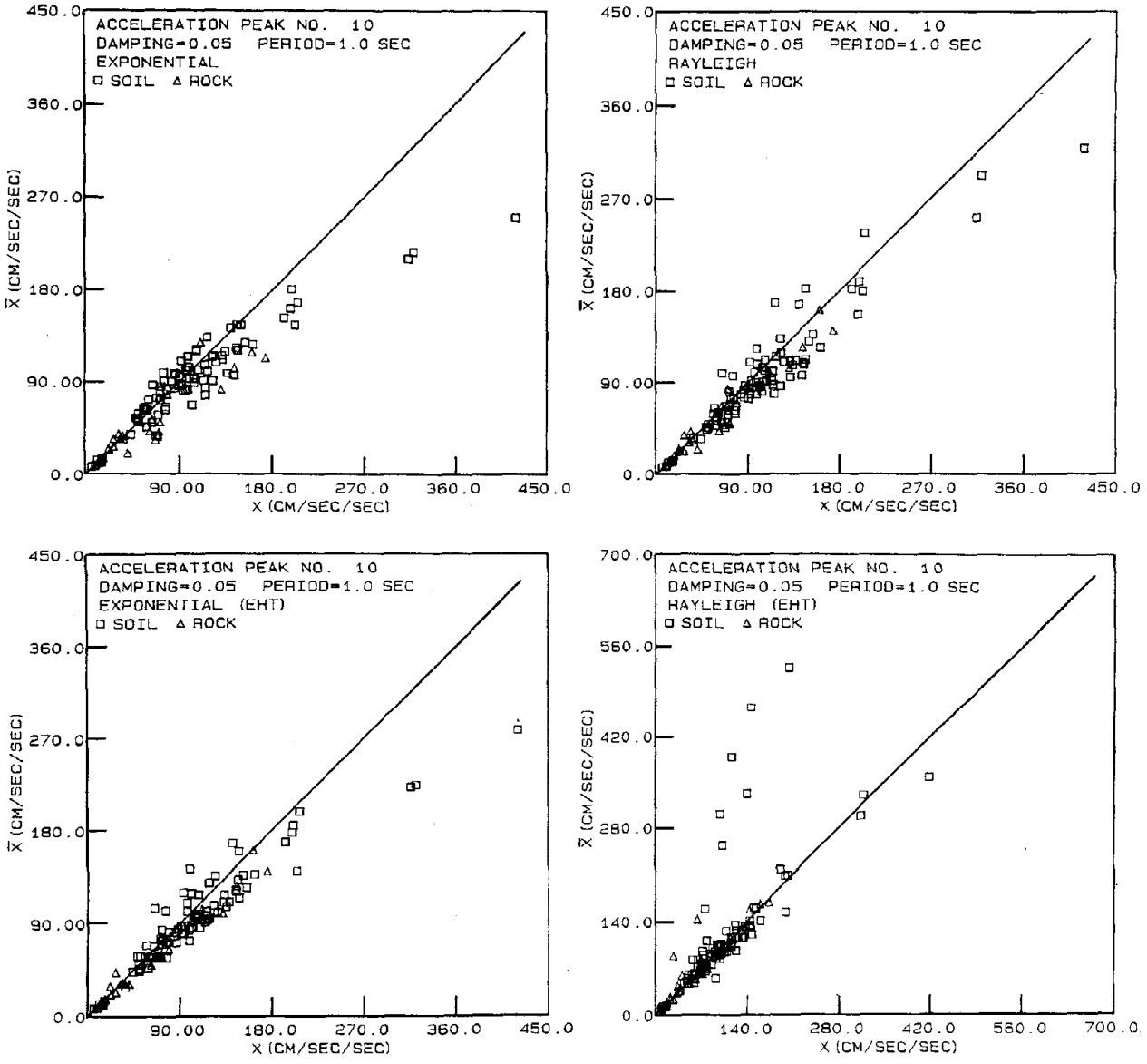

Figure 4.15 Observed X(10) vs. predicted $\bar{X}(10)$ acceleration peak from exponential, Rayleigh, exponential (EHT), and Rayleigh (EHT) distributions for SDOF oscillator with 5% damping and 1.0 second period subjected to 112 ground motion records.

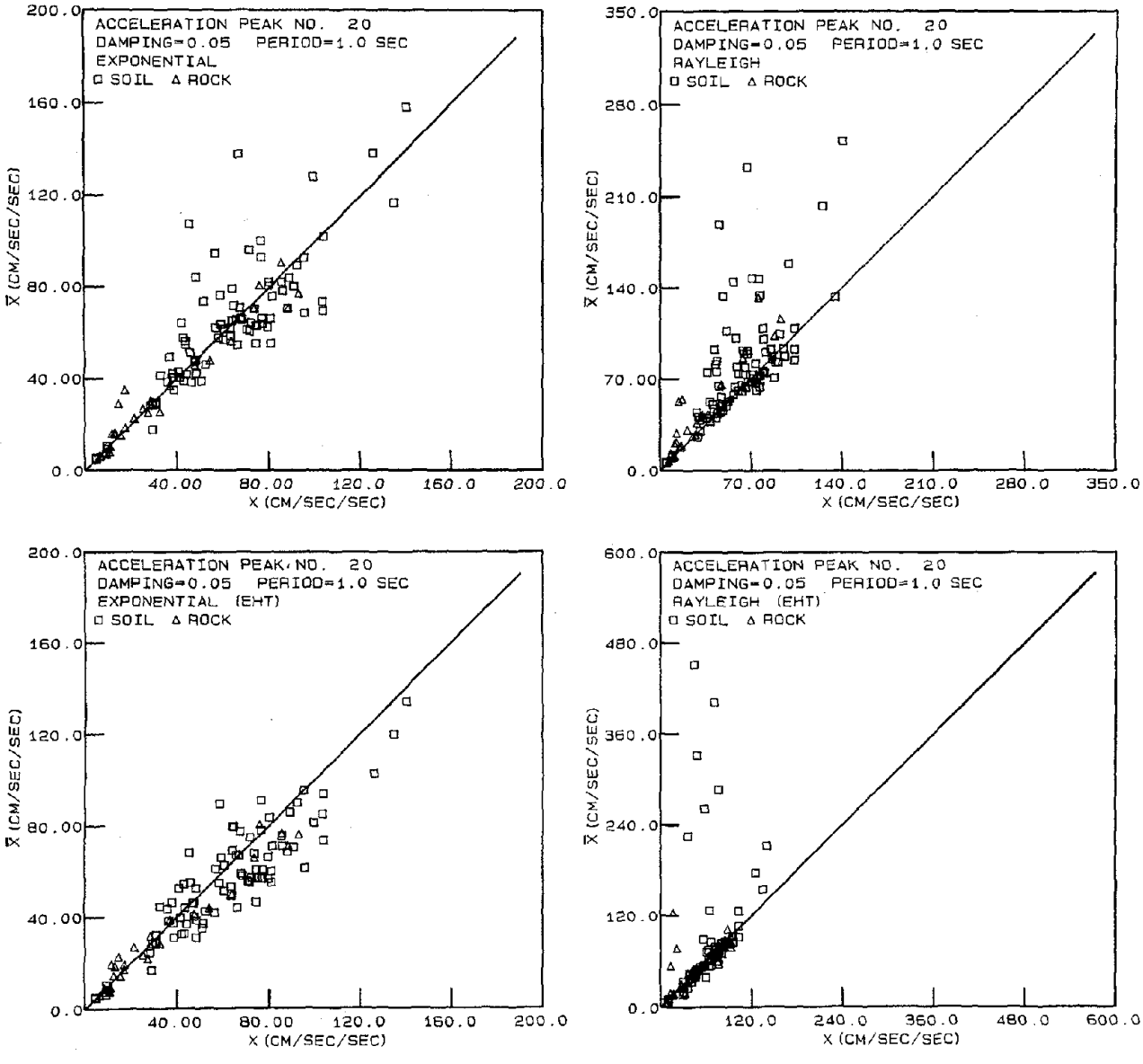

Figure 4.16 Observed X(20) vs. predicted $\bar{X}(20)$ acceleration peak from exponential, Rayleigh, exponential (EHT), and Rayleigh (EHT) distributions for SDOF oscillator with 5% damping and 1.0 second period subjected to 112 ground motion records.

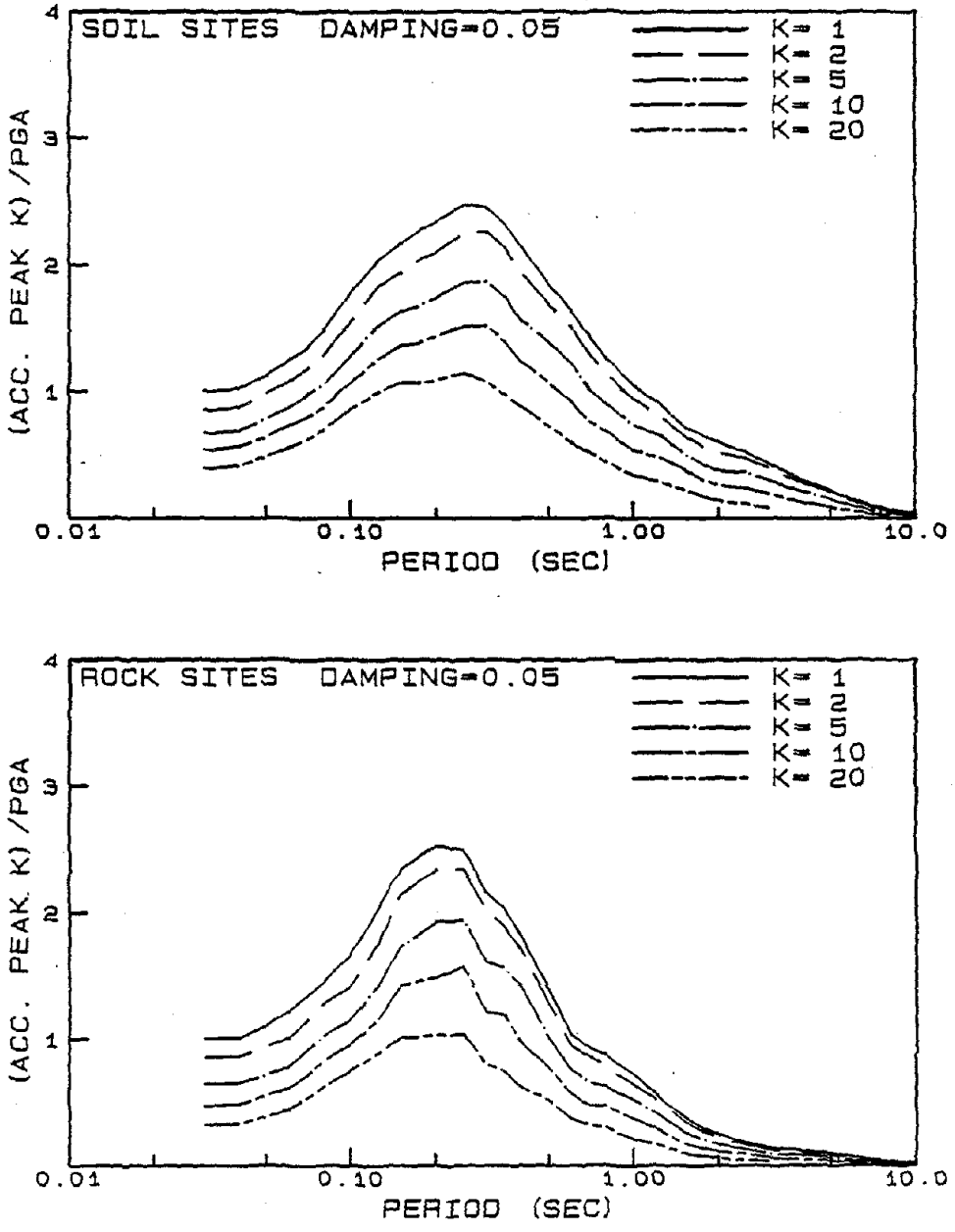

Figure 4.17 Average acceleration spectra for X(1), X(2), X(5), X(10), and X(20) for soil and rock sites for 5% critical damping.

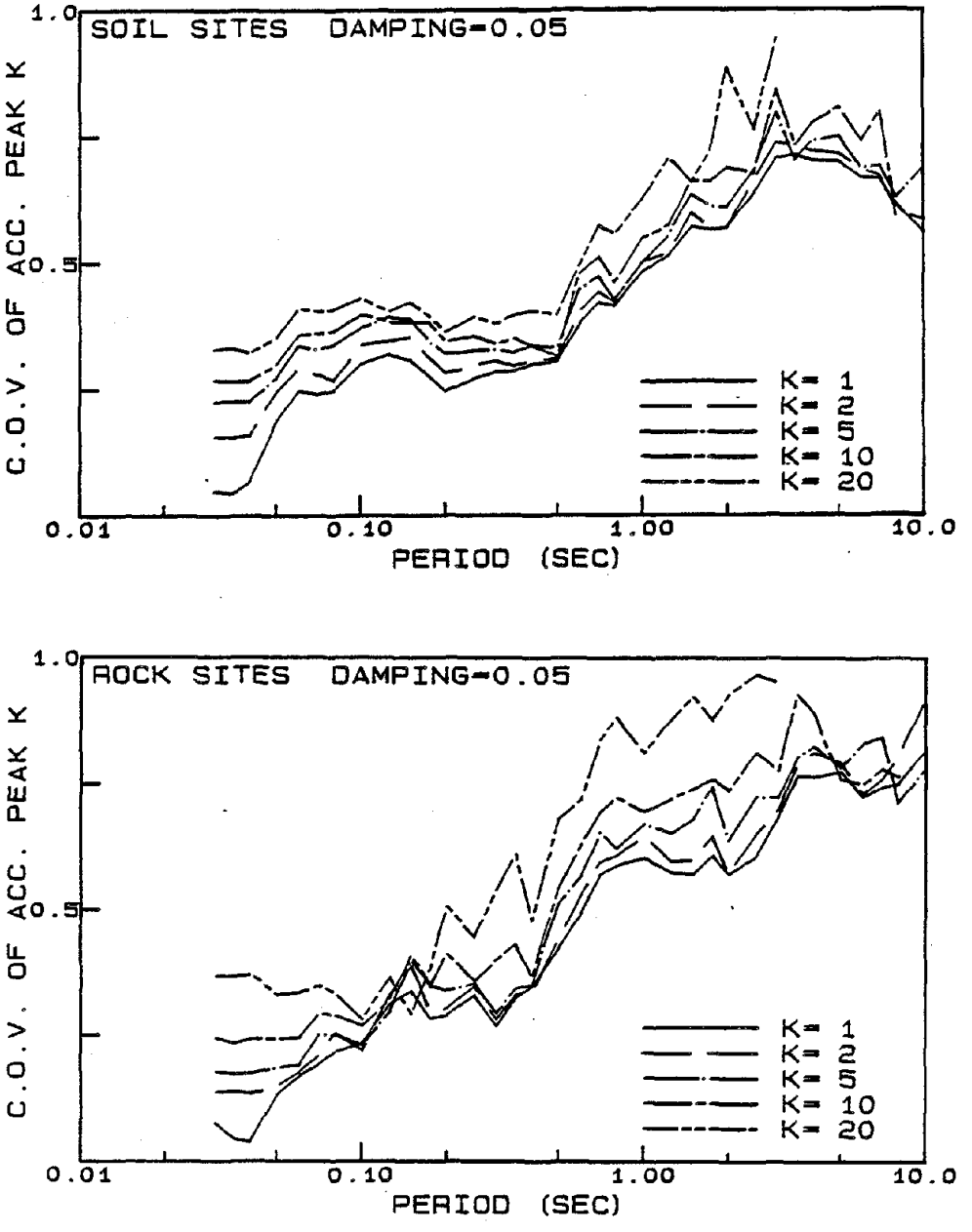

Figure 4.18 Coefficient of variation (C.O.V.) of average acceleration spectra for X(1), X(2), X(5), X(10), and X(20) for soil and rock sites for 5% damping.

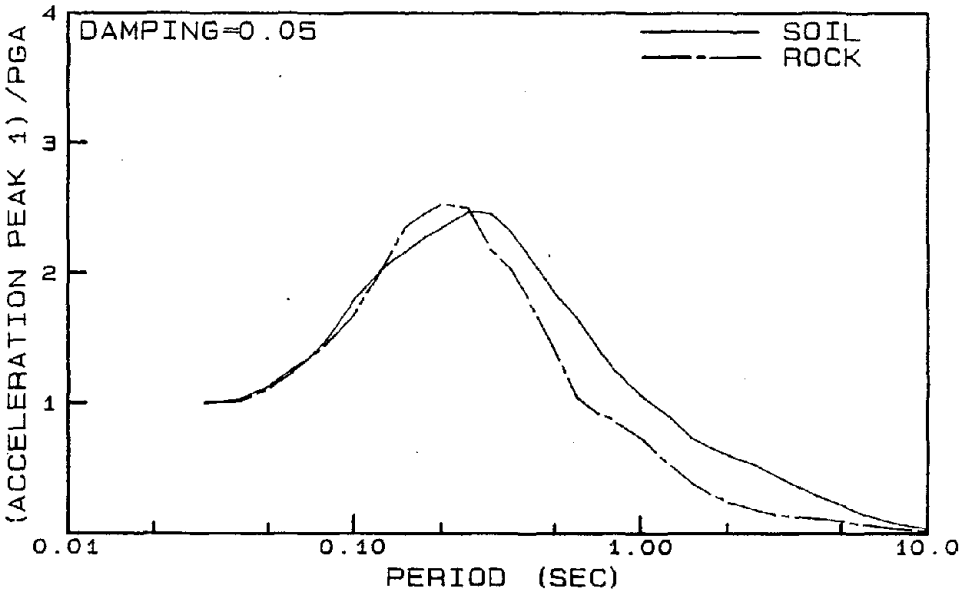

Figure 4.19 Average acceleration spectra for X(1) for soil vs. rock sites for 5% damping.

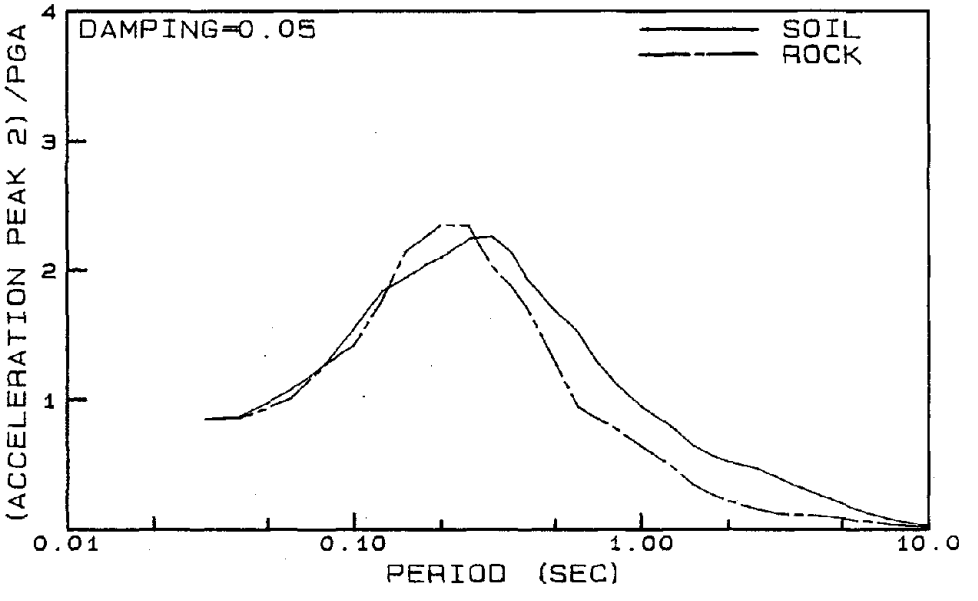

Figure 4.20 Average acceleration spectra for X(2) for soil vs. rock sites for 5% damping.

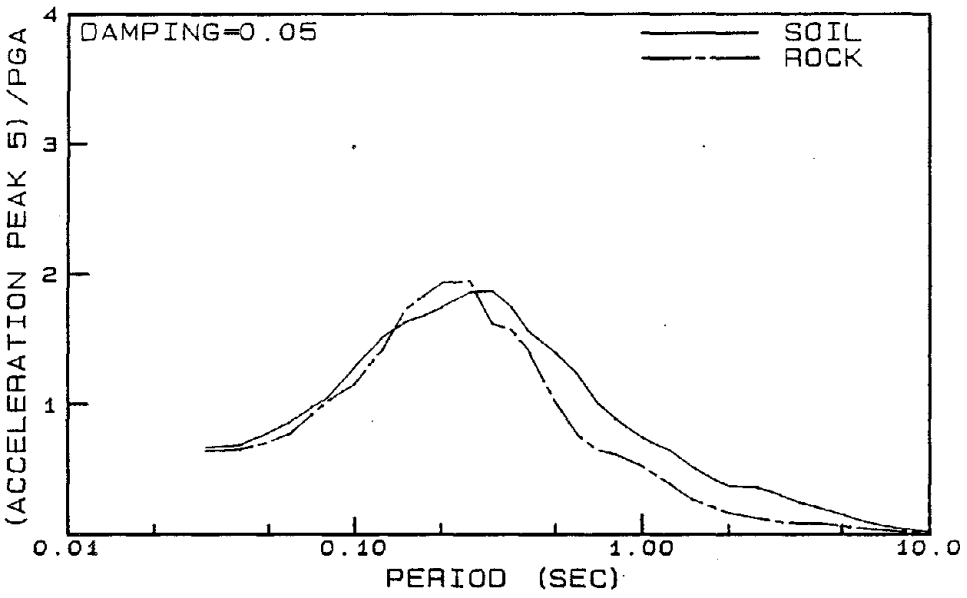

Figure 4.21 Average acceleration spectra for X(5) for soil vs. rock sites for 5% damping.

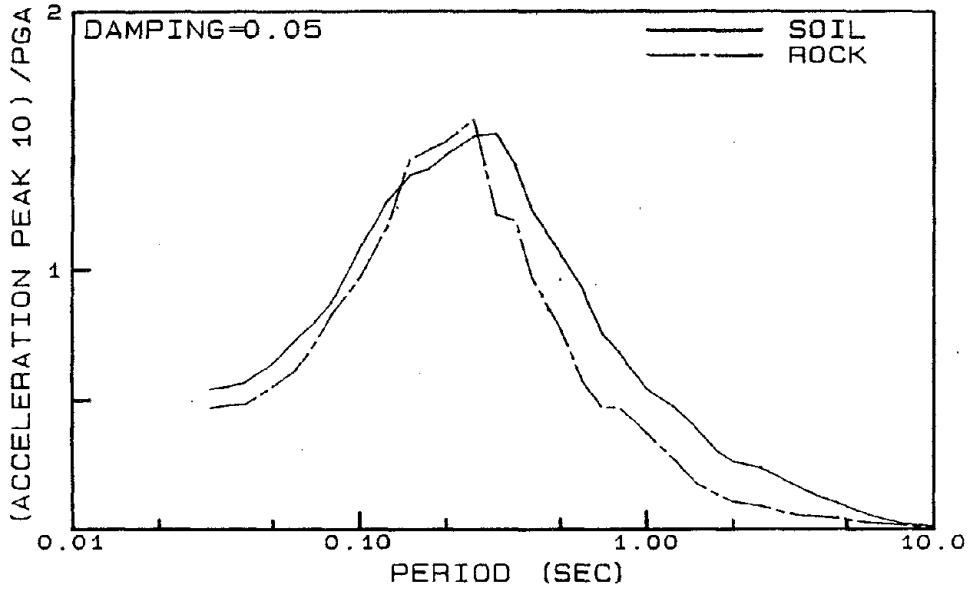

Figure 4.22 Average acceleration spectra for X(10) for soil vs. rock sites for 5% damping.

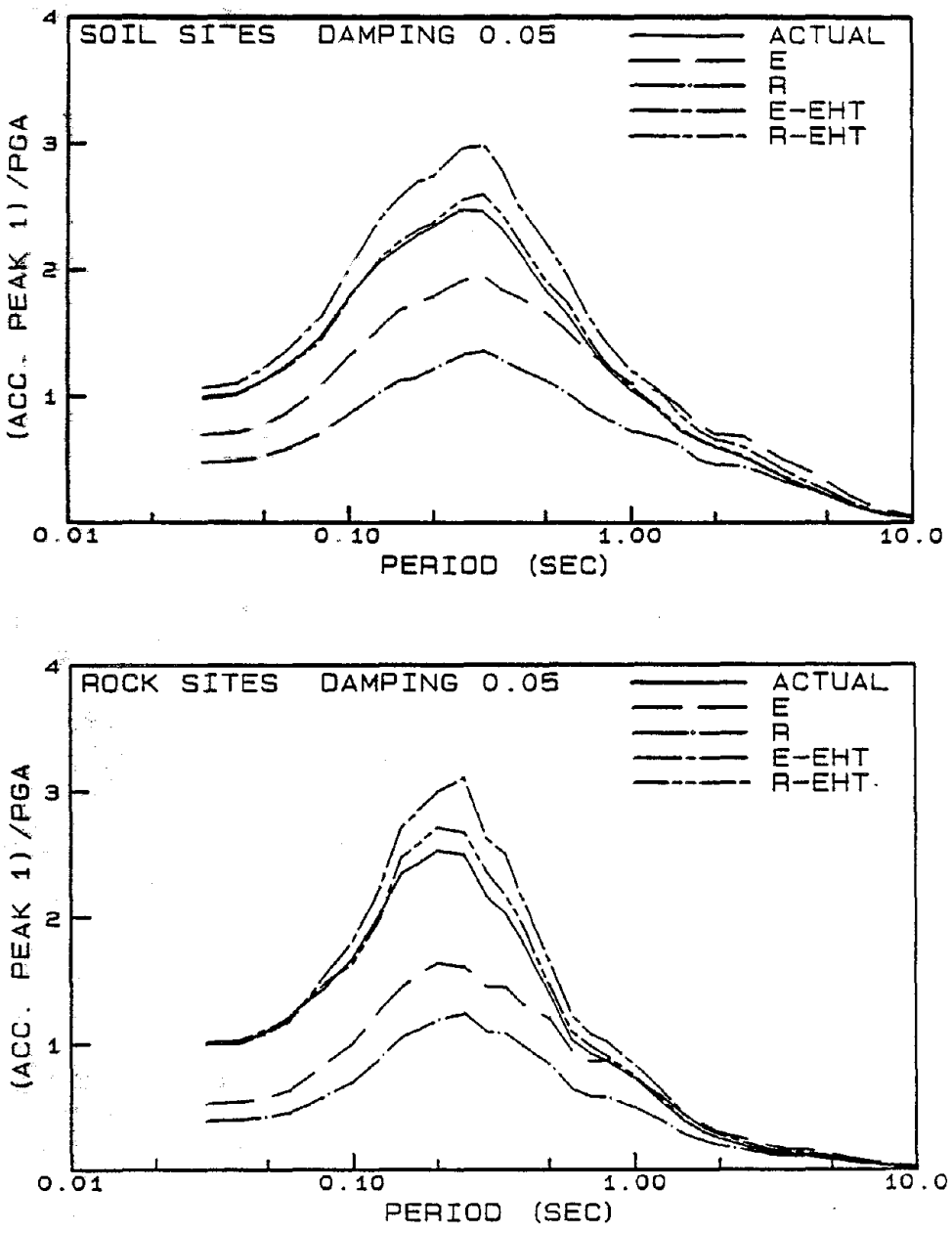

Figure 4.24 Comparison of average actual and average predicted acceleration spectra for X(1) for soil and rock sites for 5% damping.

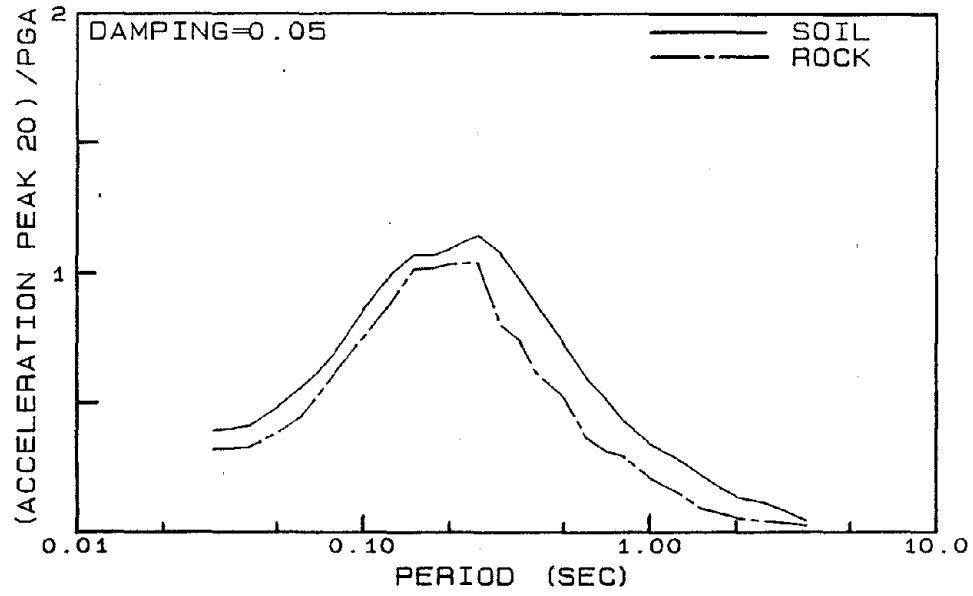

Figure 4.23 Average acceleration spectra for X(20) for soil vs. rock sites for 5% damping.

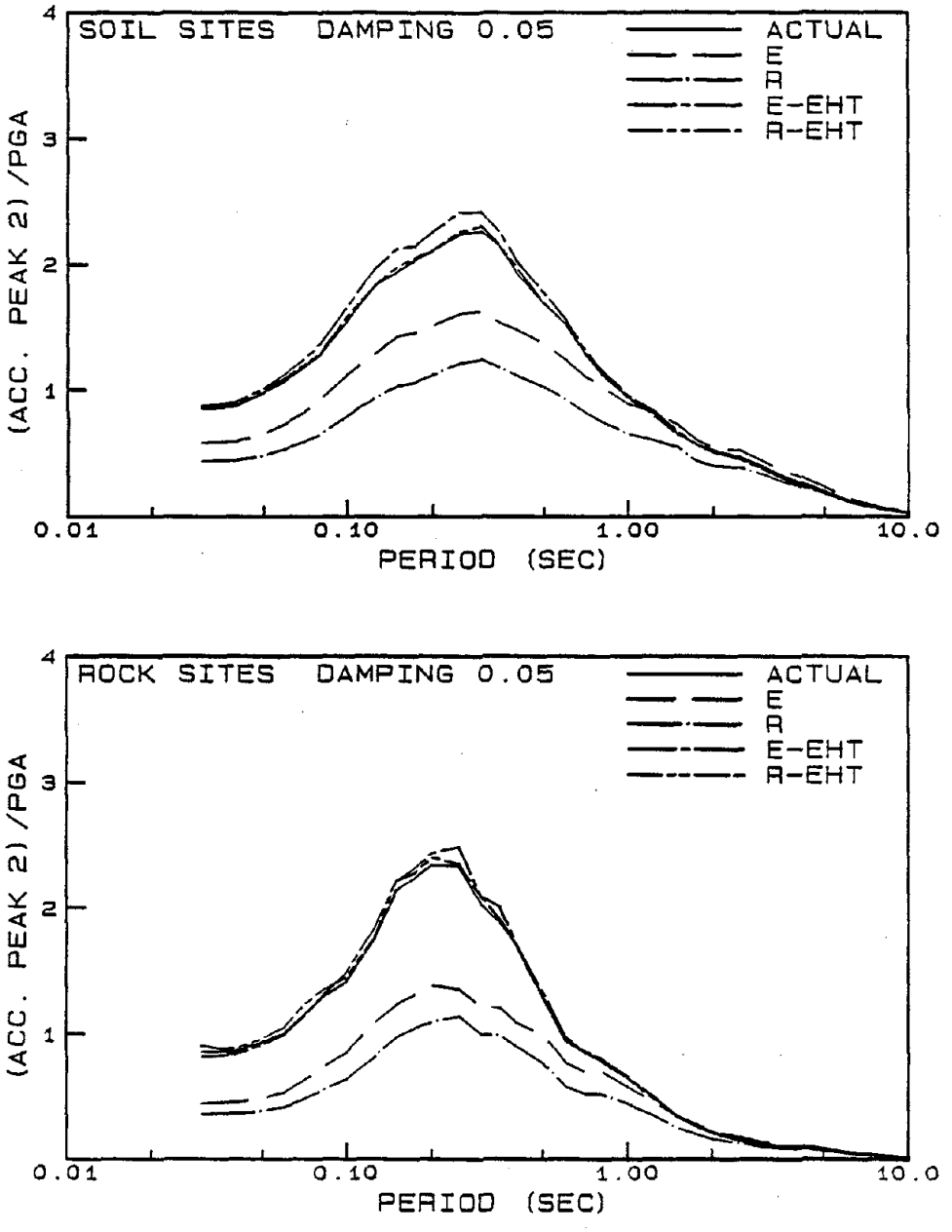

Figure 4.25 Comparison of average actual and average predicted acceleration spectra for X(2) for soil and rock sites for 5% damping.

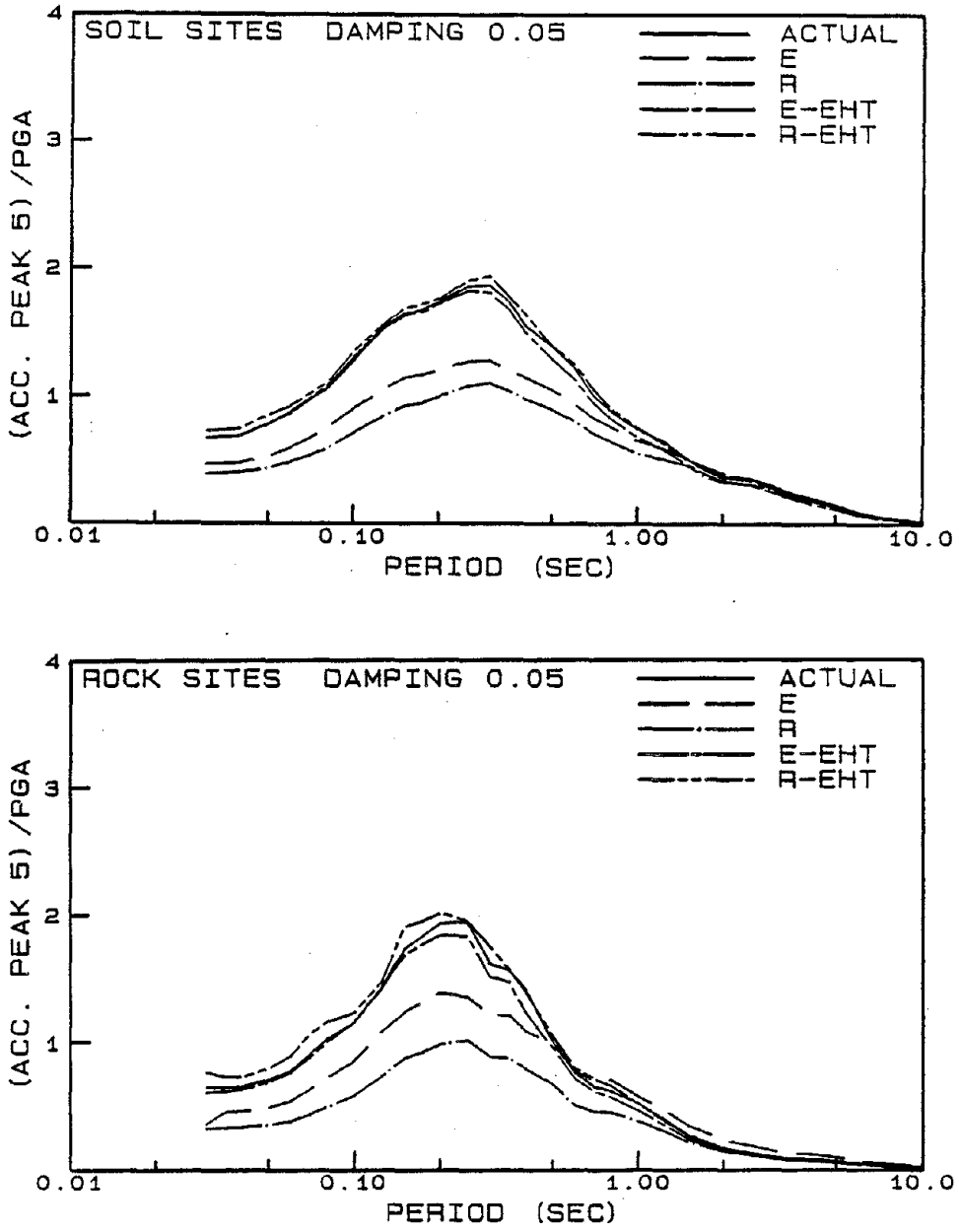

Figure 4.26 Comparison of average actual and average predicted acceleration spectra for X(5) for soil and rock sites for 5% damping.

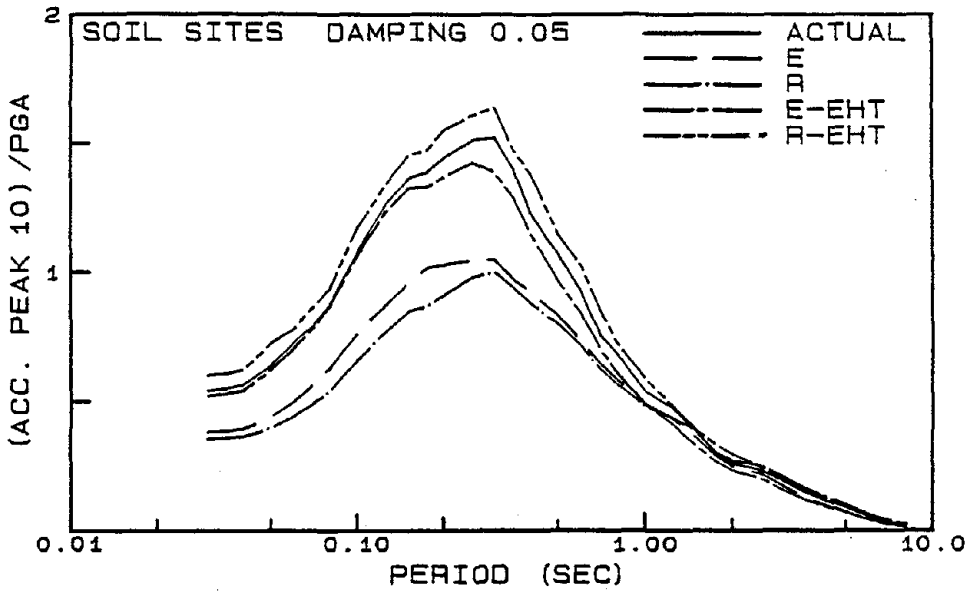

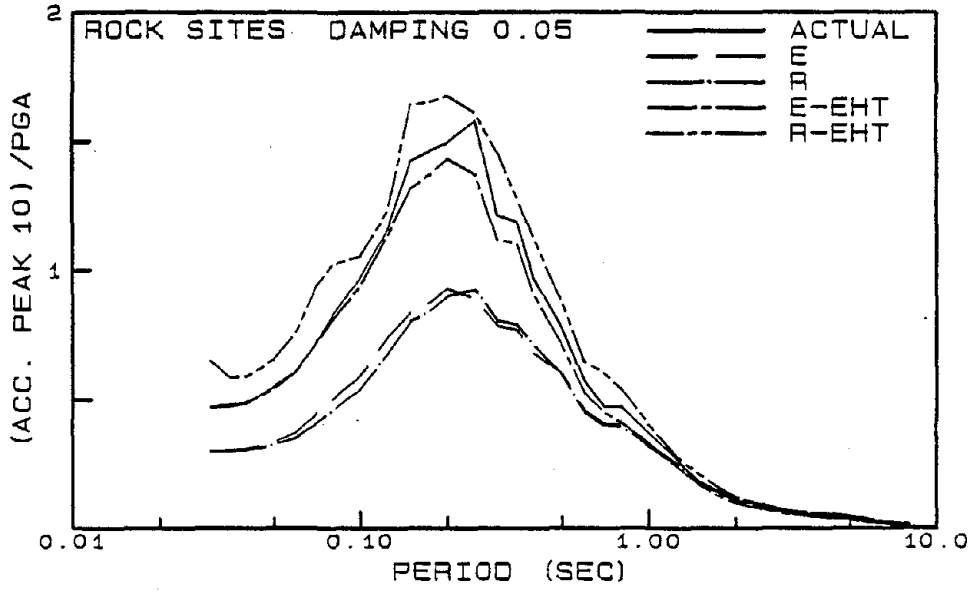

Figure 4.27 Comparison of average actual and average predicted acceleration spectra for X(10) for soil and rock sites for 5% damping.

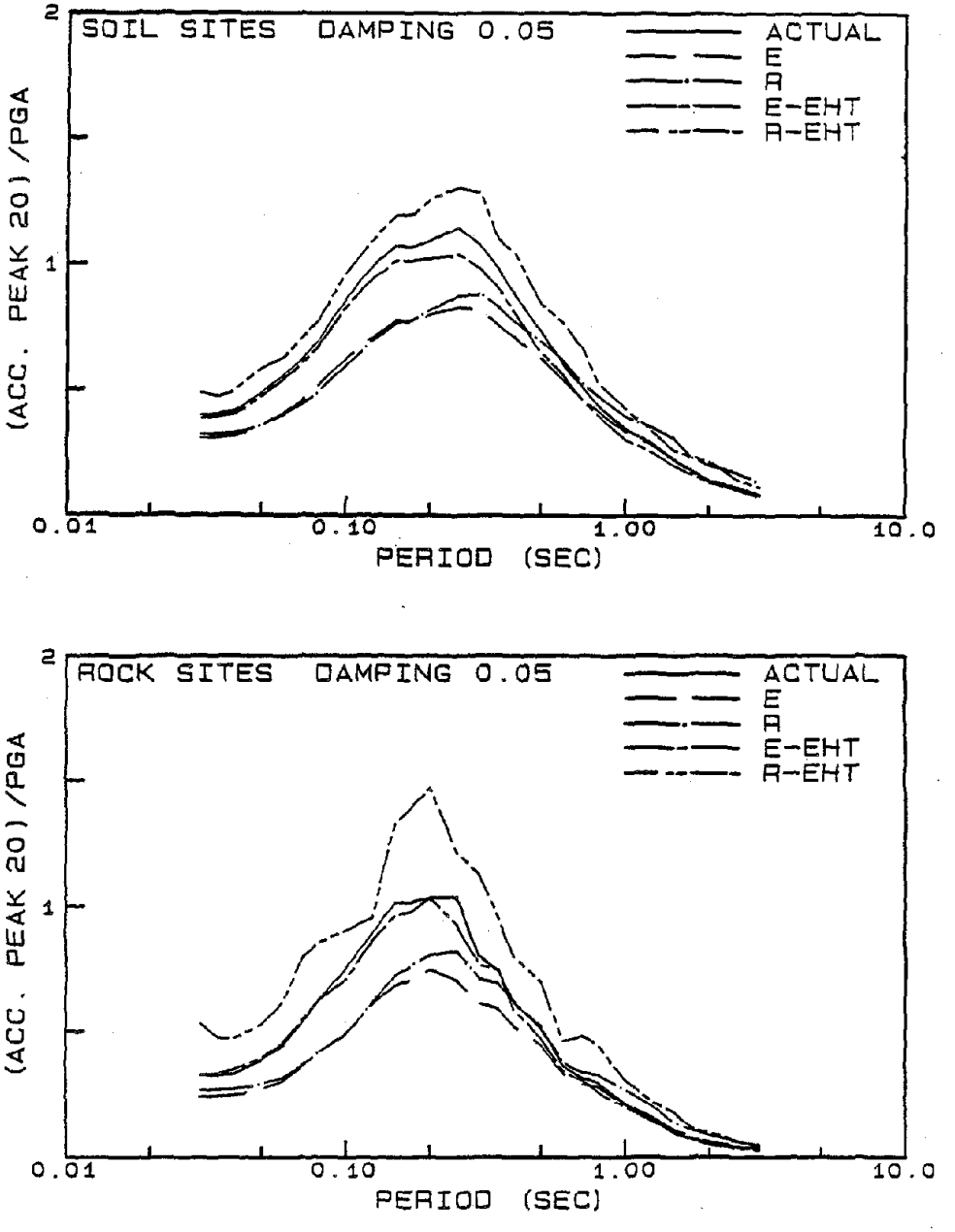

Figure 4.28 Comparison of average actual and average predicted acceleration spectra for X(20) for soil and rock sites for 5% damping.

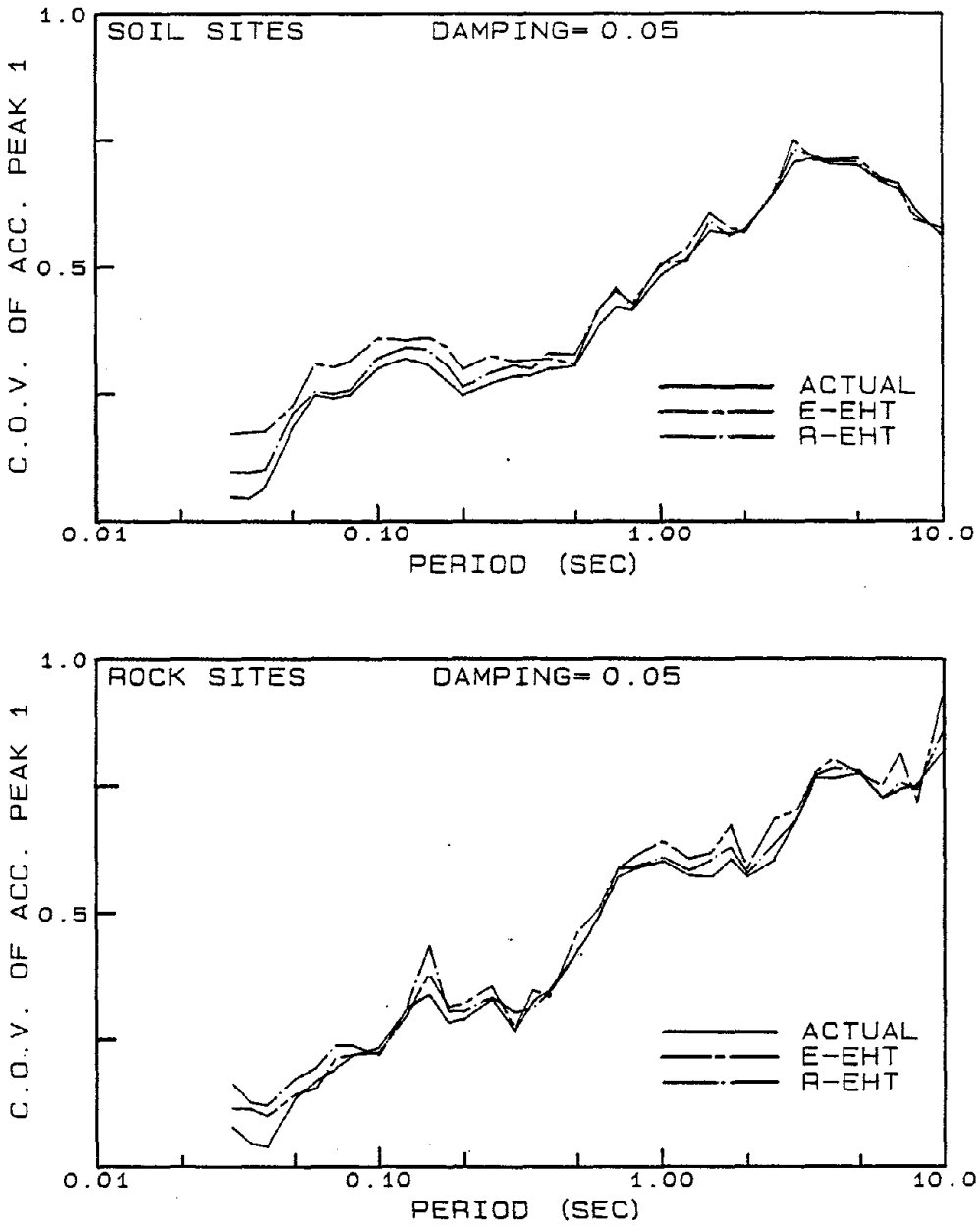

Figure 4.29 Coefficient of variation (C.O.V.) of average actual, exponential (EHT), and Rayleigh (EHT) acceleration spectra shown in Figure 4.24 for X(1) for soil and rock sites for 5% damping.

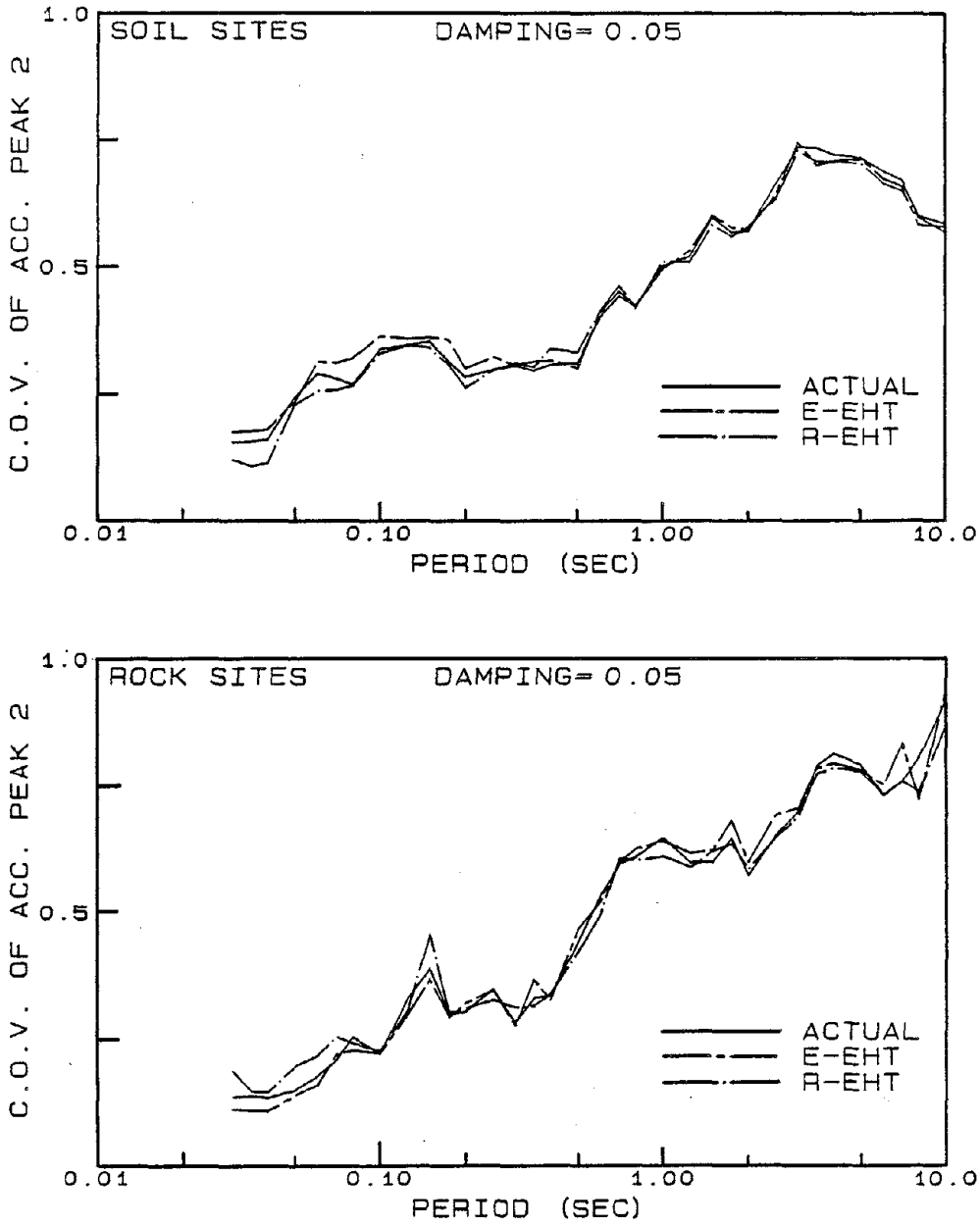

Figure 4.30 Coefficient of variation (C.O.V.) of average actual, exponential (EHT), and Rayleigh (EHT) acceleration spectra shown in Figure 4.25 for X(2) for soil and rock sites for 5% damping.

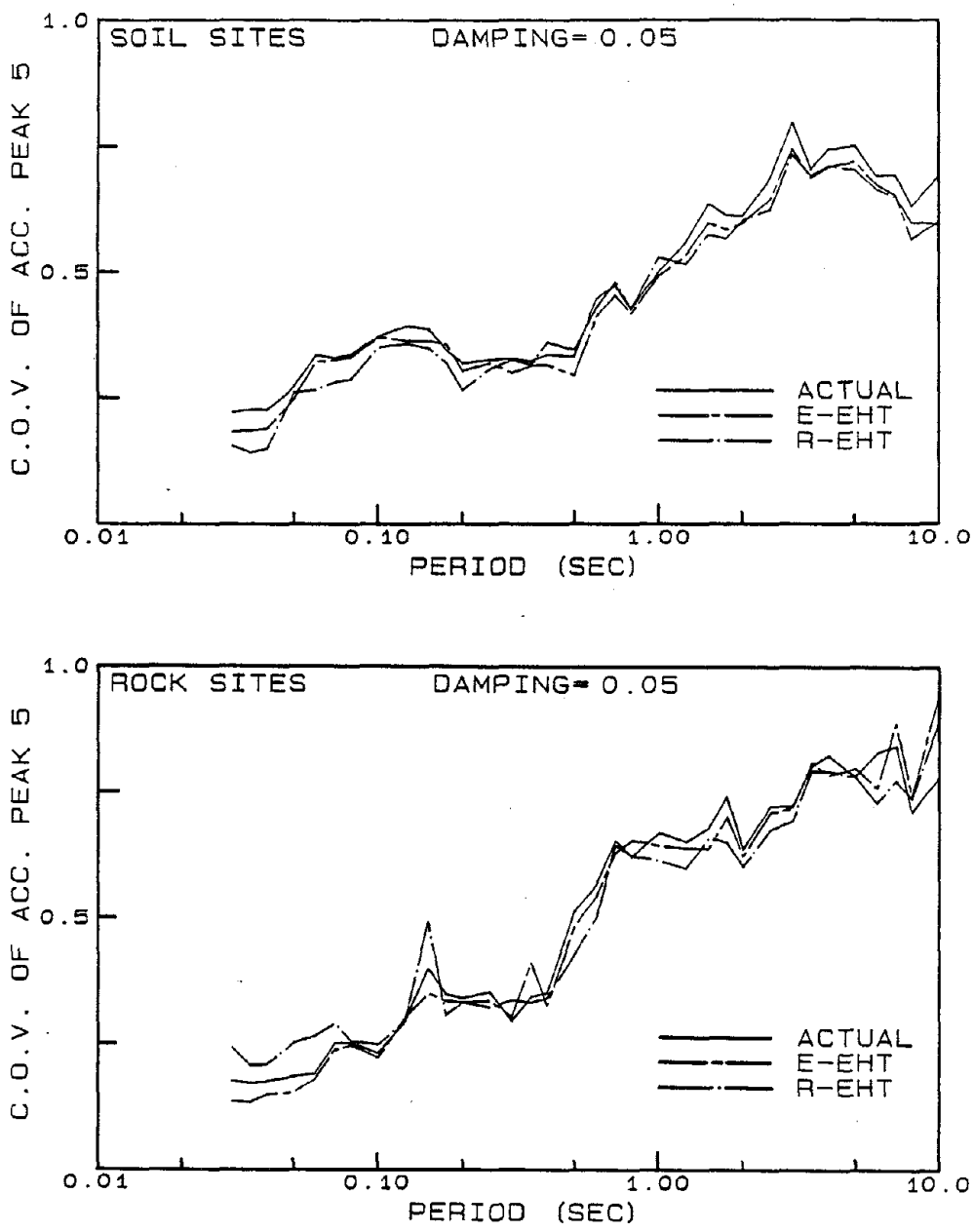

Figure 4.31 Coefficient of variation (C.O.V.) of average actual, exponential (EHT), and Rayleigh (EHT) acceleration spectra shown in Figure 4.26 for X(5) for soil and rock sites for 5% damping.

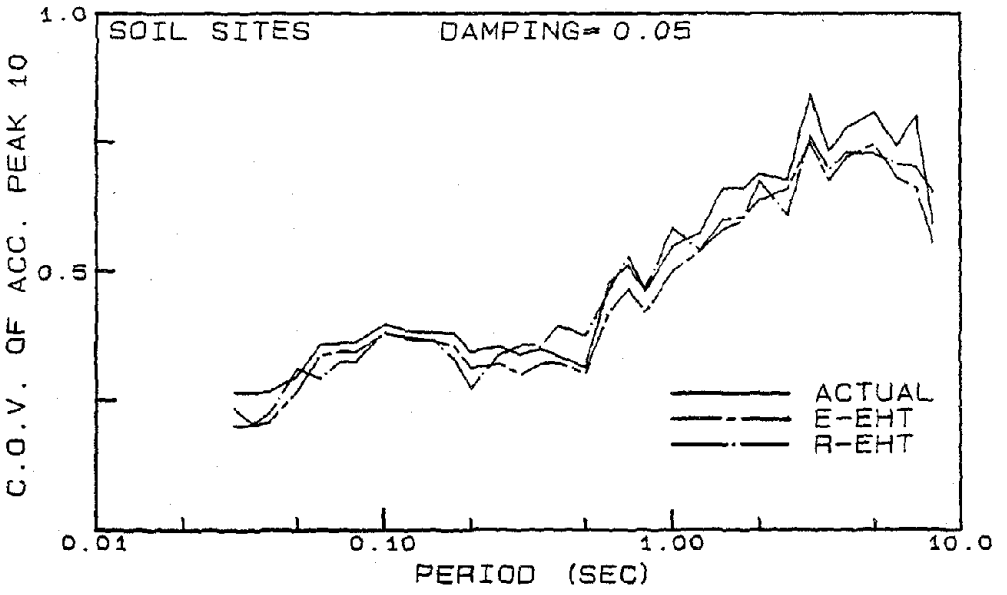

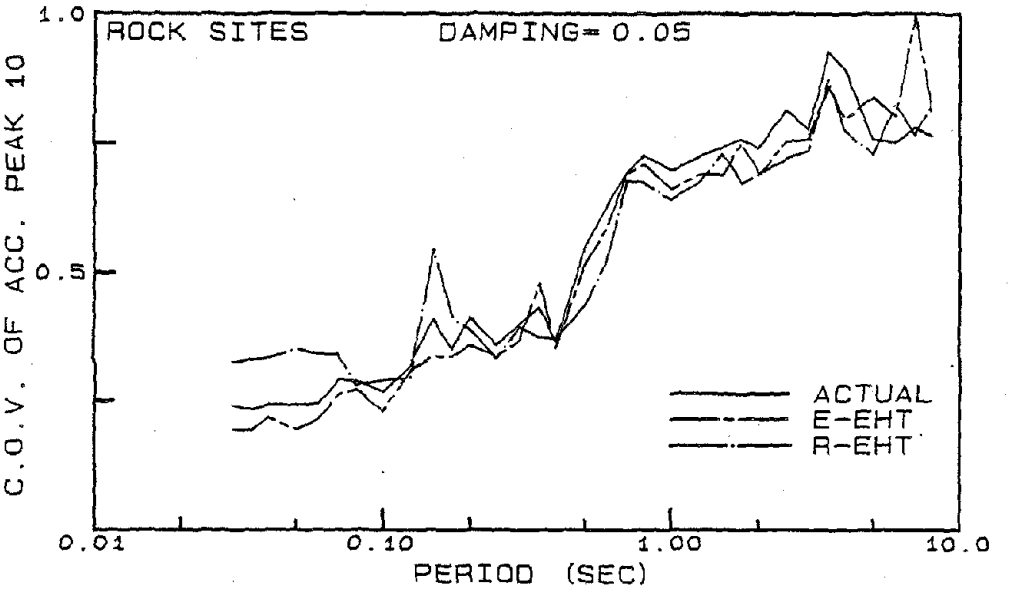

Figure 4.32 Coefficient of variation (C.O.V.) of average actual, exponential (EHT), and Rayleigh (EHT) acceleration spectra shown in Figure 4.27 for X(10) for soil and rock sites for 5% damping.

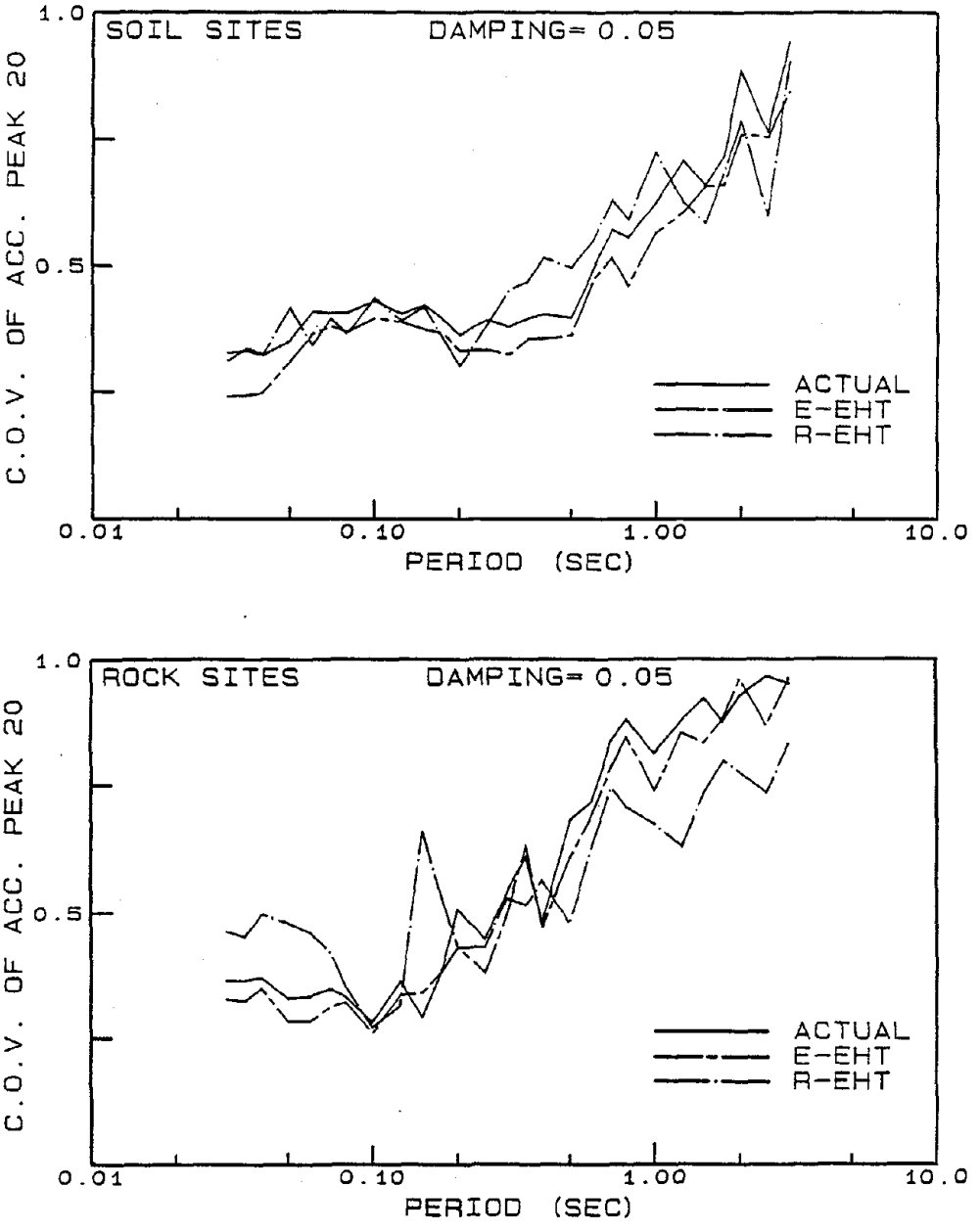

Figure 4.33 Coefficient of variation (C.O.V.) of average actual, exponential (EHT), and Rayleigh (EHT) acceleration spectra shown in Figure 4.28 for X(20) for soil and rock sites for 5% damping.

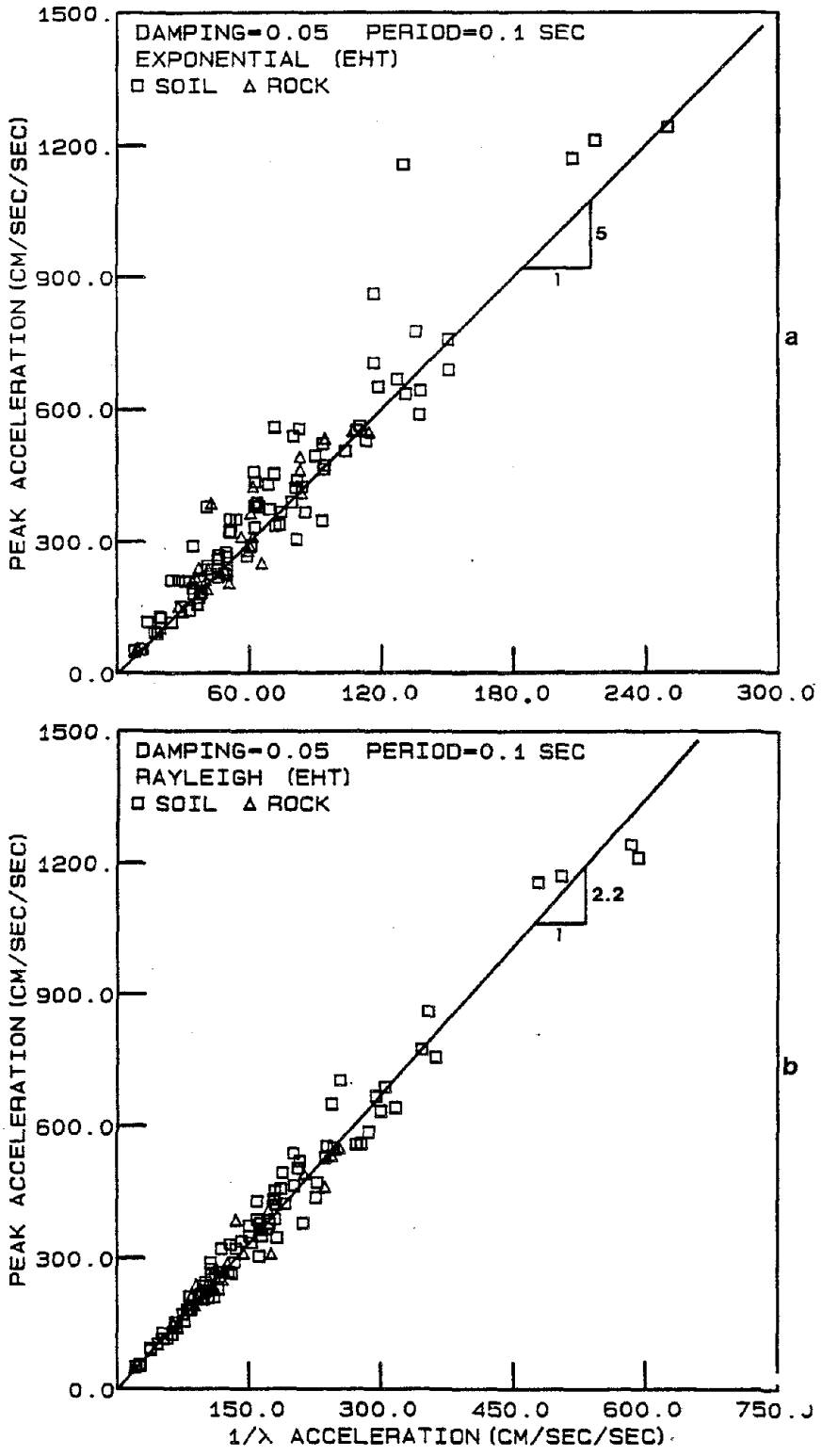

Figure 4.34 Peak acceleration vs. $1/\lambda$ for acceleration response of a SDOF oscillator with 5% damping and 0.1 second period for (a) exponential (EHT) and (b) Rayleigh (EHT) distributions. Lines shown are for reference only.

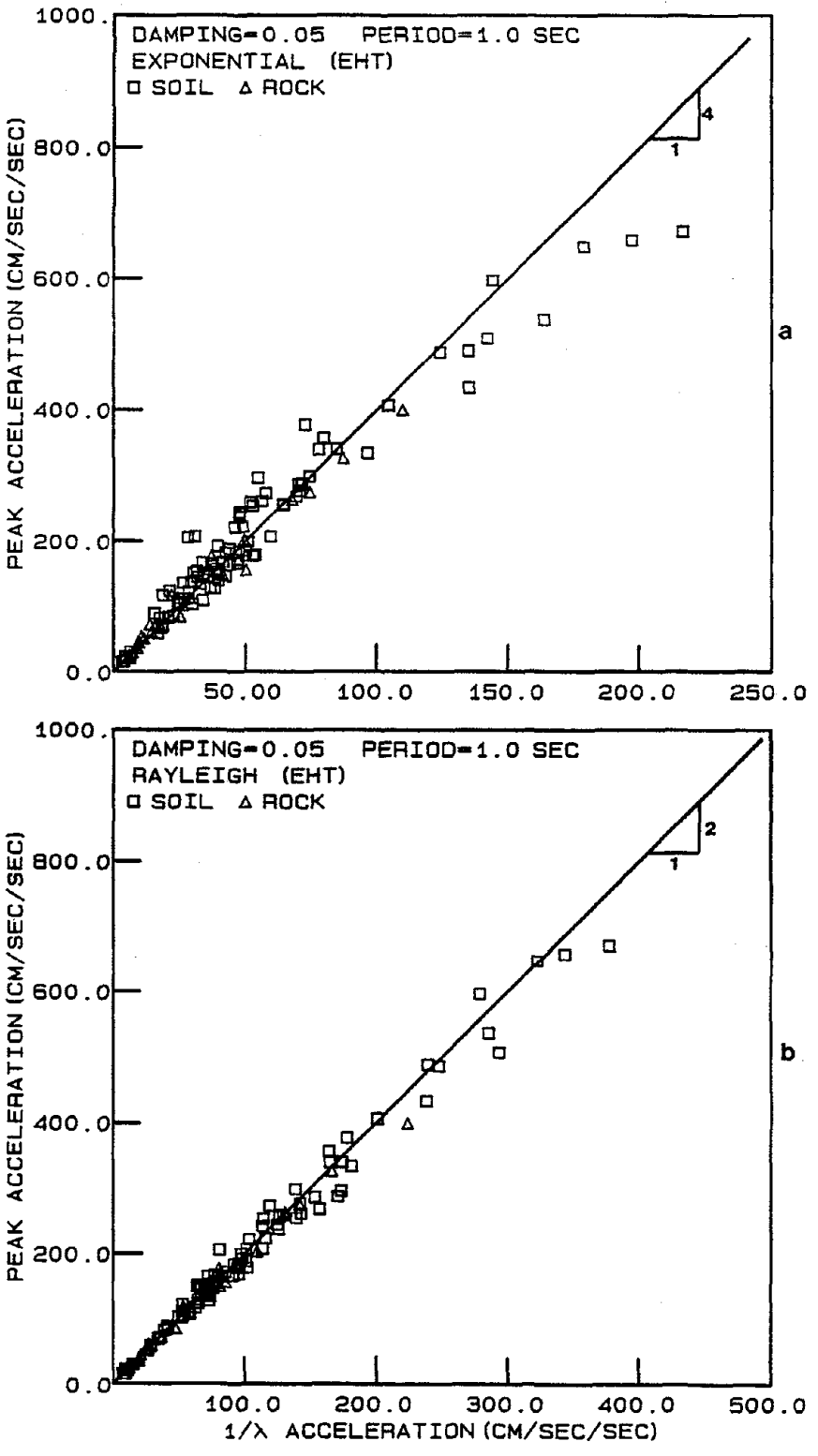

Figure 4.35 Peak acceleration vs. $1/\lambda$ for acceleration response of a SDOF oscillator with 5% damping and 1 second period for (a) exponential (EHT) and (b) Rayleigh (EHT) distributions. Lines shown are for reference only.

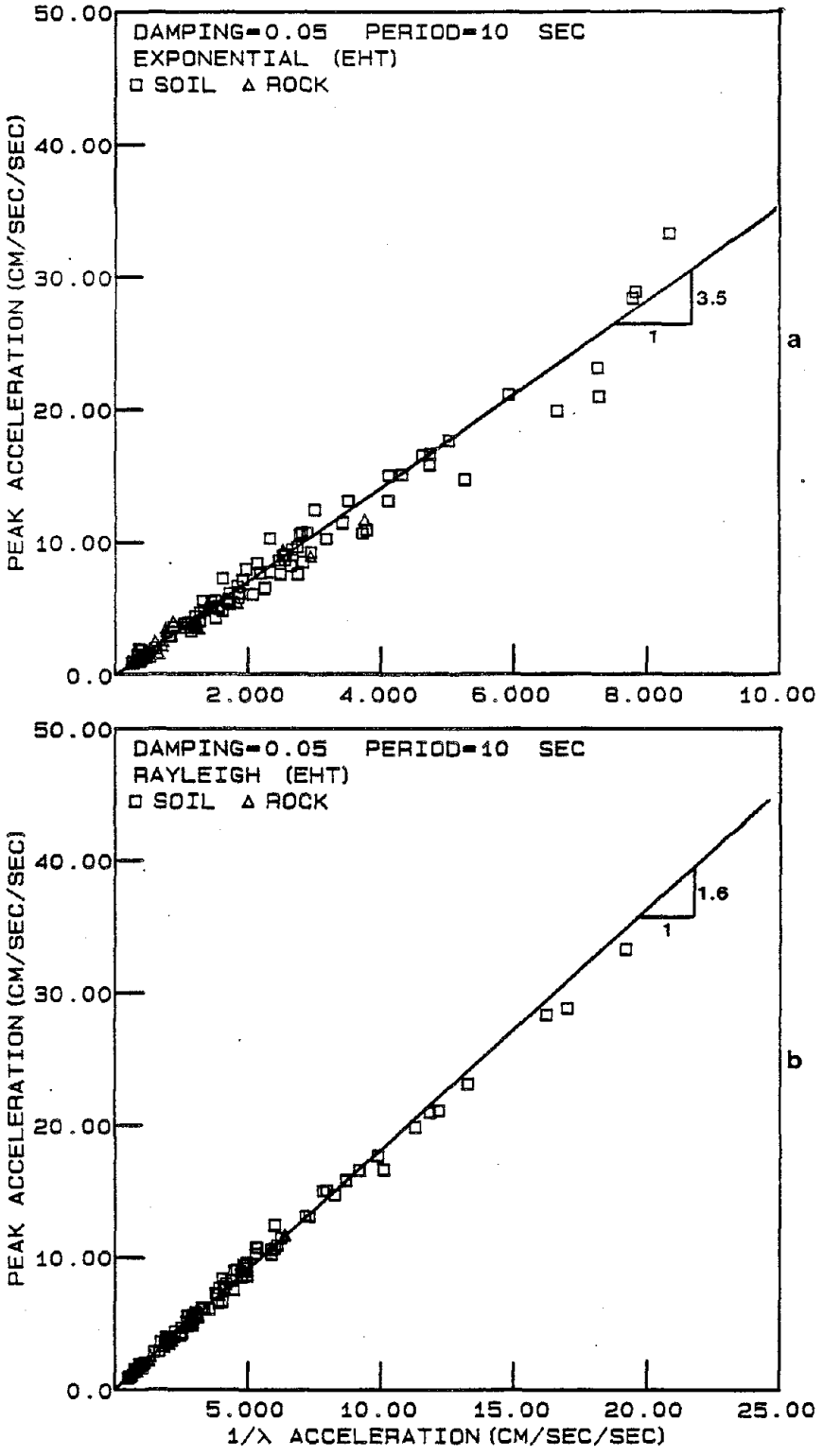

Figure 4.36 Peak acceleration vs. $1/\lambda$ for acceleration response of a SDOF oscillator with 5% damping and 10 second period for (a) exponential (EHT) and (b) Rayleigh (EHT) distributions. Lines shown are for reference only.

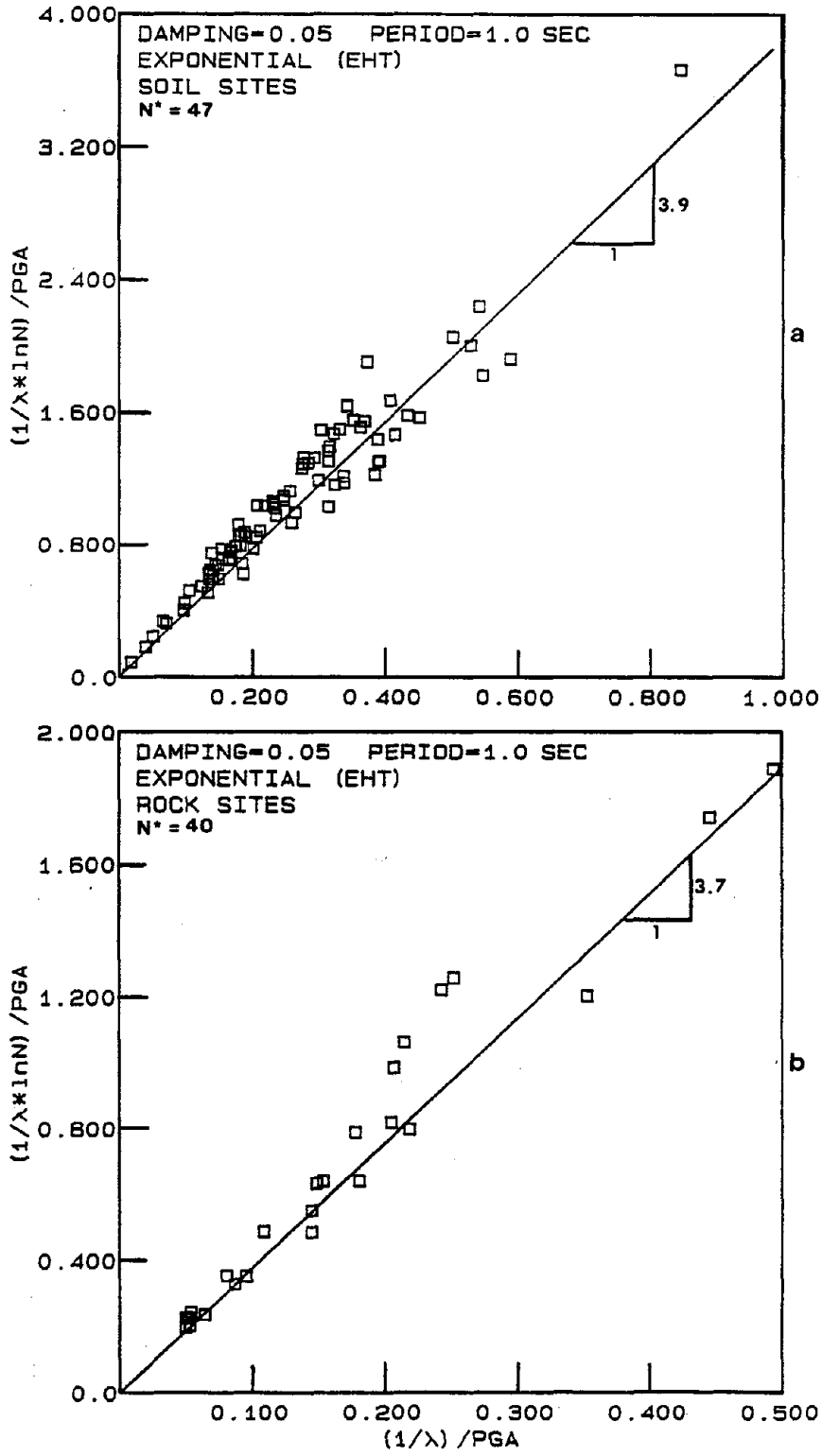

Figure 4.37 $1/\lambda \ln N$ vs. $1/\lambda$ for acceleration response of a SDOF oscillator with 5% damping and 1 second period for exponential (EHT) distribution for (a) soil and (b) rock sites. Slope of line is ln N*.

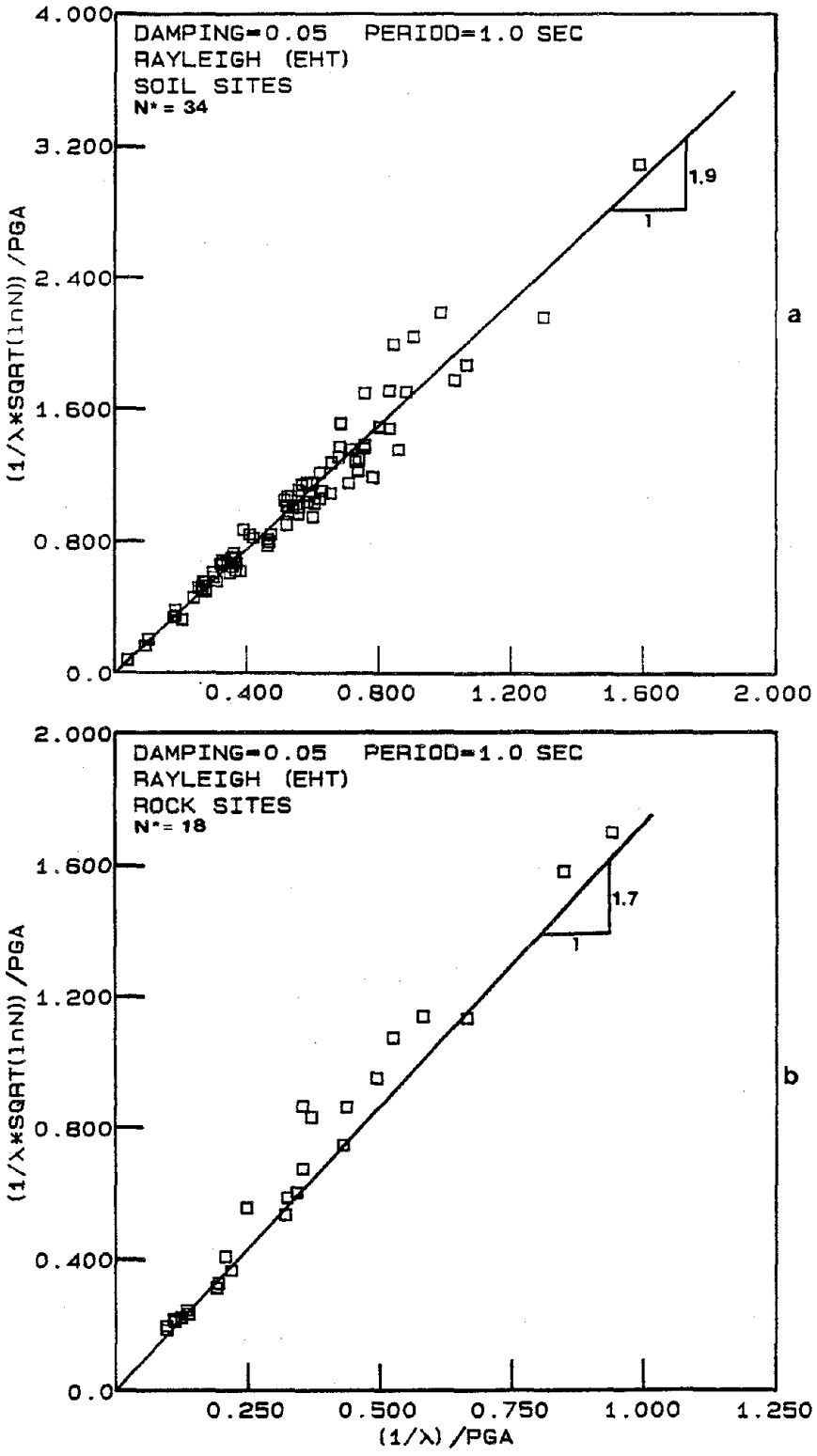

Figure 4.38 $1/\lambda\sqrt{\ln N}$ vs. $1/\lambda$ for acceleration response of a SDOF oscillator with 5% damping and 1 second period for Rayleigh (EHT) distribution for (a) soil and (b) rock sites. Slope of line is $\sqrt{\ln N^*}$.

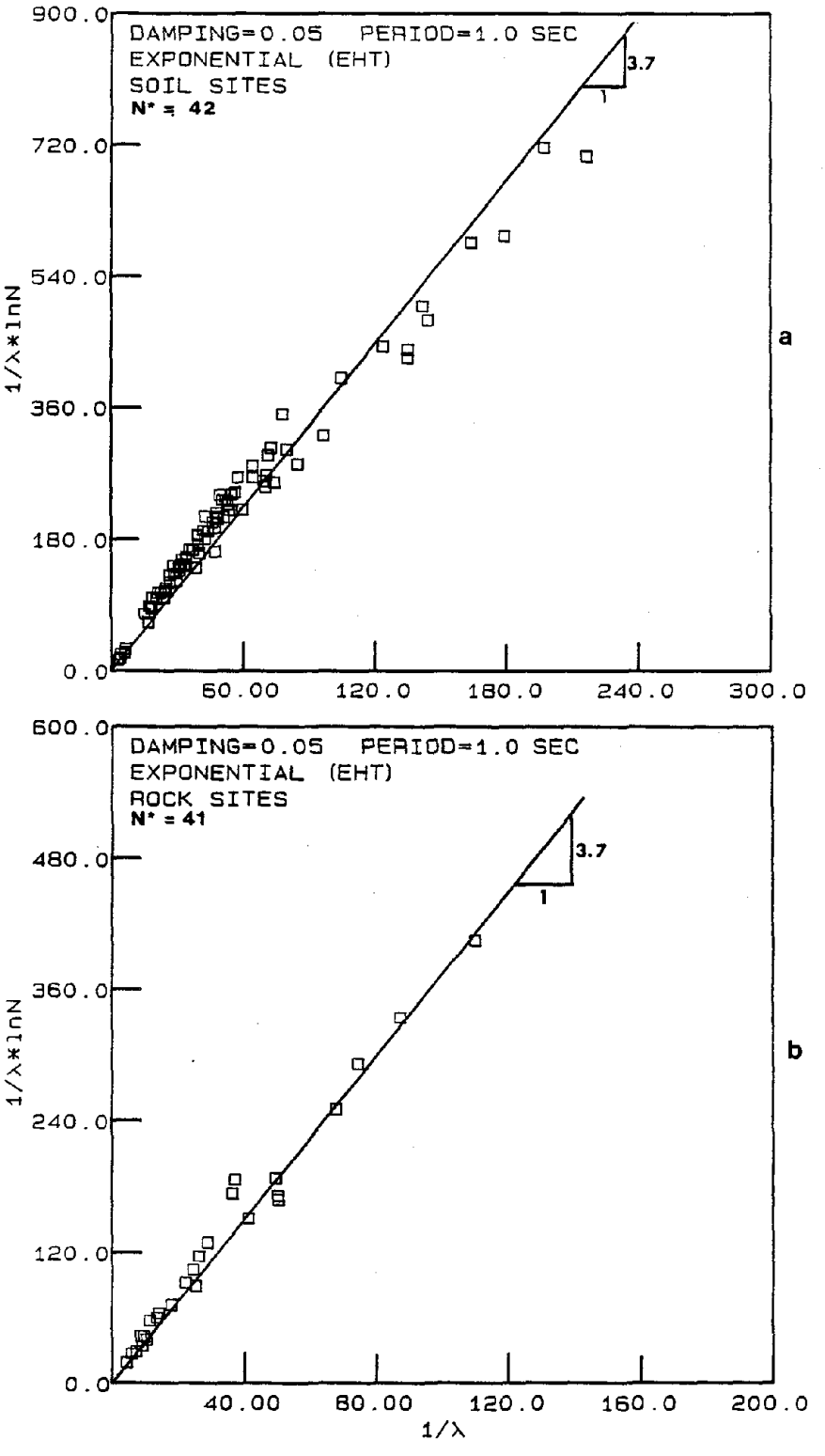

Figure 4.39 $(1/\lambda \ln N)/PGA$ vs. $(1/\lambda)/PGA$ for acceleration response of a SDOF oscillator with 5% damping and 1 second period for exponential (EHT) distribution for (a) soil and (b) rock sites. Slope of Line is ln N*.

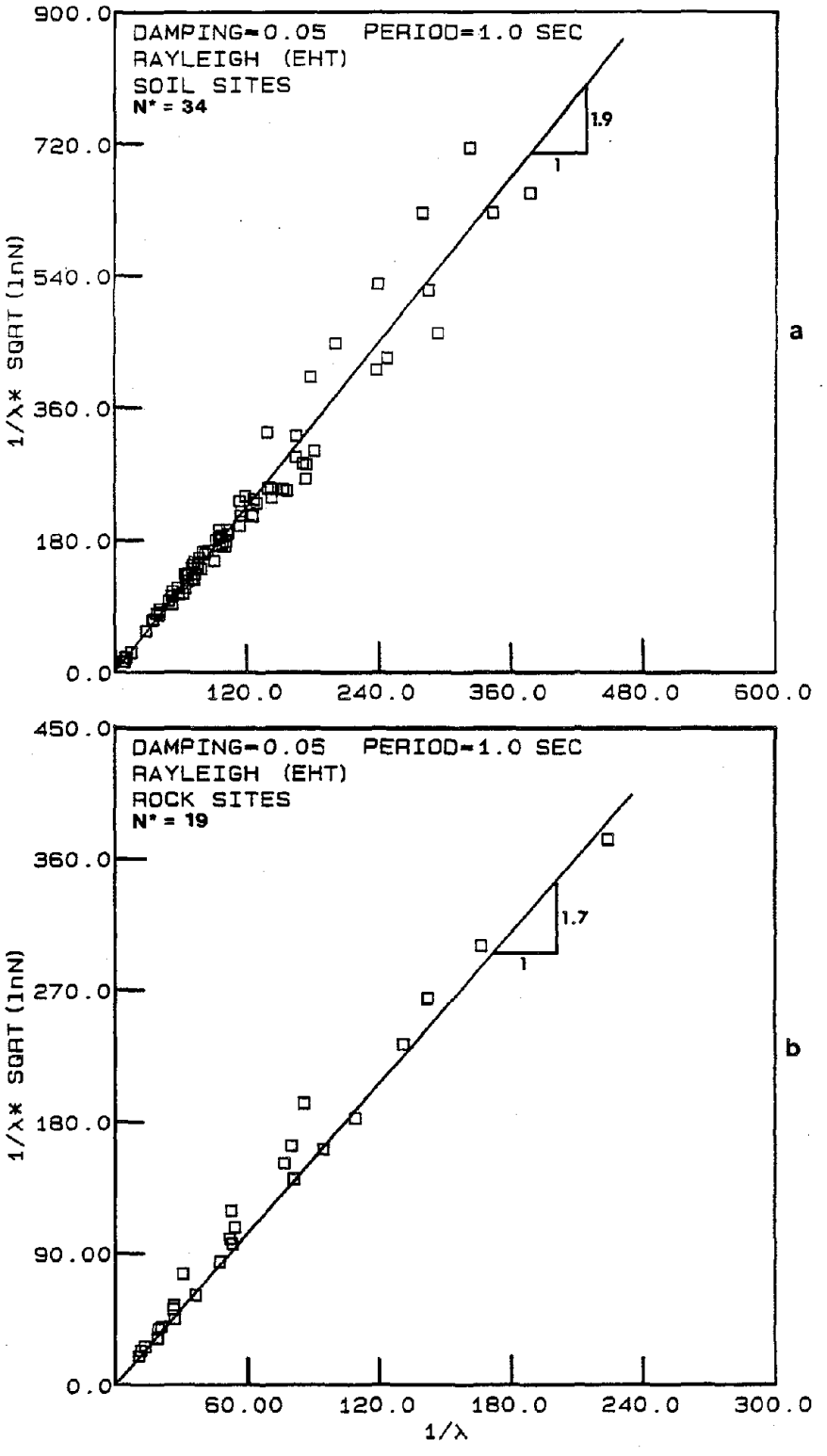

Figure 4.40 $(1/\lambda \sqrt{\ln N})/PGA$ vs. $(1/\lambda)/PGA$ for acceleration response of a SDOF oscillator with 5% damping and 1 second period for Rayleigh (EHT) distribution for (a) soil and (b) rock sites. Slope of line is $\sqrt{\ln N^*}$.

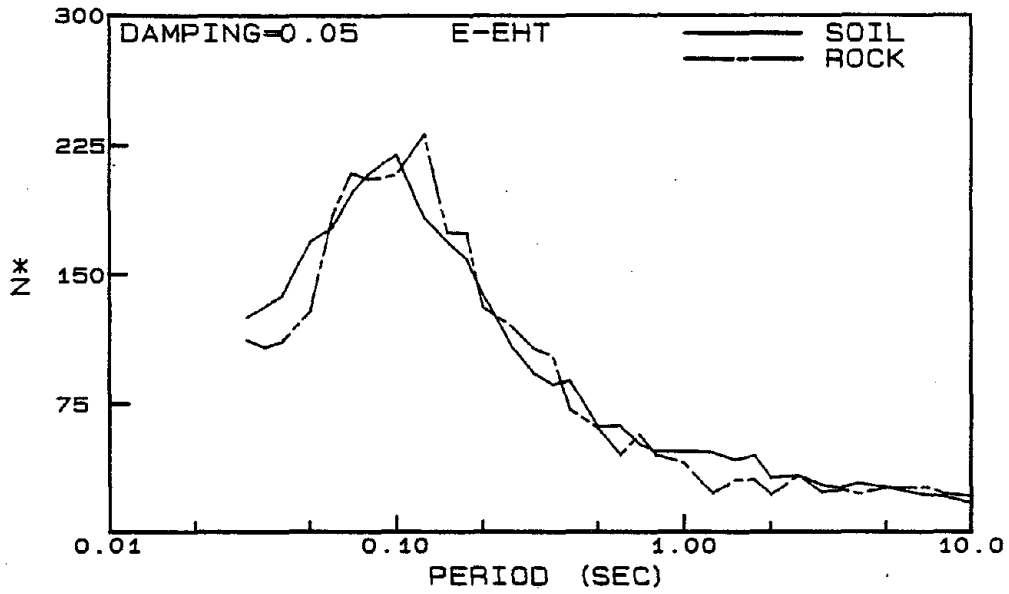

Figure 4.41 Standardized N* for exponential (EHT) distribution for SDOF oscillator with 5% damping for soil and rock sites.

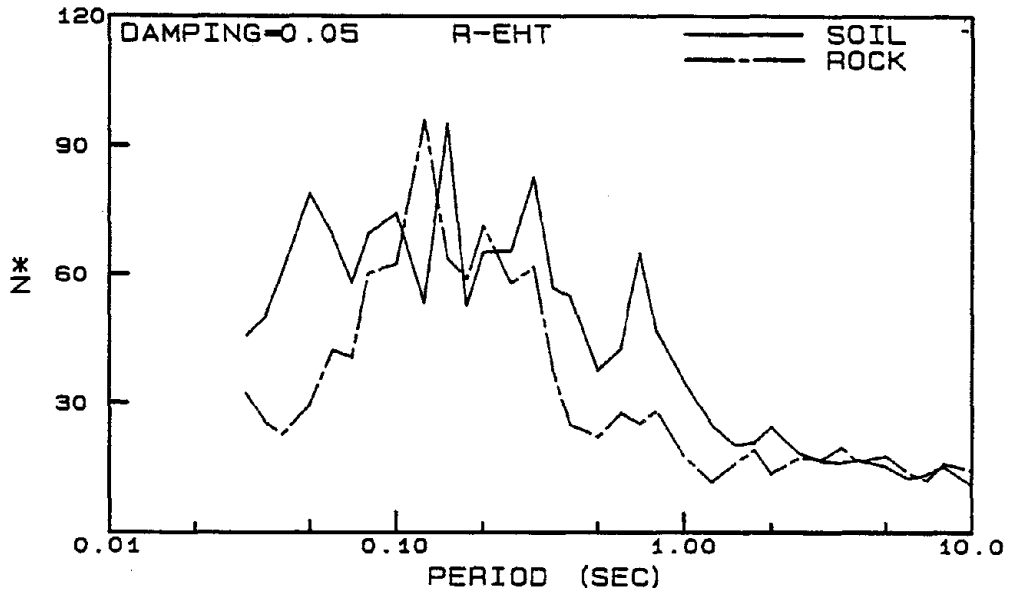

Figure 4.42 Standardized N* for Rayleigh (EHT) distribution for SDOF oscillator with 5% damping for soil and rock sites.

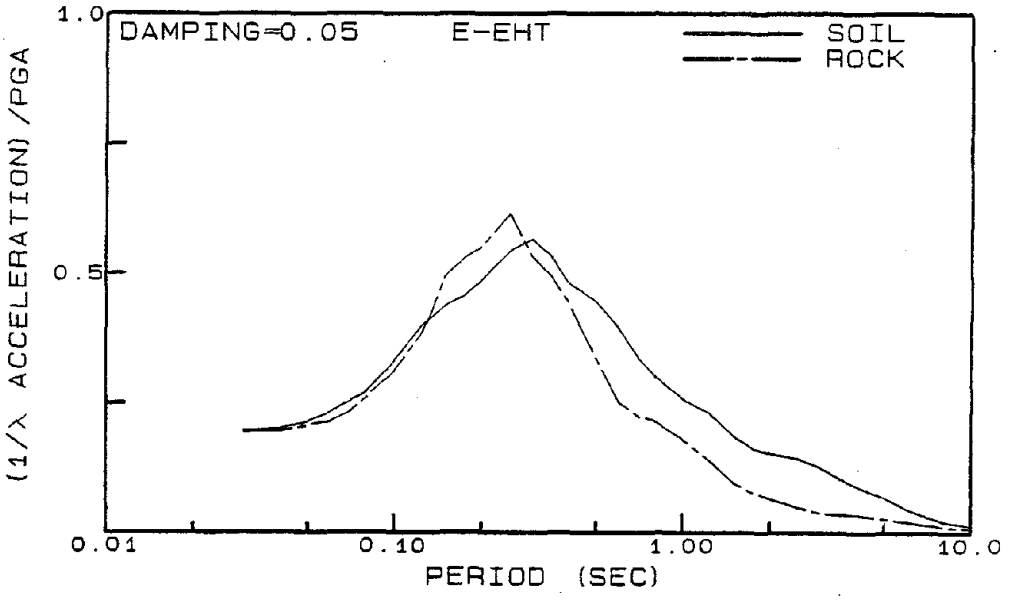

Figure 4.43 Average (1/λ) acceleration/PGA spectra for exponential (EHT) distribution for SDOF oscillator with 5% damping for soil and rock sites.

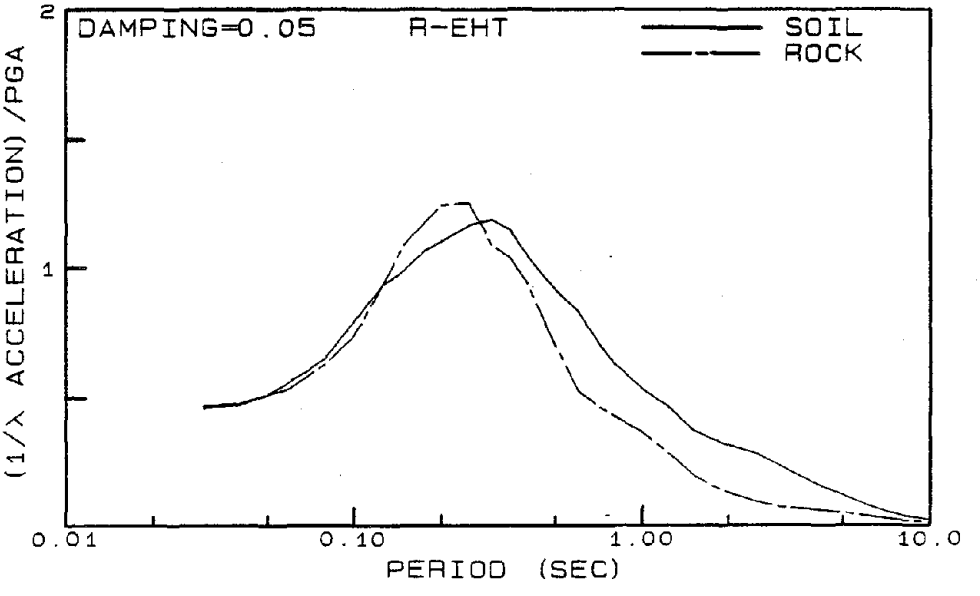

Figure 4.44 Average (1/λ) acceleration/PGA spectra for Rayleigh (EHT) distribution for SDOF oscillator with 5% damping for soil and rock sites.

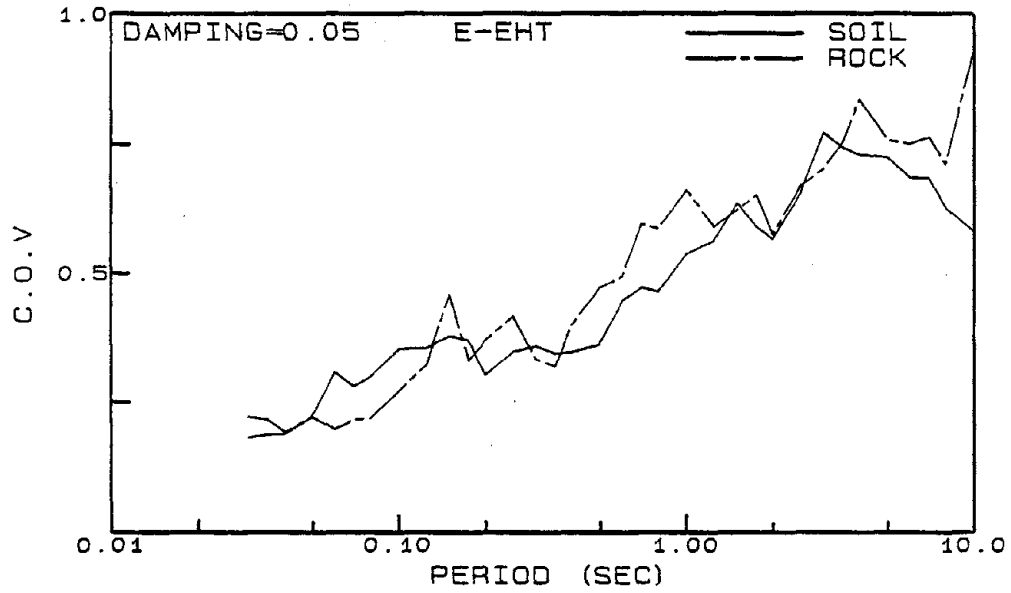

Figure 4.45 Coefficient of variation (C.O.V.) of average ($1/\lambda$) acceleration/PGA spectra for exponential (EHT) distribution for SDOF oscillator with 5% damping for soil and rock sites.

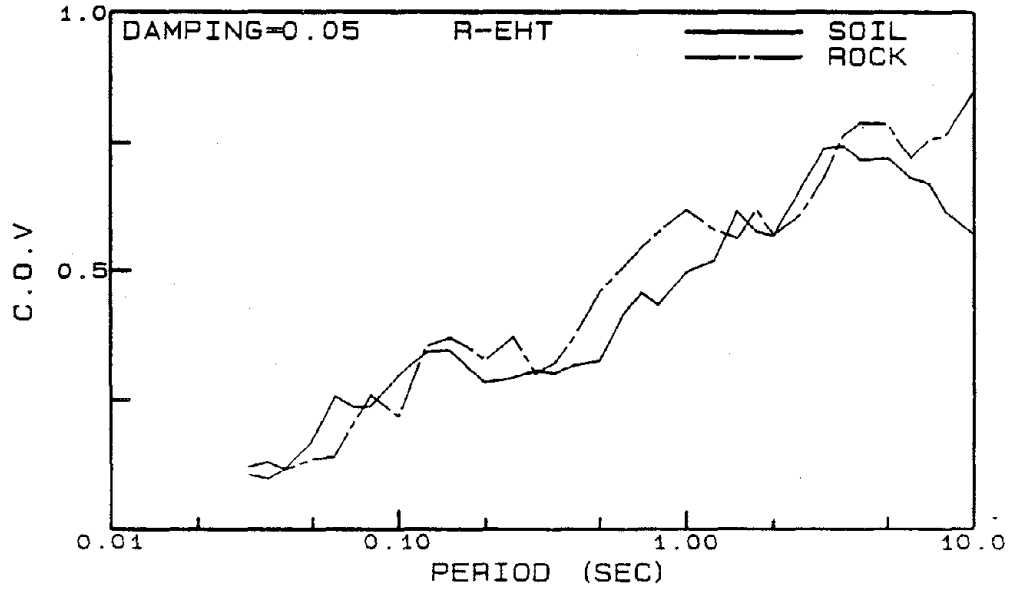

Figure 4.46 Coefficient of variation (C.O.V.) of average ($1/\lambda$) acceleration/PGA spectra for Rayleigh (EHT) distribution for SDOF oscillator with 5% damping for soil and rock sites.

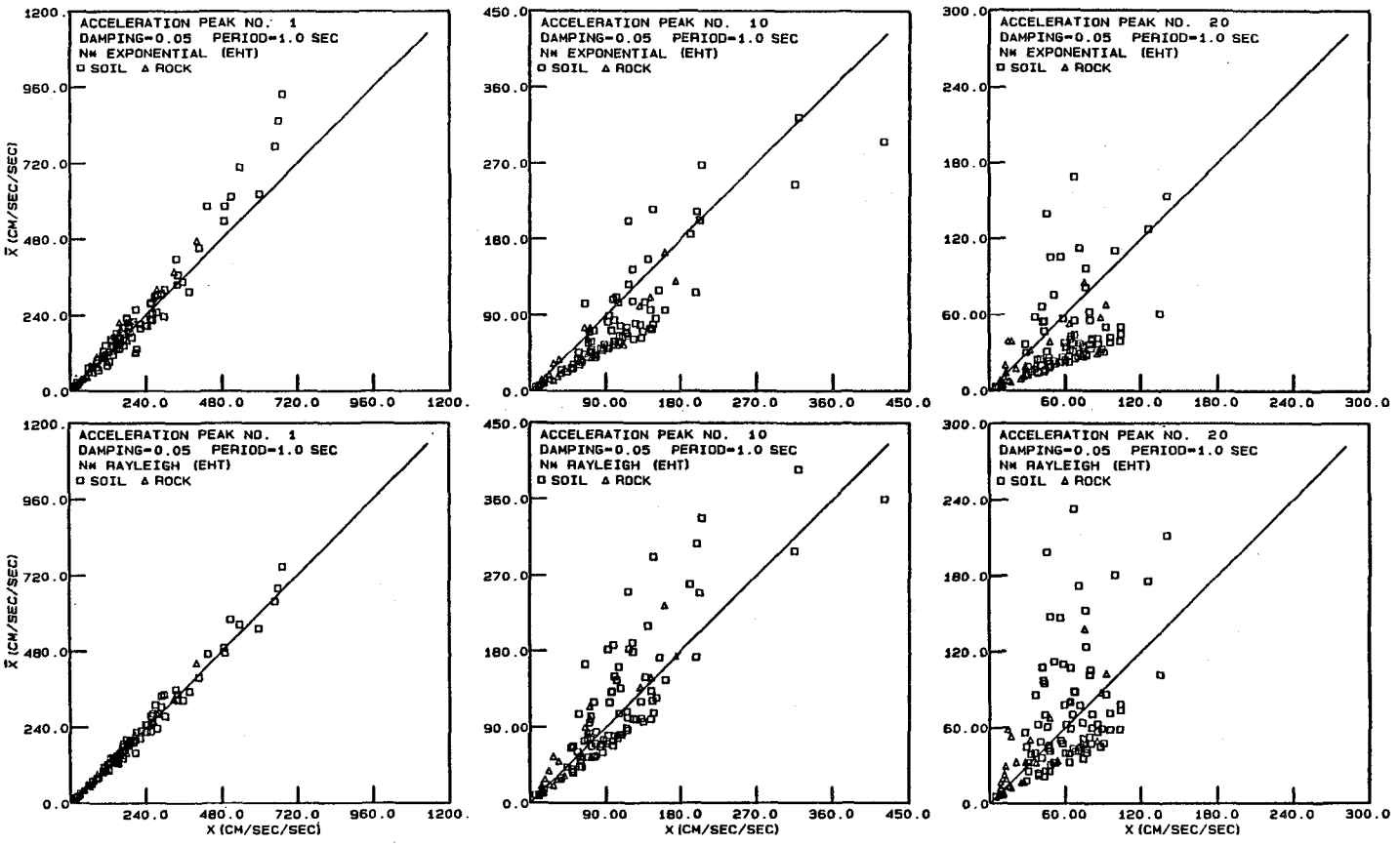

Figure 4.47 Observed vs. predicted acceleration peaks X(1), X(10), and X(20) from N* exponential (EHT) and N* Rayleigh (EHT) distributions for SDOF oscillator with 5% damping and 1 second period.

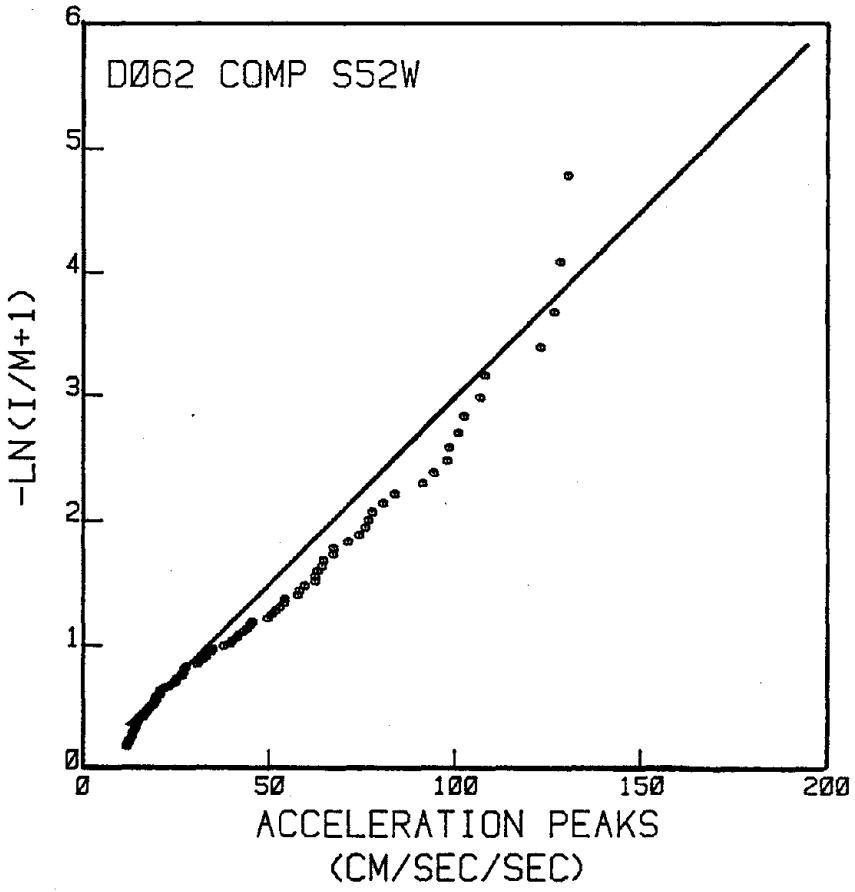

Figure 4.48 Exponential probability plot of the acceleration peaks of component S52W of the Holiday Inn Building, 1640 S. Marengo Street, recorded during the San Fernando, CA earthquake of 9 Februay 1971. The peaks plot as a Rayleigh distribution.

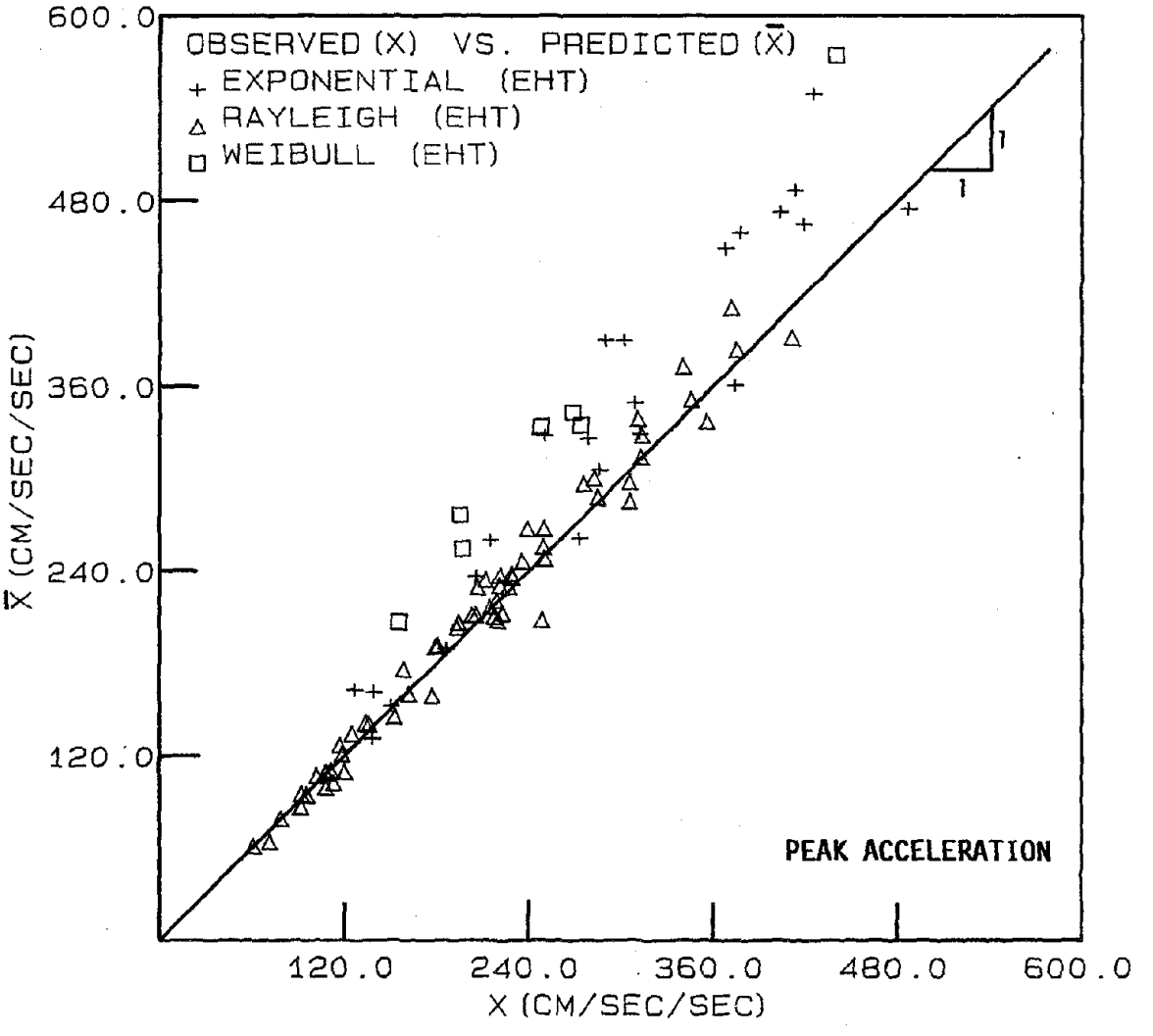

Figure 4.49 Observed X(1) vs. predicted $\bar{X}$(1) peak acceleration for recorded building response at the roof during the 1971 San Fernando, CA earthquake.

REFERENCES

Ang, A.H.-S. and W.H. Tang, (1984), Probability Concepts in Engineering Planning and Design, Vol. II, Basic Principles, New York, John Wiley & Sons, Inc.

Arias, A., (1970), "A Measure of Earthquake Intensity", in R. Hansen, ed., Seismic Design Criteria for Nuclear Power Plants, Cambridge, Massachusetts: MIT Press, pp. 438-483.

Blume, J.A., (1979), "On Instrumental vs. Effective Acceleration and Design Coefficients," Proceedings, 2nd U.S. National Conference on Earthquake Engineering, EERI, Stanford University, Stanford, CA, August 22-24, pp. 868-882.

Blume, J.A., R.L. Sharpe, and J.S. Dalal, (1972), "Recommendations for Shape of Earthquake Response Spectra," John A. Blume & Associates, San Francisco, CA, (AEC Report WASH-1254).

Bolt, B.A., (1973), "Duration of Strong Ground Motion", Proceedings, 5th World Conference on Earthquake Engineering, Rome Italy, Vol. 1, pp. 1304-1315.

Bolt, B.A., and N.A. Abrahamson, (1982), "New Attenuation Relations for Peak and Expected Accelerations of Strong Ground Motion", Bulletin of the Seismological Society of America, Vol. 72. No. 6, pp. 2307-2321.

Bond, W.E., R. Dobry, and M.J. O'Rourke, (1980), "A Study of the Engineering Characteristics of the 1971 San Fernando Earthquake Records Using Time Domain Techniques", Report No. CE-80-1, Department of Civil Engineering, Rensselaer Polytechnic Institute, Troy, New York.

Brady, A.G., V. Perez, and P.N. Mork, (1982), "Digitization and Processing of Main-Shock Ground-Motion Data from the U.S. Geological Survey Accelerograph Network", in The Imperial Valley, California Earthquake of October 15, 1979, U.S. Geological Survey Professional Paper 1254, pp. 385-406.

California Institute of Technology, Earthquake Engineering Research Laboratory, (1973), "Analysis of Strong Motion Earthquake Accelerograms, Volume II, Corrected Accelerograms and Integrated Ground Motion Velocity and Displacement Curves."

Campbell, K.W., (1985), "Strong Motion Attenuation Relations: A Ten-Year Perspective," Earthquake Spectra, Vol. 1, No. 4, August, pp. 759-804.

Chavez, D., et al., (1982), "Main Shock Location and Magnitude Determination Using Combined U.S. and Mexican Data", in The Imperial Valley, California, Earthquake of October 15, 1979, U.S. Geological Survey Profesional Paper 1254, pp. 51-54.

Cloud, W.K., (1967), "Intensity Map and Structural Damage, Parkfield, California, Earthquake of June 26, 1966," Bulletin of the Seismological Society of America, Vol. 57, No. 6, December, pp. 1161-1178.

Crandall, S.H. and W.D. Mark, (1963), Random Vibrations in Mechanical Systems, New York: Academic Press.

Deherrera, M. and T. Zsutty, (1982), "A Time Domain Analysis of Seismic Ground Motions Based on Geophysical Parameters", Stanford University, John A. Blume Earthquake Engineering Report No. 54.

Dizon, J., (1977), "Characterization of Earthquake Ground Motions", Engineer's Thesis, Stanford University.

Dobry, R., I.M. Idriss, and E. Ng, (1978), "Duration Characteristics of Horizontal Components of Strong-Motion Earthquake Records", Bulletin of the Seismological Society of America, Vol. 68, No. 5, October, pp. 1487-1520.

Donovan, N.C., B.A. Bolt, and R.V. Whitman, (1978), "Development of Expectancy Maps and Risk Analysis", ASCE, Journal of the Structural Division, Vol. 104, No. ST8, pp. 1179-1192.

Gumbel, E.J., (1958), Statistics of Extremes, Columbia University Press.

Hall, W.J., B. Mohraz, and N.M. Newmark, (1975a), "Statistical Studies of Vertical and Horizontal Earthquake Spectra," Nathan M. Newmark Consulting Engineering Services, Urbana, Illinois.

Hall, W.J., B. Mohraz, and N.M. Newmark, (1975b), "Statistical Analysis of Earthquake Response Spectra," Proceedings, International Conference on Structural Mechanics in Reactor Technology, 3rd, London.

Hanks, T.C., (1979), "b Values and $w^{-\gamma}$ Seismic Source Models: Implications for Tectonic Stress Variations Along Active Crustal Fault Zones and the Estimation of High-Frequency Strong Ground Motion," Journal of Geophysical Research, Vol. 84, No. B5, May 10, pp. 2235-2242.

Hanks, T.C., (1982), "f_{max}," Bulletin of the Seismological Society of America, Vol. 72, No.6, December, pp. 1867-1879.

Hanks, T.C. and R.K. McGuire, (1981), "The Character of High-Frequency Strong Ground Motion," Bulletin of the Seismological Society of America, Vol. 71, No. 6, December, pp. 2071-2095.

Housner, G.W., (1975), "Measures of Severity of Earthquake Ground Shaking," Proceedings, U.S. National Conference on Earthquake Engineering, EERI, Ann Arbor, Michigan, June, pp. 25-33.

Housner, G.W. and P.C. Jennings, (1977), "Earthquake Design Criteria for Structures," Earthquake Engineering Research Laboratory, California Institute of Technology, Pasadena, CA, EERL Report 77-06.

Idriss, I.M., (1978), "Characteristics of Earthquake Ground Motions," Presented at the ASCE Specialty Conference on Earthquake Engineering and Soil Dynamics, Pasadena, CA, June 19-21.

Kennedy, R.P., (1981), "Peak Acceleration as a Measure of Damage," presented at the Fourth International Seminar on Extreme-Load Design of Nuclear Power Plant Facilities, France, August.

Kiremidjian, A.S. and H.C. Shah, (1978), "Probabilistic Site-Dependent Response Spectra," Technical Report No. 29, John A. Blume Earthquake Engineering Center, Stanford University, Stanford, CA, April.

Maley, R.P. and W.K. Cloud, (1973), "Strong-Motion Accelerograph Records", in Murphy, L.M., Scientific Coordinator, San Fernando Earthquake of February 9, 1971, Vol. III: Geological and Geophysical Studies, pp. 325-348.

McCann, M.W., (1980), "RMS Acceleration and Duration of Strong Ground Motion," Technical Report No. 46, John A. Blume Earthquake Engineering Center, Stanford University, Stanford, CA.

McCann, M.W. and D.M. Boore (1983), "Variability in Ground Motions: Root Mean Square Acceleration and Peak Acceleration for the 1971 San Fernando, California, Earthquake", Bulletin of the Seismological Society of America, Vol. 73, No. 2, April, pp. 615-632.

McCann, M.W. and H.C. Shah (1979), "Determining Strong--Motion Duration of Earthquakes", Bulletin of the Seismological Society of America, Vol. 69, No. 4, August, pp. 1253-1265.

McGuire, R.K., (1978), "A Simple Model for Estimating Fourier Amplitude Spectra of Horizontal Ground Acceleration," Bulletin of the Seismological Society of America, Vol. 68, No. 3, June, pp. 803-822.

McGuire, R.K., and J.A. Barnhard, (1977), "Magnitude, Distance, and Intensity Data for C.I.T. Strong Motion Records", Journal of Research, U.S. Geological Society, Vol. 5, No. 4, July-August, pp. 437-443.

McGuire, R.K. and T.P. Barnhard, (1979), "The Usefulness of Ground Motion Duration in Predicting the Severity of Seismic Shaking," Proceedings, 2nd U.S. National Conference on Earthquake Engineering, August 22-24, Stanford University, Stanford, CA, pp. 713-722.

McGuire, R.K. and T.C. Hanks, (1980), "RMS Acceleration and Spectral Amplitudes of Strong Motion During the San Fernando Earthquake", Bulletin of the Seismological Society of America, Vol. 70, pp. 1907-1920.

Mohraz, B., (1976), "A Study of Earthquake Response Spectra for Different Geological Conditions," Bulletin of the Seismological Society of America, Vol. 66, No. 3, pp. 915-935.

Mohraz, B., W.J. Hall, and N.M. Newmark, (1972), "A Study of Vertical and Horizontal Spectra," Nathan M. Newmark Consulting Engineering Services, Urbana, Illinois (AEC Report WASH-1255).

Mortgat, C.P., (1979), "A Probabilistic Definition of Effective Acceleration", Proceedings, 2nd U.S. National Conference on Earthquake Engineering, EERI, August 22-24, Stanford University, Stanford, CA, pp. 743-752.

Mortgat, C.P. and H.C. Shah, (1978), "A Bayesian Approach to Seismic Hazard Mapping: Development of Stable Design Parameters," Technical Report No. 28, John A. Blume Earthquake Engineering Center, Stanford University, March.

Mulhern, M.R. and R.P. Maley, (1973), "Building Period Measurements Before, During, and After The San Fernando Earthquake," in The San Fernando Earthquake of February 9, 1971, United States Department of Commerce, Volume 1, Part B, pp. 725-733.

Murphy, L.M., K.V. Steinbrugge, and C. Martin Duke, (1973), "The San Fernando Earthquake", in Murphy, L.M., Scientific Coordinator, San Fernando, California, Earthquake of February 9, 1971, U.S. Dept. of Commerce, National Oceanic and Atmospheric Administration, pp. 3-4.

Nau, J. and W. Hall, (1982), An Evaluation of Scaling Methods for Earthquake Response Spectra, University of Illinois, Department of Civil Engineering, Structural Research Series No. 499.

Nau, J. and W. Hall, (1984), "Scaling Methods for Earthquake Response Spectra," ASCE, Journal of Structural Engineering, Vol. 110, No. 7, July, pp. 1533-1548.

Newland, D.E., (1975), An Introduction to Random Vibrations and Spectral Analysis, London, Longman Group Limited.

Newmark, N.M., (1976), "A Rationale for Development of Design Spectra for Diablo Canyon Reactor Facility," Report to the U.S. Nuclear Regulatory Commission, N.M. Newmark Consulting Services, September.

Newmark, N. and W. Hall, (1972), "Procedures and Criteria for Earthquake Resistant Design," NBS, Building Practices for Disaster Mitigation, Building Science Series 46, pp. 209-236.

Newmark, N.M., J.A. Blume, and K.K. Kapur, (1973), "Seismic Design Criteria for Nuclear Power Plants," ASCE, Journal of the Power Division, Vol. 99, No. PO2, pp. 287-303.

Nigam, N.C. and P.C. Jennings, (1968), "Digital Calculation of REsponse Spectra from Strong-Motion Earthquake Records", California Institute of Technology, Earthquake Engineering Research Laboratory, June.

O'Rourke, M.J., R. Serna and R.U. Johnson, (1982), "Duration of Earthquakes, Comparison Between Ground Motion and Structural Motion", Department of Civil Engineering, Report No. CE 82-3, Rensselaer Polytechnic Institute, Troy, New York, May, 67 pp.

Perez, V., (1973), "Velocity Response Envelope Spectrum as a Function of Time, for the Pacoima Dam, San Fernando Earthquake, February 9, 1971," Bulletin of the Seismological Society of America, Vol. 63, No. 1, February, pp. 299-313.

Perez, V., (1980), "Spectra of Amplitudes Sustained for a Given Number of Cycles: An Interpretation of Response Duration for Strong-Motion Earthquakes," Bulletin of the Seismological Society of America, Vol. 70, No. 5, October, pp. 1943-1954.

Perez, V. and G. Brady, (1984), "Reversing Cyclic Demands on Structural Ductility During Earthquakes", Critical Aspects of Earthquake Ground Motion and Building Damage Potential, ATC-10-1, pp. 95-104.

Ploessel, M.R. and J.E. Slosson, (1974), "Repeatable High Ground Accelerations from Earthquakes," California Geology, Vol. 27(9), September, pp. 195-199.

Prince, J., (1984), "Influence of the Number of Response Maxima on the Observed Seismic Behavior of Structures", Critical Aspects of Earthquake Ground Motion and Building Damage Potential, ATC-10-1, pp. 57-66.

Schnabel, P.B. and H.B. Seed, (1973), "Accelerations in Rock for Earthquakes in the Western United States", Bulletin of the Seismological Society of America, Vol. 63, pp. 501-516.

Seed, H.B., and I.M. Idriss, (1971), "Simplified Procedure for Evaluating Soil Liquefaction Potential," ASCE, Journal of Soil Mechanics and Foundation Division, Vol. 97, SM9, pp. 1249-1274.

Seed, H.B. , I.M. Idriss, F. Makdisi, and N. Bannerje, (1975), "Representation of Irregular Stress Time Histories by Equivalent Uniform Stress Series in Liquefaction Analyses", Earthquake Engineering Research Report No. 75-29, College of Engineering, University of California, Berkeley, CA.

Seed, H.B., R. Murarka, J. Lysmer, and I.M. Idriss, (1976a), "Relationships of Maximum Acceleration, Maximum Velocity, Distance from Source, and Local Site Conditions for Moderately Strong Earthquakes", Bulletin of the Seismological Society of America, Vol. 66, No. 4, August, pp. 1323-1342.

Seed, H.B., C. Ugas, and J. Lysmer, (1976b), "Site-Dependent Spectra for Earthquake-Resistant Design," Bulletin of the Seismological Society of America, Vol. 66, pp. 221-243.

Trifunac, M.D. and A.G. Brady, (1975), "A Study on the Duration of Strong Earthquake Ground Motion", Bulletin of the Seismological Society of America, Vol. 65, No. 3, June, pp. 581-626.

Trifunac, M.D. and B. Westermo, (1977), "Note on the Correlation of Frequency-Dependent Duration of Strong Earthquake Ground Motion with the Modified Mercalli Intensity and the Geologic Conditions at the Recording Stations," Bulletin of the Seismological Society of America, Vol. 67, No. 3, June, pp. 917-927.

Vanmarcke, E.H., (1976), "Structural Response to Earthquakes," in Lomnitz, C. and E. Rosenbleuth, editors, Seismic Risk and Engineering Decisions, Chapter 8, New York, Elsevier.

Vanmarcke, E.H. and S.-S.P. Lai, (1977), "Strong-Motion Duration of Earthquakes," Department of Civil Engineering, M.I.T. Publication R77-16.

Vanmarcke, E.H. and S.-S.P. Lai, (1980), "Strong-Motion Duration and RMS Amplitude of Earthquake Records", Bulletin of the Seismological Society of America, Vol. 70, No. 4, August, pp. 1293-1307.

Whitman, R.V., (1978), "Effective Peak Acceleration," Proceedings, 2nd International Microzonation Conference, Vol. III, San Francisco, CA, Nov. 26-Dec. 1, pp. 1247-1255.

Zsutty, T. and M. Deherrera, (1979), "A Statistical Analysis of Acceleration Peaks Based Upon the Exponential Distribution Model", Proceedings, 2nd U.S. National Conference on Earthquake Engineering, EERI, Stanford University, Stanford, CA, August 22-24, pp. 733-742.